Oxydation des composites SIC/SIC et de leurs constituants : approche expérimentale, modélisation et influence sur le comportement mécanique

Ludovic Filipuzzi

N° d'ordre : 593

THESE

PRESENTEE A

L' UNIVERSITE DE BORDEAUX I

POUR OBTENIR LE GRADE DE

DOCTEUR

Spécialité : SCIENCE DES MATERIAUX

PAR

Ludovic FILIPUZZI

Ingénieur ENSCI

OXYDATION DES COMPOSITES SIC/SIC ET DE LEURS CONSTITUANTS : APPROCHE EXPERIMENTALE, MODELISATION ET INFLUENCE SUR LE COMPORTEMENT MECANIQUE

Soutenue le 29 Mars 1991, devant la commission d'examen :

MM.	P.	HAGENMULLER.....	*Président*
	C.	GAULT.....	
	J.	LAHAYE.....	
	P.	LAMICQ.....	
	J.C.	MATHIEU.....	*Examinateurs*
	R.	NASLAIN.....	
	R.	TRESSLER.....	

- 1991 -

N° d'ordre : 593

THESE

PRESENTEE A

L' UNIVERSITE DE BORDEAUX I

POUR OBTENIR LE GRADE DE

DOCTEUR

Spécialité : SCIENCE DES MATERIAUX

PAR

Ludovic FILIPUZZI

Ingénieur ENSCI

OXYDATION DES COMPOSITES SIC/SIC ET DE LEURS CONSTITUANTS : APPROCHE EXPERIMENTALE, MODELISATION ET INFLUENCE SUR LE COMPORTEMENT MECANIQUE

Soutenue le 29 Mars 1991, devant la commission d'examen :

MM.	P.	HAGENMULLER.....	*Président*
	C.	GAULT.....	
	J.	LAHAYE.....	
	P.	LAMICQ.....	
	J.C.	MATHIEU.....	*Examinateurs*
	R.	NASLAIN.....	
	R.	TRESSLER.....	

- 1991 -

La présente étude a été réalisée au Laboratoire des Composites Thermostructuraux (Unité Mixte de Recherche 47 CNRS-SEP-UB1).

Je tiens à exprimer ma profonde gratitude à Monsieur le Professeur Roger NASLAIN, Directeur du Laboratoire, pour m'avoir accueilli au sein de son groupe de recherches et avoir accepté la direction de ce travail. Je le remercie pour avoir su me guider dans mes recherches par ses conseils judicieux.

Je remercie vivement Monsieur le Professeur Paul HAGENMULLER pour l'honneur qu'il me fait en ayant accepté la présidence de mon jury de thèse.

Monsieur le Professeur Christian GAULT, Directeur de l'Ecole Nationale Supérieure de Céramiques Industrielles de Limoges a bien voulu me faire l'honneur de juger ce travail, qu'il trouve ici l'expression de ma respectueuse reconnaissance.

Monsieur Jacques LAHAYE, Directeur de Recherches au CNRS du Centre de Recherches sur la Physico-Chimie des Surfaces Solides de Mulhouse a bien voulu me faire l'honneur de juger ce travail, qu'il trouve ici l'expression de ma sincère gratitude.

Monsieur Pierre LAMICQ, Directeur de la Recherche et Technologie à la Société Européenne de Propulsion, a bien voulu me faire l'honneur d'examiner ce travail. Je le remercie sincèrement pour son aide et ses conseils.

Monsieur Jean Claude MATHIEU, Directeur de Recherches au CNRS et Directeur du Centre de Thermodynamique et Microcalorimétrie a aimablement accepté de participer à mon jury de thèse. Je lui adresse mes sincères remerciements.

Monsieur le Professeur Richard TRESSLER, de l'Université de l'Etat de Pennsylvanie (USA) me fait l'honneur de juger ce travail, qu'il trouve ici l'expression de ma sincère gratitude.

Je tiens à remercier Monsieur Jacques THEBAULT, Ingénieur à la Société Européenne de Propulsion pour sa collaboration efficace.

Monsieur le Professeur Max SCHVOERER et Monsieur Rémi CHAPOULIE du Centre de Recherche Interdisciplinaire d'Archéologie Analytique de l'Université de Bordeaux III, Monsieur Claude JAUSSAUD du LETI de Grenoble et Madame Yolande KEEN du CEMES de l'Université de Toulouse III ont contribué à ce travail, qu'ils en soient vivement remerciés.

Je tiens à exprimer toute ma gratitude à Messieurs Gérald CAMUS, Chargé de Recherches au CNRS, pour sa collaboration efficace et amicale, Jacques DEUZET, Ingénieur à la Société Européenne de Propulsion, pour les conseils et la disponibilité qu'il m'a accordés et Francis LANGLAIS, Chargé de Recherches au CNRS pour son aimable collaboration.

Enfin, je tiens à remercier tous les membres du Laboratoire sans qui ce travail n'aurait pas pu aboutir et particulièrement J.L. BOBET, R. FEDOU, B. HUMEZ, C. LABRUGERE, F. LAMOUROUX, D. MOCAER, N. PIQUENOT, P. PLUVINAGE, F. REGNIER et J.F. VILLENEUVE.

Madame Josette FORGET et Mademoiselle Cécile DUPOUY ont contribué avec beaucoup de dévouement à la réalisation de ce mémoire, je les remercie sincèrement.

Je remercie la Société Européenne de Propulsion et le CNRS pour leur soutien financier grâce auquel cette étude a pu être menée.

SOMMAIRE

INTRODUCTION

CHAPITRE I

OXIDATION KINETICS OF SiC-BASED CERAMIC FIBERS

CHAPITRE II

OXIDATION KINETICS OF SiC DEPOSITED FROM CH_3SiCl_3/H_2 UNDER CVI-CONDITIONS

CHAPITRE III

OXIDATION MECHANISMS AND KINETICS OF 1D-SiC/C/SiC COMPOSITE MATERIALS : 1 - AN EXPERIMENTAL APPROACH

CHAPITRE IV

OXIDATION MECHANISMS AND KINETICS OF 1D-SiC/C/SiC COMPOSITE MATERIALS : 2 - MODELLING

CHAPITRE V

EFFECT OF HIGH TEMPERATURE AGEING TREATMENTS ON THE MECHANICAL BEHAVIOUR OF UNIDIRECTIONAL SiC/SiC FIBROUS COMPOSITES

INTRODUCTION

INTRODUCTION

Avant propos

L'étymologie du mot ***matériau*** qui vient du latin ***materia*** révèle que ce terme, désignant initialement le bois, recouvre les sens de ***substance*** mais aussi de ***ce qui engendre***. Cette seconde signification, oubliée aujourd'hui, n'a peut-être jamais été aussi justifiée. La multitude de nouveaux matériaux, et parmi eux les composites, qui envahissent notre vie quotidienne en témoigne.

Les matériaux composites associent des constituants de nature différente de façon à obtenir des propriétés particulières dans une ou plusieurs directions. Les perspectives de création de nouveaux matériaux, au travers du concept composite, apparaissent très vastes. Ainsi, si les matrices métalliques sont renforcées par des fibres céramiques afin d'être rigidifiées, les matrices céramiques peuvent être renforcées par des fibres métalliques ou céramiques afin de pallier leur fragilité. Les nombreuses combinaisons possibles, l'échelle à laquelle elles sont réalisées, l'orientation choisie des constituants conduisent à une large palette de matériaux aux propriétés spécifiques répondant au mieux aux exigences technologiques.

1 - Rupture des céramiques et des composites à matrice céramique (CMC)

Les CMC ont été développés principalement en vue d'applications à hautes températures sous divers environnements. Ainsi, par exemple, l'amélioration du rendement des moteurs thermiques passe par l'élévation des températures de fonctionnement. Jusqu'à maintenant, les alliages métalliques réfractaires base nickel ou cobalt étaient utilisés. Aujourd'hui, leur

température limite d'utilisation apparaît insuffisante. Le choix s'est donc orienté vers des matériaux plus réfractaires, les céramiques. Elles présentent une excellente réfractairité, de hauts modules d'élasticité, une dureté élevée, une bonne inertie chimique, des masses volumiques relativement basses et sont généralement des isolants électriques [1]. Les fortes liaisons iono-covalentes mises en jeu au sein de ces matériaux sont à la base de ces propriétés. Leur principal inconvénient est lié à leur fragilité. Les systèmes de glissement étant peu nombreux, il n'y a pas, à température ambiante, de déformation plastique comme dans le cas des métaux. Il en résulte une sensibilité très grande des céramiques aux effets d'entailles et aux défauts préexistants. L'énergie nécessaire à la propagation d'une fissure est de l'ordre de 30-300 Jm^{-2} pour les céramiques alors qu'elle dépasse souvent 10^4 Jm^{-2} pour les métaux [2]. La propagation catastrophique d'une fissure est observée dès que le facteur d'intensité de contrainte atteint sa valeur critique auprès d'un défaut. Les propriétés des céramiques sont donc gouvernées par la nature, la taille et la répartition des défauts. Ces caractéristiques étant difficilement maîtrisables, une grande dispersion de la résistance à la rupture des céramiques est généralement observée [3,4].

La première façon d'améliorer les caractéristiques mécaniques des céramiques consiste donc à limiter la taille et le nombre des défauts en maîtrisant les différentes étapes d'élaboration. Cette voie est optimisée lors de la fabrication d'éléments de petits volumes où il est plus facile de contrôler les défauts. Ainsi, les fibres céramiques à faible diamètre présentent des contraintes à rupture pouvant atteindre 3000 MPa avec des allongements à rupture de l'ordre de 1% [5].

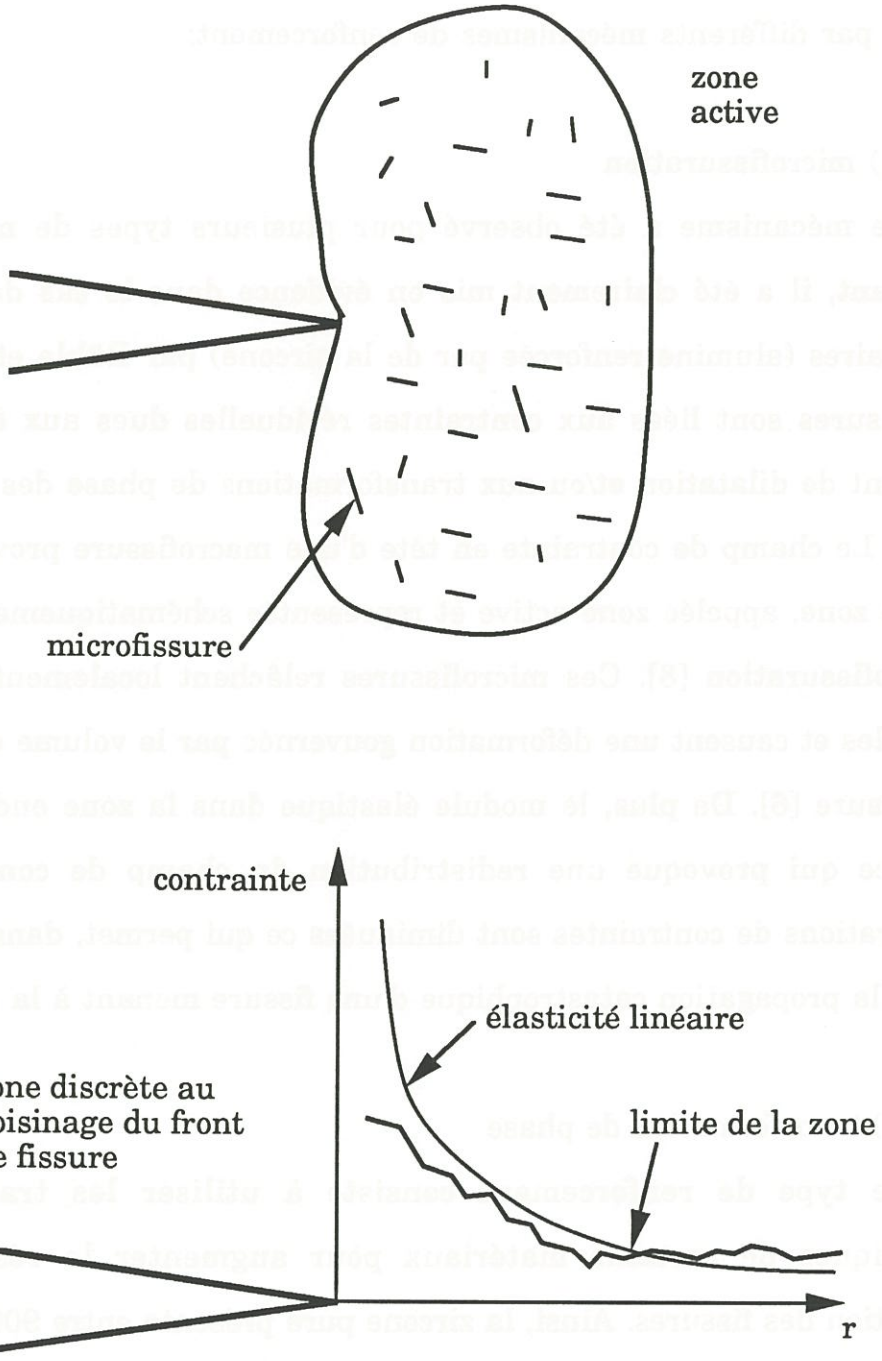

Fig. 1 : Influence de la zone active sur la répartition des contraintes au voisinage d'une fissure [8]

Le deuxième moyen consiste à essayer de freiner la progression des fissures par différents mécanismes de renforcement:

(1) microfissuration

Ce mécanisme a été observé pour plusieurs types de matériaux [6]. Cependant, il a été clairement mis en évidence dans le cas des composites particulaires (alumine renforcée par de la zircone) par Rühle et coll. [7]. Les microfissures sont liées aux contraintes résiduelles dues aux différences de coefficient de dilatation et/ou aux transformations de phase des particules de zircone. Le champ de contrainte en tête d'une macrofissure provoque sur une certaine zone, appelée zone active et représentée schématiquement à la fig. 1, la microfissuration [8]. Ces microfissures relâchent localement les tensions résiduelles et causent une déformation gouvernée par le volume déplacé par la microfissure [6]. De plus, le module élastique dans la zone endommagée est réduit ce qui provoque une redistribution du champ de contraintes. Les concentrations de contraintes sont diminuées ce qui permet, dans certains cas, d'éviter la propagation catastrophique d'une fissure menant à la rupture.

(2) transformation de phase

Ce type de renforcement consiste à utiliser les transformations allotropiques de certains matériaux pour augmenter la résistance à la propagation des fissures. Ainsi, la zircone pure présente entre 900°C et 1100°C une transformation martensitique de la structure quadratique à la structure monoclinique qui s'accompagne d'une augmentation de volume de 3 à 5 % [9]. La structure quadratique est maintenue à température ambiante sous l'effet d'agents stabilisateurs (Y_2O_3, MgO, CaO,...) et/ou de contraintes de compression. Plusieurs configurations peuvent être obtenues : les zircones

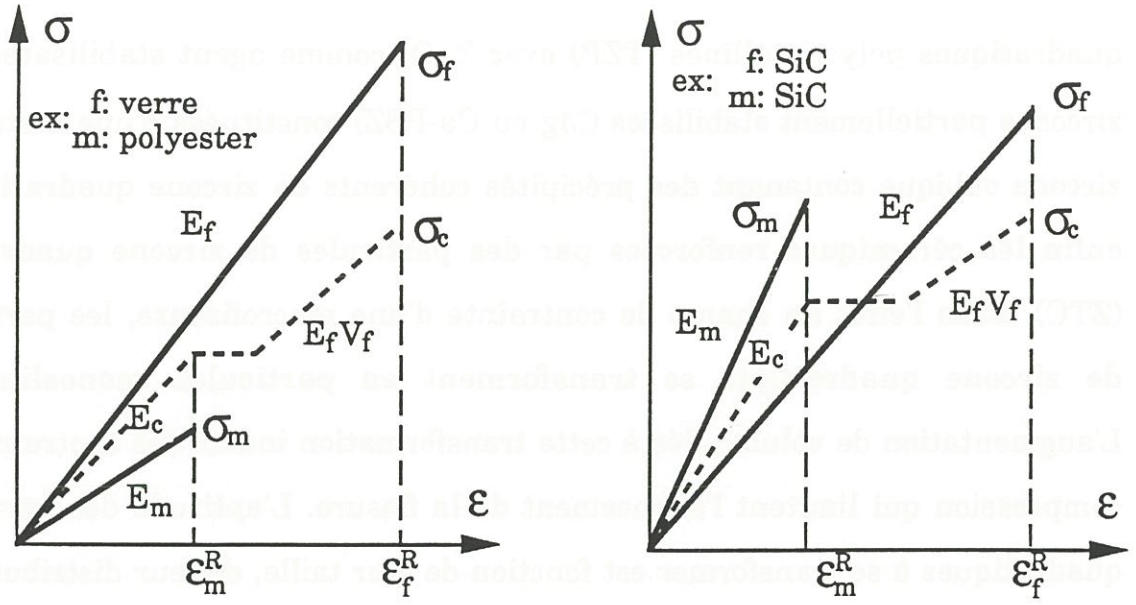

Fig. 2 : Représentation schématique du comportement endommageable de matériaux composites 1D lorsque l'allongement à rupture de la matrice est inférieur à celui des fibres [12]

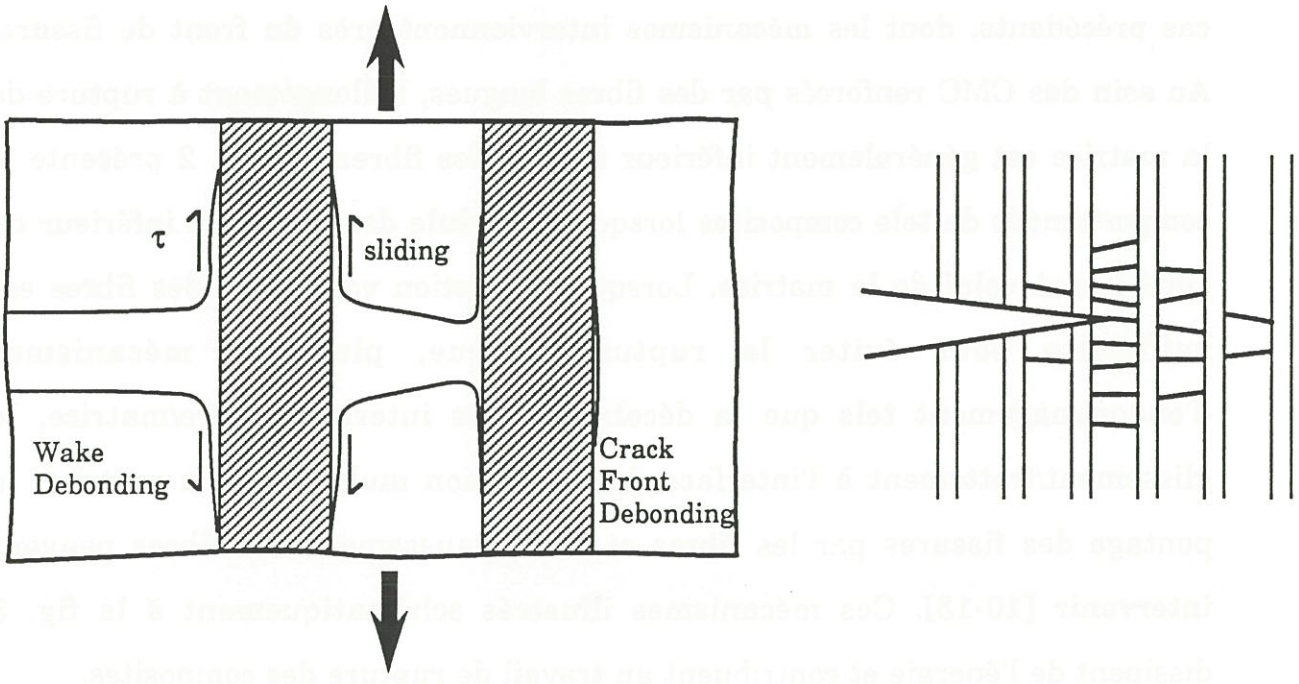

Fig. 3 : Mécanismes d'endommagement des composites à matrice fragile [10, 11]

quadratiques polycristallines (TZP) avec Y_2O_3 comme agent stabilisateur, les zircones partiellement stabilisées (Mg ou Ca-PSZ) constituées d'une matrice de zircone cubique contenant des précipités cohérents de zircone quadratique et enfin les céramiques renforcées par des particules de zircone quadratique (ZTC). Sous l'effet du champ de contrainte d'une macrofissure, les particules de zircone quadratique se transforment en particules monocliniques. L'augmentation de volume liée à cette transformation induit des contraintes de compression qui limitent l'avancement de la fissure. L'aptitude des particules quadratiques à se transformer est fonction de leur taille, de leur distribution et de leur forme.

(3) renforcement par des fibres

L'introduction d'un renfort fibreux, au sein de céramiques, permet d'obtenir des zones d'endommagement beaucoup plus étendues que dans les cas précédents, dont les mécanismes interviennent près du front de fissure. Au sein des CMC renforcés par des fibres longues, l'allongement à rupture de la matrice est généralement inférieur à celui des fibres. La fig. 2 présente le comportement de tels composites lorsque le module des fibres est inférieur ou supérieur à celui de la matrice. Lorsque la fraction volumique des fibres est suffisante pour éviter la rupture unique, plusieurs mécanismes d'endommagement tels que la décohésion des interfaces fibre/matrice, le glissement/frottement à l'interface, la fissuration multiple de la matrice, le pontage des fissures par les fibres et le déchaussement des fibres peuvent intervenir [10-13]. Ces mécanismes illustrés schématiquement à la fig. 3 dissipent de l'énergie et contribuent au travail de rupture des composites.

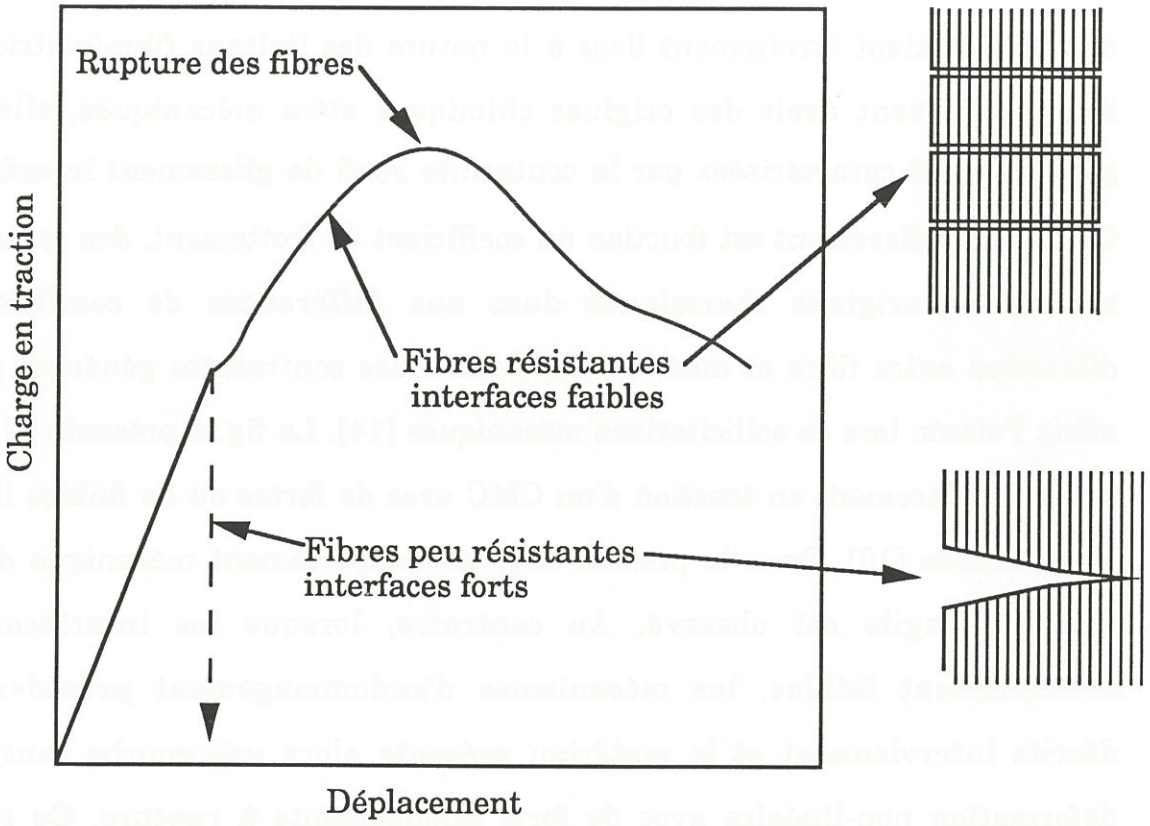

Fig. 4 : Courbe charge-déplacement en traction d'un composite à matrice céramique avec de fortes ou faibles liaisons fibre/matrice [10]

L'étude des interfaces, (ou des interphases) a montré que les propriétés des CMC étaient étroitement liées à la nature des liaisons fibre/matrice. Ces liaisons peuvent avoir des origines chimiques et/ou mécaniques, elles sont généralement caractérisées par la contrainte seuil de glissement interfacial τ. Ce seuil de glissement est fonction du coefficient de frottement, des contraintes normales d'origines thermiques dues aux différences de coefficient de dilatation entre fibre et matrice, mais aussi des contraintes générées par les effets Poisson lors de sollicitations mécaniques [14]. La fig. 4 présente la courbe force - déplacement en traction d'un CMC avec de fortes ou de faibles liaisons fibre/matrice [10]. Dans le premier cas, un comportement mécanique du type linéaire fragile est observé. Au contraire, lorsque les interfaces sont suffisamment faibles, les mécanismes d'endommagement précédemment décrits interviennent et le matériau présente alors une courbe contrainte-déformation non-linéaire avec de forts allongements à rupture. Ce type de comportement a été mis en évidence pour des composites à matrice fragile [15-17]. Alors qu'une borne supérieure pour la valeur de τ apparait nécessaire pour éviter une rupture fragile, cette valeur doit néanmoins être suffisante pour assurer le transfert de charge. D'après Aveston, Cooper et Kelly [18], le retard à la fissuration de la matrice fragile, provoqué par la présence des fibres, augmente avec la valeur de τ.

Les CMC renforcés par des fibres céramiques conjuguent donc les deux approches pour améliorer le comportement mécanique des céramiques: (i) obtention de résistances et allongements à rupture élevés par contrôle des défauts initiaux en ce qui concerne le renfort fibreux et (ii) mise en place de mécanismes d'endommagement par ajustement des liaisons fibre/matrice

permettant d'augmenter considérablement l'énergie nécessaire à la propagation des fissures et le travail de rupture des composites.

Le contrôle des interfaces lors de la fabrication des composites, mais aussi le maintien de leur intégrité à haute température dans les conditions de service, sont donc des facteurs clés pour l'utilisation de ces matériaux.

2 - Elaboration des composites SiC/SiC

2.1 - Introduction

Les premiers composites à matrice verre ou vitrocéramique renforcés par des fibres de carbone ont été élaborés il y a une vingtaine d'années [15]. Malgré leurs bonnes caractéristiques mécaniques, leur faible résistance à l'oxydation, due à la présence des fibres de carbone, a limité leur utilisation. Les composites carbone/carbone en raison de leur exceptionnelle tenue mécanique à haute température, de leur basse densité et de leur résistance à l'ablation ont été utilisés comme tuyère d'engins propulsifs et boucliers thermiques des corps de rentrée [19]. Aujourd'hui, leurs propriétés de friction leur ont ouvert de nombreuses applications dans le domaine du freinage aéronautique, ferroviaire ou automobile. Néanmoins, leur faible résistance à l'oxydation reste une limitation importante à leur généralisation. L'idée de remplacer partiellement ou complètement la matrice de carbone par du carbure de silicium a été développée par Christin et coll. [20,21]. L'évolution vers les matériaux SiC/SiC s'est effectuée suite aux développements d'une nouvelle génération de fibres SiC ex-polycarbosilane (PCS) par Yajima et coll.

[22]. Ces fibres qui se présentent sous forme de mèches multifilamentaires ont un diamètre de 15 µm en moyenne ce qui permet leur tissage. Grâce à leur caractéristiques thermomécaniques [23] et leur compatibilité chimique avec plusieurs matrices elles ont été à la base du développement des composites céramiques SiC/LAS et SiC/SiC.

2.2 - Les fibres SiC ex-PCS(*)

Les fibres sont filées à partir du PCS fondu, sous azote à une température de l'ordre de 300°C. Ensuite elles subissent un traitement de stabilisation sous air ou sous oxygène qui les rend infusibles. Au cours de ce traitement, elles s'enrichissent en oxygène. Enfin, la dernière étape consiste en une pyrolyse sous gaz inerte à une température de l'ordre de 1300°C. Le résidu obtenu est constitué d'une phase microcristallisée SiC β (taille moyenne des grains : 2,5 nm), d'aggrégats de carbone entourés d'hydrogène et d'une phase oxycarbure amorphe SiC_xO_y (avec x+y = 4) [24]. Les fibres présentent, à température ambiante, un module d'élasticité d'environ 200 GPa et une contrainte à rupture moyenne de 2800 MPa pour des longueurs de jauge de l'ordre de 10 mm. Ces caractéristiques sont maintenues jusqu'à 800°C sous argon. Au delà de 1200°C, la chute des propriétés mécaniques est très rapide [25,26]. En fait, les fibres ne sont pas stables thermodynamiquement, elles évoluent vers un état d'équilibre d'autant plus rapidement que la température est élevée. Il semble que la présence d'oxygène soit peu favorable au maintien des caractéristiques mécaniques à haute température [27]. De nombreuses études, visant à obtenir des fibres comparables mais plus réfractaires, se sont développées récemment. Ainsi, de nouveaux précurseurs organo-siliciés mais

(*) fibre Nicalon (NLM 202) de Nippon Carbon

aussi des traitements de réticulation (bombardement électronique ou rayonnement γ) ont permis d'obtenir des fibres pratiquement exemptes d'oxygène et qui conservent leur intégrité mécanique jusqu'à 1400°C [28].

2.3 - Densification de la préforme fibreuse

La préforme fibreuse peut présenter plusieurs architectures (1D, 2D, 3D, nD) suivant les propriétés que l'on veut conférer au composite. L'insertion d'une matrice réfractaire, de type SiC, au sein de ce substrat est difficilement réalisable par la technologie classique des poudres. En effet, d'une part les mécanismes mis en jeu lors du frittage seraient probablement contrariés par la présence d'un renfort rigide et, d'autre part, les températures nécessaires pour activer le frittage seraient certainement trop élevées et endommageraient les fibres. Les deux voies actuellement utilisées sont les voies liquide et gazeuse qui peuvent être éventuellement couplées pour optimiser la densification.

La première consiste à imprégner le substrat fibreux par un précurseur organosilicié, le précurseur des fibres par exemple, et à pyrolyser à une température relativement basse. Cette opération doit éventuellement être répétée plusieurs fois afin d'obtenir une bonne densification du composite. Cette méthode présente l'avantage d'être rapide.

L'infiltration chimique en phase vapeur (Chemical Vapor Infiltration : CVI) est un procédé dérivé du dépôt chimique en phase vapeur. Il consiste à déposer la matrice par réaction chimique hétérogène à partir de précurseurs gazeux au sein du substrat fibreux porté à température modérée ($\approx$ 1000°C). SiC est ainsi produit à partir d'un mélange méthyltrichlorosilane/hydrogène.

Cette méthode présente plusieurs avantages : (i) densification à basse température ce qui évite la dégradation des fibres ou des réactions chimiques fibre/matrice, (ii) réalisation de grandes pièces pouvant avoir des formes complexes et (iii) dépôt uniforme de couches de faible épaisseur (interphases, dépôts externes, ...).

Cependant, l'infiltration nécessite le transport des espèces sources et produits de réaction à travers le substrat fibreux. Pour éviter de forts gradients de concentration entre la surface et le coeur des préformes fibreuses, menant à une hétérogénéité du dépôt les transferts de masse doivent être rapides devant les phénomènes de réactions chimiques de surface. Les conditions favorables à l'homogénéité du dépôt sont les basses températures et basses pressions [29] ($T \approx 1000°C$, $5\ kPa < P < 50\ kPa$). Ces conditions opératoires impliquent que le processus de densification est lent. En revanche, un grand nombre de préformes (de formes différentes et/ou complexes) peuvent être densifiées simultanément.

2.4 - Les matériaux d'interphase

Le premier chapitre a montré l'importance des liaisons fibre/matrice sur le comportement mécanique des composites. Dans le cas des SiC/SiC, cette liaison est contrôlée par le dépôt d'une couche de pyrocarbone avant densification par SiC. L'intérêt du carbone réside dans le fait qu'il présente une structure lamellaire le plus souvent avec des défauts turbostratiques dans laquelle les feuillets ne sont que faiblement liés entre eux. Une contrainte interfaciale τ de l'ordre de quelques dizaines de MPa [30] est alors obtenue, elle

conduit à un comportement mécanique non linéaire et à un travail de rupture important.

Le nitrure de bore hexagonal, BN, présentant une structure similaire à celle du pyrocarbone a aussi été identifié comme matériau potentiel d'interphase pour les composites SiC/SiC à matrice céramique [31]. Cependant, son utilisation au stade industriel reste pour l'instant limitée. Il est intéressant de noter que de nombreux composites à fibres SiC ex-PCS et matrice verre présentent aussi une interphase de carbone. Cependant cette interphase ne résulte pas d'un dépôt préalable mais d'une évolution chimique de la fibre ou/et d'une réaction fibre/matrice au cours du processus de fabrication. Plusieurs études [32,33] ont montré que lorsque la couche de carbone, généralement amorphe, n'était pas présente, le comportement des composites était alors linéaire fragile.

3 - Oxydation des composites SiC/C/SiC

3.1 - Introduction

La présence du carbone aux interfaces fibre/matrice constitue un point faible potentiel de ces matériaux. En effet, étant donné l'importance des liaisons fibre/matrice sur le comportement mécanique, leur disparition ou leur modification pourraient avoir des conséquences importantes sur la durée de vie des matériaux.

Le comportement à l'oxydation des composites SiC/C/SiC peut être abordé, dans un premier temps, en examinant celui de chaque constituant. Cependant, bien que nécessaire cette approche n'est pas suffisante et il faudra

regarder ensuite le problème dans sa globalité avec l'interaction des différents mécanismes d'oxydation.

3.2 - Oxydation du silicium et du carbure de silicium

3.2.1 - Réactions chimiques

Le silicium et le carbure de silicium sont des matériaux semi conducteurs largement utilisés en électronique (applications à hautes températures pour SiC). La réalisation de couches électriquement isolantes, du type SiO_2, par oxydation thermique a engendré de nombreuses études sur les cinétiques d'oxydation de ces matériaux. L'utilisation de SiC, en tant que céramique structurale à haute température en environnement oxydant a aussi suscité beaucoup d'intérêt sur la tenue à l'oxydation de ces matériaux.

Thermodynamiquement, Si et SiC ne sont pas stables en atmosphère oxydante. La résistance à l'oxydation de ces matériaux est alors fonction de la **cinétique** des réactions d'oxydation. Sous fortes pressions partielles d'oxygène, il y a formation de la phase condensée SiO_2 suivant les réactions :

$$Si_{(s)} + O_{2(g)} \rightleftarrows SiO_{2(s)} \qquad (1)$$

$$SiC_{(s)} + \frac{3}{2} O_{2(g)} \rightleftarrows SiO_{2(s)} + CO_{(g)} \qquad (2)$$

$$SiC_{(s)} + 2O_{2(g)} \rightleftarrows SiO_{2(s)} + CO_{2(g)} \qquad (3)$$

Dans ce cas, l'oxydation est dite "passive" en raison de la formation de la couche d'oxyde et de son caractère protecteur.

Au contraire, sous faible pression partielle d'oxygène, il n'y a pas formation de couche condensée mais volatilisation suivant les équations :

$$Si_{(s)} + \frac{1}{2} O_{2(g)} \rightleftarrows SiO_{(g)} \qquad (4)$$

$$SiC_{(s)} + O_{2(g)} \rightleftarrows SiO_{(g)} + CO_{(g)} \qquad (5)$$

A haute température, et sous faible pression partielle d'oxygène, il peut aussi y avoir réaction entre le substrat et l'oxyde suivant les équations [34] :

$$Si_{(s)} + SiO_{2(s)} \rightleftarrows 2\,SiO_{(g)} \qquad (6)$$

$$SiC_{(s)} + 2\,SiO_{2(s)} \rightleftarrows 3\,SiO_{(g)} + CO_{(g)} \qquad (7)$$

$$SiC_{(s)} + SiO_{2(s)} \rightleftarrows 2\,SiO_{(s)} + C_{(s)} \qquad (8)$$

$$2\,SiC_{(s)} + SiO_{2(s)} \rightleftarrows 3\,Si + 2\,CO_{(g)} \qquad (9)$$

La destruction du film d'oxyde rend alors le matériau très vulnérable, l'oxydation est alors dite "active".

3.2.2 - Cinétiques d'oxydation en régime passif

Oxydation du silicium

Pour oxyder le silicium, l'oxygène doit diffuser en phase gazeuse à travers une couche limite éventuelle, puis il doit s'adsorber et se dissoudre dans la couche de SiO_2 à l'interface externe et enfin réagir avec le substrat Si pour former SiO_2.

Au cours de cette réaction, il y a augmentation de volume d'un facteur 2 environ, ce qui génère des contraintes de compression dans le film d'oxyde et de tension dans le substrat. De la façon dont ces contraintes seront relaxées (plasticité du film, fissuration, décollement) dépendra la qualité de la tenue à l'oxydation des matériaux.

Les études cinétiques ont été essentiellement réalisées à partir de mesures d'épaisseur de couche d'oxyde en fonction du temps pour des wafers monocristallins de Si. En 1965, Deal et Grove [35], ont proposé un modèle s'appuyant sur les phénomènes précédemment décrits, reliant l'épaisseur de la couche d'oxyde X au temps t par l'équation :

$$X^2 + A\,X = B\,t + X_i^2 + A\,X_i \qquad (10)$$

X_i est l'épaisseur initiale de la couche d'oxyde à t = 0. Pour de fortes épaisseurs, ou pour des temps importants, l'équation (10) devient :

$$X^2 \approx B\,t \qquad (11)$$

Cette expression est généralement connue sous le terme de "loi parabolique". B est la constante de vitesse parabolique, elle représente la diffusion de l'oxygène (sous une forme a priori quelconque) dans le film d'oxyde. Au contraire, pour des temps relativement courts l'équation (10) s'écrit :

$$X = \frac{B}{A}\,t + \frac{X_i^2}{A} + X_i \qquad (12)$$

Dans ce cas, l'épaisseur de la couche d'oxyde est proportionnelle au temps. Le rapport $\frac{B}{A}$ est la constante de vitesse linéaire, elle représente les régimes de réaction aux interfaces interne (SiO_2/Si) et externe (environnement / SiO_2).

La relation (10) a permis une bonne description des résultats expérimentaux concernant l'oxydation du Si. Il a été notamment établi, que la **perméation de l'oxygène sous forme moléculaire** à travers la couche de SiO_2 était le mécanisme limitant lors de l'oxydation du Si sous oxygène sec. L'énergie apparente d'activation reportée par Deal et Grove [35] pour ce phénomène (≈ 120 kJ/mol) est comparable à celle reportée par Norton [36] pour la perméation de l'oxygène moléculaire à travers de la silice fondue. Concernant le régime linéaire initial, une énergie apparente d'activation d'environ 190 kJ/mol comparable à celle nécessaire pour rompre une liaison Si-Si a été obtenue.

Pour les deux régimes, une dépendance linéaire est attendue avec la pression partielle d'oxygène, ce qui a été observé pour 10 kPa < P < 100 kPa. Cette étude a servi de support à l'interprétation de nombreux travaux sur les cinétiques d'oxydation de matériaux à base de silicium tels que SiC et Si_3N_4 [37-38].

Récemment, plusieurs études ont complété ou généralisé la loi linéaire-parabolique. Ainsi, des modèles plus complets, incluant en parallèle des mécanismes avec **O_2 moléculaire** et **O atomique** ont été proposés [39]. Ils permettent de rendre compte de phénomènes fins tels que la dépendance non linéaire avec la pression pour de faibles épaisseurs d'oxyde, l'oxydation initiale rapide et certains effets de composition gazeuse. D'autres [40], ont pris en compte la **diffusion d'espèces ioniques** menant à la création de charges d'espace dans la couche d'oxyde qui perturbent ensuite les phénomènes de transport. L'expression reliant le temps à l'épaisseur de la couche d'oxyde est alors une loi en puissance de la forme:

$$t = C X^{\alpha} \qquad (13)$$

où C et α sont des constantes.

Généralement, les mécanismes d'oxydation apparaissent perturbés pour de faibles pressions et de faibles épaisseurs de couche d'oxyde [40,41].

Enfin, à basse température, les contraintes générées dans la couche d'oxyde dues à l'augmentation de volume ou à la géométrie du substrat [42] sont à prendre en compte. Récemment, Doremus [43], en se basant sur des résultats d'oxydation d'alliages siliciurés, a conclu que l'oxydation du silicium pouvait difficilement être contrôlée par un régime lent de réaction à l'interface

SiO_2/Si. Le régime linéaire - parabolique, observé expérimentalement, pourrait être dû aux **contraintes** engendrées par la croissance du film d'oxyde [44]. Ces contraintes ont été mises en évidence pour une température inférieure à 950°C [45].

La présence de **vapeur d'eau** accélère la cinétique d'oxydation du silicium. La solubilité de H_2O dans la silice est beaucoup plus grande que celle de O_2 [35, 46]. En effet, H_2O réagit avec la silice pour former des liaisons Si-OH, ce qui complique la diffusion de la vapeur d'eau dans la silice. Néanmoins, plusieurs études [46,47] supportent le fait que la diffusion de H_2O dans la couche d'oxyde contrôle l'oxydation du silicium en présence de vapeur d'eau.

Notons enfin qu'une étude récente [48] a montré que la présence d'hydrogène résiduel dans la couche d'oxyde (i) augmentait sensiblement la diffusivité de l'oxygène dans la couche silice et (ii) diminuait l'énergie apparente d'activation de 113 kJ/mol à 59-83 kJ/mol.

Oxydation du carbure de silicium

Les mécanismes décrits pour l'oxydation du silicium s'appliquent pour celle de SiC. Il y a cependant plusieurs particularités.

A priori, la principale différence entre l'oxydation de SiC et de Si est liée à la production d'oxydes gazeux (CO, CO_2) qui doivent diffuser de l'interface SiC/SiO_2 à l'interface SiO_2/environnement. Cette étape, qui pourrait être limitante cinétiquement, semble au contraire rapide et ne contrôle donc pas la réaction d'oxydation [49]. Néanmoins, l'oxydation du SiC sera a priori plus lente car 2 moles ou 1,5 mole d'oxygène devront diffuser à travers la couche

d'oxyde pour former 1 mole de SiO_2 suivant que les réactions (3) ou (2) sont respectivement envisagées, au lieu de 1 mole de O_2 par mole de SiO_2 dans le cas du silicium.

Une autre différence tient à la réfractairité plus importante de SiC par rapport à Si qui permet d'envisager l'oxydation de SiC dans une gamme de température supérieure à 1400°C, qui correspond à peu près à la température de fusion de Si. Au-delà de 1400°C, une augmentation de l'énergie apparente d'activation est observée. Elle est reliée à un changement du mode de diffusion de l'oxygène dans l'oxyde, à savoir essentiellement par **perméation moléculaire à T < 1400°C** et essentiellement par **diffusion de l'oxygène sous forme ionique au-delà de 1400°C** [49]. A haute température, la cristallisation du film d'oxyde peut perturber les phénomènes de transport. Ainsi l'oxydation de SiC (CVD) entre 1550°C et 1675°C présente une transition lorsque le film d'oxyde cristallise sous forme de cristobalite. La diffusion de l'oxygène, sous forme ionique dans les deux cas, est plus lente au sein du matériau cristallisé, ce qui réduit la cinétique d'oxydation [50].

Il a été cependant reporté que la cristallisation du film d'oxyde pouvait s'accompagner de la création de défauts qui augmentent alors la cinétique d'oxydation [37].

Une autre caractéristique de SiC est la forte dépendance des cinétiques d'oxydation suivant les directions cristallographiques et les polytypes [51]. Ainsi sur des monocristaux de SiC 6H, Harris [52] a mis en évidence un rapport 7 entre les épaisseurs sur les face C $(000\bar{1})$ et Si (0001) à 1060°C sous

oxygène. Cet écart sur les cinétiques, attribué au caractère "polaire" de la structure SiC, diminue avec la température [49].

Malgré quelques tentatives [53], ce phénomène reste inexpliqué en dépit du fait qu'il ait été identifié depuis 25 ans.

La dépendance des constantes paraboliques avec la pression partielle d'oxygène présente une non linéarité qui croît avec la température [54].

Enfin, les nombreuses formes de SiC qui existent, présentent des caractéristiques différentes en termes de pureté, stoechiométrie, texture qui influencent le comportement à l'oxydation et expliquent, une certaine dispersion des résultats.

3.2.3 - Cinétiques d'oxydation en régime actif

La fig. 5 présente les transitions, établies de façon théorique ou expérimentale du régime actif au régime passif d'oxydation en fonction de la température et de la pression partielle d'oxygène. A pression partielle d'oxygène donnée, la température de transition diminue lorsque le débit diminue [55].

En régime d'oxydation active, la cinétique de consommation du SiC est linéaire [56,57]. Elle peut être contrôlée soit par la diffusion des espèces oxydantes ou des produits de réaction dans la couche limite ou par les réactions de surface.

La cinétique augmente avec la pression partielle d'oxygène jusqu'au moment où elle permet la formation de l'oxyde condensé SiO_2. La création de défauts associés à ce mode d'oxydation diminue, de façon sensible, les propriétés mécaniques de SiC [56].

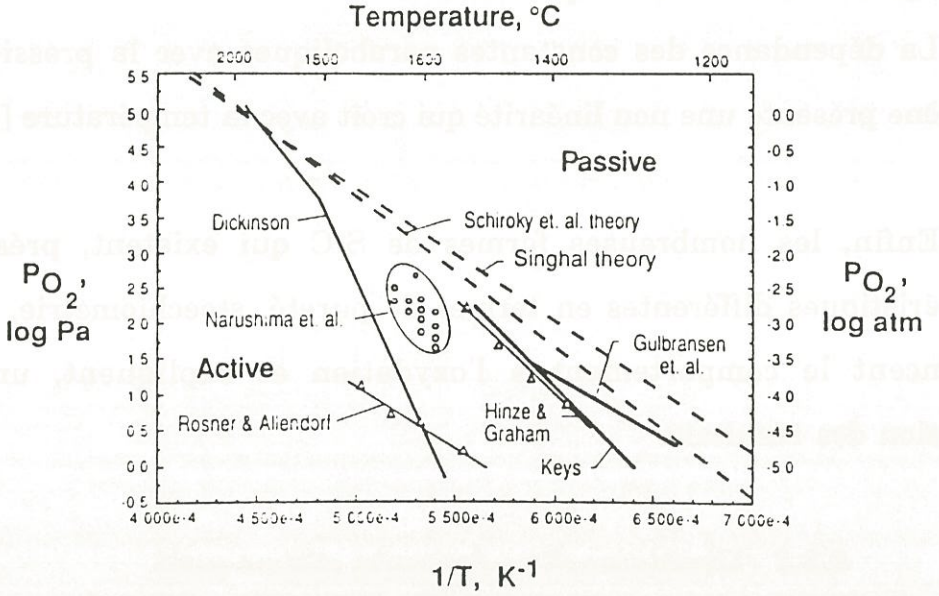

Fig. 5 : Diagramme présentant les transitions du régime actif au régime passif d'oxydation en fonction de la température et de la pression partielle d'oxygène [55]

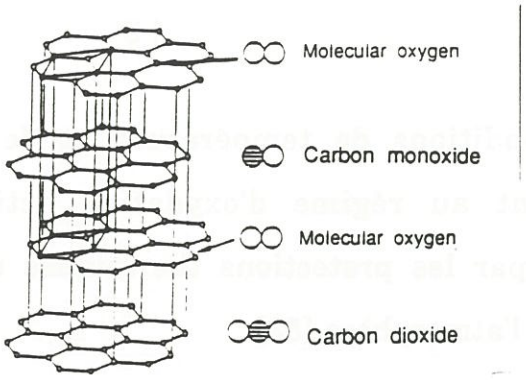

Fig. 6 : Schéma illustrant la réaction de l'oxygène moléculaire avec les plans basaux et atomes de bordure du réseau graphite pour former des oxydes de carbone [59]

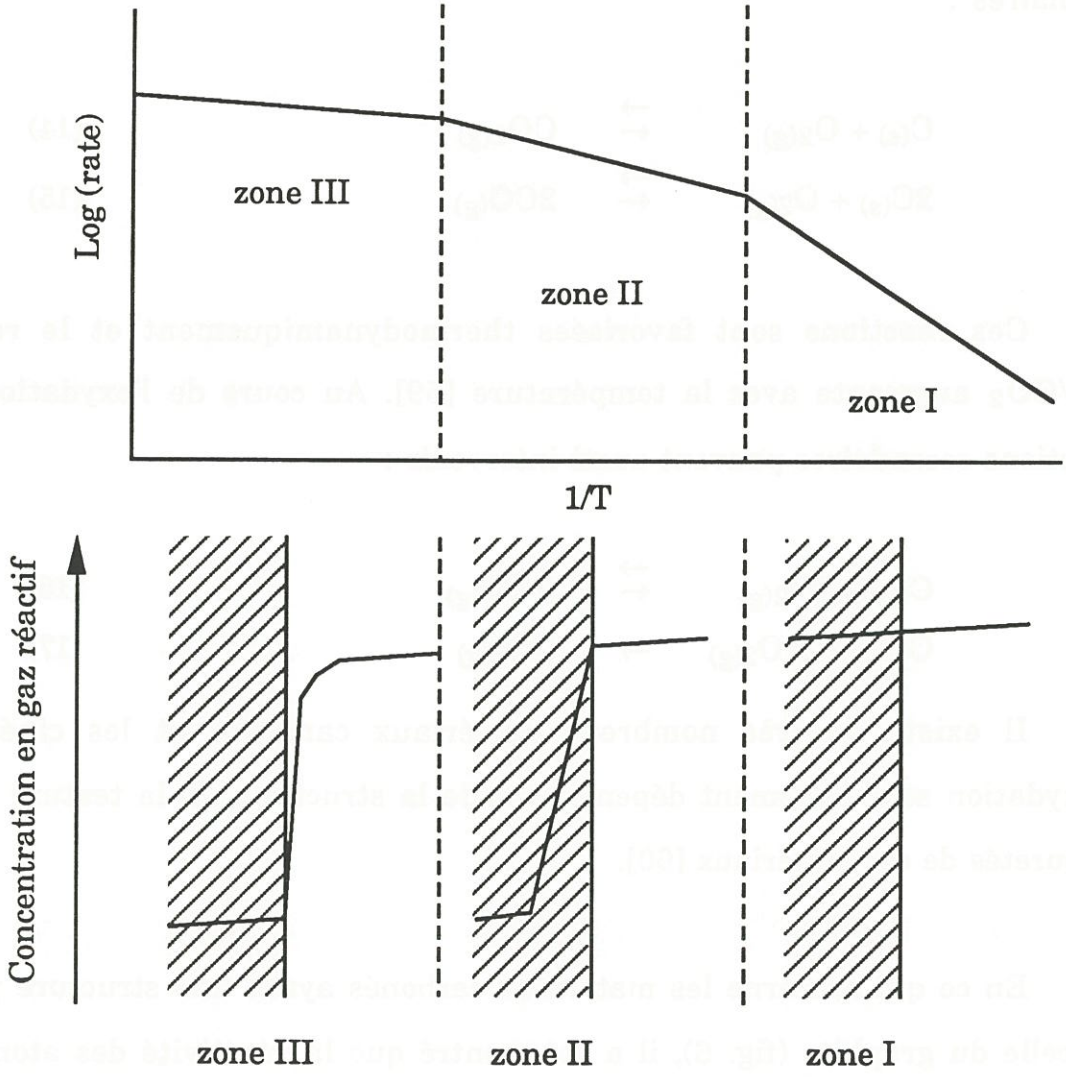

Fig. 7 : Schéma représentant la dépendance de la vitesse de gazéification du carbone avec la température et les profils de concentration attendus du gaz réactif pour chaque zone

Les conditions de température et de pression partielle d'oxygène correspondant au régime d'oxydation active, sont susceptibles d'être rencontrées par les protections thermiques d'avions spatiaux lors de leur rentrée dans l'atmosphère [58].

3.3 - Oxydation des matériaux carbonés

Le carbone s'oxyde en formant des oxydes gazeux selon les réactions primaires :

$$C_{(s)} + O_{2(g)} \rightleftarrows CO_{2(g)} \qquad (14)$$

$$2C_{(s)} + O_{2(g)} \rightleftarrows 2CO_{(g)} \qquad (15)$$

Ces réactions sont favorisées thermodynamiquement et le rapport CO/CO_2 augmente avec la température [59]. Au cours de l'oxydation, des réactions secondaires peuvent aussi intervenir :

$$C_{(s)} + CO_{2(g)} \rightleftarrows 2\,CO_{(g)} \qquad (16)$$

$$CO_{(g)} + \frac{1}{2}\,O_{2(g)} \rightarrow CO_{2(g)} \qquad (17)$$

Il existe de très nombreux matériaux carbonés et les cinétiques d'oxydation sont fortement dépendantes de la structure, de la texture et des impuretés de ces matériaux [60].

En ce qui concerne les matériaux carbonés ayant une structure proche de celle du graphite (fig. 6), il a été montré que la réactivité des atomes de bordure était nettement supérieure à celle des atomes composant les plans basaux [61]. Ces sites très réactifs sont appelés sites actifs. L'étude de la

réactivité des carbones s'appuie aujourd'hui sur ce concept des **sites actifs** [62]. Néanmoins la réactivité intrinsèque, c'est à dire la vitesse d'oxydation ramenée à l'aire des sites actifs, est sujette à des variations importantes selon le degré d'organisation des carbones. Ainsi, des rapports égaux à 17 ont été reportés pour les réactivités intrinsèques d'un pyrocarbone obtenu à 1100°C ou traité à 2000°C [63].

Les effets de texture et plus généralement d'accessibilité de l'oxygène aux surfaces réactionnelles sont à prendre en compte, particulièrement à haute température, lorsque la vitesse des actes chimiques devient grande devant celle des phénomènes diffusionnels. Pour l'oxydation des carbones purs, trois zones de température sont généralement distinguées comme l'illustre la fig. 7 [64]. La première correspond à une oxydation contrôlée par l'acte chimique et présente une forte énergie d'activation, la seconde à un régime mixte où la diffusion dans la porosité peut intervenir et la troisième où la cinétique est contrôlée par la diffusion des gaz dans la couche limite. Dans ce dernier cas, la dépendance de la vitesse d'oxydation avec la température est faible.

Enfin, certaines impuretés minérales sont susceptibles de catalyser les réactions d'oxydation (métaux de transitions, alcalins et alcalino-terreux) ou de les inhiber (composés du bore, du silicium et du phosphore). L'accessibilité de l'oxygène, ou plus généralement des espèces oxydantes, au front de réaction est une notion importante particulièrement dans le cas des composites à interphase de carbone. En effet, de part sa répartition spatiale (fine couche autour des fibres recouverte de matrice) le carbone interfacial sera a priori

moins vulnérable vis à vis de l'oxydation car mieux protégé qu'un carbone massif.

3.4 - Oxydation des composites SiC/LAS et SiC/SiC

Plusieurs travaux ont été consacrés à l'influence de traitements à haute température en environnement oxydant sur les propriétés mécaniques résiduelles des composites SiC/C/LAS.

Une fragilisation de ces composites a été observée après traitement à 650°C sous air pendant 72 h [65]. Le mode de rupture change et des fractures de type fragile apparaissent. Les contraintes interfaciales τ mesurées expérimentalement augmentent considérablement et expliquent la modification du mode rupture. Des études microstructurales en microscopie électronique à transmission ont révélé que le carbone interfacial avait disparu et que de la silice était apparue. De même la couche de NbC, souvent associée au carbone (la matrice vitreuse contenant de petites quantités de Nb_2O_5) était transformée en une couche NbO_x [66, 67]. A plus haute température (1000°C) il a été reporté que le carbone n'était pas attaqué et qu'au contraire son épaisseur augmentait [65]. D'autres études [68], ont par contre fait état de la fragilisation des composites à 1250°C sous air.

Les chemins de diffusion de l'oxygène suggérés par les auteurs sont d'une part les interfaces et d'autre part la matrice.

Les études concernant l'oxydation des SiC/C/SiC sont moins nombreuses. Globalement les mêmes remarques que sur les composites SiC/verre ont été faites, à savoir une baisse des propriétés mécaniques suite à

des vieillissements à haute température en environnement oxydant. Cette dégradation a été attribuée à la disparition du carbone interfacial et à la croissance de couche de SiO_2 sur les fibres et la matrice. Il est à noter enfin que les traitements à haute température (1400°C) pouvaientt mener à une préservation d'une partie du carbone interfacial alors qu'à basse température, pour des traitements prolongés, le carbone semble complètement oxydé [69-71].

Néanmoins, à ce jour, aucune étude n'a été consacrée spécifiquement aux mécanismes d'oxydation de ces composites et à leur cinétique.

Dans le cadre de leur utilisation, ces matériaux recevront des dépôts de surface qui tendront à les protéger contre les agressions extérieures. Cependant ces dépôts peuvent se fissurer ou se dégrader et les interphases carbonées notamment, se retrouveront alors en contact avec une atmosphère oxydante.

4 - Objectifs

Les composites SiC/C/SiC ont été développés principalement en vue d'applications à haute température en environnement oxydant. Etant donné l'importance des liaisons fibre/matrice d'une part, et la réactivité des interphases de carbone vis à vis de l'oxygène d'autre part, il est apparu nécessaire de mieux appréhender l'oxydation de ces matériaux. L'objectif de ce travail est d'arriver à une meilleure compréhension des mécanismes d'oxydation des composites SiC/C/SiC et de leurs constituants, de leur cinétique et de leur influence sur le comportement mécanique.

Le choix de l'architecture fibreuse des composites s'est orienté vers une texture **unidirectionnelle** afin de simplifier la géométrie du système, et de faciliter la compréhension des mécanismes mis en jeu.

Le mémoire s'organise autour de cinq chapitres qui peuvent être regroupés en trois axes principaux :

(i) oxydation des constituants pris isolément,

(ii) oxydation des composites avec approche expérimentale et théorique,

(iii) effet de traitements oxydants sur les propriétés mécaniques.

La première partie est constituée des **premier et second chapitres** qui présentent respectivement les résultats de cinétiques d'oxydation des fibres SiC (ex-PCS) obtenues par analyse thermogravimétrique (ATG) et de la matrice SiC (CVI) par la mesure des épaisseurs de couche d'oxyde par spectroréflectométrie(*). L'étude de la cinétique d'oxydation du troisième constituant pris isolément, l'interphase de carbone, n'a pas été effectuée. D'une part, il aurait fallu obtenir des échantillons représentatifs s'oxydant suivant les mêmes directions qu'au sein du composite. D'autre part, il a été supposé qu'à l'intérieur du composite, la contribution des phénomènes de transport, particulièrement à haute température, était prépondérante devant les mécanismes de réaction chimique du carbone avec l'oxygène.

Le **troisième chapitre** concerne l'oxydation des composites 1D-SiC/C/SiC sous un aspect expérimental. Des études cinétiques, par ATG, et morphologiques ont permis de mettre en évidence l'influence de plusieurs paramètres tels que le temps, la température, l'épaisseur d'interphase et la nature de l'atmosphère sur le

(*) collaboration C. Jaussaud, LETI, CENG, Grenoble

comportement à l'oxydation de ces matériaux. Le **quatrième chapitre** a pour objet l'interprétation des résultats précédents. Un modèle théorique, prenant en compte les phénomènes de transport et de réactions intervenant au cours de l'oxydation a été développé. Les simulations numériques effectuées ont été comparées aux résultats expérimentaux.

Enfin, le **cinquième et dernier chapitre** est en quelque sorte l'illustration des résultats acquis précédemment. Il présente l'influence des traitements à haute température sur les propriétés mécaniques résiduelles des composites 1D-SiC/C/SiC. Des corrélations entre comportement mécanique et analyses microstructurales ont été effectuées.

REFERENCES

[1] W.D. Kingery, H.K. Bowen, D.R.H. Uhlmann
"Introduction to Ceramics", Editeurs John Wiley and Sons

[2] D.C. Phillips
Encyclopedia of Materials Science, pp 1723

[3] R. Labbens
"Introduction à la mécanique de la rupture", Editions Pluralis, Paris 1980

[4] J.F. Knott
"Fundamentals of Fracture Mechanics", Butterworths, London, 1973

[5] L.C. Sawyer, R. Arons, F. Hainback, M. Jaffe et K.D. Rappaport
Ceram. Eng. and Sci. Proc., [7-8] (1985) 567-75

[6] M. Rühle et A.G. Evans
Progress in Materials Science, 33 (1989) 85-167

[7] M. Rühle, N. Claussen et A.H. Heuer (1986)
J. Am. Ceram. Soc., 69 [3] (1986) 195-97

[8] M. Bouquet
Thèse n° 395, Université de Bordeaux-I, 1989

[9] R. Stevens
"An Introduction to Zirconia", Editeur Magnesium Elektron, 1986

[10] A.G. Evans et D.B. Marshall
Acta Metall., 37 [10] (1989) 2567-83

[11] D. Rouby
"IIème Conférence Franco-Allemande sur les Céramiques Techniques", Aix-la-Chapelle, 4-6 mars 1987, pp 265-86

[12] J.M. Quenisset
"23ème Colloque du groupe français de Rhéologie", Bordeaux 1988, Editeurs CERMUB, pp 1-41

[13] R. Talreja

Proc. R. Soc. Lond., A 399 (1985) 195-216

[14] N. Piquenot, V. Arnault et D. Rouby

Actes du Colloque AMAC/CODEMAC 29-30 mars 1990, Bordeaux, Editeurs R. Naslain, J. Lamalle, J.L. Zullian, pp 81-92

[15] R.A.J. Sambel, D.H. Bowen et D.C. Phillips

J. Mater. Sci., 7 (1972) 663-75

[16] G. Bernhart, P. Lamicq et J. Macé

L'industrie céramique, 790 (1985) 51-56

[17] K.M. Prewo et J.J. Brennan

J. Mater. Sci., 15 (1980) 463-68

[18] J. Aveston, G.A. Cooper et A. Kelly

Proc. NPL Conf. on "The Properties of Fibre Composites", National Physical Laboratory, Teddington, England, Guildford, IPC Science and Technology Press Ltd, 1971 p 15

[19] B. Broquère, B. Buttazzoni et J.J. Choury

"Introduction aux Matériaux Composites" Vol 2, Editeur R. Naslain, (Editions du CNRS et de l'IMC), 1985 pp 405-438

[20] F. Christin

Thèse d'Etat n° 641, Université de Bordeaux, 1979

[21] F. Christin, R. Naslain et C. Bernard

Actes ICCM-3 "Advances in Composite Materials", Editeurs A.R. Bunsell et coll., Paris 1980, Pergamon Press 2, pp 1084-97

[22] S. Yajima, K. Okamura, T. Matsuzawa, Y. Hasegawa et T. Shishido

Nature (London), 279 [5715] (1979) 706-7

[23] G. Simon

Thèse, Ecole Nationale des Mines de Paris, 1984

[24] C. Laffon, A.M. Flanck, P. Lagarde, M. Loridjani, R. Hagège, P. Olry, J. Cotteret, J. Dixmier, J.L. Micquel, H. Hommel et A.P. Legrand

J. Mater. Sci., 24 (1989) 1503-12

[25] A.S. Fareed, P. Fang, M.J. Koczack et F.M. Ko

Am. Ceram. Soc. Bull., 66 [2] (1987) 353-58

[26] T. Mah, N.L. Hecht, D.E. Mc Cullum, J.R. Hoenigman, M.M. Kim, A.P. Katz et H.A. Lipsitt

J. Mater. Sci., 19 (1984) 1191-1201

[27] S.M. Johnson, R.D. Brittain, R.H. Lamoreaux et D.H. Rowcliffe

J. Am. Ceram. Soc., 71 [3] (1988) C132-35

[28] K. Okamura, M. Sato, T. Seguchi et S. Kawanishi
Editeur H. Ishida, Elsevier Science Publishing Co, Inc. 1990 p 209

[29] R. Naslain, J.Y. Rossignol, J.M. Quenisset et F. Langlais
"Introduction aux Matériaux Composites" Vol 2, Editeur R. Naslain, (Editions du CNRS et de l'IMC), 1985 pp 405-438

[30] V. Arnault
Thèse, INSA de Lyon, 1989

[31] R.N. Singh et M.K. Brun
Advanced Ceramic Materials, 3 [3] (1988) 235-237

[32] J.J. Brennan
"Interfacial Characterization of Glass and Glass-Ceramics Matrix/Nicalon SiC Composites" Editeurs R.E. Tressler, G.L. Messing, CG. Pantano et R.E. Newnham (Plenum Press, New York), 1986 pp 549

[33] W.K. Tredway et K.M. Prewo
Mat. Res. Soc. Symp. Proc., Vol 170 1990 pp 215-221

[34] E.A. Gulbransen et S.A. Jannsson
Oxid. Met., 4 [3] (1972) 181-201

[35] B.E. Deal et A.S. Grove
J. Appl. Phys., 36 [12] 1965 3770-78

[36] F.J. Norton

Nature 171, 701 (1961)

[37] J.A. Costello et R.E. Tressler

J. Am. Ceram. Soc., 69 [9] (1986) 674-81

[38] J. Schlichting

High Temp. High Press., 14 (1982) 717-24

[39] J.M. Delarios, C.R. Helms, D.B. Kao et B.E. Deal

Applied Surface Science, 39 (1989) 89-102

[40] D.R. Wolters et A.T.A. Zegers Van Dugnhoven

Applied Surface Science, 39 (1989) 81-88

[41] I. Trimaille et S. Rigo

Applied Surface Science, 39 (1989) 65-80

[42] P. Sutardja et W.G. Oldham

IEEE Transactions on Electron Devices, 36 [11] (1989) 2415-21

[43] R.H. Doremus

J. Appl. Phys., 66 (9) (1989) 4441-43

[44] R.H. Doremus et A. Szewczyk

J. Mater. Sci., 22 (1987) 2887

[45] S. Alexandrova, A. Szekeres et J. Kaprinarova
semicond. Sci. Technol., 4 (1989) 876-78

[46] R.H. Doremus
The Journal of Physical Chemistry, 80 [16] (1976) 1773-75

[47] D.J. Choi, D.B. Fishback et W.S Scott
J.Am. Ceram. Soc., 72 [7] (1989) 1118-23

[48] M. Susa, H. Shinohara, K. Nagata et K. S. Goto
J. Japan Inst. Metals, 54 [2] (1990) 193-200

[49] Z. Zheng, R.E. Tressler et K.E. Spear
J. Electrochem. Soc., 137 [3] (1990) 854-858

[50] T. Narushima, T. Goto et T. Hirai
J. Am. Ceram. Soc., 72 [8] (1989) 1386-90

[51] W. Von Münch et I. Pfaffender
J. Electrochem. Soc., 122 [5] (1975) 642-43

[52] R.C.A. Harris
J. Am. Ceram. Soc., 58 [1-2] (1975) 7-9

[53] J.R. Blachere et F.S Pettit
"High Temperature Corrosion of Ceramics", Noyes data corporation, Park Ridge New Jersey, 1989 pp 137-83

[54] Z. Zheng, R.E. Tressler et K.E. Spear

J. Electrochem. Soc., 137 [9] (1990) 2812-16

[55] W.L. Vaughn et H.G. Maaks

J. Am. Ceram. Soc., 73 [6] (1990) 1540-43

[56] H.E. Kim et A.J. Moorhead

J. Am. Ceram. Soc., 73 [7] (1990) 1868-72

[57] J.F. Stohr

Journées d'Etudes - Société Française des Thermiciens, Paris 20 avril 1988

[58] M.P. Bacos et M. Parlier

4ème Symposium Int. sur "Les Matériaux Utilisés en Ambiance Spatiale", Toulouse 6-9 septembre 1988

[59] M. Marsh et K. Kuo

"Introduction to Carbon Science", Editeur M. Marsh, (1989) 107-51

[60] I.W. Smith

Fuel, 57 (1978) 409

[61] N.R. Laine, F.J. Vastola et P.L Walker

J. Phys. Chem., 67 (1963) 20-30

[62] J. Lahaye, J. Dentzer, P. Soulard et P. Ehrburger
"Fundamental Issues in Control of Carbon Gasification Reactivity", Editeurs J. Lahaye et P. Ehrburger, Kluwer Academic Publishers, 1991 pp 143-162

[63] P. Ehrburger, F. Louys et J. Lahaye
Carbon, 27 [3] (1989) 389-93

[64] P.L. Walker Jr, F. Rusinko Jr. et L.G. Austin
Advan. Catalysis, 11 (1959) 133

[65] T.W. Coyle, M.M. Chan et V.V. Desmukh
"Interfaces in Polymer, Ceramic and Metal Matrix Composites" Cleveland Ohio, June 88,pp 489-501

[66] M.D. Thouless, O. Sbaizero, E. Bischoff et E.Y. Luh
Mater. Res. Soc. Symp. Proc., Vol. 120 1988 pp 333-339

[67] O. Sbaizero et S. Schmid
Materials Engineering, 1 [1] (1989) 273-280

[68] T. Mah, M.D. Mendiratta, A.P. Katz et K.S. Mazdiyasmi
Ceramic Bulletin, 66 [2] (1987) 304-308

[69] P. Lamidieu et C. Gault
Revue Phys. Appl., 23 (1988) 201-211

[70] N. Frety et M. Boussuge

Composite Science and Technology, 37 (1990) 177-189

[71] C. Gault et M. Huger

Actes du Colloque AMAC/CODEMAC 29-30 mars 1990, Bordeaux, Editeurs

R. Naslain, J. Lamalle, J.L. Zullian, pp 303-314

CHAPITRE I

OXIDATION KINETICS OF SiC-BASED CERAMIC FIBERS

INTRODUCTION AU CHAPITRE I

Fin 1987, les fibres SiC ex-polycarbosilane étaient le sujet de nombreuses études notamment en ce qui concernait leur micro ou nano structure. La tenue à l'oxydation de ces fibres était abordée principalement sous l'angle de l'évolution des caractéristiques mécaniques en fonction de la nature et de la durée des traitements oxydants. L'aspect cinétique était peu ou pas abordé.

Etant donné la nature particulière de ces fibres, à base de SiC mais contenant aussi de l'oxygène et du carbone en excès, il est apparu intéressant dans le cadre de ce travail de mener une étude sur leur cinétique d'oxydation.

Pour cela, un appareillage d'analyse thermogravimétrique a été mis en place au LCTS. Cette technique a permis de déterminer les cinétiques d'oxydation de ces fibres et de les comparer à celles de matériaux tel que le carbure de silicium pur.

Les résultats ont montré que si le comportement global à l'oxydation du SiC ex-PCS composant ces fibres était comparable à celui de SiC pur, il présente néanmoins plusieurs particularités.

Seventh Cimtec World Ceramics Congress
June 24-30 1990 Montecatini Terme Italy

OXIDATION KINETICS OF SiC-BASED CERAMIC FIBERS

L. FILIPUZZI and R. NASLAIN

Laboratoire des Composites Thermostructuraux UMR 47 CNRS-SEP-UB1
1-3 Avenue Léonard de Vinci, F - 33600 Pessac

ABSTRACT

Oxidation kinetics of SiC based polycarbosilane fibers (*) have been investigated through thermogravimetric analysis between 800°C and 1500°C in dry oxygen and in dry air for durations up to 10 hours. Oxidized fibers have been characterized in terms of elemental compositional changes, specific surface areas, structure and morphology of the oxide layers. For test temperatures ranging between 800°C and 1200°C, a parabolic law characteristic of a diffusion controlled reaction, is followed. Apparent activation energies (from 69 to 77 kJ/mol) are derived from Arrhenius plots. Their values are low compared to those reported in the literature for Si and SiC. Rather high parabolic rate constants are observed, especially at low temperatures. The presence of residual hydrogen in the ex-PCS fiber which transforms into water vapor reacting then with silica might explain this particular oxidation behavior. Beyond 1200°C, the parabolic regime is no longer respected. The crystallization of the oxide film, the formation of microcracks at high temperatures and the thermal metastability of the fibers are thought to modify the oxidation mechanisms.

KEY WORDS : SiC, Ex-PCS SiC, Oxidation, Kinetics

---

* Nicalon,ceramic grade NLM 202, from Nippon Carbon

1 - INTRODUCTION

Ceramic matrix composites (CMCs), especially SiC/SiC composites, have gaining importance for high temperature structural applications with their non-linear and non-brittle mechanical behavior[1,2], they constitute a promising application field for ceramic fibers. However, these new materials designed for application at high temperatures in oxidative conditions are not thermodynamically stable[3].

The oxidation kinetics of silicon carbide have been the subject of numerous studies for about thirty years[4]. The good oxidation resistance of SiC is due to the formation of a protective silicon dioxide layer which limits further oxidation. The results concerning oxidation kinetics of SiC are, unlike those of silicon, subjected to large variations which may be attributed to the diversity of SiC based materials (CVD, sintered with or without different impurities, single crystals...)[5]. Moreover, the oxidation behavior of SiC is function of the polytype structure and the crystalline orientation[6].

Little information exists on the oxidation kinetics of SiC-based ceramic fibers. Warren and Andersson[7,8] have investigated the oxidation behavior of first generation ex-PCS fibers(*). Between 1100°C and 1400°C, they observed that relative mass variations do not follow a parabolic law. However, their reaction rate constants, seem to be consistent with those reported in previous studies on the oxidation of SiC. More recently, Clark et al.[9,10] have characterized the microstructural and chemical changes occurring under various environments (oxidative and inert gas) in new ex-PCS fibers(**) in

---

* Nicalon fibers, from Nippon Carbon

** Standard (NLP 101) and ceramic (NLM 202) grades from Nippon Carbon

relation with their mechanical properties without giving a kinetic analysis. They observed a decrease in mechanical properties with heat treatments.

Yarn SiC-based fibers are prepared from polycarbosilane precursors. After melt-spinning, they are stabilized in air and then pyrolysed in an inert atmosphere up to about 1200°C. The resultant material is assumed to consist of a continuum of SiC crystals (with a medium size of about 2.5 nm) and tetrahedral SiC_xO_y (with $x + y = 4$) units and contains free aromatic carbon aggregates surrounded by hydrogen atoms[11]. The oxygen content is about 10 to 15 wt %.

Ex-PCS fibers are not stable in inert atmosphere at high temperatures. A significant weight loss is observed at temperatures of about 1250°C[12]. It is worthy of note that Luthra[13] predicted, on the basis of thermochemical considerations, that CO should be the predominant gas over the fiber whereas experimentally (Knudsen cell effusion) SiO has been observed to be the major species[14]. The aim of the present contribution is to study the oxidation behavior of ex-PCS SiC-based fibers in order to give an insight into the mechanisms involved in these reactions.

2 - EXPERIMENTAL PROCEDURE

Thermogravimetric analysis (TGA)(+) has been used to determine the oxidation behavior of samples of ex-PCS fibers between 800°C and 1500°C. The tests were performed under flowing dry oxygen(++) ($H_2O \leq 2$ ppm) with a flow rate of approximately 1 lh^{-1} and a total pressure of 100 kPa as well as under either air and static low oxygen pressure atmospheres (1 and 10 kPa). Fibers

---

+ TAG 24 S16 SETARAM sensibility 10^{-6}g

++ Oxygen N48 Alphagaz

were supplied in the form of sized yarns (about 500 filaments per yarn). Each sample consisted of 100 mg of fibers obtained by cutting the yarns in 1 cm length and was set in an alumina crucible(§). After purging and filling the analysis chamber with oxygen, the sample was heated at a rate of 10°C min^{-1} up to 700°C in an alumina tube(§) to remove the polyvinyl acetate sizing. Then, the sample was heated at a rate of 30°C min^{-1} up to the final temperature for ageing periods of about 10 hours. The temperature was controlled with a Pt/PtRh 10 % thermocouple set inside the crucible. The mass variations recorded before the sample temperature stabilization, were not taken into account for the determination of oxidation rate constants.

The specific surface area was measured using Kr adsorption technique at boiling nitrogen temperature according to the B.E.T. method. Chemical(*) and electron microprobe(**) analyses on desized and oxidized fibers were performed to determine the compositional changes. The structure and morphology of oxide layers were characterized by X ray diffraction (CuKα radiation), Auger electron spectroscopy (AES)(+), secondary ion mass spectroscopy in combination with Ar ion sputtering (SIMS) and scanning electron microscope (SEM). Fiber diameters were measured on micrographs from polished cross sections of fibers embedded in a SiC matrix obtained by chemical vapor infiltration (CVI).

---

§ High purity alumina (> 99.9 %)

* CNRS, Service Central d'Analyses Vernaison

** CAMEBAX

\+ PHI 590 SAM Perkin Elmer

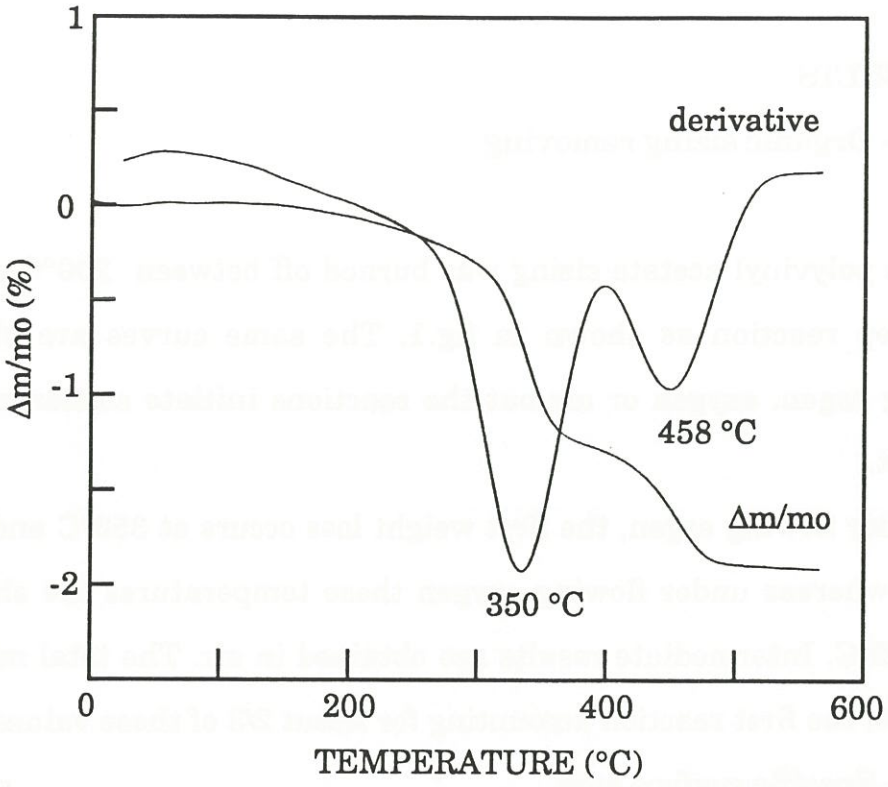

FIGURE 1

Sizing pyrolysis in flowing argon (heating rate : 10°C min-1).

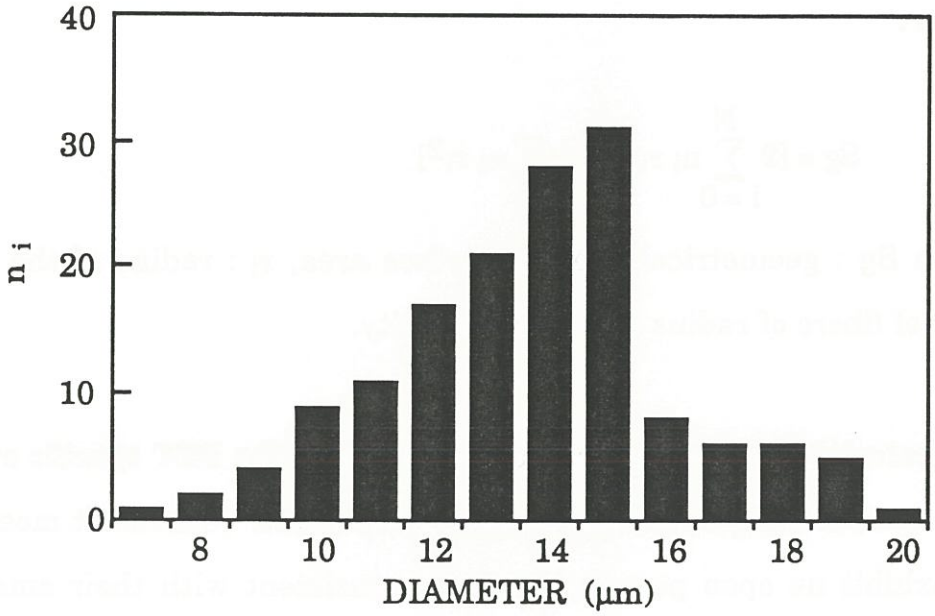

FIGURE 2

Fiber diameter distribution in a yarn (mean diameter:13.7 μm).

3 - RESULTS

3.1 - Organic sizing removing

The polyvinyl acetate sizing was burned off between 200°C and 500°C in a two step reaction as shown in fig.1. The same curves are obtained under flowing argon, oxygen or air but the reactions initiate sooner when oxygen is present.

Under flowing argon, the first weight loss occurs at 350°C and the second at 458°C whereas under flowing oxygen these temperatures are shifted to 308°C and 402°C. Intermediate results are obtained in air. The total mass loss is 1.4-1.8 wt%, the first reaction accounting for about 2/3 of these values.

3.2 - Specific surface area

The specific surface area (measured by the BET technique) is 0.11 m^2g^{-1}. The fiber diameter distribution in a yarn is presented in fig.2. The geometrical specific surface area can be calculated from this distribution using the equation :

$$Sg = [2 \sum_{i=0}^{N} n_i r_i] \; / [\rho \sum n_i r_i^2] \qquad (1)$$

with Sg : geometrical specific surface area, r_i : radius of the fiber i, n_i : number of fibers of radius r_i, ρ : fiber density.

The calculations lead to a value of 0.11m^2g^{-1}. The BET specific surface area is thus equal to the geometrical surface of the fibers. This result means that the fibers exhibit no open porosity which is consistent with their smooth aspect observed by SEM. The values of the specific surface area of oxidized fibers at 800°C, 165 h in air and 1200°C, 10 h in air are respectively 0.11 and 0.10 m^2g^{-1}.

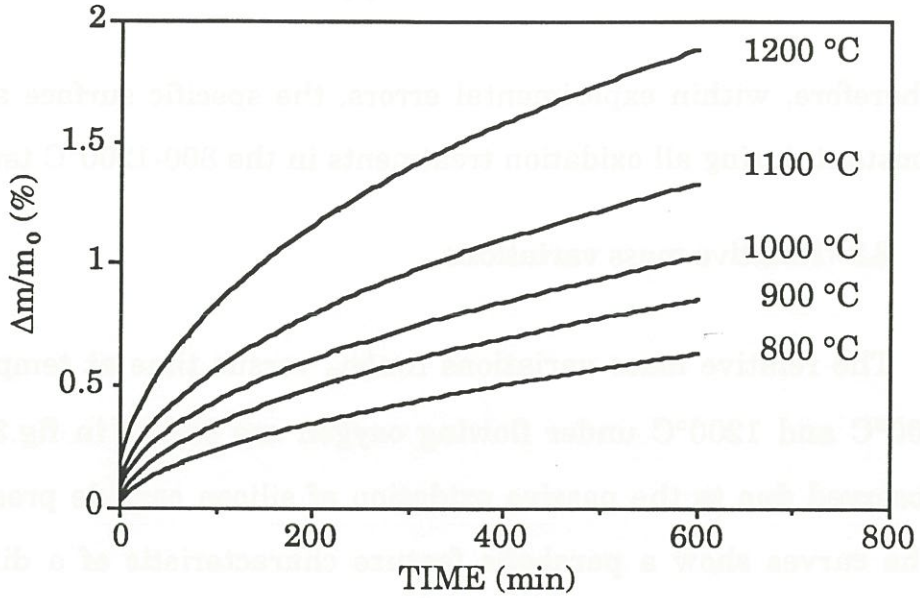

FIGURE 3

Relative mass variations versus time between 800°C and 1200°C during oxidation under flowing dry oxygen (P= 100 kPa).

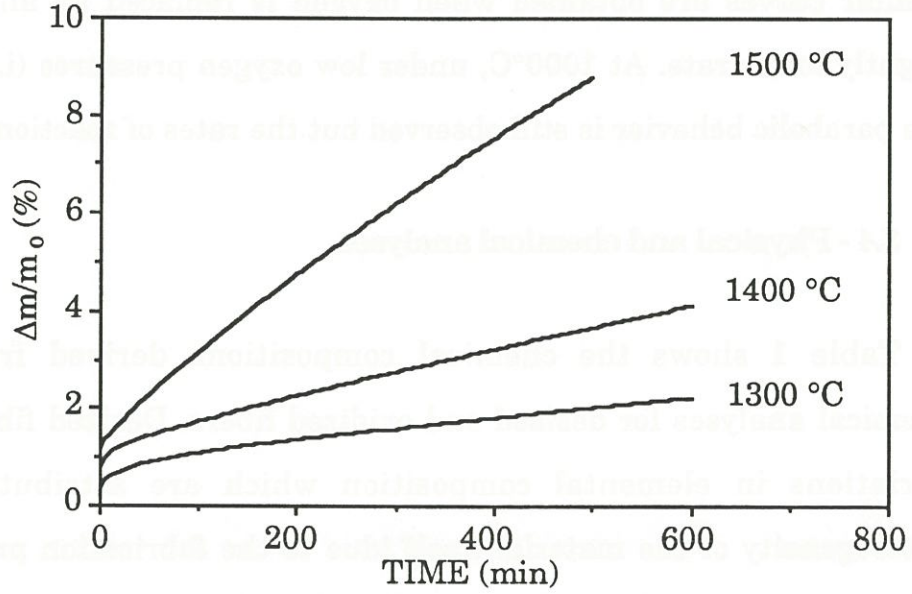

FIGURE 4

Relative mass variations versus time between 1300°C and 1500°C during oxidation under flowing dry oxygen (P= 100 kPa).

Therefore, within experimental errors, the specific surface area is considered constant during all oxidation treatments in the 800-1200°C temperature range.

3.3 - Relative mass variations

The relative mass variations $\Delta m/m_0$ versus time at temperatures between 800°C and 1200°C under flowing oxygen are shown in fig.3. Mass gains are observed due to the passive oxidation of silicon carbide present in the fibers. The curves show a parabolic feature characteristic of a diffusion controlled reaction. Beyond 1200°C the parabolic behavior is no more respected : at 1300°C and 1400°C, a quasi-linear law seems to follow a short parabolic-like initial period, as shown in fig.4. At 1500°C, the oxidation kinetics are strongly accelerated.

In the range 800°C to 1200°C, more especially studied in the present work, similar curves are obtained when oxygen is replaced by air with however a slightly lower rate. At 1000°C, under low oxygen pressures (i.e. 1 and 10 kPa), the parabolic behavior is still observed but the rates of reaction are lower.

3.4 - Physical and chemical analyses

Table 1 shows the chemical compositions derived from quantitative chemical analyses for desized and oxidized fibers. Desized fibers exhibit slight variations in elemental composition which are attributed to a certain heterogeneity of the material itself (due to the fabrication process). Hydrogen was not measured although it was thought to be present. As a matter of fact, it was previously reported[15] that the elemental composition of SiC-based fibers in the as-prepared state was Si : 55 wt%, C : 34 wt%, O : 11 wt% and H : 0,06 wt% which is in agreement with our results for the major elements. An increase in

the oxygen content and a decrease in the carbon content are respectively observed when fibers are oxidized. After dissolution of silica in HF aqueous solution, the composition obtained is similar to that of desized fibers.

Electron microprobe analyses show that there is no variation of the bulk composition during oxidation treatments up to 1400°C, 20 h in air. It also reveals no variation in elemental composition in the fiber at the micron scale.

Elements	desized (wt. %)*	Oxidized 800°C 165 h (wt. %)**	Oxidized 1400°C 20 h (wt. %)**	Oxidized 800°C 165 h + HF leached (wt. %)**
Si	57.3	55.1	51.7	56.6
C	30.0	26.9	12.3	30.8
O	12.7	18.0	36.0	12.6

* averaged on 4 analyses, ** averaged on 2 analyses

TABLE 1
Chemical analyses of ex-PCS fibers after various chemical or/and thermal treatments

On the basis of the X-ray diffraction data, cristobalite is detected in the oxide scale for treatments performed at 1100°C (duration : 10 h). At lower temperatures, amorphous silica was identified by AES. Combined with Ar ion sputtering, this technique was used to characterize the oxide/fiber interface. A pure SiC (CVI) sample was oxidized for purpose of comparison. In both cases, a sharp interface (with no intermediate phase) has been observed. This result was confirmed by SIMS analyses on oxidized fibers. An oxide film (about 5 nm in thickness) was observed on desized fibers. In addition to the major elements, hydrogen was detected in the bulk of desized fibers but its concentration has not been quantified. Futhermore, oxidized fibers present a hydrogen content

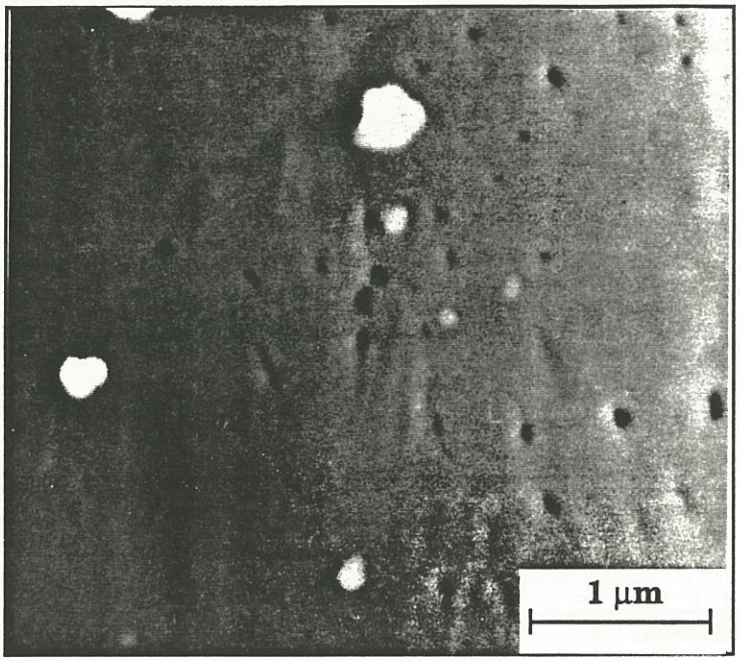

FIGURE 5

SEM micrograph of a fiber oxidized at 900°C, 100 h, in air.

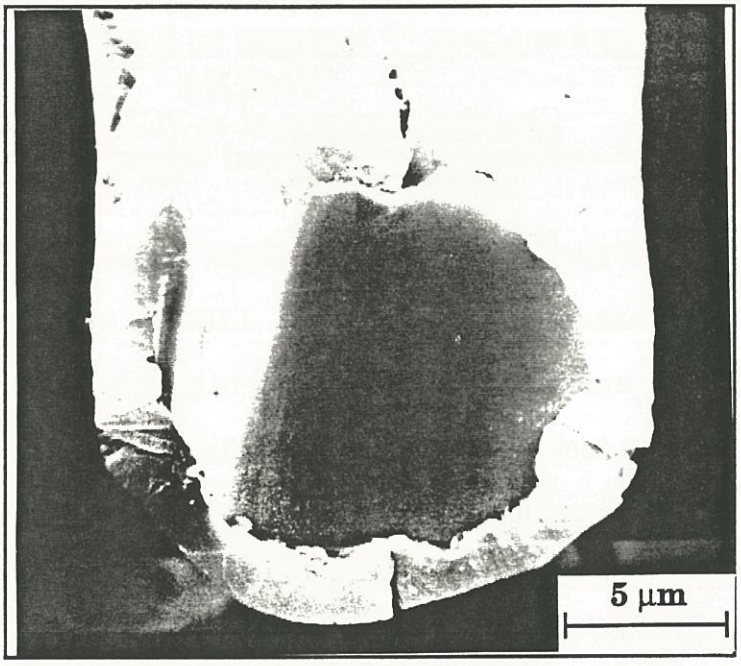

FIGURE 6

SEM micrograph of a fiber oxidized at 1500°C, 10 h, in O2.

quasi-constant, in the silica scale and at the oxide/fiber interface, and lower than that in desized fibers.

At low temperatures (800-1000°C), numerous small pores are observed at the surface of the oxide scale as shown in fig.5. At higher temperatures, the oxide layers have a cracked appearance as shown in fig.6, and in some cases the fibers are preferentially attacked at the basis of the cracks.

4 - DISCUSSION

4.1 - Sizing pyrolysis

The mass loss at 350°C and 458°C is assigned to decomposition reactions of polyvinyl acetate (PVA). Fareed et al.[16] observed by differential scanning calorimetry two exothermic peaks occurring at 374°C and 467°C that they assigned to oxidation reactions. The first step is probably due to removal of acetic acid and the second to that of aromatic hydrocarbons, such as benzene, toluene, styrene, etc... as reported by previous researchers[17]. The ratio of the mass of acetic acid over the total mass of PVA is about 2/3 which is, in fact, that experimentally observed for the first reaction in the present work.

4.2 - Oxidation kinetics

The oxidation behavior of ex-PCS SiC fibers is function of their microstructure and chemical composition. For instance, the occurrence of free carbon could lead to the formation of a partially or even non-protective oxide layer and to an enhanced in depth penetration of oxygen in the fiber. The ratio

of the molar volume of silica to that calculated for an ex-PCS fiber (from its chemical analysis) is about 1.35. Therefore, the oxide layer should be protective as in the case of SiC or silicon, a feature which should lead to a similar oxidation behavior. However, the occurrence of free carbon as well as combined oxygen and residual hydrogen in ex-PCS fibers may modify the oxidation kinetics.

The oxygen already present in the fiber is assumed to contribute to the formation of the silica layer, thus the oxygen flux required to oxidize the material would be lower than for pure SiC. Conversely, an additional flux of oxygen would be necessary to increase the thickness of the SiO_2 film owing to the presence of free carbon. The difference observed between the SiC and Si kinetics rate constants has already been explained on this basis[5]. Thus, the presence of these two elements (i.e. O from the oxicarbide phase SiC_xO_y and free carbon) would increase the ratio of the reaction product flux (namely CO or CO_2) to that of the oxidative species. Finally, residual hydrogen in the fiber could lead to water vapor formation whose role is known to be important in the oxidation of Si or SiC[18,19].

In a cylindrical geometry, the surface through which molecules diffuse is not constant, the external surface of the oxide layer being larger than the internal one and both of them changing vs time. Assuming that the reaction is diffusion controlled, the application of first Fick's law leads to the following equation :

$$\left[(1-\alpha)\ln(1-\alpha)-(1-\alpha)+\frac{\alpha(\Delta-1)+1}{(\Delta-1)}\ln(1+(\Delta-1)\alpha)-\frac{\alpha(\Delta-1)+1}{(\Delta-1)}\right]_{\alpha_i}^{\alpha}=K_1 t \quad (2)$$

with α : conversion rate, α_i : initial conversion rate, Δ : ratio of product to reactant molar volumes, K_1 : reaction rate constant, t : time.

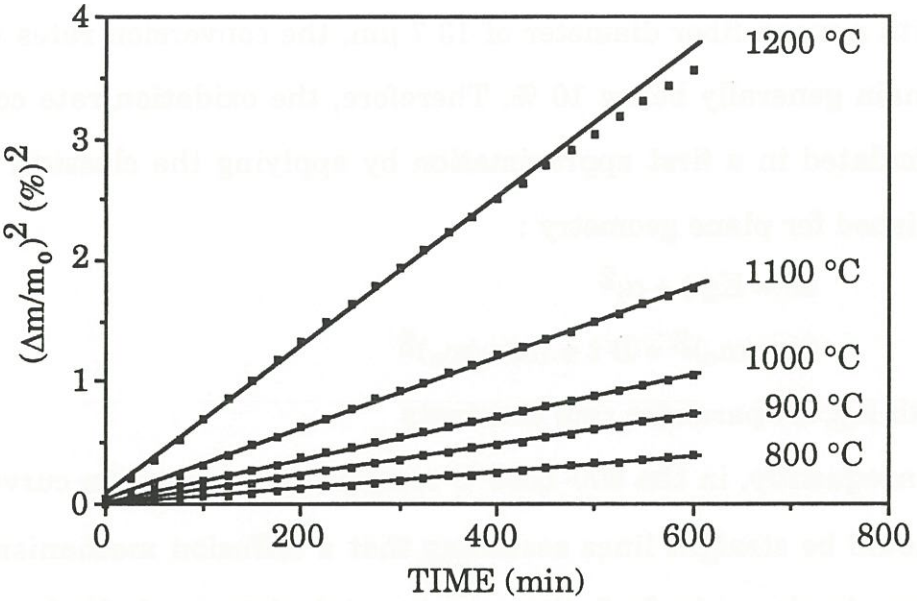

FIGURE 7

Curves $(\Delta m/m_o)^2$ versus time for different temperatures under dry oxygen (P = 100 kPa).

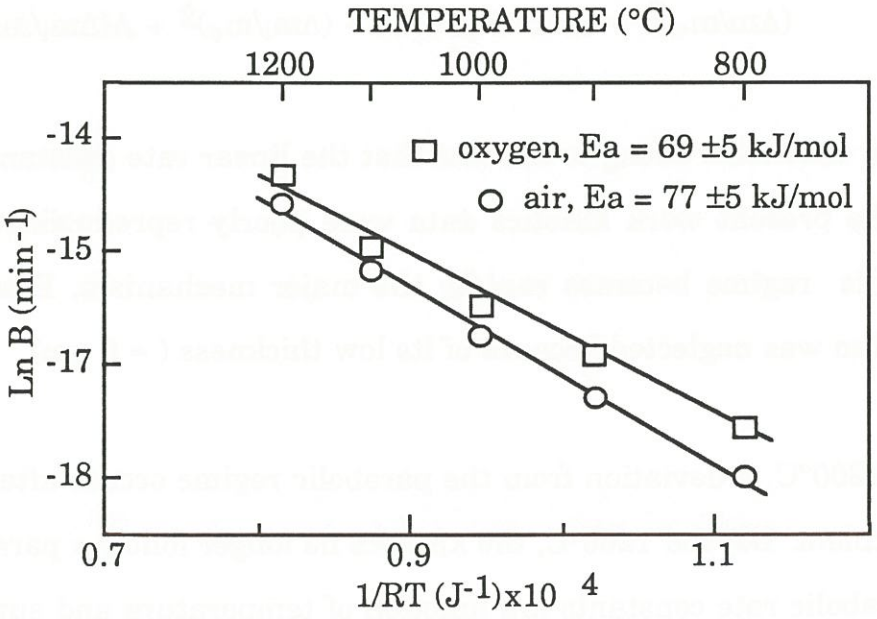

FIGURE 8

Thermal variations of parabolic rate constants in dry oxygen and in dry air (P = 100 kPa).

With a mean fiber diameter of 13.7 μm, the conversion rates were observed to remain generally below 10 %. Therefore, the oxidation rate constants could be calculated in a first approximation by applying the classical parabolic law established for plane geometry :

$$\alpha^2 = K_2\, t + \alpha_i^2 \qquad (3)$$

or $$(\Delta m/m_o)^2 = B\, t + (\Delta m_i/m_o)^2 \qquad (4)$$

with K_2, B : parabolic rate constants

Consequently, in the 800-1200°C temperature range, the curves $(\Delta m/m_o)^2 = f(t)$ should be straight lines assuming that a diffusion mechanism controls the reaction. As shown in fig.7, the experimental data are indeed quite well fitted by straight lines.

The linear-parabolic model[18] leading to the following equation :

$$(\Delta m/m_o)^2 + A(\Delta m/m_o) = Bt + (\Delta m_i/m_o)^2 + A(\Delta m_i/m_o) \qquad (5)$$

was not used here owing to the fact that the linear rate constants, B/A, derived from the present work kinetics data were poorly reproducible. Moreover, the parabolic regime becomes rapidly the major mechanism. Finally, the initial oxide film was neglected because of its low thickness (≈ 5 nm).

At 1200°C, a deviation from the parabolic regime occurs after about 4 hours of treatment. Beyond 1200°C, the kinetics no longer follow a parabolic law.

Parabolic rate constants are function of temperature and supposed to follow an Arrhenius law :

$$B = B_o \exp \frac{-Ea}{RT} \qquad (6)$$

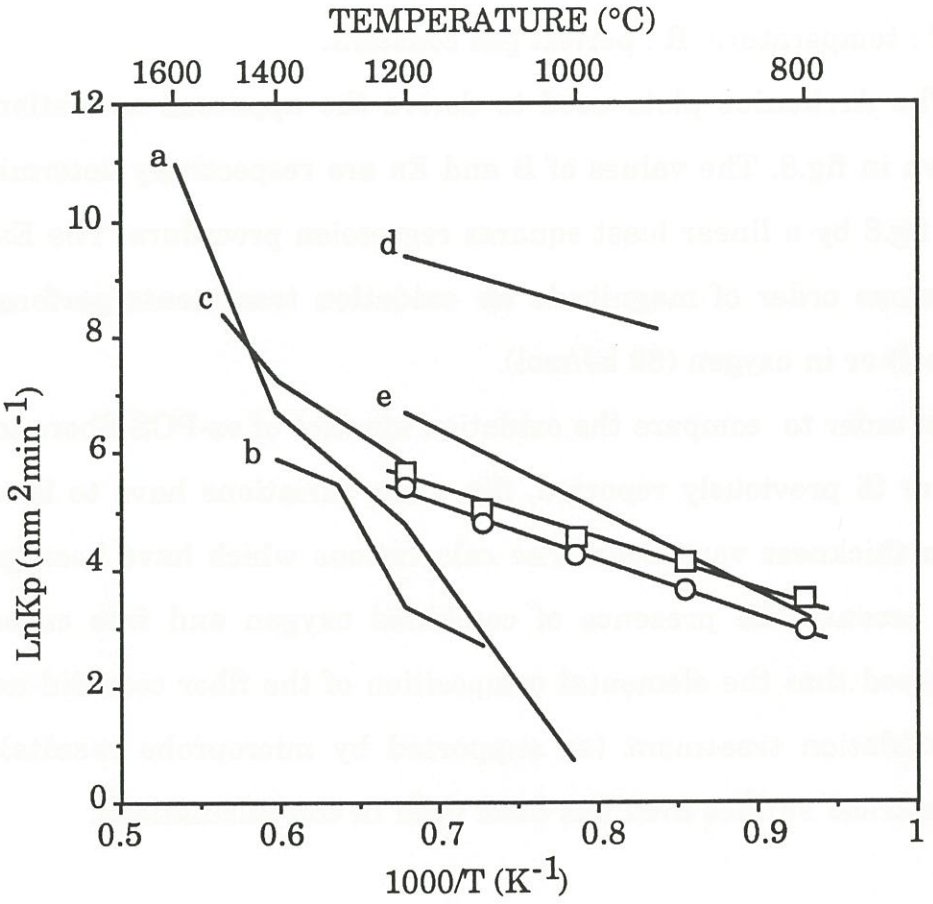

FIGURE 9

Thermal variations of parabolic rate constants for different Si or SiC-based materials: □ ex-PCS fibers in dry oxygen,○ ex-PCS fibers in dry air (present work), (a) SiC in dry oxygen[20], (b) ex-PCS fibers in air[8] , (c) SiC (CNTD) in dry oxygen[5], (d) Si in wet oxygen[18], (e) Si in dry oxygen[18].

with B_0 : preexponential coefficient, Ea : apparent activation energy,

T : temperature, R : perfect gas constant.

The Arrhenius plots used to derive the apparent activation energies are shown in fig.8. The values of B and Ea are respectively determined from fig.7 and fig.8 by a linear least squares regression procedure. The Ea values are of the same order of magnitude for oxidation treatments performed in air (77 kJ/mol) or in oxygen (69 kJ/mol).

In order to compare the oxidation kinetics of ex-PCS fibers to those of pure SiC or Si previously reported, the mass variations have to be converted into oxide thickness variations. The calculations which have been performed took into account the presence of combined oxygen and free carbon. They also supposed that the elemental composition of the fiber core did not vary during an oxidation treatment (as supported by microprobe results). Finally, the geometrical surface area has been used in the calculations.

The experimental validation of the relations used for the conversion of mass into thickness variations has been achieved by measuring : (i) the thickness of the oxide scale by SEM or/and (ii) the diameter of oxidized fibers by laser interferometry before and after leaching the oxide layer with a HF aqueous solution. A good correlation was obtained by both methods leading to a difference of less then 10 % between measured and calculated thicknesses.

The thermal variations of the parabolic rate constants are shown in fig.9 for ex-PCS fibers as calculated in the present work together with those previously reported by Warren et al.[8] for first generation ex-PCS fibers as well as for several SiC and Si materials. The values of the parabolic rate constants obtained in the present work for ex-PCS fibers are higher than those reported

by Warren et al.[8], principally because they used a much higher specific surface area value (i.e. 1 m^2g^{-1} instead of 0.11m^2g^{-1}). These authors have mentionned a cubic regime[7] between 1100°C and 1400°C whereas a deviation from parabolic regime is observed after only a few hours at 1200°C in the present study.

At low temperatures, the kinetics seem to be relatively fast and similar to that of silicon in dry oxygen whereas at 1200°C they seem to be similar to that of SiC.

In fact, there is little information on the oxidation of SiC in the 800-1200°C temperature range. In previous studies[6,20], high values of Ea have been obtained (150 - 200 kJ/mol). Schlichting[21] observed also a Ea value higher for SiC than for Si (120 kJ/mol). He explained this difference on the basis of structural considerations: silica could be in a reduced state SiO_{2-x} for Si and stoichiometric for SiC.

The oxygen molecular permeation through the growing silica layer is supposed to be the controlling mechanism in the oxidation of SiC-based materials at low temperatures. The values of Ea obtained in the present work, for a material with a complex chemical composition in dry air or in dry oxygen, are therefore lower than those associated with the oxidation of pure silicon and even more with those of pure SiC.

Hydrogen present in a combined state in the bulk of the fibers leads to the formation of free H_2 and H_2O during an oxidation treatment[22]. These two species can dissolve in and react with SiO_2 to form Si-H and Si-OH bonds which break the Si-O-Si lattice[23]. The activation energy for molecular diffusion is assimilated to an elastic strain energy of the lattice[24]. Hence, lower Ea values are expected when some Si-H and Si-OH bonds are present in the silica lattice.

Under wet oxygen, silicon is oxidized faster than in dry oxygen as shown in fig.9. It is worthy of note that the Ea value derived in this case[18] is 68 kJ/mol i.e. of the same order than that reported by Moulson and Roberts[25] for the diffusion of H_2O in fused silica (77 kJ/mol). The presence of water vapor, even in low proportions, is known to enhance the oxidation of SiC[19-20], but the mechanisms controlling the reaction are not yet fully understood.

In the case of ex-PCS fibers, water vapor is produced from residual hydrogen present in the fiber. It seems unlikely that the H_2/H_2O diffusion from internal to external interfaces may control the oxidation reaction since H_2/H_2O fluxes have been reported to be higher than the oxygen flux in amorphous silica[23].

On the other hand, the diffusion of the O_2 molecules through a silica layer containing hydroxyl groups and Si-H bonds could be the limiting step of the reaction. This mechanism agrees with the parabolic regime and could explain the low Ea value which have been obtained in the present work. Nevertheless in a permeation mechanism, the parabolic rate constants should be proportional to the oxygen partial pressure. In the present work, the ratio of air to oxygen parabolic rate constants is about 0.7 to 0.8 instead of 0.2 expected. This feature is not yet clearly understood.

The oxide film morphology is also an important parameter. The small pores observed at the surface of the oxide scale (fig.5) are probably formed by the outward diffusion of gaseous oxidation products (CO, CO_2, H_2O, H_2). Moreover, the oxidation of both the SiC_xO_y phase and C aggregates could lead to a silica layer less compact than that occurring during the oxidation of pure

SiC. The diffusion of oxidative species through a porous silica could also explain the observed kinetics with low Ea values.

The diffusion of reaction products (CO, CO_2) as a rate controlling step has been ruled out because previous work[26] has shown that carbonaceous species diffuse readily through silica.

The deviation from parabolic regime after a few hours at 1200°C could be assigned to the crystallization of the oxide films. The diffusion through cristobalite could reduce the oxidant transport if no defects are simultaneously created[5]. The presence of hydrogen and water vapor is known to enhance the crystallization of the oxide layer[19,20] and could explain that cristobalite is detected at temperatures as low as 1100°C.

The microcracks observed in oxidized fibers may have several origins. They could be formed during cooling due to : (i) a coefficient of thermal expansion mismatch between the oxide scale and the fiber or (ii) the $\beta \rightarrow \alpha$ transformation of cristobalite at about 270°C. These microcracks could also result from stresses arising from the oxide film growth due to a density difference between the fiber and its oxide or from crystallization. As shown in fig.6, preferential oxidation at the ends of microcracks occurs. The parabolic regime is then no longer respected.

Finally, thermal stability effects cannot be ruled out at high temperatures in ex-PCS fibers. Although, at 1400°C no change in the elemental composition is recorded in the fiber core, they might influence the oxidation reaction.

5 - CONCLUSION

The oxidation kinetics of ex-PCS fibers between 800°C and 1500°C as derived from TGA experiments performed in dry oxygen or in dry air, exhibit the following main features : (i) passive oxidation occurs due to the formation of an amorphous and/or crystallized (cristobalite) silicon dioxide layer. Between 800°C and 1200°C, kinetics obey a parabolic law which is no longer followed beyond 1200°C, (ii) in the diffusional regime, the apparent activation energy values are low (69-77 kJ/mol) compared to those usually accepted for the oxidation of silicon or pure SiC, (iii) the parabolic rate constants are higher, expecially at low temperatures than those for pure SiC, (iv) residual hydrogen in the ex-PCS fibers, thought to react with silica, and/or micropores in the oxide layer could explain the low values of the apparent activation energy, (v) over 1200°C, crystallization of the oxide scale, microcracks formation and thermal metastability of the ex-PCS fibers are thought to modify the oxidation kinetics.

ACKNOWLEDGEMENTS

The authors acknowledge the contribution of M. Lahaye (CUMENSE) to the X-ray and AES microprobe analyses as well as that of G. Camus and J. Thébault (from SEP) to usefull discussions. This work has been supported by CNRS and the Société Européenne de Propulsion via a grant given to L. Filipuzzi.

REFERENCES

1) P.J. Lamicq, G.A. Bernhart, M.M. Dauchier and J.G. Macé, Am. Ceram. Soc. Bull. 65 [2] (1986) 336-38.

2) R. Naslain, J.Y. Rossignol, J.M. Quenisset, F. Langlais in "Introduction aux Matériaux Composites" Vol.2 (R.Naslain, ed.) CNRS/IMC, Bordeaux 1985, pp. 439-91.

3) E.A. Gulbransen and S.A. Jansson, Oxid. Met. 4 [3] (1972) 181-201.

4) G. Ervin, Jr, J. Am. Ceram. Soc. 41 [9] (1958) 347-52.

5) J.A. Costello and R.E. Tressler, J. Am. Ceram. Soc. 69 [9] (1986) 674-81.

6) R.C.A. Harris, J. Am. Ceram. Soc. 58 [1-2] (1975) 7-9.

7) C.H. Andersson and R. Warren, Proc. 9 th Int. Symp. on reactivity of Solids, Cracow, Poland, 1980, pp. 585-89.

8) R. Warren, C.H. Andersson, Composites 15 [2] (1984) 101-11.

9) T.J. Clark, M. Jaffe, J. Rabe, N. Langley, Ceram. Eng. Sci. Proc. 7 [7,8] (1986) 901-13.

10) T.J. Clark, E.R. Prack, M.I. Haider, L.C. Sawyer, Ceram. Eng. Sci. Proc. 8 [7,8] (1987) 717-31.

11) C. Laffon, A.M. Flanck, P. Lagarde, M. Loridjani, R. Hagege, P. Olry, J. Cotteret, J. Dixmier, J.L. Micquel, H. Hommel, A.P. Legrand, J. Mater. Sci. 24 (1989) 1503-12.

12) M.M. Jaskowiak, J.A. Dilarlo, J. Am. Ceram. Soc 72 [2] (1989) 192-97.

13) K.L. Luthra, J. Am. Ceram. Soc. 69 [10] (1986) C231-33.

14) S.M. Johnson, R.D. Brittain, R.H. Lamoreaux, D.J. Rowcliffe, J. Am. Ceram. Soc. 71 [3] (1988) C132-35.

15) S. Yajima, K. Okamura, T. Matsuzawa, Y. Hasegawa, T. Shishido, Nature (London) 279 [5715] (1979) 706-7.

16) A.S. Fareed, P. Fang, M.J. Koczak, F.M. Ko, Am. Ceram. Soc. Bull. 66 [2] (1987) 353-58.

17) A. Ballistreri, S. Foti, G. Montaudo, E. Scamporrino, J. Polym. Sci. 18 (1980) 1147-53.

18) B. E. Deal and A.S. Grove, J. Appl. Phys. 36 [12] (1965) 3770-78.

19) R.E. Tressler, J.A. Costello and Z. Zheng, 1985, Exp. Symp. Ind. Heat Exchange Technol. 6-8 Nov 1985, pp. 307-14.

20) E. Fitzer and R. Ebi in Silicon Carbide 1973 (R. C. Marshall, J.W. Faust and C.E. Ryan eds.), University of South Carolina Press, Columbia SC, 1973 pp. 320-28.

21) J. Schlichting, High Temp. High Press. 14 (1982) 717-24.

22) C. Guterl, CRPCSS-Mulhouse, Internal report, July 1989.

23) R.H. Doremus, Glass Science, Wiley New York 1973, 229-232.

24) O.L. Anderson and D.A. Stuart, J. Am. Ceram. Soc. 37 [12] (1954) 573-80.

25) A.J. Moulson and J.P. Roberts, Trans. Faraday Soc. 57 (1961) 1208-16.

26) Z. Zheng, R.E. Tressler, K.E. Spear, 91th Annual Meeting Am. Ceram. Soc. 23-27 April 1989 Indianapolis.

CHAPITRE II

OXIDATION KINETICS OF SiC DEPOSITED FROM CH_3SiCl_3/H_2 UNDER CVI-CONDITIONS

INTRODUCTION AU CHAPITRE II

A aucun moment de cette thèse, l'objectif n'a été d'étudier les mécanismes fondamentaux à la base de l'oxydation du carbure de silicium. Si l'étude concernant l'oxydation du SiC ex-PCS contenait, a priori, plusieurs inconnues (influence du carbone ou de l'oxygène en excès), celle concernant le SiC déposé ou infiltré chimiquement en phase vapeur s'annonçait plus classique. Il faut néanmoins souligner que, d'une part la dispersion des résultats de cinétique, disponibles dans la bibliographie, les rendait difficilement utilisables et que, d'autre part, ce matériau réalisé dans des conditions de température et de pression particulières n'avait pas été étudié d'un point de vue cinétique.

L'objectif premier de ce travail était donc la détermination des valeurs des constantes paraboliques de vitesse. Il a été réalisé grâce à la collaboration de C. Jaussaud du LETI de Grenoble, qui a mis à notre disposition une technique permettant de mesurer les épaisseurs de couche d'oxyde formée par oxydation d'un substrat SiC. La connaissance des valeurs des constantes paraboliques de vitesse, concernant les fibres et la matrice, était une étape nécessaire à l'interprétation qualitative et quantitative du comportement à l'oxydation des composites.

Soumis à "Journal of Materials Science"

OXIDATION KINETICS OF SiC DEPOSITED FROM CH_3SiCl_3/H_2 UNDER CVI-CONDITIONS

L. FILIPUZZI, R. NASLAIN
Laboratoire des Composites Thermostructuraux, UMR-47
(CNRS-SEP-UB1), Europarc, 1-3, Av. L. de Vinci
33600 - Pessac, France
and
C. JAUSSAUD
CENG LETI
85 x 38041- Grenoble, France

ABSTRACT

Oxidation tests are performed on SiC deposits prepared from CH_3SiCl_3/H_2 under CVI-conditions, at temperatures ranging from 900°C to 1500°C under a flow of pure oxygen at 100 kPa (passive oxidation regime). The kinetics of growth of the silica layer are established from thickness measurements performed by spectroreflectometry. They obey classical parabolic laws from which rate constants are calculated. Within 1000°C-1400°C, the oxidation process is thermally activated with an apparent activation energy of 128 kJ mol^{-1}. Beyond 1400°C and below 1000°C, an increase in the activation energy is observed which is thought to be related to a change in the mechanism of the oxygen transport across the silica layer for T >1400°C and tentatively to stress effects for T <1000°C. The kinetics data are compared to those measured on silicon single crystals (used as a standard) and to other reported data on SiC.

KEY WORDS : SiC, Silicon, CVD/CVI, Oxidation, Kinetics

1 - INTRODUCTION

Silicon carbide is one of the most promising ceramic materials for structural applications at high temperatures owing to its refractory character, low density, excellent mechanical properties and good resistance to oxidation [1]. This latter property is related to the formation of a protective layer of silica and is effective at medium temperatures and high enough oxygen pressures (passive oxidation regime) [2].

Silicon carbide ceramics often contain impurities whose nature and concentration depend on the processing techniques. SiC ceramics prepared according to the powder metallurgy route contain a significant amount of sintering aids (e.g. boron, aluminium, yttrium, etc...). On the other hand, silicon carbide chemically deposited from gaseous precursors (e.g. CH_3SiCl_3/H_2) exhibits a much higher degree of purity as long as the organometallic source has been carefully purified (however, a contamination by the deposition chamber material (usually stainless steel) or/and the substrate remains possible). These impurities are known to modify the oxidation behavior of SiC-ceramics. Finally, the oxidation rate of SiC-crystals depends also on the nature of the polytypes and the crystal orientation [2,3].

An important family of ceramic matrix composites (CMC) consisting of SiC-based fibers embedded in a SiC-matrix, referred to as SiC/SiC composites are being used in rocket engine nozzles and space craft heat shield [4]. In these composites, the SiC-matrix is infiltrated in the pore network of SiC-based fiber preforms by chemical vapor infiltration (CVI), a process derived from the well known chemical vapor deposition (CVD) technique [5]. SiC/SiC composites

exhibit, with respect to monolithic SiC, a non linear mechanical behavior under tension loading, a higher resistance to crack propagation (by almost two orders of magnitude) and to thermal shocks. This outstanding behavior for a ceramic material is observed only when the fibers are weakly bonded to the matrix, a requirement which is achieved through the use of a thin layer of a soft material, referred to as the interphase (e.g. pyrocarbon or boron nitride), between the matrix and the fibers [6]. The non-linear stress-strain behavior of SiC/SiC composites under tension loading is related to the occurrence of various damaging phenomena including a progressive microcracking of the SiC-matrix and fiber-matrix debonding [7]. These damaging phenomena, when they take place in a composite maintained at high temperatures in atmospheres containing oxygen, result in new reactive surfaces and oxygen diffusion path ways. Therefore, the knowledge of the oxidation kinetics of the SiC-matrix (which has been deposited under specific conditions) is necessary for the modelling of the oxidation behavior of SiC/SiC composites.

The aim of the present contribution was to establish the oxidation kinetics of SiC deposits, prepared under CVI-conditions, and to compare the data with those corresponding to silicon (used as a standard) and other SiC-ceramics.

2 - EXPERIMENTAL

2.1 - Samples

The **samples** used in the present study were SiC-layers (≈ 120 μm in thickness), deposited from a CH_3SiCl_3/H_2 mixture under CVI-conditions (i.e. T

(a)

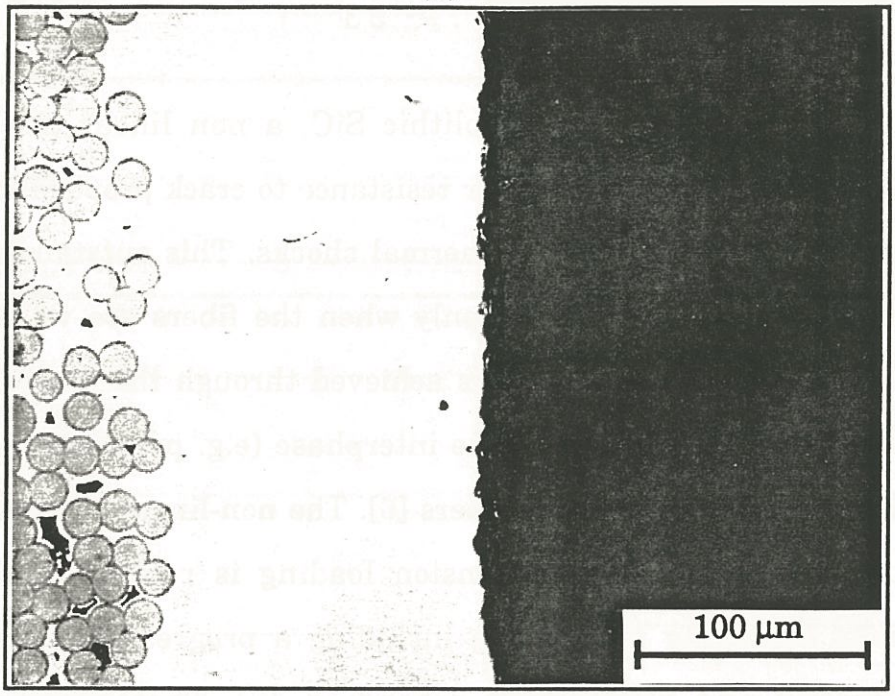

(b)

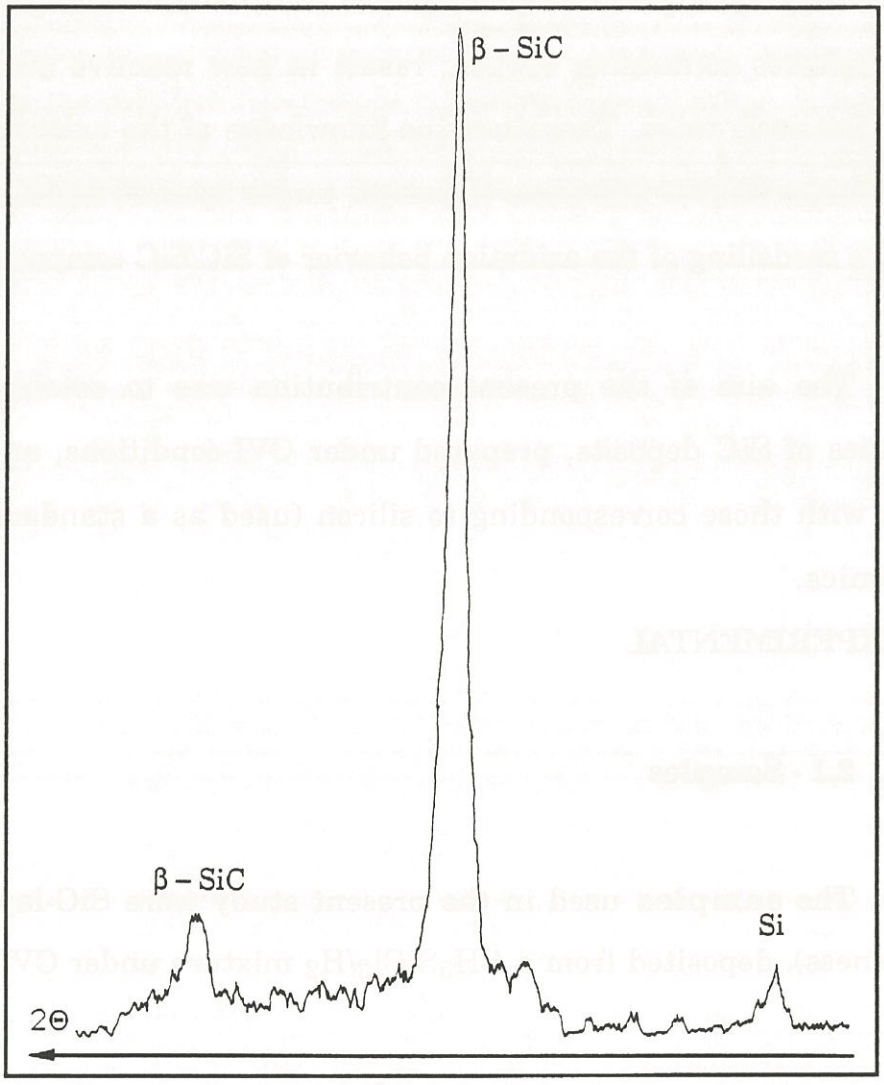

Fig. 1: Nature of the SiC deposits prepared from CH_3SiCl_3/H_2 under CVI-conditions: (a) optical micrograph of the SiC layer deposited on the external surface of the fiber preform; (b) XRD spectrum of the SiC layer.

≈ 1000°C and P < 50 kPa), on the external surface of a SiC-based fiber(*) preform. The isothermal / isobaric (ICVI) process has been described in detail eslsewhere [4]. It will be sufficient to recall here that in ICVI the overall deposition process is rate-controlled by the kinetics of the chemical surface reactions and not by mass transfers (of the reactants and products) in the gas phase. As a result, SiC is formed both in the pore network of the preform (infiltration) and on its external surface (coating). At the end of the process, the pores become progressively sealed by the SiC-deposit. Here, the preform has been maintained in the CVI-chamber a time long enough in order to grow a SiC coating of about 120 μm in thickness (fig. 1a). The SiC-coating was polycrystalline (β-modification or 3C-polytype) with (111) planes preferentially orientated parallel to the substrate. Trace amounts of free silicon were detected by X-ray diffraction (fig. 1b). However, no significant departure from the stoichiometric Si/C = 1 ratio was observed from the results of electron probe microanalysis (standard : SiC single crystal). Therefore, it was assumed that the silicon in excess was present as isolated precipitates within a stoichiometric SiC phase. The infiltrated/coated SiC/SiC composite was then : (i) cut with a diamond saw in small cubes 3 x 3 x 3 mm^3 and one of their faces i.e. that with the 150 μm SiC-coating, was polished with a diamond paste (1μm grain size), (ii) ultrasonic cleaned in acetone and alcool baths and finally (iii) dried. It was assumed that the 150 μm coating was representative of the SiC-matrix deposited simultaneously in the pore network of the fiber preform.

The oxidation tests, which are described below, were also performed on **silicon single crystals** (orientation : 111) cut with a diamond saw in an undoped silicon wafer(**) 300 μm in thickness, and used as a standard (since their

(*) Nicalon fiber (NLM 202 ceramic grade) from Nippon Carbon
(**) from IBM

oxidation kinetics have been studied in a detailed manner by many researchers).

2.2 - Oxidation tests

All the oxidation tests were performed, within the temperature range 900°C-1500°C, with an electric furnace equipped with a tube and sample holder made of pure alumina(*) and heated with a carbon resistance.

In each test, the alumina tube was first evacuated with a vacuum pump (residual pressure : 1 Pa) and then swept with a flow of pure dry oxygen (H_2O < 2 ppm)(**). The oxidation test was performed with an oxygen flow of 1 liter per hour under a pressure of 100 kPa. Temperature was raised at a rate of 60°C per minute and controlled with a Pt/Pt-10%Rh thermocouple set below the sample.

2.3 - Characterization of the silica layer

The kinetics of growth of the silica layer were assessed from thickness measurements, performed by **spectro-reflectrometry**(***) [8]. The accuracy of the measurements was established to be ± 5 nm for x < 200 nm and ± 2 nm for x > 200 nm.

The nature of the silica layer was characterized by X-ray diffraction (CuKα radiation) and optical microscopy in reflexion.

(*) > 99.9 % alumina from
(**) N48 oxygen from Alphagaz
(***) Nanospec/AST model 201

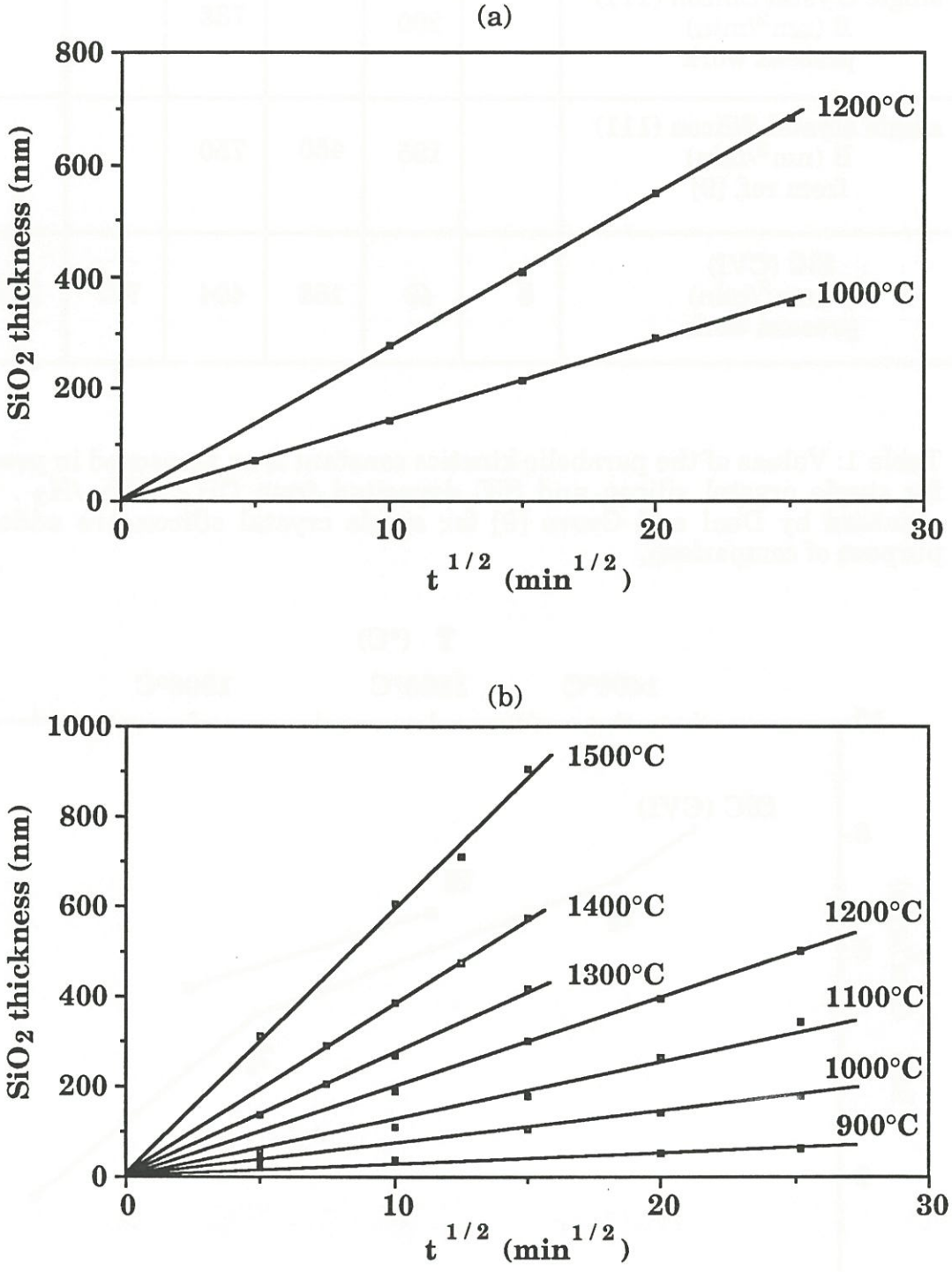

Fig. 2: Kinetics of growth of the silica layer in pure oxygen of: (a) single crystal silicon (111); (b) SiC deposits prepared under CVI-conditions.

Temperature (°C)	900	1000	1100	1200	1300	1400	1500
single crystal Silicon (111) B (nm^2/min) present work		200		735			
single crystal Silicon (111) B (nm^2/min) from ref. [9]		195	450	750			
SiC (CVI) B (nm^2/min) present work	5	49	188	404	777	1406	3365

Table 1: Values of the parabolic kinetics constant B as measured in present work for single crystal silicon and SiC deposited from $CH_3\ SiCl_3\ /H_2$. The data obtained by Deal and Grove [9] for single crystal silicon are added for the purpose of comparison.

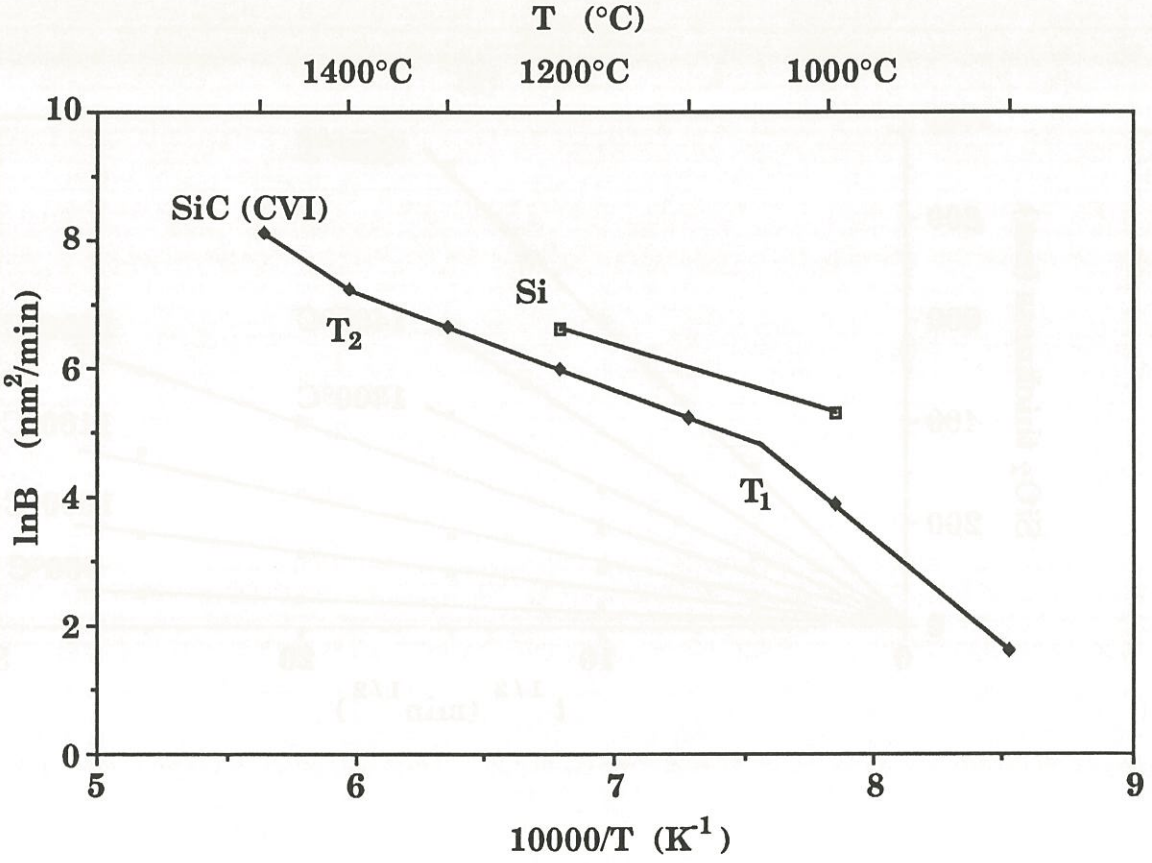

Fig. 3: Arrhenius plots of the thermal variations of the parabolic rate constants B for the single crystal silicon (111) and SiC deposits prepared under CVI-conditions.

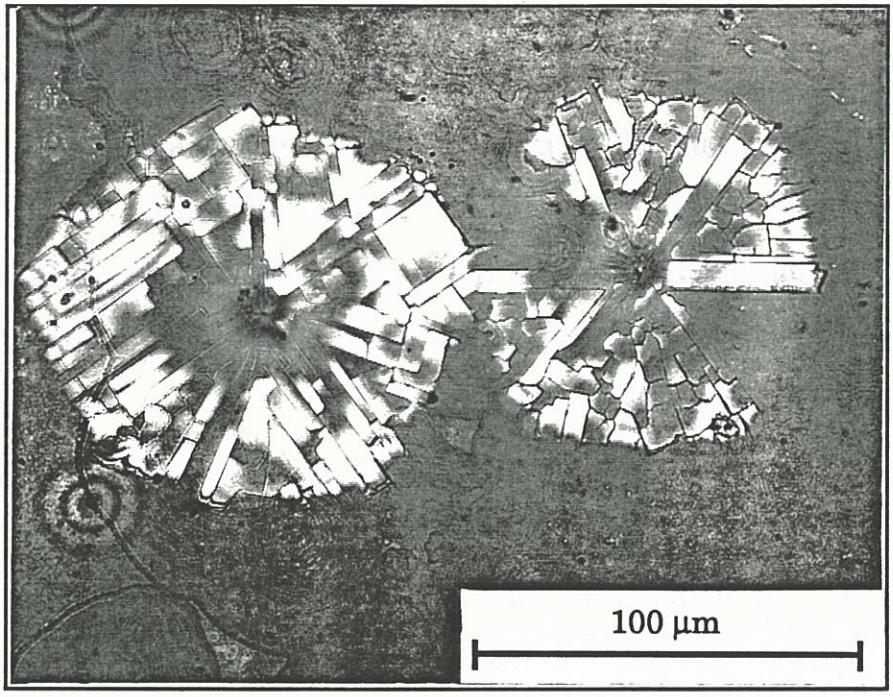

Fig. 4: Optical micrograph of the surface of a SiC (CVI) sample maintained 225 min at 1500°C under a flow of pure oxygen (P=100kPa) showing crystals of cristobalite.

3 - RESULTS

The variation of the **silica layer thickness, x,** as a function of the square root of the oxidation test duration t at a given temperature T, are shown in fig.2. Linear relationships $x = f(t^{1/2})$ are observed for all the oxidation tests, in agreement with the results of the previous studies reported on the oxidation of both silicon and silicon carbide [2,9].

The values of the **parabolic kinetics constant B** defined according to the parabolic equation : $x = B^{1/2} t^{1/2}$ were calculated, by a least squares linear regression procedure, from the slopes of the straight lines shown in fig. 2. They are listed in table I as well as those previously reported in the literature for silicon single crystal (111).

The thermal variations of the parabolic kinetics constant B are shown in fig. 3 as Arrhenius plots $LnB = f(1/T)$.

The silica layers formed during the oxidation tests are usually amorphous. Cristobalite has been observed only for the oxidation tests performed under the most severe conditions, i.e. T=1500°C and t > 150 mn (fig. 4).

4 - DISCUSSION

The values of the parabolic rate constant B which have been calculated in the present work for silicon single crystals (111) are very close to those reported by Deal and Grove [9]. This feature suggests that our oxidation test conditions

(nature of the tube, sample holder, oxygen purity) were clean enough. On the other hand, Choi et al. have reported much higher (x 7) B values for the same material and have assigned this increase in the kinetics of growth of the silica layer to the presence of impurities in their alumina tube [10].

A shown in fig. 3, silicon single crystals exhibit a higher oxidation rate in pure oxygen than SiC CVI/CVD deposits, in agreement with the conclusion drawn by Costello and Tressler for pure materials [11]. As an example, at 1200°C, there is a factor of 2 between the values of the parabolic rate constants, B(Si) and B(SiC), of silicon single crystal and SiC CVI/CVD deposits. At lower temperatures, the α = B(Si)/B(SiC) ratio is higher (e.g. it is equal to 4 at 1000°C).

The explanation which has been given to justify the higher B values for silicon single crystals is based on the hypothesis that an additional oxygen flux is necessary to oxidize the carbon of SiC with respect to that required for the oxidation of silicon [2]. Considering that oxidation occurs according to the following equations :

$$Si + O_2 \rightarrow SiO_2 \qquad (1)$$

$$SiC + \frac{3}{2} O_2 \rightarrow SiO_2 + CO \qquad (2)$$

$$SiC + 2\,O_2 \rightarrow SiO_2 + CO_2 \qquad (3)$$

1 mole of oxygen per silica mole is necessary to oxidize silicon with respect to 3/2 or 2 for SiC depending on whether equation (2) or (3) is selected. Therefore, from these considerations an α = B(Si)/B(SiC) ratio equal to 1.5-2 is expected for

oxidation tests performed in similar conditions. Costello and Tressler have indeed reported α values in the range of 2-2.5 for oxidation tests performed at 1200-1400°C on silicon and SiC 6H (0001 face) single crystals and concluded that the oxidation of SiC may proceed according to equation (3) [2]. However, Zheng et al. have reported higher α-values, i.e. $\alpha = 4$ for oxidation tests run with similar materials (silicon and SiC 4H (0001 face) [11]. Futhermore, Schiroky et al. have published a comparative study of the oxidation of silicon SiC (CVD) and Si_3N_4 (CVD) [12]. From their data, we have calculated that an α ratio of about 5 exists between silicon and SiC (CVD). All these results suggest that the hypothesis based on the additional oxygen flux necessary to oxidize the carbon from SiC (with respect to that necessary to oxidize silicon) is not enough in itself to explain the differences observed experimentally in the B constants between Si and SiC. Other hidden factors might well be involved.

As shown in fig. 3, the Arrhenius plots observed for SiC (CVD/CVI) is complex and can be analysed on the basis of three domains. Between T_1 = 1100°C and T_2 = 1400°C, the Arrhenius plot is a linear segment corresponding to an apparent activation energy of 128 kJ mol^{-1}, a value which is in agreement with those reported previously [2,11]. Beyond 1400°C an increase in the slope of the Arrhenius plot is observed. This transition has been mentioned by other researchers and assigned to a change in the transfer of oxygen across the silica layer [2,13] : oxygen can diffuse through silica either as **molecular species** by permeation or as **ionic species** in the crystal network. Since the latter mechanism has a high activation energy, it is thought to become rate-controlling at high temperatures. In the same manner, another increase in the slope of the Arrhenius plot (and therefore in the apparent activation energy) is noticed below 1100°C. This transition at a low temperature is not

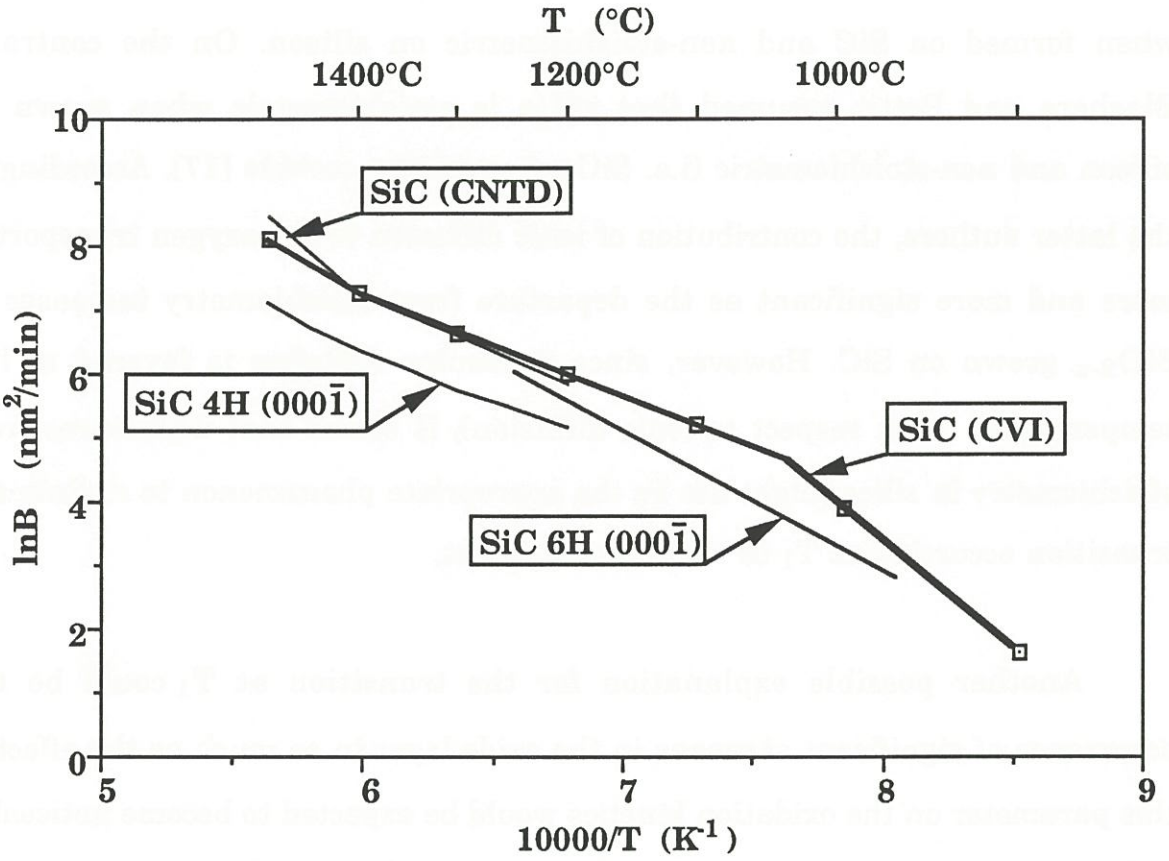

Fig. 5: Thermal variations of the parabolic rate constants B for SiC (CVI) (present work), SiC (CNTD) [2], 4H-SiC polytype [11] and 6H-SiC polytype [16].

observed for silicon (or if it does occur, it is less noticeable). On the contrary, it has been mentioned already by several authors for SiC [14-16]. According to them (see for example ref [15]), this difference between silicon and SiC could be related to **composition defects** in the silica layer which could be stoichiometric when formed on SiC and non-stoichiometric on silicon. On the contrary, Blachere and Pettit assumed that silica is stoichiometric when grown on silicon and non-stoichiometric (i.e. SiO_{2-x}) on silicon carbide [17]. According to the latter authors, the contribution of ionic diffusion to the oxygen transport is more and more significant as the departure from stoichiometry increases in SiO_{2-x} grown on SiC. However, since molecular diffusion is favored at low temperatures (with respect to ionic diffusion), it seems that departures from stoichiometry in silica might not be the appropriate phenomenon to explain the transition occurring at T_1 in the Arrhenius plot.

Another possible explanation for the transition at T_1 could be the occurrence of significant **stresses** in the oxide layer in as much as the effect of this parameter on the oxidation kinetics would be expected to become noticeable at low temperatures. As a matter of fact, such an hypothesis has been already discussed for silicon [18-20]. Stresses arise in the oxide layer due to the volume increase inherent to silicon or SiC oxidation. They can influence the oxidant diffusivity in SiO_2 and are particularly noticeable for low oxide thicknesses [20]. Since the oxidation kinetics of SiC is lower than that of silicon, the importance of stress effects may be more pronounced for SiC than for silicon.

Finally, the oxidation kinetics rates of SiC (CVD/CVI) measured in the present work are compared to those mentioned in the literature for different SiC-ceramics, in fig. 5. At high temperatures ($T > 1200°C$) our data are very

close to those reported by Costello and Tressler for SiC (CNTD)(*), prepared according to a modified CVD-technique and which contains also some free silicon. On the other hand, the B values measured in present work are higher, generally speaking, than those mentioned for the hexagonal SiC polytypes (4 H and 6 H) although the thermal variations of the B constants are very similar [11,16].

5 - CONCLUSION

The oxidation kinetics of silicon carbide, deposited from CH_3SiCl_3/H_2 on a SiC-based fiber preform under CVI-conditions, were studied from oxidation tests performed under a flow of pure oxygen (P = 100 kPa) for temperatures ranging from 900°C to 1500°C (passive oxidation regime), with the following main conclusions : (i) - the kinetics of growth of the silica layer obey parabolic laws, (ii) between 1100°C and 1400°C, the oxidation process is thermally activated with an apparent activation energy of 128 kJ mol^{-1} (iii) beyond 1400°C, an increase in the apparent activation energy is observed which is thought to be related to a change occurring in the mechanism of the oxygen transport across the silica layer, (iv) below 1100°C, another increase in the apparent activation energy also occurs which has been tentatively assigned to the effect of stresses in the oxide layer.

ACKNOWLEDGEMENTS

This work has been supported by both CNRS and SEP through a grant given to L.F. The SiC(CVI) samples were prepared by SEP-Bordeaux.

(*) Controlled Nucleation Thermally Deposited

REFERENCES

[1] J.L. Chermant in "Les céramiques thermomécaniques", Presse du CNRS, Paris, 1989.

[2] J.A. Costello and R.E. Tressler, J. Am. Ceram. Soc. 69 [9] (1986) 674-81.

[3] W. Von Münch and I. Pfaffender, J. Electrochem. Soc. 122 [5] (1975) 642-43.

[4] J.C. Cavalier, A. Lacombe and J.M. Rouges, Proc. Third European Conference on composite materials (A.R. Bunsell, P. Lamicq, A. Massiah Eds) 20-23 March 1989 Bordeaux France pp 99-110.

[5] R. Naslain, J.Y. Rossignol, J.M. Quenisset and F. Langlais in "Introduction aux Matériaux Composites", Vol.2 (R. Naslain Ed.) CNRS/IMC Bordeaux 1985 pp 439-91.

[6] A.J. Caputo, D.P. Stinton, R.A. Lowden and T.M. Besman, Am. Ceram. Soc. Bull. 66 [2] (1987) 368-72.

[7] M. Bouquet, J.M. Birbis and J.M. Quenisset, Comp. Sci. and Technology 37 (1990) 223-48.

[8] W.G. Spitzer, M. Tanenbaum, J. Appl. Phys. 32 (1961) 744.

[9] B.E. Deal and A.S. Grove, J. Appl. Phys. 36 [12] (1965) 3770-78.

[10] D.J. Choi, D.B. Fishback and W.S Scott, J. Am. Ceram. Soc. 72 [7] (1989) 1118-23.

[11] Z. Zheng, R.E. Tressler and K.E. Spear, J. Electrochem. Soc. 137 [3] (1990) 854-58.

[12] G.H. Shiroky, R.J. Price and J.E. Sheehan, GA Project 3799, December 1986.

[13] Z. Zheng, R.E. Tressler and K.E. Spear, J. Electrochem. Soc. 137 [9] (1990) 2812-16.

[14] E. Fitzer and R. Ebi in Silicon carbide 1973 (R.C. Marshall, J.W. Faust and C.E. Ryan Eds.) University of South Carolina Press, Columbia SC 1973 pp 320-28.

[15] J. Schlichting, High Temp. High Press. 14 (1982) 717-24.

[16] R.C.A. Harris, J. Am. Ceram. Soc. 58 [1-2] (1975) 7-9.

[17] J.R. Blachere and F.S Pettit in High Temperature Corrosion of Ceramics, Noyes data corporation,Park Ridge New Jersey, 1989 pp 137-83.

[18] R.H. Doremus and A. Szewczyk, J. Mater. Sci. 22 (1987) 2887-92.

[19] S. Alexandeova, A. Szekeres and J. Koprinarova, Semicond. Sci. Technol. 4 (1989) 876-78.

[20] P. Sutardja and W.G. Oldham, IEEE Transactions on Electron Devices 36 [11] (1989) 2415-21.

CHAPITRE III

OXIDATION MECHANISMS AND KINETICS OF 1D-SiC/C/SiC COMPOSITE MATERIALS : 1 - AN EXPERIMENTAL APPROACH

INTRODUCTION AU CHAPITRE III

Il eût été logique que la troisième partie de ce travail soit consacrée à l'oxydation du troisième constituant, **l'interphase de carbone**. Néanmoins, en raison de problèmes liés à la difficulté d'obtenir des échantillons représentatifs et à l'importance préssentie des phénomènes de transport à haute température, il a été jugé intéressant de passer directement à l'étude du comportement des composites. Des matériaux à texture unidirectionnelle* ont été choisis afin de simplifier la géométrie du problème.

L'analyse thermogravimétrique a été largement utilisée pour établir le comportement à l'oxydation de ces matériaux. Cette méthode est en effet particulièrement bien adaptée, dans la mesure où l'oxydation de chaque constituant mène à une variation de masse (négative pour le carbone et positive pour les carbures). Les analyses ont été effectuées dans des conditions différentes, ce qui a permis de préciser l'influence de plusieurs paramètres.

Un autre point important concernait l'étude de l'évolution de la morphologie des composites avec les traitements d'oxydation. Plusieurs méthodes ont été mises à contribution notamment les méthodes de microscopie (optique, électronique à balayage et en transmission). Suite à des contacts antérieurs, une méthode basée sur l'émission de cathodoluminescence, permettant de détecter et cartographier la silice formée par oxydation a été développée**. Les résultat de ce travail sont présentés en annexe 1.

---

* élaborés à la Société Européenne de Propulsion

** étude conduite en collaboration avec le CRIAA de l'Université de Bordeaux III

Soumis à "Journal of the American Ceramic Society"

OXIDATION MECHANISMS AND KINETICS OF 1D-SiC/C/SiC COMPOSITE MATERIALS : 1 - AN EXPERIMENTAL APPROACH

L. FILIPUZZI, G. CAMUS, R. NASLAIN
Laboratoire des Composites Thermostructuraux, UMR-47
(CNRS-SEP-UB1), Europarc, 1-3 Av. Léonard de Vinci
33600 - Pessac, France
and
J. THEBAULT
Société Européenne de Propulsion, B.P. 37
33165 - Saint Médard en Jalles, France

ABSTRACT

The oxidation of unidirectional 1D-SiC(ex-PCS)/C/SiC(CVI) model composites has been investigated through an experimental approach based on thermogravimetric analyses, optical/electron microscopy and electrical measurements. The influence of initial carbon interphase thickness, total pressure, oxygen partial pressure and fiber orientation on the oxidation kinetics of uncoated or partially SiC-coated composites is presented and discussed. The oxidation process involves three main phenomena : (i) a reaction of oxygen with the carbon interphase resulting in the formation of annular pores around the fibers, (ii) a diffusion transfer of oxygen and carbon oxides along the pores and (iii) a reaction of oxygen with the pore walls leading to the growth of silica layers on both the fibers and matrix. In composites with a thin carbon interphase (e.g. 0.1 μm) treated at high temperatures in oxidizing atmospheres the pore entrances are rapidly sealed by silica and the in-depth oxidation is thus slowed down significantly. Under such conditions, the oxidation damages are limited to the vicinity of the external surface and the materials exhibit a self-healing character. Conversely, long exposures at low temperatures give rise to the formation of a network of microcracks in the matrix related to mechanical stresses arising from the in-situ SiC/SiO_2 conversion. Finally, the self healing character is not observed in composites

with a thick carbon interphase (e.g. 1 μm) since carbon is totally consumed before silica could seal the pores resulting from the oxidation of the interphase.

KEY WORDS : Oxidation, SiC, Carbon, Kinetics, Ex-PCS fibers, SiC/C/SiC Composites

1 - INTRODUCTION

Ceramic matrix composites (CMC) reinforced with continuous fibers exhibit attractive properties such as low densities, high elastic moduli and high strengths at elevated temperatures. Thus, they are considered as materials with a high potential in various fields of applications including engines and re-entry thermal protection for spacecrafts. More specifically, CVI- processed SiC matrix composites reinforced with ex-polycarbosilane SiC - based fibers(*), referred to as SiC/SiC composites, have been designed and developed to improve the damage tolerance of the inherently brittle SiC monolithic ceramics while retaining their outstanding stiffness, high temperature strength and oxidation resistance (in the so-called passive oxidation regime) [1]. The toughness of ceramic materials can be improved significantly by fiber reinforcement. Thus, in continuous fiber reinforced ceramics, several well identified mechanisms (i.e. matrix microcracking, fiber/matrix debonding and fiber pull out) contribute to increase, in a dramatic manner, the work of fracture and resistance to crack propagation and to avoid catastrophic failure [2,3]. The onset of these energy dissipating mechanisms is usually associated with the non-linear feature of the deformational response of the materials. Hence, non-linear tensile behaviors with strains to rupture ranging from 0.2 to 0.9 % (depending on the process and architecture of the reinforcement) have been reported for SiC/SiC composites [4-6].

(*) Nicalon fibers (NLM 202 ceramic grade) from Nippon Carbon

SiC-based materials exhibit generally an excellent oxidation resistance owing to the formation of a protective layer of silica (passive oxidation layer) which limits further oxidation. Recent studies have shown that it is also the case for the basic components of the SiC/SiC composites, i.e. the CVI-processed SiC-matrix and the ex-PCS Si-C-O fibers(*) [7-8].

However, it is now well established that the mechanical properties of CMC depend upon the fiber-matrix bonding [9,10]. Thus, the energy dissipating mechanisms which have been mentioned above, take place only when a low enough shear strength interface is provided between the matrix and the fibers. This is usually achieved through the interposition of a thin layer of a compliant material (e.g. carbon or hex-BN), referred to as the **interphase**. This interphase is either deposited on the fiber surface prior to the infiltration of the matrix or /and formed in-situ as the result of a chemical reaction occurring near (or at) the fiber/matrix interface during the high temperature step of the CMC processing [11-13]. It is thought that the reactivity of the carbon interphase towards oxygen might be a weak point of such materials when exposed to oxidizing atmospheres unless they have been properly protected by a suitable coating. Previous works on SiC/C/SiC and SiC/C/Glass ceramic composites have shown the detrimental effects of high temperature exposures in oxidizing environments [14-17]. This behavior is clearly related to changes taking place in the fiber-matrix interfacial region. The carbon interphase is thought to be consumed by oxidation and replaced by oxide phases (e.g. silica) giving rise to a dramatic increase in the interfacial debonding/sliding resistance [10]. Then the overall mechanical behavior changes from a tough to a brittle character governed in this latter case by a

single dominant macroflaw when failure occurs [5,14]. Conversely, it has been also established that the tensile failure strength of SiC/SiC composites at room temperature remains unchanged after aging in air at 1200°C (with even a significant improvement in the failure strain) when the materials have been protected by an external coating [6]. However, if the effects of exposures to high temperature oxidizing atmospheres on the mechanical behavior of CMC have been some what clarified, no detailed study has been specifically devoted to the oxidation mechanisms.

The aim of the present contribution was to evidence, through an experimental approach, the influence of several parameters (e.g. temperature, time, interphase thickness, atmosphere) on the oxidation behavior of SiC/C/SiC composites and to identify the mechanisms which were involved. In order to enhance the oxidation phenomena and to facilitate their understanding, the experiments were performed on model unidirectional composites (unprotected or partially protected by a coating), which are referred to as 1D-SiC/C/SiC composites. The modelling of the oxidation phenomena is treated in a companion article [18].

2 - EXPERIMENTAL

2.1 - The model 1D-SiC/C/SiC composites

The model composite materials used in the present study consist of a SiC-matrix (formed according to the so-called isothermal-isobaric CVI process) reinforced with 0° plies of **ex-PCS Si-C-O fibers**(*). The fibrous preform

(*) Nicalon fibers (NLM 202 ceramic grade) from Nippon Carbon

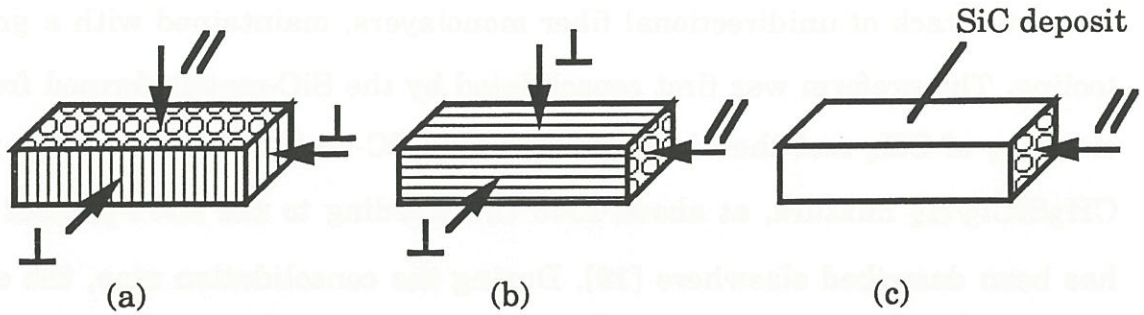

Fig. 1 : 1D - SiC/C/SiC specimens used in the study : (a,b) uncoated specimens (A or B), (c) partially coated specimens (A_c or B_c) (the arrows show the directions along which oxidation can proceed, i.e. parallel (//) or perpendicular (⊥) to the fiber axis).

Material	Apparent density g. cm^{-3}	Open Porosity (%)	Specific surface area m^2/g
A	2.25	19	0.08
B	2.22	18	0.05
A_c	2.56	8	0.06
B_c	2.51	6	0.06

Table I : Main physical characteristics of a received material (A, B : uncoated ; A_c, B_c : partially coated sample).

was a 0° stack of unidirectional fiber monolayers, maintained with a graphite tooling. The preform was first consolidated by the SiC-matrix formed from the cracking of CH_4 and then infiltrated by the SiC-matrix formed in situ from a CH_3SiCl_3/H_2 mixture, at about 1000°C, according to the ICVI-process which has been described elsewhere [19]. During the consolidation step, the ex-PCS Si-C-O fibers were coated with a layer of **pyrocarbon** (the interphase) whose mean thickness was either 0.1 or 1 μm. The related 1D-SiC/C/SiC composites will be futher referred to as **material A** (interphase thickness : 0.1 μm) and **material B** (interphase thickness: 1 μm). The reinforcement orientation and surface treatment of the samples of A and B (3 x 3 x 10-13 mm^3) are shown schematically in fig. 1. The samples were either uncoated or partially coated with a layer of SiC (about 60 μm in thickness). **Uncoated** specimens have had all their faces ground so that oxidation could take place through all the specimen sides. Besides, the specimens were cut and machined with the fibers axis being either parallel (//) or perpendicular (⊥) to the larger length of the specimens (fig. 1a, b). **Coated** specimens (referred to as A_c and B_c) were elaborated by submitting the surface machined specimens to an additionnal CVD step in order to seal the remaining open porosity and to protect the fibers and interphases with a rather thick layer of SiC. Subsequently, two opposite faces of the specimens were surface machined so that oxidation could take place mainly along one single direction, i.e. parallel to the fiber axis (fig. 1c).

2.2 - Oxidation tests and material characterization

Thermogravimetric analysis (TGA)(**) was used to record continuously the variations of the relative mass change ($\Delta m/m_o$, with $m_o \approx 0.3$ g) versus

(**) TAG 24 S16 TGA APPARATUS FROM SETARAM (sensitivity : 10^{-6} g)

time as the sample was heated from room temperature to the test temperature T and then maintained isothermally at T. In order to separate properly the temperature effect from the chemical effect (i.e. due to reaction between the sample and the atmosphere), TGA experiments were first run in helium (P = 100 kPa) with a constant heating rate of 10°C per min. up to a maximum temperature of 1800°C. In that case, the crucible and the tube were in graphite and temperature was measured with a W-Re/W-Re thermocouple. Oxidation tests were conducted at a constant temperature T (with 700°C < T < 1500°C) for a duration of 10 hours, with high purity alumina tube and sample holder. Temperature was measured in this case with a Pt/Pt-Rh10% thermocouple, the heating rate being either 30 or 60°C per min, up to the test temperature T. Most of the experiments have been performed in a flow of dry oxygen (P = 100 kPa ; oxygen flow rate : 1 l per hour)(*). However, a few tests were also conducted in air (P = 100 kPa) as well as under a static atmosphere of pure oxygen (P = 1 - 5 kPa).

The materials have been characterized in terms of **density** (by mass versus volume measures), **residual open porosity** (using a mercury porosimetry technique)(**) and **specific surface area** (according to the BET-technique : Kr adsorption). The microstructural change occurring during the oxidation treatments have been characterized by optical microscopy, scanning/transmission **electron microscopy** and **cathodoluminescence**. The latter technique was used to assess the formation of silica in the materials (silica exhibits a characteristic blue luminescence at $\lambda \approx 450$ nm when irradiated with an electron beam) [20]. Finally, the presence or absence of

---

(*) pure oxygen (ref. N 48) from Alphagaz (H_2O : < 2 ppm)

(**) model 9200 from Micromeritics

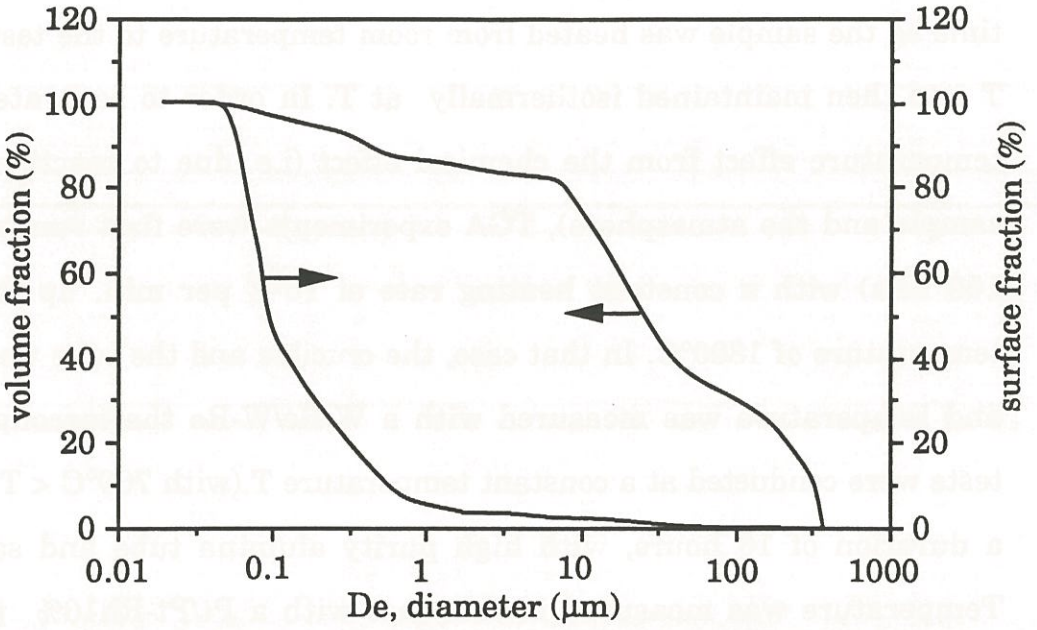

Fig 2: Cumulative distribution of open porosity and surface in as received material B_c as measured by mercury porosimetry

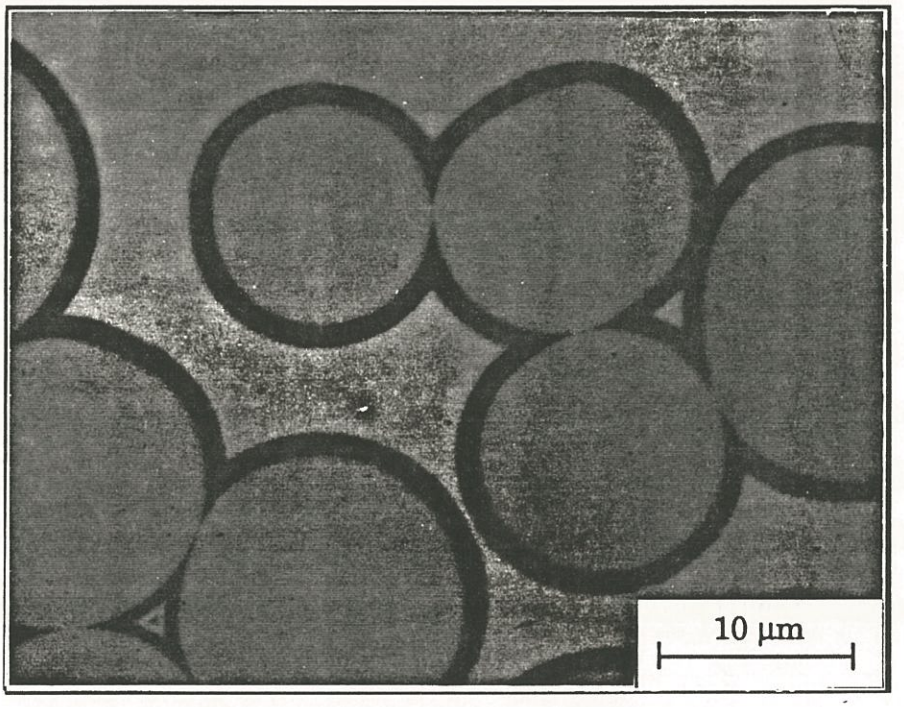

Fig. 3: SEM micrograph under (backscattered electron imaging mode) of material B.

carbon interphases in the samples, after the oxidation tests, has been evidenced by electrical conductivity measurements.

3 - RESULTS

3.1 - Characterization of as-received materials

The main physical properties, i.e. density, open porosity and specific area of the uncoated and partially coated materials, are listed in table I. Both mass/volume measurements and mercury porosimetry data yield close apparent density values. The open porosity which stands just below 20 % for the uncoated materials, falls to about 6-8 % for the partially coated materials owing to the fact that a large fraction of the residual open pores were sealed by SiC during the additional CVD step. Specific surface area measurements performed by both mercury porosimetry and BET methods lead to similar values which are below 0.1 $m^2\ g^{-1}$.

The cumulative distribution of the open porosity and specific surface area, as measured by mercury porosimetry, is shown in fig. 2, for material B_c. Two populations of pores are observed : (i) a population of pores whose equivalent pore diameters, De, are of the order of several hundreds of μm and (ii) a population of pores with $6 < De < 40$ μm. It is worthy of note that the contribution of the very small pores ($De < 0.1$ μm) to the specific surface area is very important.

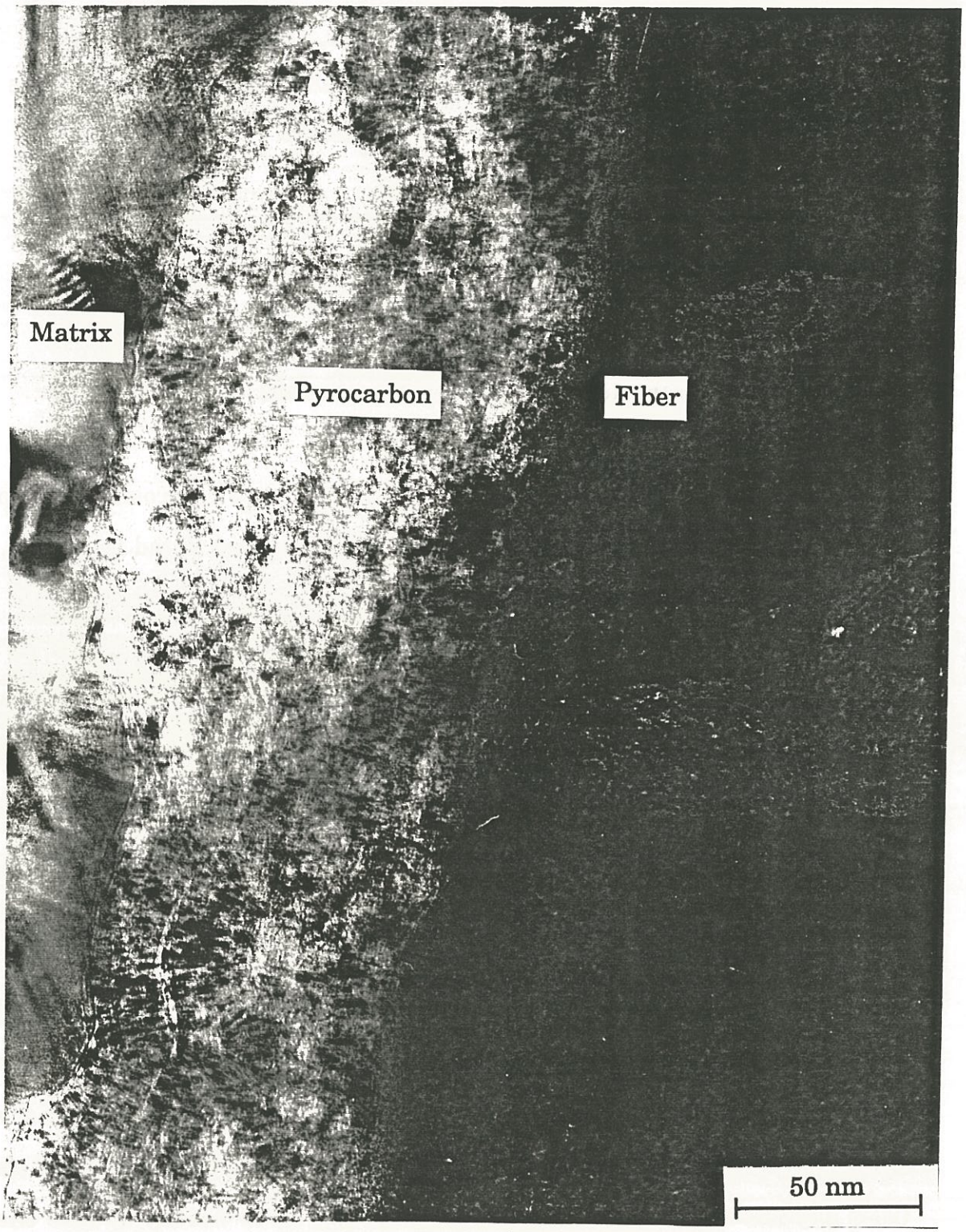

Fig. 4 : TEM micrograph (bright field) of material A (as received).

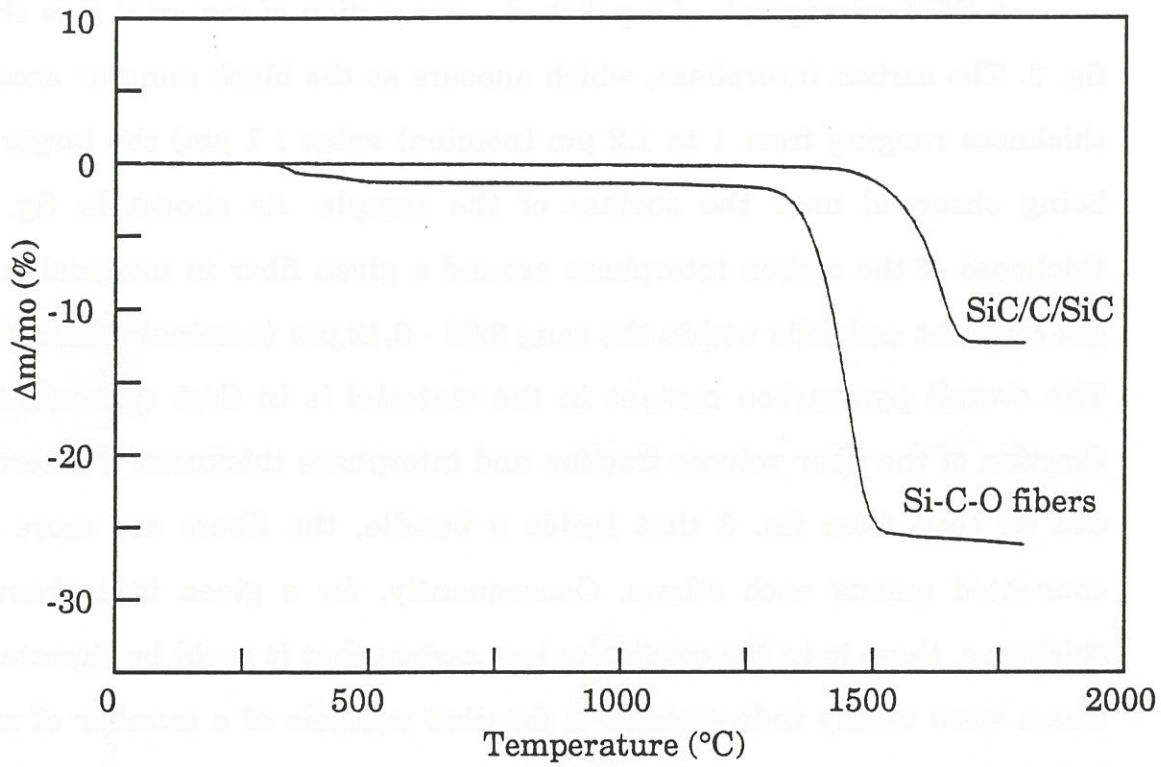

Fig. 5 : Continuous relative mass change Δm/mo as a function of temperature for ex-PCS Si-C-O fibers and a SiC/C/SiC composite under flowing helium (heating rate : 10°C min-1).

A SEM-micrograph of a polished cross-section of material B is shown in fig. 3. The carbon interphase, which appears as the black annular area, has a thickness ranging from 1 to 1.2 μm (nominal value : 1 μm) the larger values being observed near the surface of the sample. As shown in fig. 4, the thickness of the carbon interphase around a given fiber in material A is also not constant and falls within the rang 0.08 - 0,12 μm (nominal value : 0.1 μm). The overall pyrocarbon content in the material is in first approximation, a function of the fiber volume fraction and interphase thickness. Futhermore, it can be seen from fig. 3 that inside a bundle, the fibers are more or less connected among each others. Consequently, for a given interphase mean thickness, there is in the composite less carbon that it could be expected if the fibers were totally independent. A detailed analysis of a number of material polished cross-section has allowed to establish that each fiber has an average of two points of contact with surrounding fibers. From this feature, it has been calculated that the carbon interphase volume fractions were 1.1 % for material A and 9.7 % for material B (appendix 1). Finally, the optical activity of the thick carbon interphase (1 μm) was measured to be of the order of 10° which suggests that the pyrocarbon deposit has, in this case, a smooth laminar microstructure [21].

3.2 - Thermogravimetric analyses in an inert atmosphere

The TGA curves corresponding to an uncoated SiC/C/SiC composite (material A) and ex-PCS Si-C-O fibers (for purpose of comparison) heated up to 1800°C in helium (heating rate : 10°C per min.) are shown in fig. 5. Both materials exhibit a similar behavior : (i) a wide plateau extending from room temperature to a high temperature Td and (ii) an important weight loss beyond

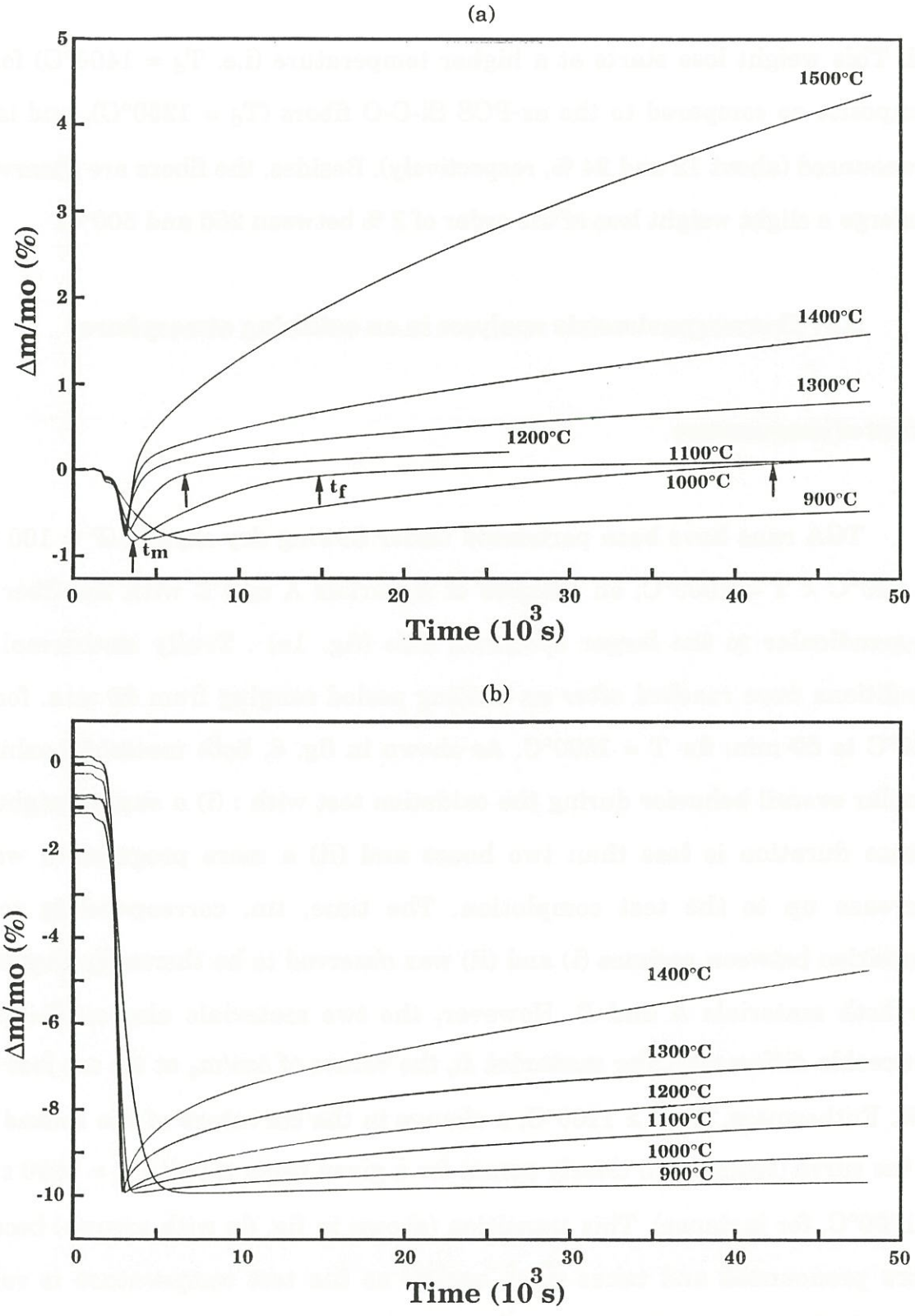

Fig. 6 : Variations of the relative mass Δm/mo as a function of time for uncoated materials with fiber axis perpendicular to the larger length under flowing oxygen (P=100 kPa): (a) material A (e = 0.1 μm) (b) material B (e = 1 μm).

Td. This weight loss starts at a higher temperature (i.e. T_d = 1400°C) for the composite as compared to the ex-PCS Si-C-O fibers (T_d = 1250°C), and is less pronounced (about 12 and 24 %, respectively). Besides, the fibers are observed to undergo a slight weight loss of the order of 2 % between 250 and 500°C.

3.3 - Thermogravimetric analyses in an oxidizing atmosphere

Effect of temperature

TGA runs have been performed under flowing dry oxygen (P = 100 kPa) at 900°C < T < 1500°C, on samples of materials A and B with the fiber axis perpendicular to the larger specimen side (fig. 1a) . Trully isothermal test conditions were reached after an heating period ranging from 30 min. for T = 900°C to 50 min. for T = 1500°C. As shown in fig. 6, both materials exhibit a similar overall behavior during the oxidation test with : (i) a sharp weight loss whose duration is less than two hours and (ii) a more progressive weight increase up to the test completion. The time, tm, corresponding to the transition between regimes (i) and (ii) was observed to be thermally dependent for both materials A and B. However, the two materials also exhibit some noticeable differences. For **material A**, the values of $\Delta m/m_0$ at tm are less than 1 %. Futhermore, for T ≥ 1100°C, a change in the curvature of the second part of the curve (regime (ii)) clearly occurs for a given time, tf (with t_f = 7500 s at T = 1200°C, for instance). This transition (shown in fig. 6a with arrows) becomes more pronounced and takes place earlier as the test temperature is raised. Beyond tf, the general trend in the $\Delta m/m_0 = f(t)$ variations is still a weight increase but with a much lower rate. For **material B**, the weight loss values (regime (i)) are much higher (reaching 10 %) and no change in the oxidation

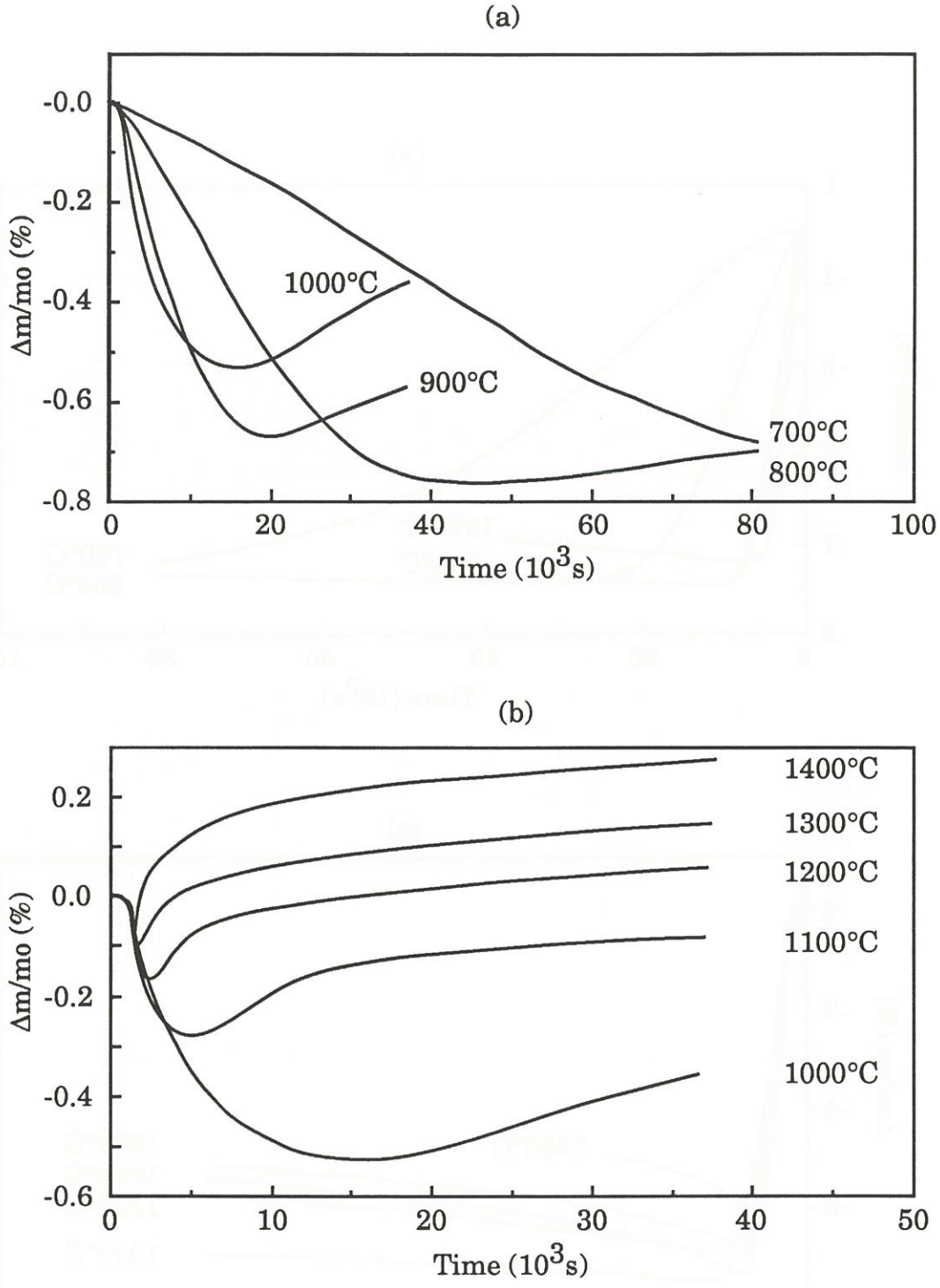

Fig.7 : Variations of the relative mass Δm/mo as a function of time for materials A_C in flowing oxygen (P = 100 kPa) at different temperatures : (a) 700 °C< T < 1000°C ; (b) 1000°C < T < 1400°C.

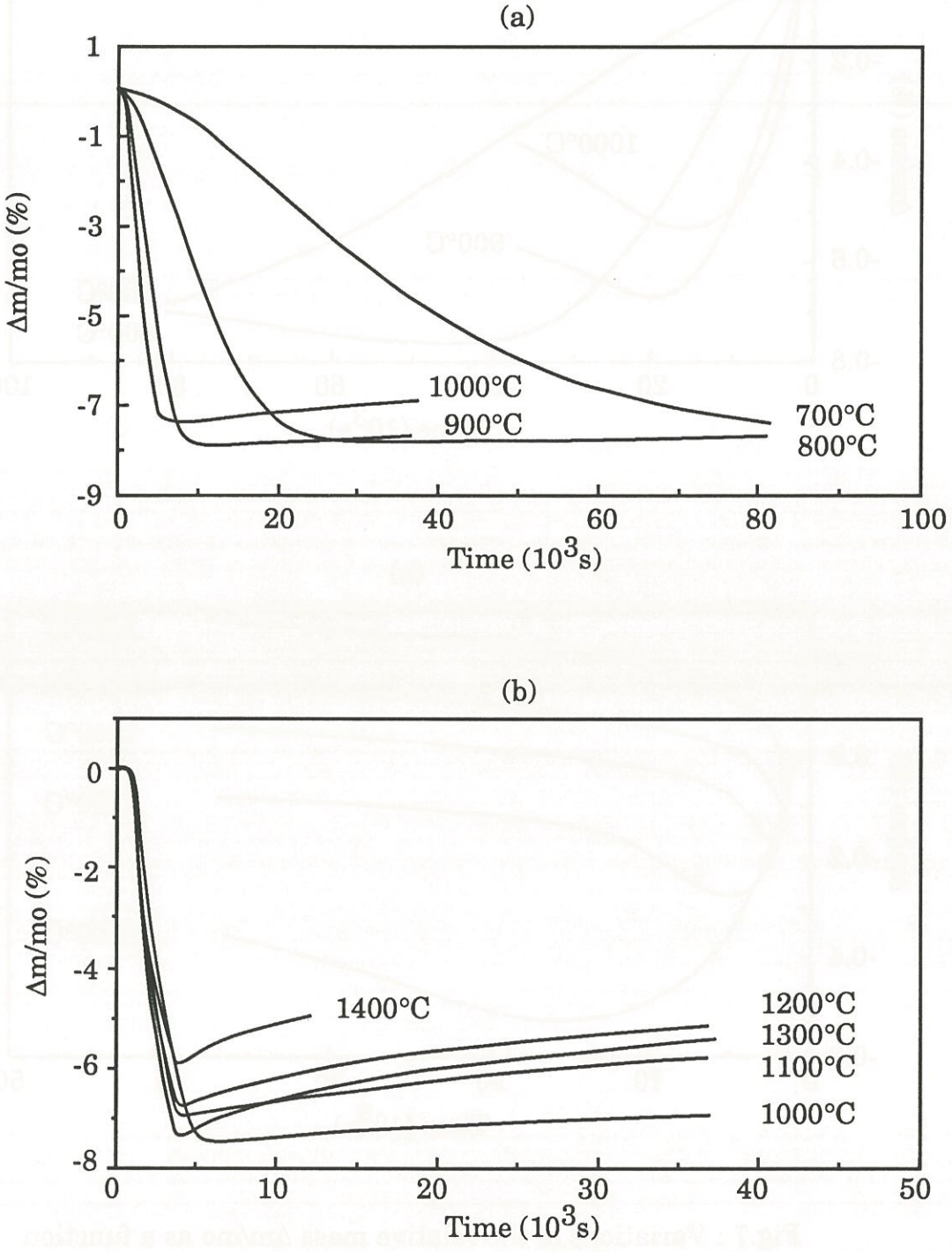

Fig. 8 : Variations of the relative mass Δm/mo as a function of time for materials B_c in flowing oxygen (P = 100 kPa) at different temperatures : (a) 700 °C< T < 1000°C ; (b) 1000°C < T < 1400°C.

kinetics is observed in regime (ii). In this case of material B, it should be mentioned that the $\Delta m/m_0 = f(t)$ curves have been translated along the y-axis to let their minima lie on the same horizontal (fig. 6b).

Fig. 7 and 8 show the effect of the oxidation test temperature (700°C < T < 1400°C) on the $\Delta m/m_0 = f(t)$ curves, for the partially coated **materials A_c and B_c**. The heating rate used to reach the test temperature was in this case 60°C per min. Temperature has a strong effect on the weight loss rate for 700°C < T < 1000°C whereas its effect is not significant for high temperature tests (1000°C < T < 1400°C). For **material A_c**, the weight loss clearly decreases when temperature is raised, i.e. from about 0.8 % for T = 800°C to less than 0.1 % for T = 1400°C. As for the uncoated materials, a transition is observed at t_f in the oxidation kinetics in regime (ii) which takes place earlier when the test temperature is raised. For **material B_c**, the weight loss is close to ~ 7 % whatever the temperature except for T = 1400°C where it is slightly below 6 %.

Effect of oxygen flow rate

The effect of the oxygen flow rate has been investigated on samples B_c at T = 1000°C. The results of the test have shown that an increase of the oxygen flow rate from 1l/hr. to 10 l/hr. did not result in any change in the $\Delta m/m_0 = f(t)$ curve.

Effect of atmosphere composition and pressure

The influence of the test atmosphere on the oxidation kinetics was studied on samples of materials A and B (with the fiber axis perpendicular to

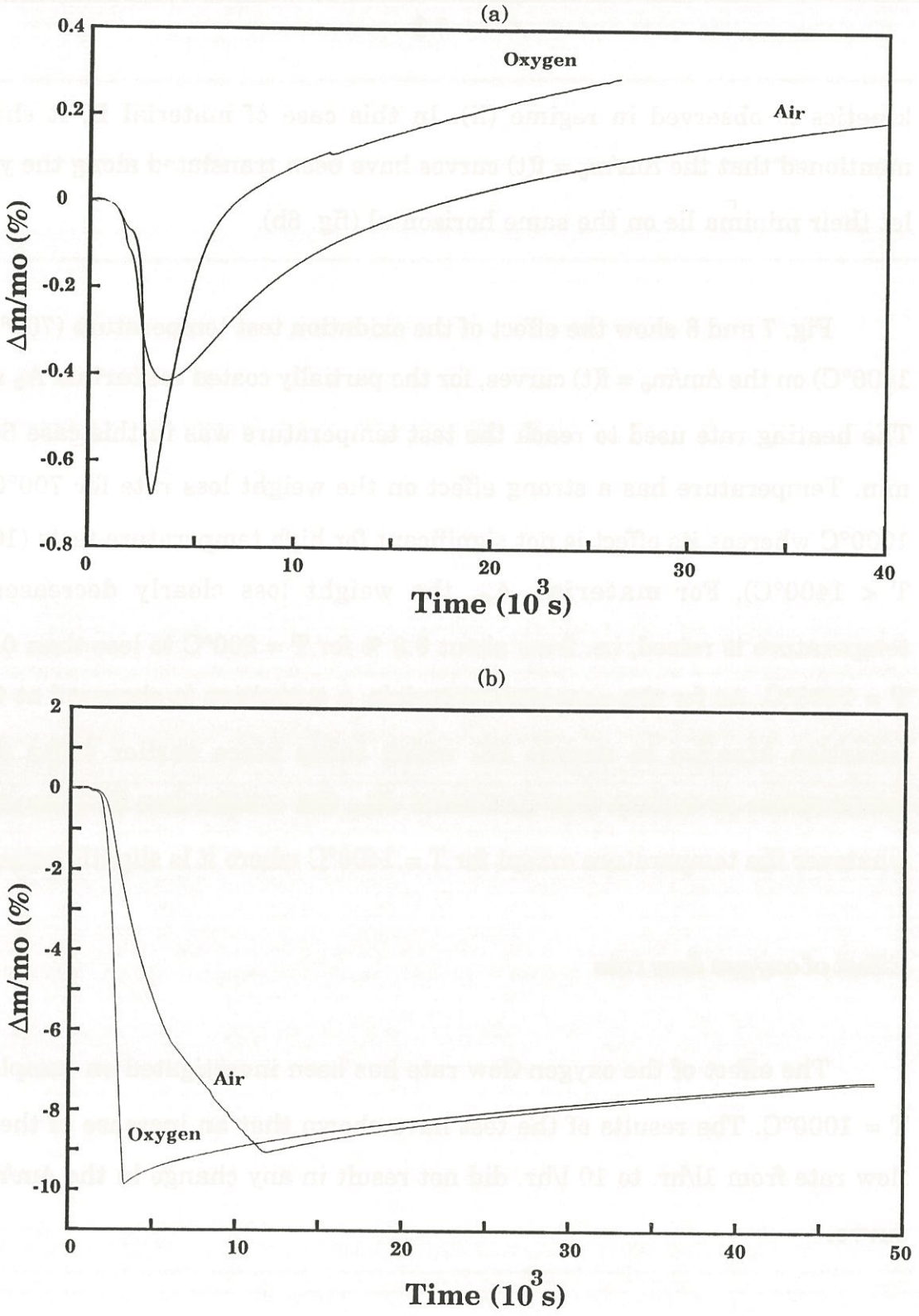

Fig. 9 : Influence of the atmosphere on the variation of the relative mass Δm/mo as a function of time at T = 1200°C, P = 100 kPa for material A (e = 0.1 μm) (a) and material B (e = 1 μm) (b).

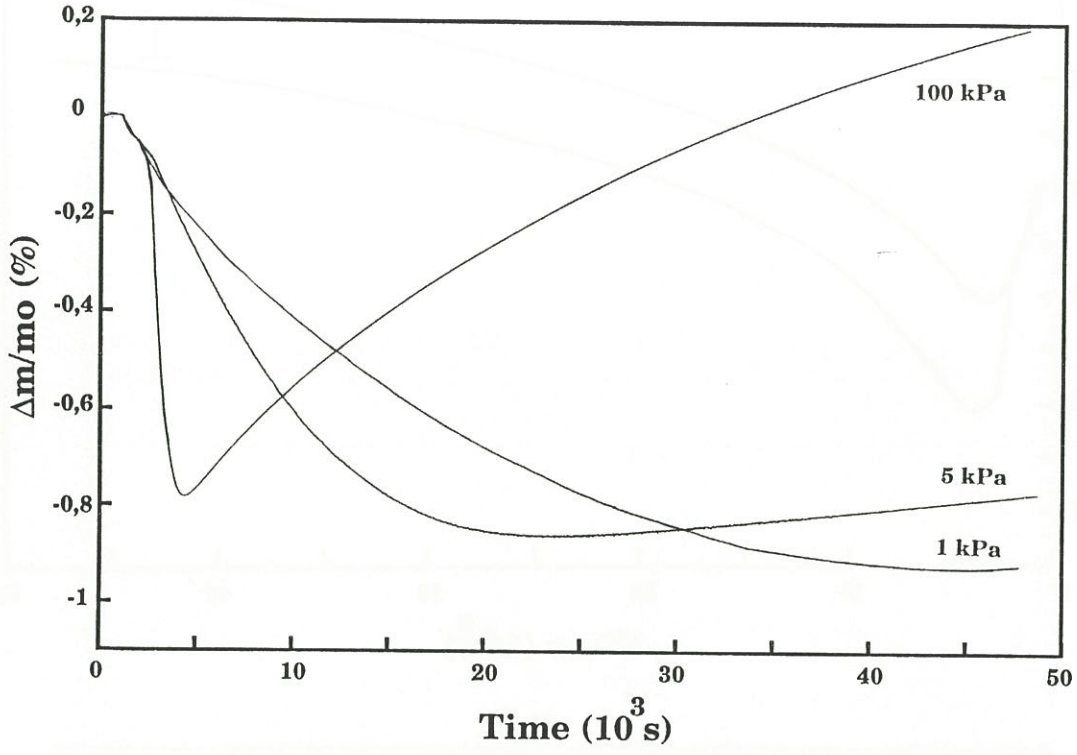

Fig. 10 : Influence of the total pressure on the variation of the relative mass Δm/mo as a function of time at T = 1000°C in oxygen for material A (e = 0.1 μm).

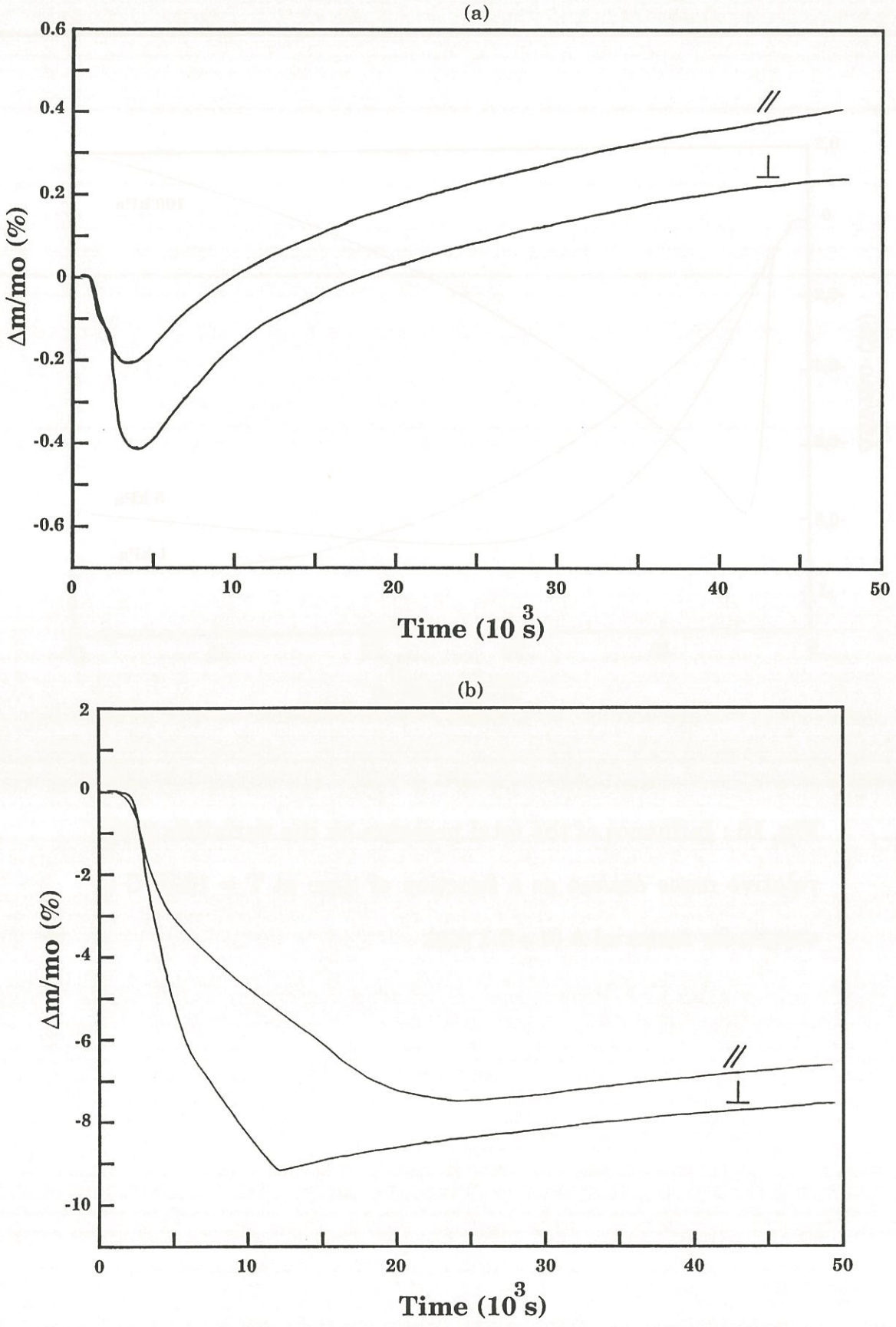

Fig. 11 : Influence of fiber orientation on the variation of the relative mass Δm/mo as a function of time at T = 1200°C, in air, P = 100 kPa for material A (e = 0.1 μm) (a) and material B (e = 1 μm) (b).

the larger specimen face). The tests were run at T = 1200°C under flowing dry oxygen or air at P = 100 kPa. Experiments were also performed at T = 1000°C under an atmosphere of dry oxygen at various pressures (static conditions) but only for materials A. The results of these tests are shown in fig. 9 and 10.

Switching from oxygen to air results mainly in a decrease in the weight loss rate. Therefore, the transition from regime (i) to regime (ii) is not as well apparent for tests run in air as it is when oxygen is used (fig. 9). In the same manner, the weight loss rate is strongly reduced when the oxygen pressure is lowered from 100 kPa to 1 kPa for the tests run under static conditions (fig. 10).

Effect of fiber orientation

Oxidation tests have been performed on materials A and B in which the fiber were oriented either parallel or perpendicular to the larger specimen face (fig. 11a, b), at T = 1200°C and P = 100 kPa in air. For material A, the weight loss is slightly reduced when the fiber orientation is changed from the ($\perp$) to the (//) configurations (i.e. from 0.2 % to 0.4 %) whereas, for materials B, the main feature is a change in the weight loss rate. Conversely, the weight increase kinetics (regime (ii)) are almost the same for the two fiber orientations, for both materials A and B.

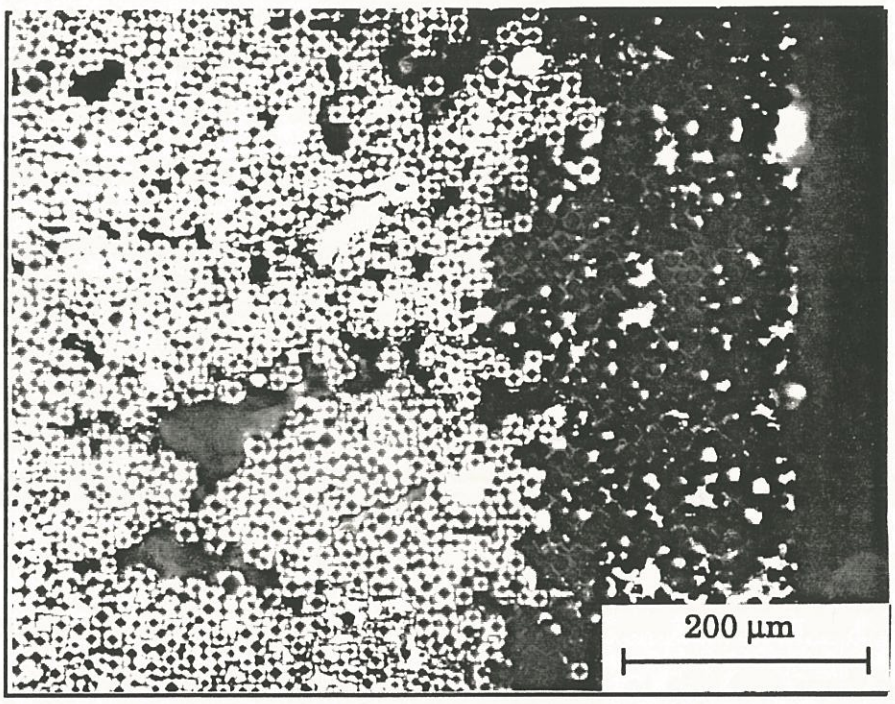

Fig. 12 : Optical micrograph in polarized light of a polished cross section of material B oxidized in air at P = 100 kPa and T = 1200°C (heating time + 10 min).

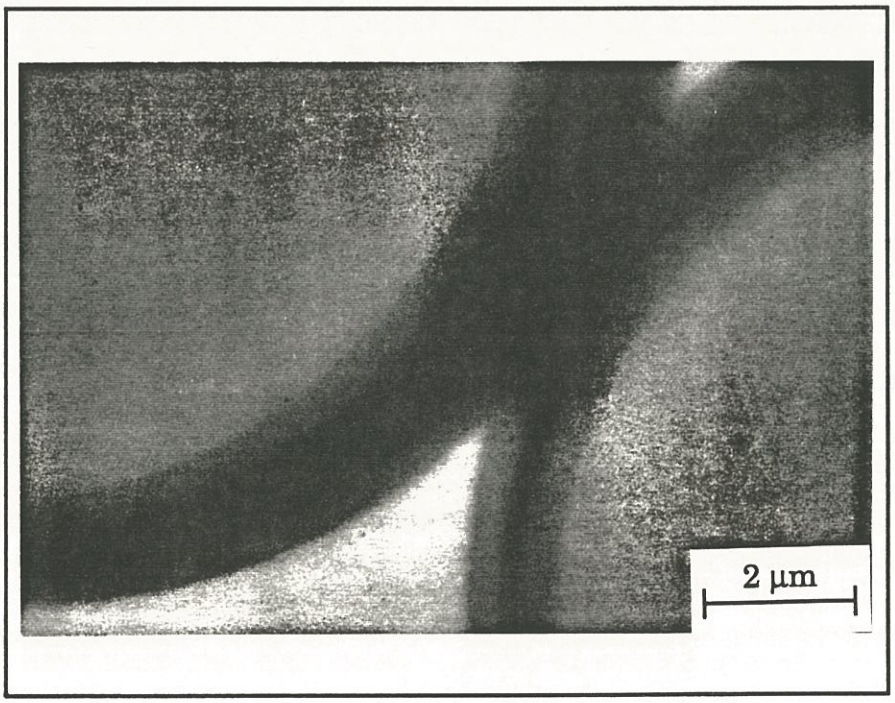

Fig. 13 : SEM micrograph (backscattered electron imaging mode) of a polished cross section of material B oxidized in flowing oxygen (P = 100 kPa, T = 1200°C, t = 10 hours).

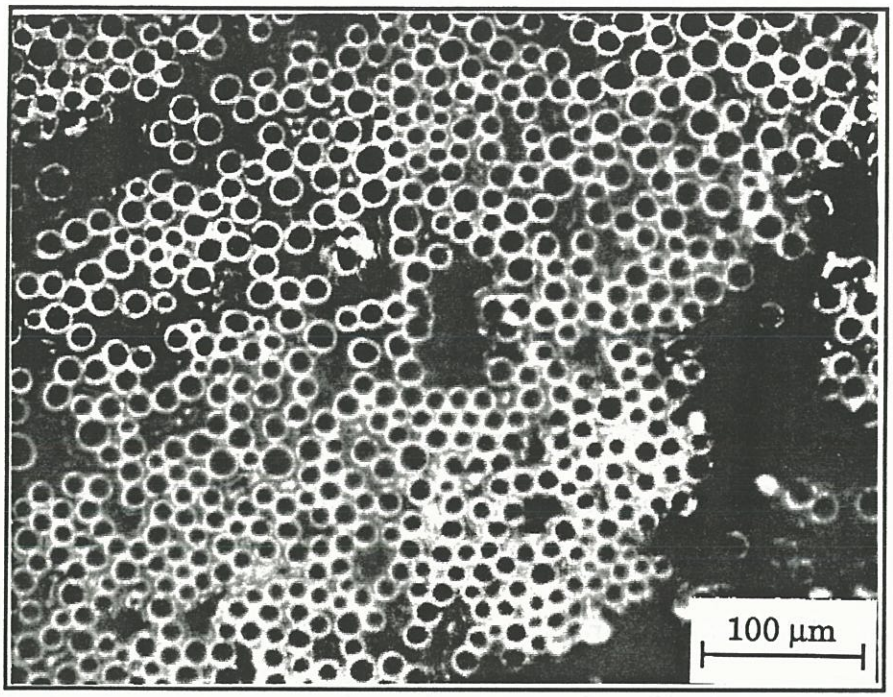

Fig. 14 : Cathodoluminescence of a polished cross section of material B oxidized in air (P = 100 kPa ; T = 900°C, t = 140 hours).

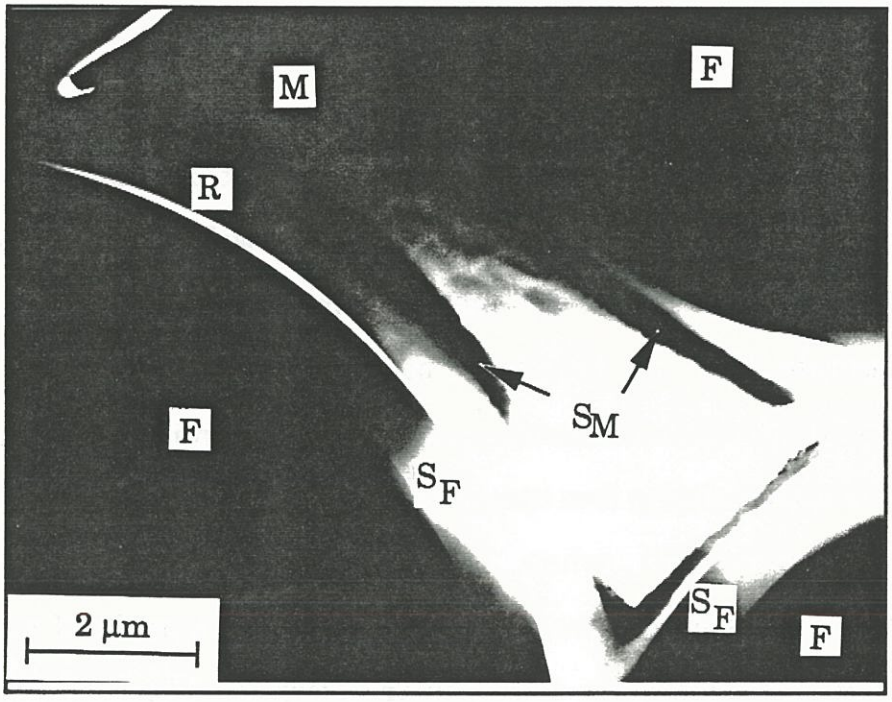

Fig 15 : TEM micrograph (bright field) of material B oxidized in oxygen (P = 100 kPa ; T = 1300°C, t = 10 hours): F = fiber; M = emplacement of the matrix; S_F = silica on the fiber; S_M = silica on the matrix; R = embedding resin.

3.4 - Morphological analysis of the oxidized materials

Uncoated materials

Optical and SEM observations were first performed on materials with a thick interphase (material B) in order to assess the effect of the oxidation treatment on each constituent of the composite, i.e. the ex-PCS Si-C-O fibers, the SiC CVI-matrix and the carbon interphase. As shown in fig. 12, the pyrocarbon interphase is easily detected in polarised light. It clearly appears that oxidation has partly consumed the carbon interphase : the oxidation reaction front has started from the sample surface and then has moved in-depth along a direction perpendicular to that surface (i.e. perpendicular to the fiber axis in this particular sample).

As the thick carbon interphase is consumed, annular pores are formed within which both the fibers and matrix are in turn submitted to oxidation. As a result, a thin layer of oxide is formed on the wall of the pores (i.e. on both the Si-C-O fiber surface and SiC matrix), appearing as deep-grey phase in SEM-micrographs (fig. 13). This layer of oxide has been assigned to silica on the basis of both cathodoluminescence and transmission electron microscopy (TEM)/electron energy loss spectroscopy (EELS). Silica is known to give rise to a blue luminescence when irradiated with an electron beam. The cathodoluminescence micrograph of an oxidized sample of material B, shown in fig. 14, clearly reveals the annular layers of silica which have been formed around the fibers after the oxidation of the thick carbon interphases. The oxide layers formed on both the fiber and matrix sides of the annular pores are also

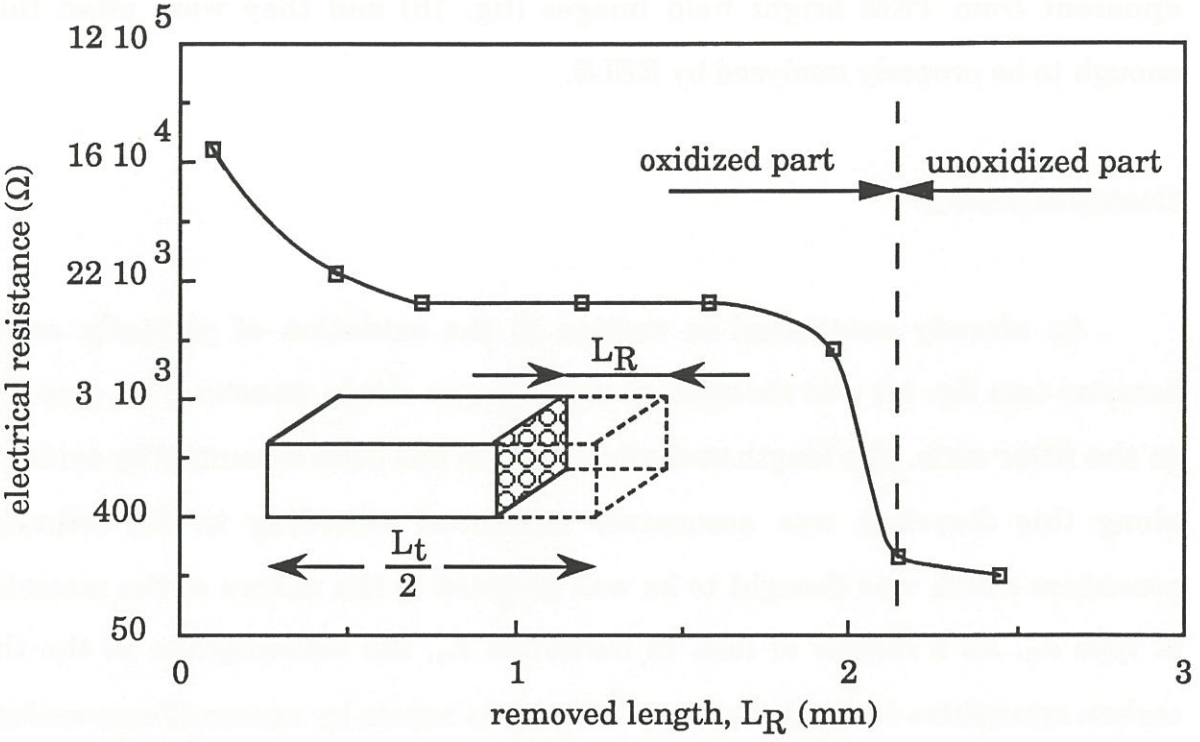

Fig. 16 : Ohmic resistance versus removed length l_R for an A_c material oxidized in oxygen (P = 100 kPa ; T = 1200°C, t = 10 hours).

Temperature (°C)	**900**	**1000**	**1100**	**1200**	**1300**
L_R, length over which carbon is oxidized (mm)	> 6.5	> 6.6	3.4 ± 0.2	2.2 ± 0.2	1.5 ± 0.2

Table II: Lengths over which carbon is oxidized for A_c specimens oxidized in oxygen (P = 100 kPa, t = 10 hours) as a function of test temperature.

apparent from TEM bright field images (fig. 15) and they were often thick enough to be properly analysed by EELS.

Coated materials

As already mentioned in section 2, the oxidation of partially coated samples (see fig. 1c) was thought to occur in one single direction, i.e. **parallel to the fiber axis**. The length over which carbon has been consumed by oxidation along this direction was accurately measured according to the following procedure which was thought to be well adapted to the nature of the materials of type A_c. As a matter of fact, in materials A_c, the consumption of the thin carbon interphase by oxidation was not easy to assess by means of conventional microscopy methods. Since pyrocarbon was known to exhibit a rather high electrical conductivity as compared to both SiC ans silica, **ohmic resistance measurements** were used to determine quantitatively the thickness of that part of the sample in which the carbon interphase has been consumed. First, the sample was cut in the middle. Then, the measurements were performed between two opposite faces, perpendicular to the fiber axis (fig. 1c), of an A_c sample previously oxidized 10 hours at T = 1200°C, one of these faces being ground between two successive measurements in order to remove progressively the oxidized part. Fig. 16 shows one example of the variations of the ohmic resistance as a function of the thickness L_R of material removed by grinding. A sharp transition takes place at the level of the oxidation front which is thus accurately located in the sample. The values of L_R measured for 900°C < T < 1300°C are listed in table II. They clearly show that L_R in the materials of type A_c decreases as the test temperature is raised. Conversely, the measurements performed under similar conditions on materials of type B_c

(a)

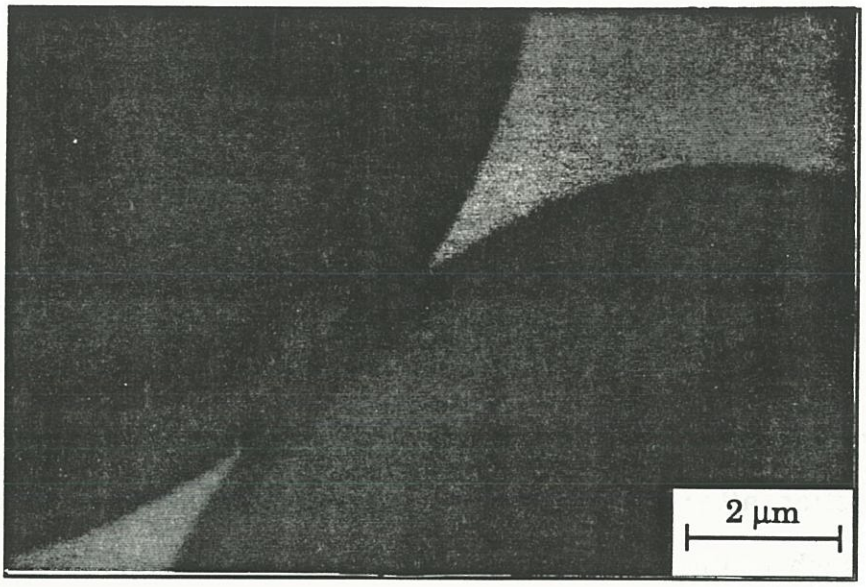

(b)

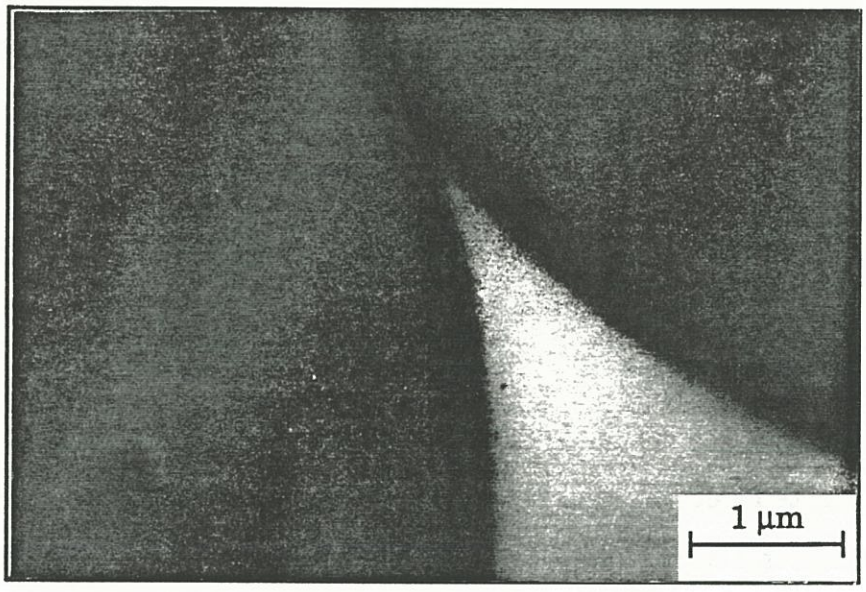

Fig. 17 : SEM micrographs (backscattered electron imaging mode) of polished cross sections of material A_C oxidized in oxygen (P = 100 kPa, T = 1200°C, t = 10 hours): (a) very near the external surface, (b) at a distance of 1 mm from the surface.

have shown that the carbon interphase was totally consumed after 10 hours of oxidation treatment for test temperature ranging from 900°C to 1300°C.

In oxidized samples of **material A_c**, the degree of filling of the annular pore (resulting from the consumption of the thin carbon interphase) by silica depends on the distance from the pore entrance, at a given test temperature. Near the specimen surface, silica was observed to fill totally the annular pore cross-section after an oxidation treatment of 10 hours at 1200°C in oxygen. Under such conditions, silica appears as a continuous deep-grey ring (≈ 0,3 μm in thickness) between the Si-C-O fiber and the SiC CVI-matrix, as shown in fig. 17a. At a distance of 1 mm from the sample surface, two distinct silica layers are already present in the annular pore as shown in fig 17b, that formed on the fiber surface (≈ 0.2 μm in thickness) being thicker than that formed on the pure SiC-matrix. Very similar features were observed after an exposure of 10 hours at 1000°C in oxygen, namely : (i) a single silica layer (≈ 0.3 μm thick) filling the entire annular pore cross section near the specimen surface and (ii) two distinct silica layers separated by a residual pore in cross-section located in the middle of the specimen (i.e. at about 6.6 mm from the specimen surface), the silica layer on the fiber surface being thicker than that formed on the matrix side. On the other hand, no difference was observed between cross section located near the surface or in the middle of the specimen for **material B_c** in which the thickness of the initial carbon interphase and thus the width of the annular pore are much larger (i.e. 1 μm). As shown in fig. 13, the silica layers formed on the fibers and on the matrix after an exposure of 10 hours in oxygen at T = 1200°C, have almost the same thickness and are separated by a rather large residual pore.

(a)

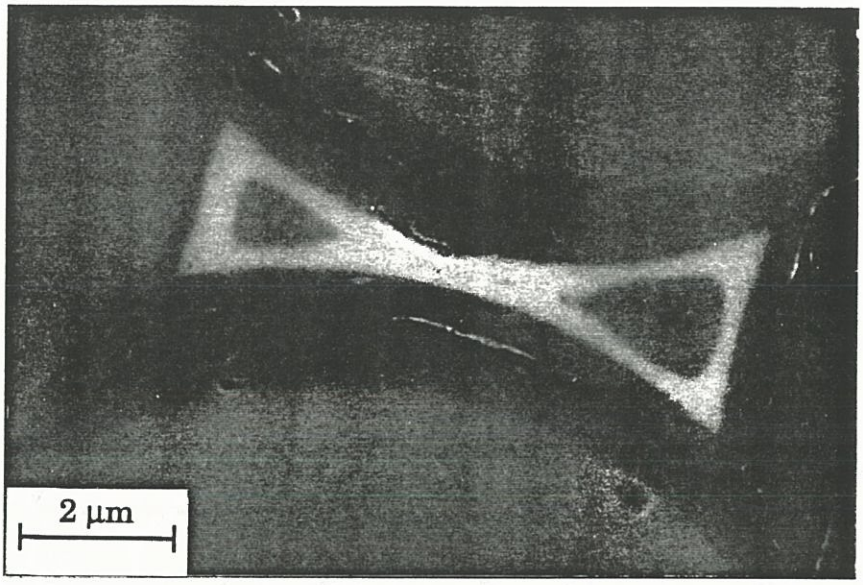

(b)

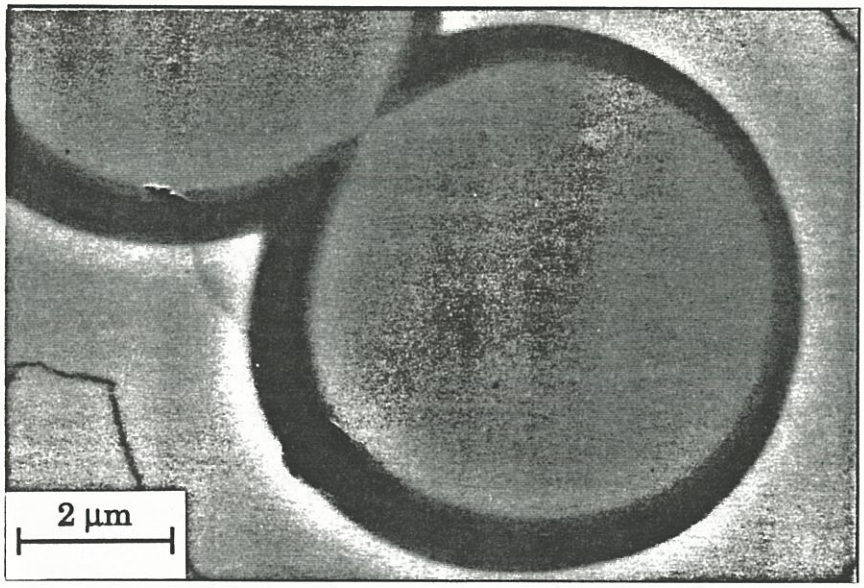

Fig. 18 : SEM micrographs (backscattered electron imaging mode) of polished cross sections of material B_c after an exposure of 10 hours in oxygen (P = 100 kPa) at T = 1200°C : (a) very near the specimen surface and (b) from the bulk.

(a)

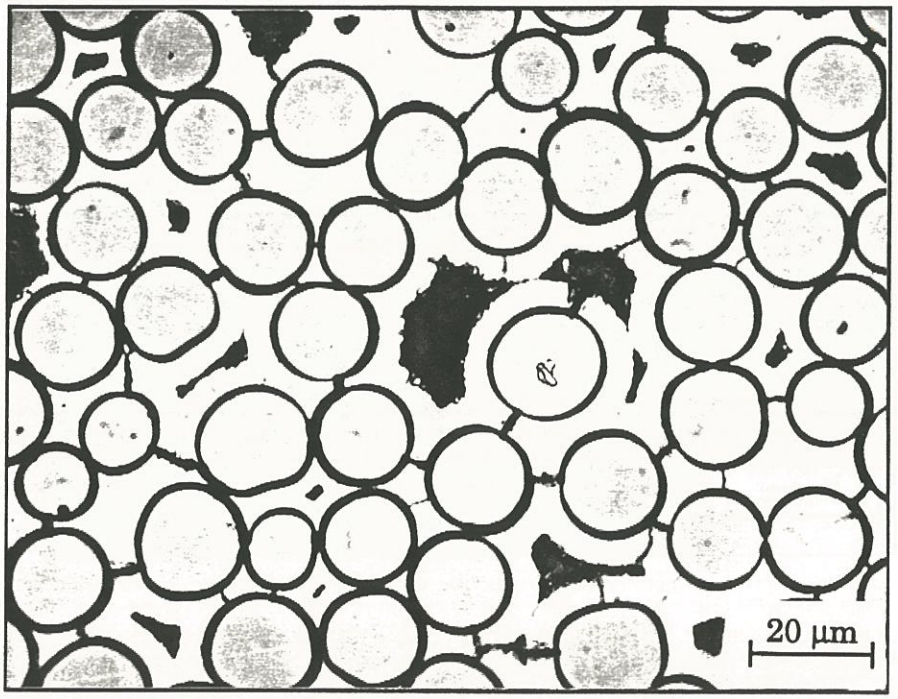

(b)

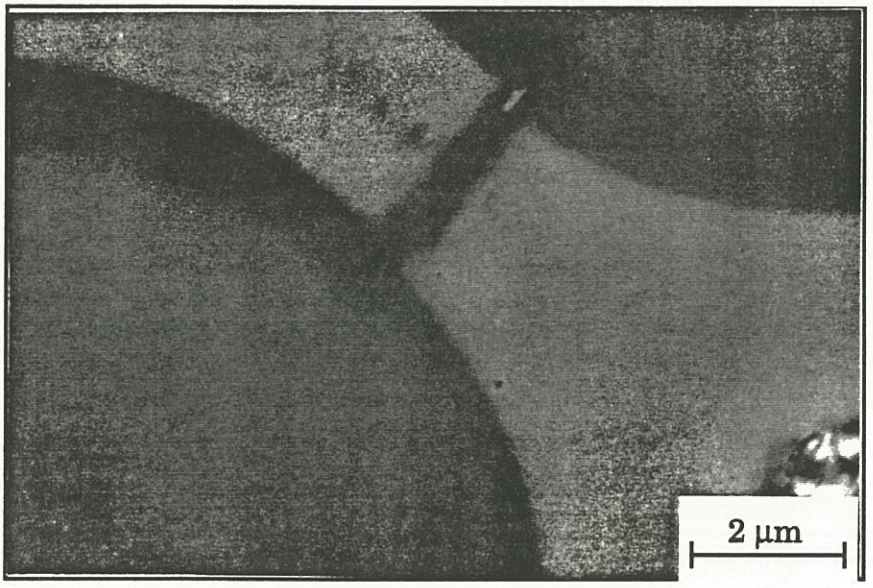

Fig. 19a, b : Optical micrographs of polished cross sections of 1D-SiC/C/SiC composites after an exposure of 300 hours in air (P = 100 kPa) at 900°C : (a), (b) material A

(c)

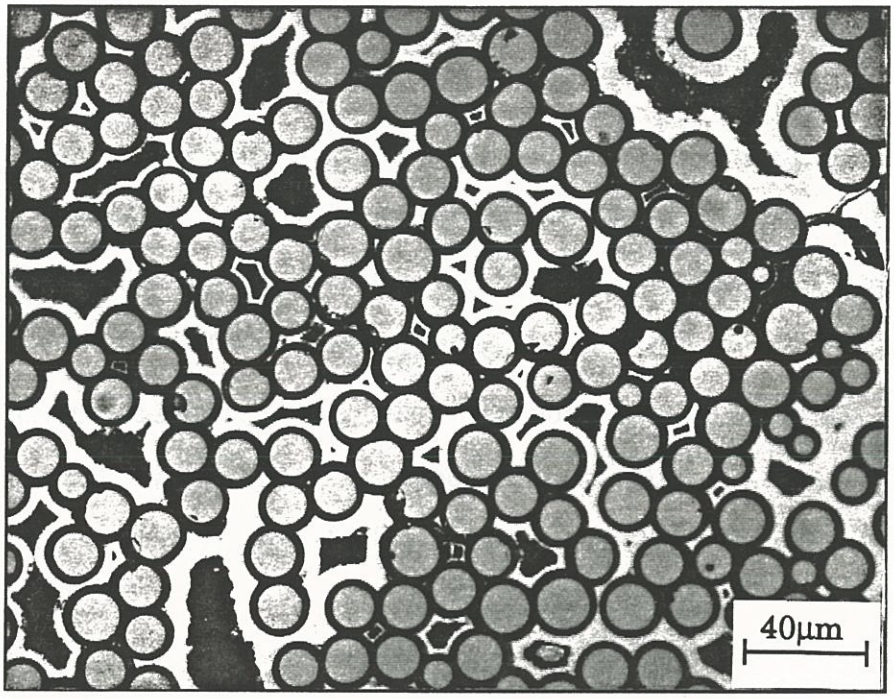

Fig. 19 c : Optical micrograph of polished cross section of 1D-SiC/C/SiC composites after an exposure of 300 hours in air (P = 100 kPa) at 900°C : (c) material B

Additional morphological features

The growth of the silica layers takes place not only at the fiber/matrix interfaces when the carbon interphase has been consumed by oxidation, as already discussed, but also on the wall of the open pores actually present in ceramic matrices infiltrated according to the CVI-process [19]. An example of such a dog-bone cross section pore, with its inner silica coating is shown in fig. 18a (note that the left part of the pore has been totally filled with silica whereas the right part, which was of a slightly larger size, still contains a residual porosity.

As shown in fig. 18b, the removal of the carbon interphase in material B usually debonds the fibers from the matrix. Moreover, since the width of the annular pore is here rather large ($\approx$ 1 μm), a given fiber may move off axis.

Finally, after a long exposure in air at 900°C, a 1D-SiC/C/SiC composite with a thin interphase (material A) was observed to exhibit : (i) thicker silica layers at the fiber/matrice interfaces as it could be expected and, more interestingly (ii) numerous **microcracks** between adjacent fibers or between a fiber and a residual matrix pore (fig. 19a). Some of these microcracks appear to be totally filled with silica and a preferential oxidation of the fiber may be observed at the extremity of the cracks (fig. 19b). On the contrary, after the same oxidation treatment, such microcracks were not observed in the composites with the thick carbon interphase (material B) (fig. 19c). It is worthy of note that no microcracks were formed in both materials A and B when the oxidation treatments were performed at higher temperatures.

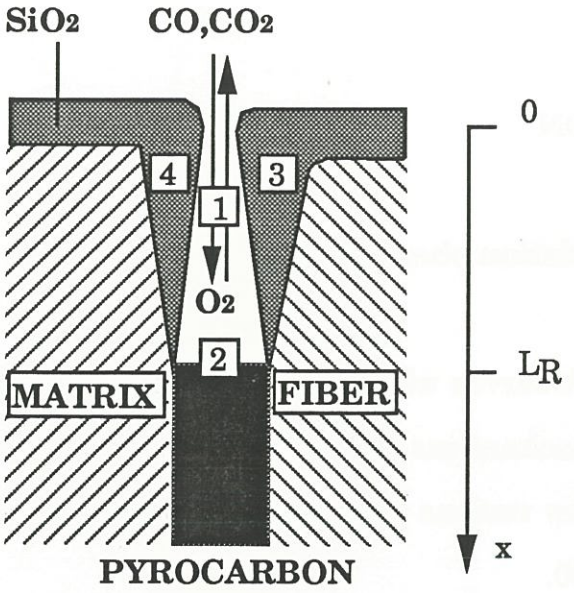

Fig. 20 : Schematic representation of SiC/C/SiC oxidation mechanisms (1) gas phase diffusion of oxygen in the pore, (2) reaction of oxygen with the carbon interphase, (3) diffusion of oxygen in SiO_2 and reaction with the fiber, (4) diffusion of oxygen in SiO_2 and reaction with the matrix.

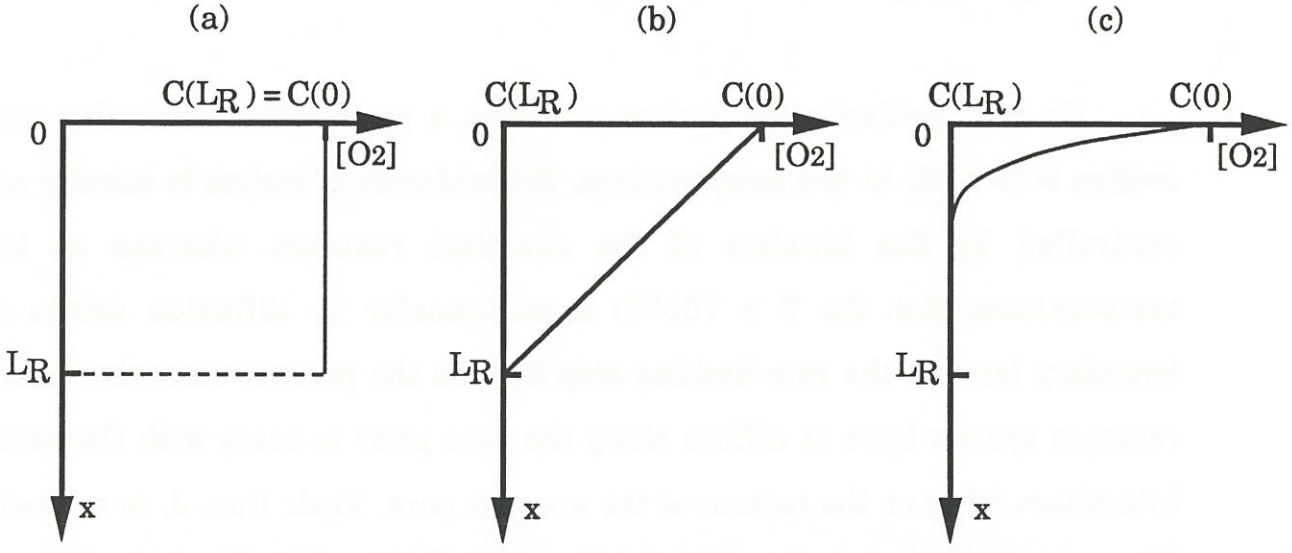

Fig. 21 : Schematic representation of expected oxygen concentration profiles for different conditions. The predominant mechanisms are: (a) reaction of oxygen with the carbon, (b) gaseous mass transport along the pore, (c) oxidation of the fibers and the matrix.

4 - DISCUSSION

4.1 - Oxidation phenomena

The TGA-curves which have been presented in section 3 obviously show that several mechanisms are present in the oxidation process of 1D-SiC/C/SiC composites. The various phenomena thought to take place are schematically shown in fig. 20.

(i)- The oxidation process is assumed to start with the **oxidation of the carbon interphase** giving rise to an evolution of gaseous carbon oxides according to the following equations :

$$C_{(s)} + O_{2\,(g)} \rightarrow CO_{2\,(g)} \quad (1)$$

$$2C_{(s)} + O_{2\,(g)} \rightarrow 2CO_{\,(g)} \quad (2)$$

As the gasification of carbon proceeds, a pore with an annular cross-section is formed. At low temperatures, the oxidation of carbon is usually rate-controlled by the kinetics of the chemical reaction whereas at high temperatures (i.e. for T > 700°C) mass transfer by diffusion across the boundary layer is the rate limiting step [22]. In the present case, the gaseous reactant species have to diffuse along the pore prior to react with the carbon interphase lying at the bottom of the annular pore. Their flux, J, is related to the concentration gradient along the pore dC/dx and to their diffusion coefficient D, according to the first Fick's law :

$$J = - D \frac{dC}{dx} \quad (3)$$

Taking into account the thickness of the carbon interphase and thus the width of the related annular pores, the gaseous species mass transfer along the pore is thought to occur with a contribution of both molecular diffusion regime (limited by collisions between molecules) and Knudsen diffusion regime (limited by collisions of molecules with the wall). The resulting effective diffusion coefficient is defined according to the following Bosanquet equation :

$$D^{-1} = D_M^{-1} + D_K^{-1} \quad (4)$$

where D_M is the molecular diffusion coefficient and D_K the Knudsen diffusion coefficient. The former is dependent on both the pressure P and temperature T [24] and the latter on temperature only [25], according to the two following equations :

$$D_M = \alpha T^{1.75} P^{-1} \quad (5)$$

$$D_K = \alpha' a T^{0.5} \quad (6)$$

where α and α' are coefficients and **a** is a characteristic dimension of the pore (i.e. its width).

(ii)- The ex-PCS Si-C-O fibers and the SiC CVI-matrix react also with oxygen leading to the formation, in the so-called passive oxidation regime, of both condensed and gaseous oxide species, i.e. SiO_2 and CO/CO_2 respectively. For pure SiC, the oxidation reaction can be depicted according to the two following equations [26]:

$$SiC_{(s)} + 2\,O_{2(g)} \rightarrow SiO_{2(s)} + CO_{2(g)} \quad (7)$$

$$SiC_{(s)} + 3/2\,O_{2(g)} \rightarrow SiO_{2(s)} + CO_{(g)} \quad (7')$$

Ex-PCS SiC, i.e. the residue resulting from the pyrolysis of an oxygen-cured polycarbosilane, is not pure silicon carbide. It has been recently described as a continuum of SiC-crystals (with a mean size of about 2.5 nm) and tetrahedral units SiC_xO_y (with $x + y = 4$) containing free aromatic carbon clusters surrounded by some hydrogen atoms, the oxygen content being of the order of 13 wt. % [27]. Nevertheless, it has been assumed that the oxidation of the ex-PCS Si-C-O fibers involves the same chemical reactions than those mentioned for pure SiC, the corresponding equations being characterized by different stoichiometric coefficients [28]. Finally, the growth of the silica layers on Si-based ceramics, is known to be rate-limited by diffusion of the reactant species in the scales (in the passive oxidation regime) and generally obey classical parabolic laws [26].

(iii)- In the oxidation process of 1D-SiC/C/SiC composites, there will be obviously a **competition** between the gas phase diffusion of oxygen along the annular pores resulting from the consumption of the carbon interphase, on one hand, and the chemical reaction (equations (7), (7')) taking place between oxygen and the pore walls (consisting of both ex-PCS Si-C-O fibers and SiC CVI-matrix), on the other hand. As shown schematically in fig. 21, various oxygen concentration profiles might be observed along the pore, depending on the result of that competition. If the chemical reaction kinetics are the rate-limiting step for the pyrocarbon oxidation and oxygen consumption by SiC and Si-C-O along the pore is low (i.e. at low temperatures), then a low oxygen concentration gradient is expected along the pore and the length of carbon

consumed would have little effect on the gasification rate of carbon (case (a)). Conversely, if the chemical reaction corresponding to the oxidation of carbon is very fast, then the oxygen concentration at the bottom of the pore (i.e. at $x = l_c$) will be nearly equal to zero and diffusion mass transfer along the pore would be rate controlling. As long as carbon is still present and being reacting with oxygen, the diffusion path lengths of the gaseous reactants (and products) would increase and, as a result, the carbon consumption rate would decrease as a function of time (case (b)). Finally, if the oxygen consumption by the pore walls (i.e. by SiC and Si-C-O) is high, than the oxygen residual flux near the bottom of the pore available for the oxidation of the pyrocarbon interphase might be reduced to low values (case (c)). In a given oxidation test, more than one of these cases might be involved as the carbon interphase is consumed.

External mass transfers have not been considered in the present analysis because of the small characteristic dimension of the annular pores (i.e. 0.1 or 1 μm). This choice is supported by the fact that the overall oxidation kinetics were observed not to depend on the oxygen gas flow for T = 1000°C ; P = 100 kPa and Q (O_2) ranging from 1 to 10 l per hour (as mentioned in section 3.3).

The growth of the silica layers on the pore wall results in a progressive decrease in the pore characteristic dimension (i.e. its width). When the pore becomes sealed by silica near the sample surface, the reactant would have to diffuse through a condensed phase, silica, before entering that part of the pore which is not yet filled with silica. This phenomenon would dramatically reduce the oxygen flux available for the in-pore chemical oxidation reactions.

Finally, it is worthy of note that the thermal dependence of the diffusion coefficients D_M and D_K (equations (5) and (6)) is lower than that of the parabolic rate constant corresponding to the oxidation of SiC which is known to obey an Arrhenius law (i.e. an $e^{-Ea/RT}$ temperature dependence). Thus, low temperatures would favor diffusion phenomena in the gas phase along the pore and oxidation in the bulk of the material whereas high temperatures are expected to enhance the oxidation of the carbide species from the pore wall and the near-surface oxidation of the composite. This feature is very similar to that previously reported for the oxidation process of reaction bonded silicon nitride [29].

4.2 - Thermogravimetric analyses

4.2.1 - Thermal stability of 1D-SiC/C/SiC composites

As shown in fig. 5, both the 1D-SiC/C/SiC composites and the ex-PCS Si-C-O fibers from which they have been prepared, undergo significant weight loss when they are heated in helium at high temperatures.

(i)- The small weight loss observed between 250 and 500°C for the **as-received ex-PCS Si-C-O fibers**, can be assigned to the pyrolysis of the organic sizing (i.e. polyvinyl acetate) [28]. The second and much more significant weight loss (i.e. ≈ 24 wt.%) occurring beyond 1250°C is related to a well established decomposition process of oxygen cured polycarbosilane precursors [30-31]. When temperature is high enough, the ternary SiC_xO_y phase is thought to undergo a decomposition/crystallization which yield an evolution of gaseous

oxides (namely SiO and CO) and a solid residue consisting of a mixture of SiC crystals of rather large mean size and free carbon. This process, whose kinetics are dependent both temperature and pressure, was reported to start from the fiber surface with a front moving versus time radially towards the fiber axis as the time is increased.

(ii)- the **1D-SiC/C/SiC composites** are observed to undergo a similar weight loss at high temperatures (fig. 5). However, it is limited to 12 wt% and it takes place at a higher temperature. Since the fiber weight fraction in the composites is about 51%, this weight loss can be assigned almost entirely to the decomposition of the ex-PCS Si-C-O fibers within the SiC-matrix. The fact that the decomposition of the fibers is shifted towards the high temperatures by 150°C seems to be due to a kinetic effect. Obviously, the release of the gaseous SiO and CO species from the surface of the fibers located far from the composite external surface should be more difficult than for the non-embedded fibers. As a result, SiO and CO could be present in the pores of the composites with rather high partial pressures shifting thus the thermodynamic equilibria responsible for the fiber decomposition process.

The impedding effect of the SiC CVI-matrix upon the fiber decomposition process explains why the SiC(ex-PCS)/C/SiC(CVI) composites were reported to keep a significant percentage of their room temperature failure stress at high temperatures [1,6]. As an example, it has been shown that the mechanical properties of a 1D-SiC/C/SiC composite remain almost unchanged in terms of Young's modulus and strain to rupture while the stress at first damage and the stress to rupture are more severely affected, after an ageing treatment of 100 hours in helium at T = 1400°C and P = 100 kPa [5]. Thus, the thermal

stability effects which might occur in SiC/C/SiC composites at T ≤ 1400°C will be considered in the following discussion as second order effects with respect to those related to the oxidation phenomena.

4.2.2 - Oxidation behavior of 1D-SiC / C / SiC composites

As shown in fig. 6, the main features of the TGA curves recorded for experiments performed in atmospheres containing oxygen are : (i) a weight loss taking place at the beginning of the test and then (ii) a weight increase whose value raises versus time up to the test completion.

(i)- The **mass loss** at the beginning of the test can be mainly assigned to the **oxidation of the carbon interphase**. For the uncoated materials (i.e. materials A and B), the weight loss values do not appear to depend on the test temperature, a feature which suggests that the carbon interphase might be totally consumed (fig. 6). It should be kept in mind that TGA-curves represent the addition of all the phenomena schematically depicted in fig. 20. Nevertheless, the observed maximum weight loss values, i.e. 0.8% for material A and 9% for material B, are of the same orders than the carbon interphase contents which have been calculated for the two materials, i.e. 1.1 wt.% for e = 0.1 μm and 9.7 wt.% for e = 1 μm.

As already pointed out in section 3, fibers are not independent from each other with respect to oxidation. As a matter of fact, the carbon interphase layers are very often connected to each other so that the oxidation process can propagate either parallel or/and perpendicular to the fiber axis, as illustrated in fig. 12. Obviously, as the interphase thickness increases, the number of

interconnected pyrocarbon interphase layers is raised. Since for uncoated materials oxidation occurs via all the specimen faces, the carbon surface area in contact with oxygen changes versus time (which is not the case for the coated materials A_c and B_c). Therefore, the detailed analysis of the TGA-curve features should be done with care for the uncoated A and B materials.

(ii)- the **weight increase**, beyond t = tm, can be obviously related to the **oxidation** of both the **SiC and Si-C-O** phases since equations (7) and (7') are characterized by overall weight increases and give raise to the **formation of silica** whose occurrence in the materials has been clearly established in section 3-4.

For **materials B**, the weight increase exhibits two features which are characteristic of solid diffusion diffusion controlled reactions : the weight increase rate decreases versus time and it is thermally dependent.

For **materials A**, the transition observed at tf in the oxidation kinetics of the carbide phase, during oxidation treatments performed at a high enough test temperature, can be assigned to the progressive sealing of the annular pores (whose width is very small in these materials) by silica, reducing thus the overall internal surface area of the carbide/oxycarbide phases. Beyond tf, a weight increase still occurs but with a much lower rate since the oxidation phenomena responsible for this weight increase are now limited to the external surfaces (whose extension is more limited than that of the annular pores). The fact that tf is observed to decrease with raising test temperatures (fig. 6a) can be justified by the temperature dependence of the parabolic rate constants corresponding to the passive oxidation of both the ex-PCS Si-C-O

fibers and SiC CVI-matrix : an increase in these constants due to a temperature effect should lower the time necessary to seal annular pores with silica.

It should be mentioned that the carbide oxidation occurs both in the annular pores resulting from the consumption of the carbon interphase and at external surfaces of the composites. External surfaces consist of both the six faces of the sample and the walls of the intrinsic pores present initially in the CVI-matrix, as already mentioned. Considering the intrinsic pore distribution reported in fig. 2, the actual carbide surface seen by oxygen, at a given time, will be different from that which can be calculated from the initial specific surface area and it will change with time. As a matter of fact, significant oxygen concentration gradients could arise in small pores as oxidation proceeds. Besides, these small pores will be rapidly sealed with silica, lowering thus the external surface area (fig. 18a).

(iii)- In partially **coated samples** (materials A_c and B_c), oxidation should occur only parallel to the fiber axis (fig. 1c) thus the surface of carbon in contact with oxygen should be constant. On the basis of this feature, it was expected that the weight loss corresponding to the consumption of carbon at low temperatures should progressively decrease versus time since the diffusion path of the reactants in the gas phase is increasing. As shown in fig. 7a, this is not the case at the beginning of the oxidation process since the weight loss rate is observed to increase. However, it is known that the active surface area is not constant during the oxidation of carbon : pitting and surface etching effects can change the effective surface area [32]. Louys has

reported recently that the oxidation rate of pyrocarbon and other materials raises almost linearly with the conversion rate up to 10% and has suggested that this feature could be related to an increase in the surface seen by oxygen [33]. The strong thermal dependence of the gasification rate for 700°C < T < 900°C (fig. 7a) might be related to the predominant role played by the chemical reaction kinetics at low temperatures. At higher temperatures (fig. 7b), on the other hand, gas phase mass transfer by diffusion in the pores becomes the prevailing phenomenon explaining thus that the overall oxidation kinetics depend only very slightly on temperature.

For **materials A_c**, the maximum weight loss was observed to decrease with raising temperature suggesting that the thin carbon interphase (e = 0.1 μm) has not been totally consumed by oxidation, an assumption which is supported by the data shown in table II. As long as t < tf, the annular pores remain open. Therefore, for $t_m < t < t_f$, the annular pores are not closed whereas a weight increase occurs, a feature which suggests that the carbon oxidation rate is significantly reduced. As temperature is raised, the growth rate of the silica layers in the pores is faster, the oxygen consumption by the pore wall is higher whereas the increase in the gas phase mass transfer rate is relatively small. As a result, the length over which carbon is consumed is observed to decrease, as shown in table II.

Conversely, for **materials B_c**, the thick carbon interphase is thought to have been entirely consumed whatever the temperature. Under such conditions, the annular pores resulting from the oxidation of the carbon interphase has a characteristic dimension which is too large to allow a

complete filling by silica near the specimen surface within the time/temperature ranges investigated here, as shown in fig. 17b.

(iv)- When **pure oxygen is replaced by air**, the oxygen partial pressure is divided by a factor close to 5. As a result, the oxidation rates of both the carbon and carbide (oxycarbide) phases are slowed down : the growth of the silica layers on SiC and Si-C-O is slower than in pure oxygen and the annular pores remain open for a longer time, as shown in fig. 9. Besides, lowering the oxygen partial pressure decreases the oxygen concentration gradients, reducing thus the oxygen flux along the pores available for the oxidation reactions.

Reducing the **total oxygen pressure** has a similar effect. At low pressures, the Knudsen diffusion becomes the predominant mechanism and it does not depend on pressure (equation (6)). As a consequence, the carbon oxidation rate is strongly lowered owing to the reduction of the oxygen concentration gradient, as shown in fig. 10. It is worthy of note that the low pressure TGA-experiments have been performed under static conditions. Under such conditions, the effect of the external mass transfers in the gas phase, on the overall oxidation kinetics of the composite, might be more significant than for experiments performed under flowing oxygen.

(v)- As already mentioned in section 3.3, oxidation occurs both parallel and perpendicular to the fiber axis in uncoated samples of both materials A and B (fig. 1a, b). It appears from fig. 11 that oxidation is not as fast in the $\perp$ direction as in the // direction. The diffusion path that oxygen has to follow in order to reach the carbon interphase, in a direction perpendicular to the fiber axis is more tortuous and more important, it can be eventually interrupted

when fibers or complete fiber tows are isolated from one another by the SiC CVI-matrix. This latter factor is expected to be more effective in the composite with a thin interphase.

4.3 - Morphological features of oxidized 1D-SiC/CSiC composites

The morphological features of oxidized 1D-SiC/C/SiC composites which have been described in section 3.4, are consistent with the oxidation model depicted in section 4.2 and illustrated schematically in fig. 20.

(i)- The growth of a **silica layer**, within the annular pores resulting from the in-depth oxidation of the carbon interphase (according to equations (1) or (2)), on both the ex-PCS Si-C-O fibers and SiC CVI-matrix (according to equations (7) or (7')), has been clearly established, as shown in fig. 13 and 15. Furthermore, the **sealing of the annular pore** entrance by the silica scale, predicted by the model, for composites with a thin carbon interphase and for oxidation treatments performed at a high enough temperature, is clearly apparent in fig. 17a. Moreover the thickness of the single silica layer actually measured, i.e. 0.3 μm, is in fair agreement with the calculated value, i.e. 0.26 μm expected for an annular pore width equal to 0.1 μm (the thickness of the initial pyrocarbon interphase in samples of materials A or A_c) when it becomes sealed by silica.

(ii)- For **materials B_c**, in which oxidation proceeds along the fiber axis, the consumption of the thick carbon interphase (e = 1 μm) yields an annular pore of large size in which the oxygen concentration gradient is thought to be rather weak (when carbon is completely consumed) and the oxygen transfer

easy. This feature could explain that the morphology of the material, as observed from polished cross-sections cut perpendicular to the fiber axis, is almost the same near the external surface and in the middle of the sample with **two distinct silica layers** (one grown on the fibers and the other on the matrix) with about the same thickness (fig. 18).

For **materials A_c**, the thickness of the two silica layers in the middle of oxidized samples are very different, as observed from polished cross-sections (fig.) that of the layer grown on the ex-PCS Si-C-O fibers being larger, a result which is apparently surprising when compared to what has been reported for materials B_c (fig. 18). An explanation could be found in the conditions under which the silica scales have grown. In material B_c, the fibers and matrix might have been in contact with a high p_{O2} atmosphere owing to the easy diffusion of oxygen along the annular pore of relatively large width. Conversely, in material A_c, the silica layers on the pore walls might have grown in a low p_{O2} atmophere due to the much lower pore width. It is anticipated that the influence of the oxygen partial pressure on the oxidation kinetics of the ex-PCS Si-C-O fibers and pure SiC CVI-matrix might be different, an assumption which could account for the difference observed here in the thickness of the silica layers [7, 8].

The **fiber offset** in the annular pores, which has been observed after oxidation treatments performed on the composites with the thick carbon interphase (material B or B_c), is a direct consequence of the fiber/matrix debonding resulting from the carbon interphase release (according to equations (1) or (2)) (fig. 18b). Thus, when such a phenomenon occurs, it is

clear that a longer exposure to oxygen will be necessary to seal the annular pore with silica.

(iii)- It has been established in section 3.4 that 1D-SiC/C/SiC composites may ro may not exhibit **microcracks** after long exposures in air, depending on the values of the test temperature and carbon interphase thickness. This feature is also consistent with the oxidation model.

Generally speaking, microcracks are present in composites with the thin carbon interphase (materials A or A_c) after oxidation treatments performed at rather low temperatures, e.g. 900°C (fig. 20a). Moreover, silica is present in some of these microcracks and the fibers are preferentially oxidized at the tip of the microcracks (as shown by a higher thickness of the silica scale). These features strongly suggest that the microcracks were already present at high temperatures and do not result from the effect of a thermal expansion mismatch between the material components, during cooling. The microcracks are thought to result from the mechanical stresses arising in a rigid body, from the **positive volume change** related to the conversion of SiC into SiO_2 according to equations (7) or (7'). As a matter of fact, when the annular pores become sealed, the silica layers formed on both the fibers and matrix near the pore entrance are in contact. Diffusion of oxygen towards the SiC and Si-C-O walls still continues across the silica scale, thus more silica is formed at the SiC/SiO_2 and $Si\text{-}C\text{-}O/SiO_2$ interfaces. Since the SiC/SiO_2 conversion takes place with a positive volume change, internal stresses (thought to be both radial and circumferencial owing to the cylindrical geometry of the fiber/matrix interface) are generated which yield matrix microcracking. It is noteworthy that these cracks occur preferentially in the matrix bridges of low

thicknesses (fig. 20a). After propagation, the microcracks become interconnected, matrix block displacements occur which still enlarge the microcracks and the oxygen diffusion through this new pore network yields a new formation of silica.

Conversely, no microcracks are formed in 1D-SiC/C/SiC composites with a thick carbon interphase (materials B or B_c) submitted to the same treatment in air (T = 900°C ; P = 100 kPa ; t = 300 hours). Under such conditions, the width of the annular pores was too large (e = 1 μm) and the kinetics of formation of SiO_2 too low, to allow the two silica layers formed in the pores on the fibers and matrix, respectively, to be in contact. Thus no mechanical stress was induced in the matrix.

Finally, no microcracks are formed in 1D-SiC/C/SiC composites with a thin carbon interphase (e = 0.1 μm) during oxidation tests performed at high temperatures (i.e. T =1200°C). It is thought that under such conditions, the viscosity of the silica glass resulting from the oxidation of SiC or Si-C-O is low enough to allow internal stress release by viscous flow.

5 - CONCLUSION

On the basis of the data reported in section 3 and the discussion presented in section 4, the following main conclusions can be drawn :

(i)- the thermal stability of ex-PCS Si-C-O ceramic fibers in an inert atmosphere is significantly improved when such fibers are embedded in a SiC CVI-matrix. This feature is consistent with the fact that SiC(ex-

PCS)/C/SiC(CVI) composites were reported to be usable beyond the temperature (i.e. 1100°C - 1200°C) at which the fibers begin to undergo their decomposition process.

(ii)- In oxidizing environments, several mechanisms are involved in the oxidation of 1D-SiC/C/SiC model composites, namely : the gasification of the carbon interphase which leaves pores of annular section, the gas phase diffusion of oxygen and carbon oxides along these pores (in molecular or Knudsen regimes) and, finally, the reaction of oxygen with the pore walls resulting in the growth of silica layers. The growth of silica reduces the width of the pores and can even seal the pore entrances.

(iii)- As expected from the thermal dependences of in-pore diffusion ($T^{0.5}$ or $T^{1.75}$) and SiC (or Si-C-O) oxidation reaction ($e^{-Ea/RT}$), respectively, the oxidation of both uncoated and partially SiC-coated 1D-SiC/C/SiC composites occurs in the bulk at low temperatures whereas it is limited to the surface at high temperatures (particularly when the carbon interphase is thin).

(iv)- Matrix microcracking occurs in uncoated (or partially SiC-coated) 1D-SiC/C/SiC composites with a thin carbon interphase, during oxidation treatments at low temperatures, related to internal mechanical stresses generated by the SiC/SiO_2 conversion which takes place with a positive volume change. This phenomenon is no longer observed at high temperatures and/or for composites with a thick carbon interphase.

(v)- From the oxidation point of view, materials with a **thin carbon interphase** have the best behavior particularly when used at high temperatures and in

atmospheres with a high oxygen partial pressure (passive regime). Under such conditions, 1D-SiC/C/SiC composites behave as **self-healing materials** even when uncoated.

The quantitative description of the oxidation kinetics of 1D-SiC/C/SiC model composites is presented in a companion paper [18].

ACKNOWLEDGEMENTS

This work has been supported by both CNRS and SEP through a grant given to one of us (L. F.). The authors are indebted to SEP for providing the model materials. They acknowledged the contributions of R. Chapoulie and M. Schvoerer (CRIAA) to the cathololuminescence analysis, C. Labrugère (LCTS) and Y. Keen (CEMES-LOE) to the TEM characterization and finally F. Lamouroux (LCTS) to fruitfull discussions.

APPENDIX - 1

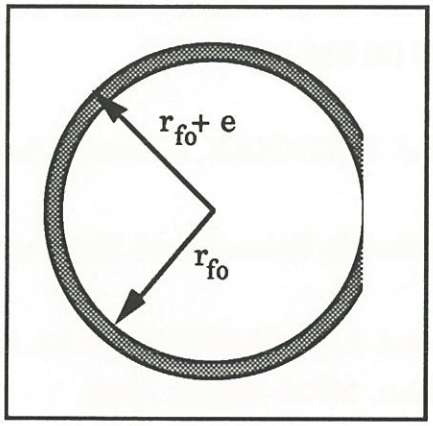

Fig. A1: Schematic representation of the composite

The surface of carbon associated with one fiber having n points of contact is :

$$S_c = \pi((r_{fo} + e)^2 - r_{fo}^{\ 2}) - n\,[(r_{fo} + e)^2\,(\frac{\pi}{2} - \mathrm{Arcsin}(\frac{r_{fo}}{r_{fo} + e})) - r_{fo}\,\sqrt{(r_{fo} + e)^2 - r_{fo}^{\ 2}}\,]$$

Then the carbon content is derived by using the relation :

$$\text{Carbon content} = \frac{\rho_c V_f}{\rho_{comp}} \frac{S_c}{\pi\, r_f^{\ 2}}$$

with r_f : average radius of carbon (7 μm)

e : thickness of interphase (0.1 or 1 μm)

V_f : volume fraction (0.45)

ρ_c : density of carbon (2 gcm^{-3})

ρ_{comp} : density of composite (in the text)

n : number of contact point (2)

For material with an external layer as for partially coated materials the carbon content is obtained with the same relation with taking care to calculate the average fiber volume fraction which is smaller due to the presence of the external layer.

REFERENCES

[1] P.J. LAMICQ, G.A. BERNHART, M.M. DAUCHIER and J.G. MACE, Am. Ceram. Soc. Bull., 65 [2] 336-338 (1986).

[2] K. PREWO and J.J. BRENNAN, J. Mater. Sci., 15 [2] 463-468 (1980).

[3] A.G. EVANS, Materials Science and Engineering, A(107) 227-239 (1989).

[4] M. BOUQUET and J.M. QUENISSET in Amac/Codemac, Eds. R. Naslain, J. Lamalle, J.C. Zulian, 29/30 March 1990.

[5] L. FILIPUZZI, G. CAMUS, J. THEBAULT and R. NASLAIN, 11th RISO International Symposium on Metallurgy and Materials Science, Eds. J.J. Bentzen, J.B. Bilde-Sorensen, N. Christiansen, A. Horsewell, B. Ralph, Roskilde Denmark, 1990 pp 283-289.

[6] J.C. CAVALIER, A. LACOMBE and J.M. ROUGES, "Ceramic Matrix Composites : New Materials with very High Performances" in "Developments in the Science and Technology of Composite Materials (A.R. Bunsell et al. eds), Proc. ECCM-3, Bordeaux, March 20-23, 1989, pp 99-100, Elsevier Applied Science, London and New York.

[7] L. FILIPUZZI, R. NASLAIN and C. JAUSSAUD, (Submitted to J. Mater. Sci.).

[8] L. FILIPUZZI and R. NASLAIN, 7th Cimtec, Montecatini Terme, June 24-30 1990.

[9] H.C. CAO, E. BISCHOFF, O. SBAIZERO, M. RUHLE, A.G. EVANS, D.B. MARSHALL and J.J. BRENNAN, J. Amer. Ceram. Soc., 73 [6] 1691-99 (1990).

[10] D.H. GRANDE, J.F. MANDELL and H.C.C. HONG "Fibre-Matrix Bond Strengh Studies of Glass, Ceramic and Metal Matrix Composites", J. Mater. Sci., 23 311-328 (1988).

[11] A.J. CAPUTO, D. P. STINTON, R.A. LOWDEN and T.M. BESMAN, Am. Ceram. Soc. Bull., 66 [2] 368-72 (1987).

[12] J.J. BRENNAN "Interfacial Characteristics of Glass-Ceramic Matrix/SiC Fiber Composites", J. de Physique, Colloque C5 Suppl., 10 [49] 791-809 (1988).

[13] R. NASLAIN, O. DUGNE, A. GUETTE, J. SEVELY C. ROBIN-BROSSE, J.P. ROCHER and J. COTTERET, J. Amer. Ceram. Soc. (in press).

[14] N. FRETY and M. BOUSSUGE, Comp. Sci. Technol., 37 177-189 (1990).

[15] G. GAULT and M. HUGER in Matériaux Composites pour applications à hautes températures, Proc., Edited by R. Naslain, J. Lamalle and Z.L. Zulian (AMAC/CODEMAC) publications, Paris and Bordeaux, pp 303-14 (1990).

[16] R.L. STEWART, K. CHYUNG, M.P. TAYLOR and R.F. COOPER, Fracture Mechanics of Ceramics Vol 7, Edited by R.C. Brandt, A.G. Evans, D.P.H. Hasselman and F.F.Lange, Plenum Press New York p 3 (1986).

[17] O. SBAIZERO and C. SCHMID, Materials Engineering Vol.1 [1] 273-80 (1989).

[18] L. FILIPUZZI and R. NASLAIN, "Oxidation Mechanisms and Kinetics of 1D-SiC/C/SiC Composite Materials", 2-Modelling" (to be published).

[19] R. NASLAIN, J.Y. ROSSIGNOL, P. HAGENMULLER, F. CHRISTIN, L. HERAUD and J.J. CHOURY, Synthesis Properties of New Composite Materials for High Temperature Applications Based on Carbon Fibers and C-SiC or C-TiC Hybrid Matrices Rev. Chimie Minérale, 18 544-564 (1981).

[20] C. ITOH, K. TANIMURA and N. ITOH, J. Phys. C. Solid State Phys., 17 4693-4702 (1988).

[21] F. DOUX in "Les Carbones Eclaires en Lumiere Polarisée", (1989).

[22] K.L. LUTHRA, Carbon, 26 [2] 217-24 (1988) .

[23] G.F. HEWITT in "Chemistry and Physics of Carbon" (Edited by P.L Walker, Jr) Vol 1, Marcel Dekker Inc. New York, 73-120 (1965).

[24] E.N. FULLER and J.C. GIDDINGS, Ind. Eng. Chem., 58 [5] 18 (1966).

[25] M. KNUDSEN Ann. Physik, 28 75-130 (1909).

[26] J.A. COSTELLO and R.E. TRESSLER, J. Am. Ceram. Soc., 69 [9] 674-681 (1986).

[27] C. LAFFON, A.M. FLANCK, P. LAGARDE, M. LORIDJANI, R. HAGEGE, P. OLRY, J. COTTERET, J. DIXMIER, J.L. MICQUEL, H. HOMMEL, A.P. LEGRAND, J. Mater. Sci., 24 1503-1512 (1989).

[28] L. FILIPUZZI and R. NASLAIN, Proc. 7 th CIMTEC, Montecatini Terme, June 24-30 1990 (in press).

[29] G. GRATHWOHL and F. THUMMLER, J. Mater. Sci., 13 1177 (1978).

[30] M.M. JASKOWIAK, J.A. DICARLO, J. Am. Ceram. Soc., 72 [2] 192-97 (1989).

[31] E. BOUILLON, D. MOCAER, J.F. VILLENEUVE, R. PAILLER, R. NASLAIN, M. MONTHIOUX, A. OBERLIN, C. GUIMON and G. PFISTER, (Submitted to J. Mater. Sci.).

[32] H. MARSH and K. KUO in "Introduction to carbon Science" Edited by H. Marsh 107-51 (1989).

[33] F. LOUYS, Thesis,Univ. Mulhouse (1987).

CHAPITRE IV

OXIDATION MECHANISMS AND KINETICS OF 1D-SiC/C/SiC COMPOSITE MATERIALS : 2 - MODELLING

INTRODUCTION AU CHAPITRE IV

Ayant généré des données expérimentales, l'étape suivante consistait à interpréter ces résultats. Il est rapidement apparu que plusieurs phénomènes se produisaient simultanément et que l'exploitation qualitative et quantitative des courbes cinétiques établies par ATG était très délicate. Etant donné la complexité des mécanismes mis en jeu, il était nécessaire d'avoir une approche théorique indépendante afin d'éviter une interprétation sommaire, voire érronée et en tout cas insatisfaisante, des résultats expérimentaux.

La première phase a consisté à identifier les mécanismes physiques et chimiques mis en jeu lors de l'oxydation. Ensuite, il a fallu formaliser ces phénomènes sous forme d'équations et de conditions aux limites. Enfin, la dernière étape a été la résolution numérique de ces équations qui n'admettaient pas de solutions analytiques. Au cours du développement de ce programme, la compréhension qualitative des mécanismes s'est améliorée et les hypothèses initiales ont été progressivement modifiées.

Chronologiquement, l'étude de la diffusion et réaction simultanée d'une espèce gazeuse dans un pore cylindrique avec formation d'une espèce condensée, a été la première étape de ce travail. L'une des premières hypothèse à vérifier était de savoir si le problème pouvait être considéré ou non comme quasi stationnaire, ce qui permet alors le découplage des variables de temps et d'espace et simplifie considérablement les équations et la résolution numérique. Ce point a été étudié et fait l'objet de l'annexe 2. La seconde étape a consisté à introduire le carbone et à considérer une géométrie proche de celle du composite. La méthode de résolution numérique utilisée est présentée à l' annexe 3.

Soumis à "Journal of the American Ceramic Society"

OXIDATION MECHANISMS AND KINETICS OF 1D-SiC/C/SiC COMPOSITE MATERIALS : 2- MODELLING

L. FILIPUZZI and R. NASLAIN
Laboratoire des Composites Thermostructuraux, UMR-47
(CNRS-SEP-UB1), Europarc, 1-3, Av. L. de Vinci
33600 - Pessac, France

ABSTRACT

A model, based on a simple axisymmetrical fiber/interphase/matrix assembly is derived to depict the oxidation behavior of 1D-SiC (ex-PCS)/C/SiC (CVI) composites. It takes into account : (i) the changes versus time of the geometry of the annular pore resulting from the consumption by oxidation of the carbon interphase, (ii) the mass transfers by diffusion along the pore of the reactant and product and (iii) the chemical reactions with oxygen of both the pore walls (yielding silica) and the pore bottom consisting of carbon. The model gives : the gaseous species concentration and silica thickness profiles along the pore, the length of carbon consumed by oxidation and the relative weight parameter change. The model depicts in a satisfactory manner the features of the TGA-curves recorded on actual composites and it is in excellent agreement with the measurements of the carbon interphase lengths consumed by oxidation. It shows that the oxidation resistance of 1D-SiC/C/SiC composites is better at high temperatures and for thin carbon interphases. Under such conditions, the materials exhibit a self-healing behavior.

KEY WORDS : SiC/C/SiC Composites, Carbon interphase, SiC-CVI Matrix, Ex-PCS fibers, Oxidation, Kinetics, Modelling

1 - INTRODUCTION

One of the main advantages of **ceramic matrix composites** (CMCs), such as the SiC/SiC or SiC/LAS composites reinforced with continuous SiC-based fibers(*), with respect to the more conventional C/C composites, lies in their better oxidation resistance. SiC-based ceramics are known to exhibit an excellent behavior in oxidizing atmospheres owing to the formation of a **protective silica scale** which slows down the oxidation rate as long as the oxidation conditions remain those of the so-called passive oxidation regime [1,2].

Most CMCs behave mechanically as non-linear materials in tension loading when they have been properly processed. This property, which is rather uncommon for a ceramic material (most ceramics fail at a low strain within their linear elastic domain) is directly related to the occurrence of various well identified damaging phenomena such as : matrix microcracking, fiber/matrix debonding and fiber pull out. It is now well established that high toughness is observed in CMCs only when the fiber/matrix coupling is weak enough. This requirement is usually achieved through the use of an interfacial compliant material, referred to as the **interphase**, the most common interphase material being carbon [3]. Carbon interphase is either deposited on the SiC fiber surface from a gaseous precursor (e.g. CH_4) prior to the infiltration of the SiC-matrix in SiC/SiC composites processed by chemical vapor infiltration (CVI) or it is formed in-situ in hot-pressed SiC/LAS composites, as the result of a chemical reaction taking place at the fiber/matrix interfaces during processing [4].

(*) ex-polycarbosilane Nicalon fibers from Nippon Carbon

From the standpoint of oxidation (passive oxidation regime) the carbon interphases in both SiC/SiC and SiC/LAS composites might become the weak point of the materials. Carbon is readily oxidized at temperatures as low as 500°C with formation of gaseous oxides [5]. The release of the carbon interphases by oxidation modifies strongly the fiber/matrix coupling and consequently the mechanical behavior of both SiC/SiC and SIC/LAS composites [6-10]. Therefore, a coating (e.g. SiC for SiC/SiC composites) is often used to prevent an extensive in-depth diffusion of oxygen via the carbon interphases although some of these composites have been reported to exhibit a self-healing character [7].

It thus appears that the analysis and understanding of the oxidation behavior of CMCs are key issues. Within this scope, an **experimental approach** of the oxidation behavior of 1D-SiC/C/SiC model composites has been presented in a companion article [10]. The materials consisted of continuous ex-PCS Si-C-O fibers(*) embedded unidirectionally by CVI in a SiC-matrix, according to a process which has been described elsewhere [11]. It has been shown that an oxidation treatment resulted in : the consumption of the carbon interphase (released as CO/CO_2 gaseous species) and the formation of an **annular pore** (whose width was 0.1 - 1 μm) around each fiber. Thus, the reactants and products have to diffuse along very narrow pores whose length and width change versus time owing to chemical reactions occurring with the pore walls (oxidation of the SiC from the fibers and matrix with formation of silica layers) and pore bottom (oxidation of the carbon interphase). After a long enough exposure, the oxidation rate of the carbon interphase was observed to be

(*) ex-polycarbosilane Nicalon fibers from Nippon Carbon

significantly reduced. Moreover, under specific conditions (i.e. high temperatures, high oxygen partial pressures and thin carbon interphase), the oxidation was limited to the composite external surface owing to an early sealing of the annular pore entrances by silica [10].

Bernstein and Koger have already **modelled** the oxidation kinetics of a thin layer of carbon inserted between two plates of silicon or silicon nitride and reported that the carbon length consumed was proportional to the square root of time [12]. However, their model did not take into account neither the reactant consumption due to reaction with the walls nor the resulting change in the pore width. Although the carbon consumption rate was reported to decrease versus time, the model could not take into account the fact that it might even stop.

Thiele has studied the diffusion in a **cylindrical pore** of a gas reacting with the pore wall but with the assumption that no change occurred in the pore dimensions [13]. The so-called Thiele modulus m (an adimensional number) has been derived from his work to characterize the competition between diffusion and chemical reaction in a cylindrical pore : when $m < 1$, the concentration gradient of a given gaseous species along the pore is weak whereas when m is large (e.g. $m > 5$), a strong depletion in the concentration is observed at mid-pore length. Petersen has used a similar approach to depict the gasification of carbon in a cylindrical straight pore, taking into account the local change in the pore radius resulting from the chemical reaction [14]. Ramachandran and Smith have presented a model in which the chemical reaction with the pore wall resulted in the formation of a condensed product, the kinetics of growth of the deposit being controlled by both reaction and

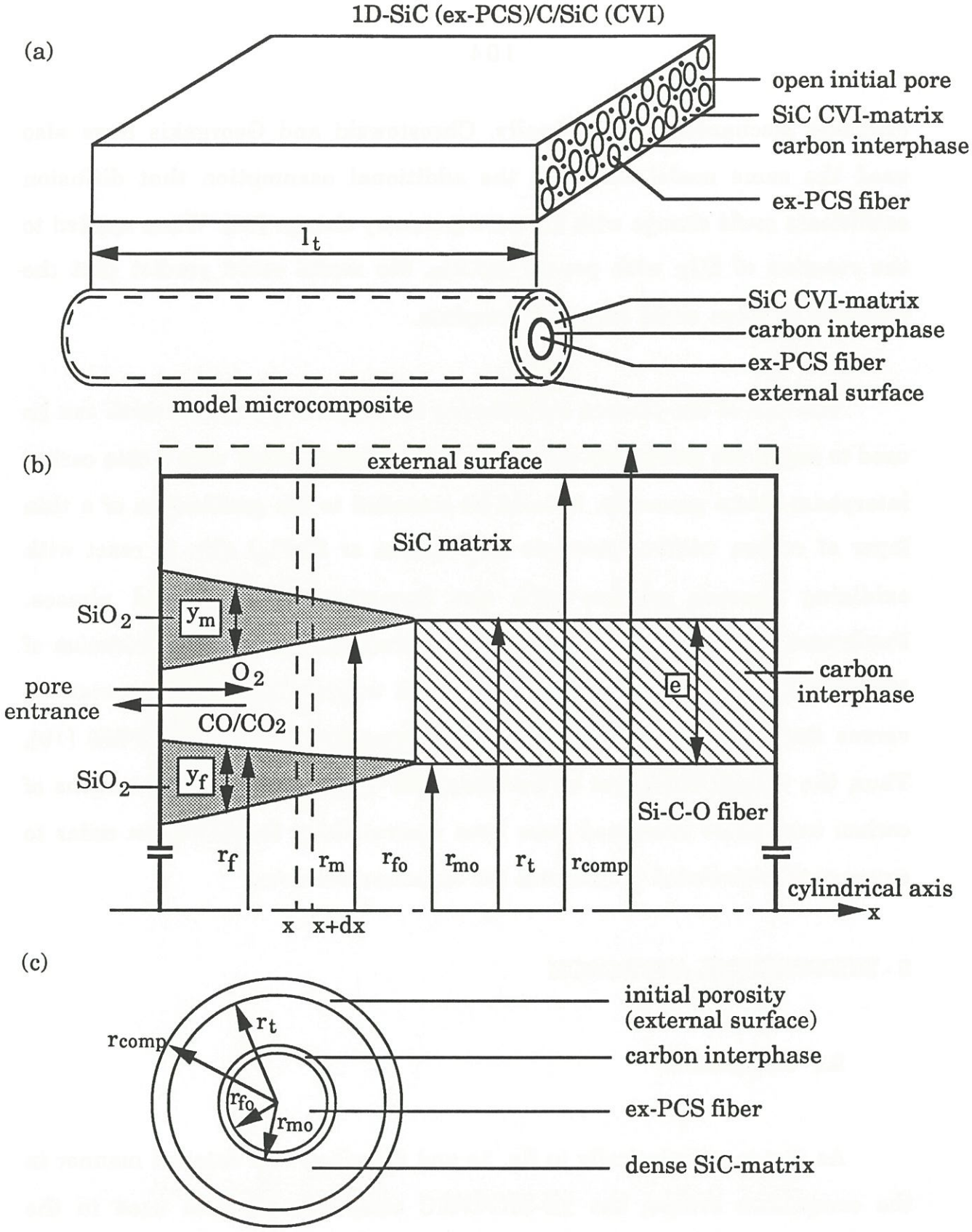

Fig. 1: Geometry of the microcomposite used to model the oxidation of 1D-SiC/C/SiC composites prepared by CVI: (a) relation between the model microcomposite and the sample used for the TGA experiments, (b) details of the microcomposite after an exposure to an oxidizing atmosphere (longitudinal partial section) and (c) cross-section (schematic)

diffusion mechanisms [15]. Finally, Chrostowski and Georgakis have also used the same model but with the additional assumption that diffusion coefficients could change with the pore geometry change [16]. When applied to the reaction of SO_2 with porous $CaCO_3$, the model could predict that the chemical reaction could remain incomplete.

The aim of the present contribution is to derive a **model** which can be used to depict the **oxidation of 1D-SiC/C/SiC composites** with a thin carbon interphase. More generally, it could be extended to the gasification of a thin layer of carbon within materials (e.g. silicon or Si_3N_4) able to react with oxidizing gaseous species with the formation of condensed phases. Furthermore and as already shown in the companion article, the oxidation of 1D-SiC/C/SiC composites results in an overall weight change whose variations versus time have been studied by thermogravimetric analysis (TGA) [10]. Thus, the weight variations of the composite versus time and the lengths of carbon interphase consumed have been derived from the model, in order to compare the calculated values with the experimental data.

2 - THEORETICAL APPROACH

2.1 - Hypotheses

As shown schematically in fig. 1a and described in a detailed manner in the companion article, the 1D-SiC/C/SiC composite samples used in the present work consist of ex-polycarbosilane (PCS) fibers running parallel to each others in one single direction, which have been first coated with pyrocarbon (thickness : 0.1 or 1 μm) and their assembly was then infiltrated

with a SiC-matrix, according to the CVI-process [11]. They also contain, in the as-prepared state, a residual open porosity owing to the fact that in the CVI-process : (i) the open pores of very small size are not infiltrated, (ii) the infiltration of a 1D-preform (which occurs mainly along the fiber direction) is more difficult than that of e.g. a 2D-preform made from fabrics and (iii) the infiltration is usually stopped before it has proceeded to completion. Thus, 1D-SiC/C/SiC composites can be depicted, from an oxidation stand-point, on the basis of five components : (i) the ex-PCS fibers, (ii) the SiC-CVI matrix, (iii) the carbon interphase, (iv) the initial open porosity (which is of the order of 10 %) and (v) the external surfaces. During an exposure at high temperatures in an oxidizing atmosphere, the five components react with oxygen : the carbon interphase is consumed with the formation of **gaseous carbon oxides** (CO or/and CO_2) and an **annular pore** around each fiber (fig. 1b) whereas all the other components give rise to the formation of a **silica scale** (as long as the oxidation corresponds to the passive regime). The consumption of the carbon interphase yields a weight loss and the oxidation of the SiC (or SiC-based) surfaces a weight increase. In the following, the porosity resulting from the carbon interphase consumption (consisting of the annular pores) will be referred to as the **internal porosity or internal surface** whereas that corresponding to both the initial open porosity and sample surfaces will be referred to as the **external surface**.

The 1D-SiC (ex-PCS)/C/SiC (CVI) composites actually used for the TGA-experiments will be modelled, in the following, as a hypothetical elemental composite, shown schematically in fig. 1a-c, referred to as 1D-SiC/C/SiC microcomposite. The microcomposite is an axisymmetrical assembly of : (i) one single ex-PCS Si-C-O straight fiber (assumed to be of constant diameter

2 r_{fo}), (ii) a layer of carbon interphase with a constant thickness e (with e = 0.1 or 1 μm), (iii) a shell of dense SiC-matrix with a constant thickness $r_t - r_{mo}$ and finally (iv) a "shell of porosity" taking into account the occurrence of the open porosity present in SiC/C/SiC composites elaborated by CVI. The microcomposite has the same length l_t as the actual composites. The matrix shell thickness $r_t - r_{mo}$ (or the value of r_t since r_{mo} is fixed by those of the fiber radius and interphase thickness) and thus the matrix volume fraction, are defined by the following conditions : the value of the fiber volume fraction, on the one hand, that of the density, on the other hand, are the same in the microcomposite and in the actual composites (appendix - A11). The density condition is used to take into account the occurrence of the open porosity of the CVI-matrix. One should add to the microcomposite as it has been defined above an **external surface** defined as the specific surface area measured by mercury porosimetry on the composites actually used for the TGA-experiments. Therefore, the oxidation of the model microcomposite will be treated in two steps in the following : (i) the oxidation taking place in the **internal porosity** (i.e. that of the annular pore walls and carbon interphase) and (ii) the oxidation of the **external surface** (i.e. that corresponding actually to the external faces and initial open porosity of the composite sample).

In the modelling procedure, the chemical reactions between the oxidizing reactant and the three main material components (the ex-PCS fibers, the carbon interphase and the SiC-matrix) are assumed to be **irreversible** and to take place at **constant** temperature and pressure.

It is further assumed that : (i) oxidation proceeds **equally** via the two bases of the microcomposite (that of carbon leading to gaseous oxides only

whereas that of the fibers and matrix yields both gaseous species and a condensed phase, silica which progressively reduces the cross-section of the annular pore, (ii) the concentration is contant in a given cross section of the annular pore (no radial gradients), (iii) the mass transfers outside the annular pore are fast with respect to those occurring inside and (iv) mass transfers by convection in the annular pore are neglected. Finally, it is assumed that the gaseous species concentrations reach their steady state values rapidly with respect to the pore geometry change. This latter hypothesis corresponds to a **steady state** regime which will allow us to **separate the time and space variables.**

2.2 - Chemical reactions

The **oxidation of carbon** in an atmosphere of oxygen results in the formation of gaseous carbon oxides, with an overall **weight loss**, according to the two following equations :

$$C + O_2 \rightarrow CO_2 \quad (1)$$

$$2C + O_2 \rightarrow 2CO \quad (2)$$

Assuming that equilibrium is reached, **thermodynamic** considerations predict that the reaction corresponding to equation (1) is favored at low temperatures ($T < 700°C$) whereas that related to equation (2) is preponderant at high temperatures : the CO/CO_2 ratio thus increasing as temperature is raised [17]. Since pressure remains constant, the fact that in equation (2) there is an increase in the mole number of the gaseous species, when (2) is shifted to the right, is expected to change locally the mass transfers in the pore.

From a **kinetic** standpoint, the oxidation of carbon at low temperatures is known to be rate-limited by the kinetics of the chemical reaction. Generally speaking, reaction rate constants are known to obey Arrhenius laws. However, the values of the reaction rate constants corresponding to the oxidation of carbon depend upon a number of parameters including : the state of crystallization, the microstructure and texture, the crystallographic directions, and the amount of impurities. Values higher than 25 have been reported for the ratio between the rate constants of the oxidation reactions of a graphite single crystal when they take place along the axes **a** and **c**, respectively. Furthermore, for the same material, values of the reaction order with respect to oxygen equal to 0.21 and 0.30 have been mentioned for oxidation tests performed in the $<11\bar{2}0>$ and $<10\bar{1}0>$ directions (for T = 812°C and 1.3 < P < 13 kPa) [18] whereas values close to 0.5 - 0.6 were published by different authors [5].

The **oxidation of silicon carbide**, when it occurs under the passive oxidation regime conditions, results in the formation of both gaseous products (i.e. CO or/and CO_2) and a condensed phase, silica, through which the oxidizing species have to diffuse in order to react with SiC. Under such conditions, the oxidation of SiC corresponds to the two following equations :

$$SiC + 2O_2 \rightarrow SiO_2 + CO_2 \quad (3)$$

$$SiC + \frac{3}{2}O_2 \rightarrow SiO_2 + CO \quad (4)$$

Temperature (°C)	900	1000	1100	1200
B_f^* (nm^2min^{-1}) SiC ex PCS	5	49	188	404
B_m^* (nm^2min^{-1}) SiC CVI	58	83	139	285
p_f	0,5	0,5	0,5	0,5
p_m	0,9	0,8	0,7	0,6

Table I : Values of the parabolic rate constant B* and of the oxygen concentration exponent p for Si-C-O (ex-PCS) fibers and SiC CVI-matrix for temperatures ranging from 900°C to 1200°C.

One should emphasize that the **ex-PCS fibers**, which result from the pyrolysis of oxygen-cured PCS green fibers, do not consist of pure SiC, their overall composition being close to $Si_{0.38}\ C_{0.47}\ O_{0.15}$. They have been reported to contain significant amounts of oxygen (bonded to silicon in tetrahedral SiC_xO_y species) and free carbon (as well as trace amounts of hydrogen) [19,20]. However, their oxidation behavior has been observed to be rather similar to that of pure SiC (but with different oxidation kinetics) and will be depicted as corresponding to the two following equations [21] :

$$Si_{0.38}\ C_{0.47}\ O_{0.15} + 0.77\ O_2 \rightarrow 0.38\ SiO_2 + 0.47\ CO_2 \qquad (3')$$

$$Si_{0.38}\ C_{0.47}\ O_{0.15} + 0.54\ O_2 \rightarrow 0.38\ SiO_2 + 0.47\ CO \qquad (4')$$

In reactions (3), (3'), (4) and (4') there is a decrease in the overall mole number of the gaseous species when they are totally shifted to the right, a feature which will be responsible for an additional oxygen flux in the pore, in opposition to what has been mentioned for reaction (2).

The parabolic rate constants B* related to the growth of the silica scale on both SiC (CVI) and ex-PCS fibers obey Arrhenius laws and their values are listed in table I for various oxidation test temperatures [21,22]. Furthermore, their variations as a function of the oxygen partial pressure are not linear [23,24]. In the following, it will be assumed that the variations of the parabolic rate constants B as a function of the oxygen concentration obey the following equation :

$$B = B^* (C/C^*)^p \qquad (5)$$

where B* and C* are the parabolic rate constant (m^2s^{-1}) and oxygen concentration (mol m^{-3}) at P = 100 kPa in pure oxygen, respectively. The values of the exponent p have been : (i) extrapolated from the data available in the literature (limited to T ≥ 1200°C) for SiC [21] and (ii) derived from TGA oxidation tests (performed for 1 < P < 100 kPa) for ex-PCS fibers [25].

It appears from equations (3) to (4') that the oxidation of both the SiC CVI-matrix and ex-PCS fiber syields an overall **weight increase**. Furthermore, the SiC/SiO_2 conversion as well as the $Si\text{-}C\text{-}O/SiO_2$ conversion (for the ex-PCS fibers) take place with a **positive volume change** : the ratio between the molar volumes of the condensed product SiO_2 and initial ceramic material from which it has been formed, is equal to about 2 and 1.35 for SiC (CVI) and Si-C-O (ex-PCS), respectively. As a consequence, the annular pore resulting from the oxidation of the carbon interphase will become progressively filled with silica as the oxidation of the SiC (or Si-C-O) pore walls proceeds.

In the oxidation of the three components of the material, the gaseous product is CO or/and CO_2. In the following, the calculations have been performed taking into account either equations (1), (3) and (3') or equations (2), (4) and (4') in order to involve the O_2/CO_2 and O_2/CO couples. Conversely, secondary reactions which might occur either between C and CO_2 or CO and O_2, corresponding to the following equations :

$$C + CO_2 \rightarrow 2CO \qquad (5)$$

$$CO + \frac{1}{2}O_2 \rightarrow CO_2 \qquad (6)$$

or between CO_2 and the silicon carbide (or oxicarbide) were not taken into account.

2.3 - Oxidation of the internal porosity : model and boundary conditions

The equation of mass conservation used to depict the variations of the concentration C of a given species as a function of time and space coordinates, in a non-stationary regime is [26] :

$$\frac{\partial C}{\partial t} + \nabla N = R \qquad (7)$$

where R in mol m^{-3} s^{-1} is a term taking into account the consumption or formation of the chemical species involved and N in mol m^{-2} s^{-1} the absolute molar flux. Under the condition of steady state regime, equation (7) becomes :

$$\nabla N = R \qquad (7')$$

Referring now to fig. 1b, which shows schematically the pore geometry at an exposure time t, let A be the oxidizing species (i.e. molecular oxygen O_2) and A' the gaseous species resulting from the chemical reaction between A and the three components of the material (i.e. A' is either CO_2 or CO). Let then consider two cross-sections of the pore located at x and x+dx, at a given time t the conservation equation of the mole number of species A diffusing across the slice of material of the thickness dx during dt can be written as :

$$\frac{S(x + dx)\ \ N_A(x + dx) - S(x)\, N_A(x)}{dx} = R_A(x) \qquad (8)$$

where S is the area of the annular pore cross-section with :

$$S = \pi (r_m^2 - r_f^2) \qquad (9)$$

and $R_A(x)$, in mol m^{-1} s^{-1}, is the number of moles of species A consumed by reaction with the pore walls per unit length. If dx is allowed to tend towards zero, then equation (8) can be rewritten as :

$$\frac{d(SN_A)}{dx} = R_A \qquad (8')$$

where N_A, the absolute molar flux of species A, is given by :

$$N_A = - D_A \frac{dC_A}{dx} + \frac{C_A}{C_o} \sum_i N_i \qquad (10)$$

where C_o is the total concentration.

The first term in the right hand side of equation (10) is the true **diffusion flux** (first Fick equation) whereas the second is the **Stefan flow** resulting from the fact that the total mole number of the gaseous species is not constant during the oxidation process in the pore, as already mentioned in section 2.2 (see equations (2), (3 or 3') and (4 or 4')).

As a matter of fact D_A, the coefficient of diffusion in the gas phase is an **effective diffusion coefficient** taking into account : (i) the molecular diffusion

regime in which diffusion is controlled by the collisions between the molecules and (ii) the Knudsen diffusion regime in which diffusion results from the collisions of the molecules with the wall. It is defined according to the Bosanquet equation [27] :

$$D_A^{-1} = D_M^{-1} + D_K^{-1} \qquad (11)$$

where D_M is the **binary diffusion coefficient** (diffusion of A in A' or A' in A) in molecular regime and D_K is the **Knudsen diffusion coefficient**. The equations (A4) and (A7'), which have been used to calculate the values of D_M and D_K are given in appendix A2. Since D_K is a function of the space variable x (which is not the case for D_M), D_A is itself a function of x.

If one assumes that only two different gaseous species are present, the expression of the Stefan flow (second term in the right hand side of equation (10) can be rewritten as :

$$\frac{C_A}{C_o} \sum_i N_i = \frac{C_A}{C_o} (N_A + N_{A'}) \qquad (12)$$

Furthermore, if there is only one simple chemical reaction involved, then the respective mole numbers of A and A' are proportional to each other. Their ratio, which is given by the reaction equation, is also valid for the related fluxes. In the present case, three reactions are involved corresponding either to equations (1), (3) (3') or (2), (4), (4'). Moreover, the two reactions of A with the fiber and matrix occur at the same depth x in the pore whereas that of A with the carbon interphase takes place only at the pore bottoms, i.e. for $x = l_r$. Thus,

at $x = l_r$, the ratio between the molar fluxes of A and A' will be given by the stoichiometric coefficients of equations (1) or (2) whereas at the pore entrance, i.e. at $x = 0$, it will depend on the relative weights of the three reactions in the oxidation process. Let α be the ratio between the molar fluxes of A' and A, then :

$$N_{A'} = - \alpha N_A \tag{13}$$

with : $$\alpha = \frac{a_f n_{Af} + a_m n_{Am} + a_c n_{Ac}}{n_{Af} + n_{Am} + n_{Ac}} \tag{14}$$

where n_{Af}, n_{Am} and n_{Ac} are the mole numbers of A consumed in the pore at t during dt per unit length by the oxidation of the fibers, the matrix and the carbon interphase respectively, whereas a_f, a_m and a_c are the mole numbers of A' which are formed per mole of A consumed by the reactions involving the fibers, the matrix and the carbon interphase.

Combining equations (10), (12) and (13), N_A can be expressed as :

$$N_A = - \frac{D_A C_o}{C_o - C_A (1-\alpha)} \frac{dC_A}{dx} \tag{15}$$

The oxidation of both the fibers and matrix results in the formation of a condensed phase, silica, through which the reactant and product gaseous species have to diffuse. Assuming that the reactions are rate-limited by the diffusion phenomena in the solid state, the rates of growth of the silica layers formed on the fibers and matrix can be written respectively as :

$$\frac{d\,[y_m(t)]}{dt} = \frac{B_m^*(\frac{C_A}{C^*})^{p_m}}{2y_m(t)} \qquad (16)$$

$$\frac{d\,[y_f(t)]}{dt} = \frac{B_f^*(\frac{C_A}{C^*})^{p_f}}{2y_f(t)} \qquad (16')$$

y_m and y_f are the thickness of silica scale on the matrix and on the fiber.

These growth kinetic laws were derived for **plane geometry.** Nevertheless, they have been applied here since the thickness of the oxide layers is always much lower than the fiber and matrix radii.

The mole number of A, which is consumed by reaction with the pore wall (fibers and matrix) at t, during dt and per unit length, can be expressed as :

$$R_A = \frac{\pi g_m r_{mo} \rho_s B_m^*(\frac{C_A}{C^*})^{p_m}}{y_m M_s} + \frac{\pi g_f r_{fo} \rho_s B_f^*(\frac{C_A}{C^*})^{p_f}}{y_f M_s} \qquad (17)$$

where g_f and g_m are the mole numbers of A necessary to form one mole of silica.

After having combined equations (8'), (9), (15) and (17), the differential equation which has to be solved, at each time t, is :

$$\frac{d}{dx}\left[(r_m^2 - r_f^2)\frac{(-D_A C_o)}{C_o - C_A(1-\alpha)}\frac{dC_A}{dx}\right] = \frac{g_m r_{mo}\rho_s B_m^*(\frac{C_A}{C^*})^{p_m}}{y_m M_s} + \frac{g_f r_{fo}\rho_s B_f^*(\frac{C_A}{C^*})^{p_f}}{y_f M_s} \quad (18)$$

all the second order terms, i.e. $\frac{dr_m}{dx}$, $\frac{dr_f}{dx}$, $\frac{dD_A}{dx}$, and $\frac{d\alpha}{dx}$, being taken into account in the resolution procedure.

Boundary conditions

The boundary conditions in the pore are given by :

for x = o $\qquad C_A = C_o \qquad (19)$

for x = l_r $\qquad \frac{-D_A C_o}{C_o - C_A(1-\alpha)}\frac{dC_A}{dx} = k(C_A)^{Pc} \qquad (19')$

Equation (19') is derived from the fact that the diffusion flux of A at x = l_r is equal to the consumption flux of A with the carbon interphase at the bottom of the pore.

The concentration profile of A along the pore being calculated, then the oxidation rate of the carbon interphase at t is given by :

$$\frac{d(l_r)}{dt} = -b\, D_A(l_r)\frac{M_c}{\rho_c}\left(\frac{dC_A}{dx}\right)_{l_r}\frac{C_o}{C_o + C_A(l_r)} \quad (20)$$

where b is the mole number of carbon oxidized per mole of A : its value is 1 and 2 for equations (1) and (2), respectively. Equation (20) will be used in the following to calculate at time t the increase in the carbon length which is consumed by oxidation.

The boundary condition expressed by equation (19') is valid as long as the carbon interphase is not totally consumed. When this is no longer the case, a single straight pore with two open ends is formed. Under such conditions, the molar flux should be nil in the center of the pore, for symmetry consideration, and a new boundary condition equation has to be used, i.e. :

$$\text{for } x = \frac{l_t}{2} \qquad \frac{dC_A}{dx} = 0 \qquad (19'')$$

The other boundary condition (equation (19)) remaining valid.

Numerical solution

The second order differential equation (18) could not be solved analytically. Therefore, a **numerical integration** based on a classical Runge and Kutta algorithm [30] was used to solve equations (18) to (19''), (16) and (16'). An iterative method has been defined to determine the unknown boundary conditions necessary for the respect of known boundary conditions.

The results of the calculations were expressed as : (i) the concentration profiles of the various gaseous species as well as the **silica thickness profiles,**

constituent	chemical nature	$G=\Delta m/m$ ($g\ mol^{-1}$)
interphase	C	-12
matrix	SiC	+20
fiber	$Si_{0.38}C_{0.47}O_{0.15}$	+4.1

Table II : Molar weight changes resulting from the oxidation of ex-PCS fibers, SiC-matrix and C-interphase

along the annular pore, for each value of time t and (ii) **the length of carbon consumed** by oxidation at each t.

Relative weight change $(\Delta m/m_o)_i$

The oxidation of the three components results in different weight changes whose molar values are listed in table II. Since the advancement of each chemical reaction taking place in the annular pore, i.e. corresponding to the oxidation of carbon, SiC-matrix and Si-C-O fibers, is known at any given time t from the model, it is thus possible to calculate the variations of the relative mass of the microcomposite versus time due to the **internal surface** oxidation.

At this level and in order to achieve a better fit with the experimental TGA data, a correction was applied to the volume fraction of the carbon interphase in the model microcomposite, in order to take into account the occurrence of direct contacts between adjacent fibers in the actual 1D-SiC/C/SiC composites. It has been shown in the companion article that each fiber has an average of two direct contacts with neigboring fibers [10]. This feature slightly lowers the volume fraction of the carbon interphase in the composites with respect to that calculated from thickness measurements. A correction taken into account this effect was made which consists in substracting some carbon from the ring corresponding to the interphase in a cross-section of the microcomposite. The correction was applied only to the calculation of the relative weight change. In the following, this relative weight

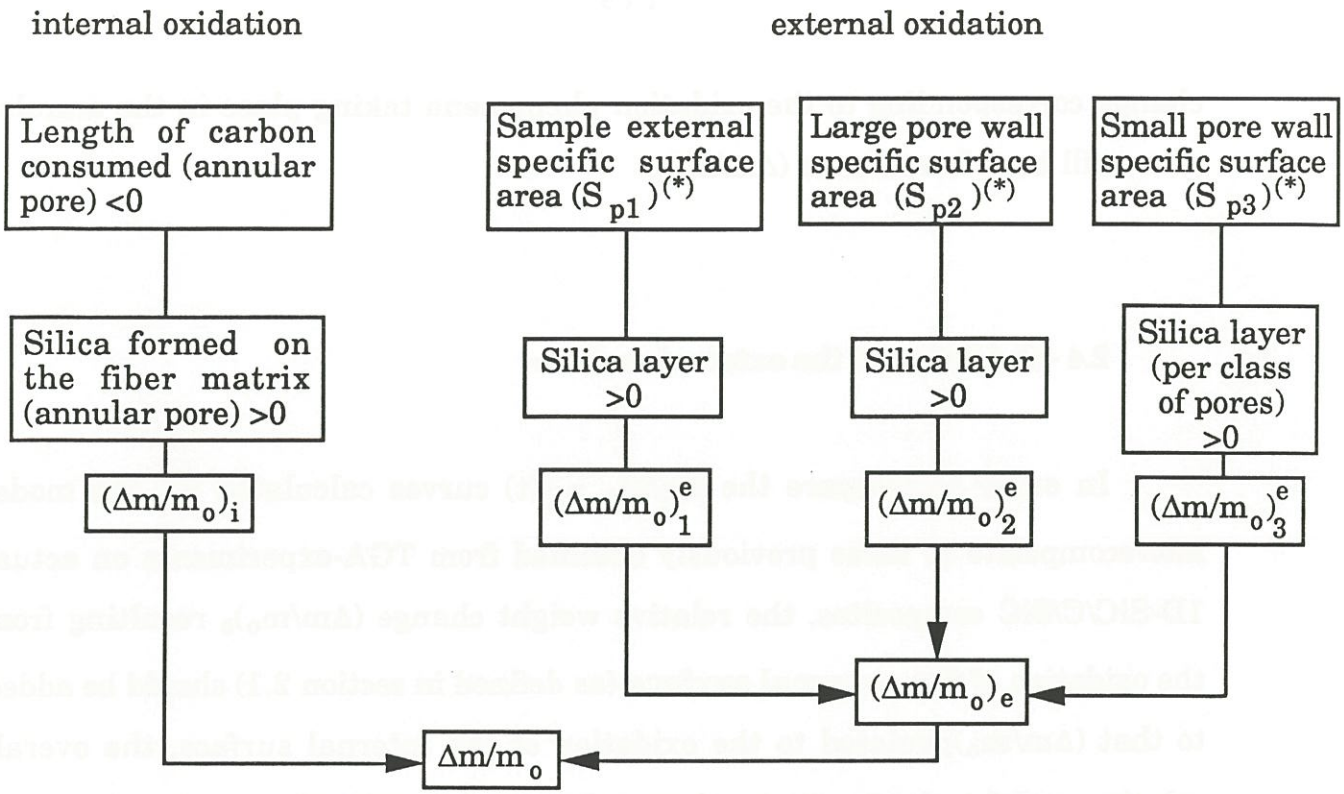

Fig. 2 : Procedure used to calculate the relative weight change due to oxidation: <0 : weight loss; >0 : weight increase; (*) $S_{p1} + S_{p2} + S_{p3} = 0.06\ m^2 g^{-1}$ with $S_{p1} = 6\ 10^{-4}\ m^2 g^{-1}$; $S_{p2} = 4\ 10^{-3}\ m^2 g^{-1}$ and $S_{p3} = 5.6\ 10^{-2}\ m^2 g^{-1}$

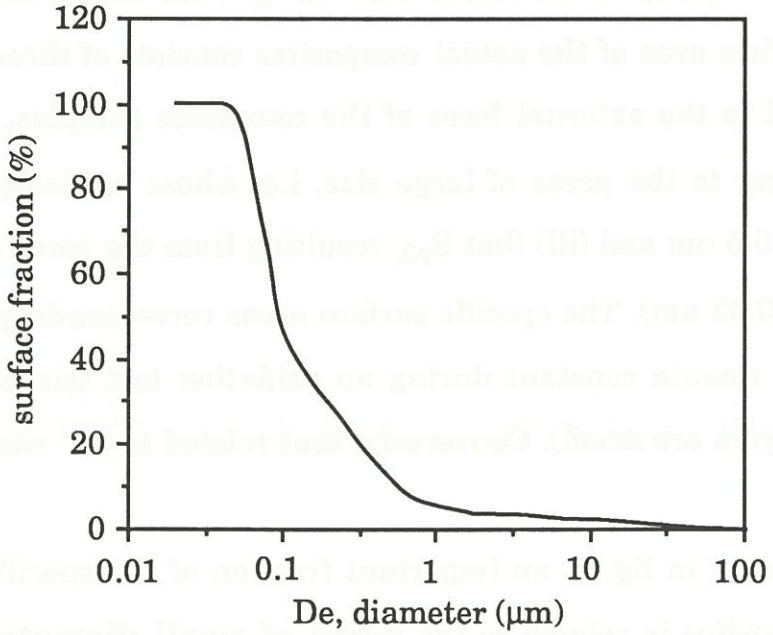

Fig 3: Cumulative distribution a of specific surface area in as received material B_c as measured by mercury porosimetry

change corresponding to the oxidation phenomena taking place in the annular pore, will be referred to as $(\Delta m/m_o)_i$.

2.4 - Oxidation of the external surface

In order to compare the $\Delta m/m_o = f(t)$ curves calculated for the model microcomposite to those previously obtained from TGA-experiments on actual 1D-SiC/C/SiC composites, the relative weight change $(\Delta m/m_o)_e$ resulting from the oxidation of **the external surface** (as defined in section 2.1) should be added to that $(\Delta m/m_o)_i$ related to the oxidation of the internal surface, the overall relative weight change $\Delta m/m_o$ being thus $\Delta m/m_o = (\Delta m/m_o)_i + (\Delta m/m_o)_e$, as shown in fig. 2.

The external **specific** surface area of the model microcomposite is assumed to be equal to that measured by mercury porosimetry on actual 1D-SiC/C/SiC composites, i.e. about 0.06 $m^2\ g^{-1}$. As shown in fig. 2 and 3, the specific surface area of the actual composites consists of three components : (i) that related to the external faces of the composite samples, S_{p1}, (ii) that S_{p2} corresponding to the pores of large size, i.e. whose equivalent diameters are larger than 0,5 um and (iii) that S_{p3}, resulting from the pores of small sizes (i.e. from 0,5 to 0,02 um). The specific surface areas corresponding to (i) and (ii) are assumed to remain constant during an oxidation test (since the thickness of the silica layers are small). Conversely, that related to (iii) varies versus time.

As shown in fig. 3, an important fraction of the specific surface area of actual composites is related to the **pores of small diameters**. However, the

reactive surface actually seen by oxygen for this pore family during an oxidation test, is thought to be rapidly lower than the value which has been measured initially by mercury porosimetry since : (i) the diffusion resistance in such very small pores is important (high Thiele modulus) and large concentration gradients are expected to be present between the pore entrance and pore center and (ii) the growth of the silica layer near the pore entrance should seal very rapidly such pores. The oxidation of the small pore family initially present in 1D-SiC/C/SiC composites appears thus to have some common features with that of RBSN ceramics [31].

In the **model microcomposite**, the external surface is assumed to consist mainly of the wall surface of **cylindrical pores**, parallel to the fiber axis and whose diameters range from 0.02 to 0.5 um. The equations which have been used to depict quantitatively their oxidation are, generally speaking, those previously given for the wall of the annular pores resulting from the release of the carbon interphase, with the following differences : (i) the pore cross-section is no longer annular but circular, (ii) the boundary condition at pore mid-length (assuming that the pores are open at both ends) in that expressed by equation (19''), i.e. the molar flux of A is nil at $l_t/2$ and (iii) the assumption that the growth of silica on the pore wall is taking place in plane geometry is no longer acceptable and thus the growth law corresponding to cylindrical geometry has to be used (appendix-A3).

2.5 - Calculation of the variations of $\Delta m/m_o$ versus time

The overall relative mass change $\Delta m/m_o$ related to the oxidation of the model microcomposite, at a given time t, is calculated as shown in fig. 2,

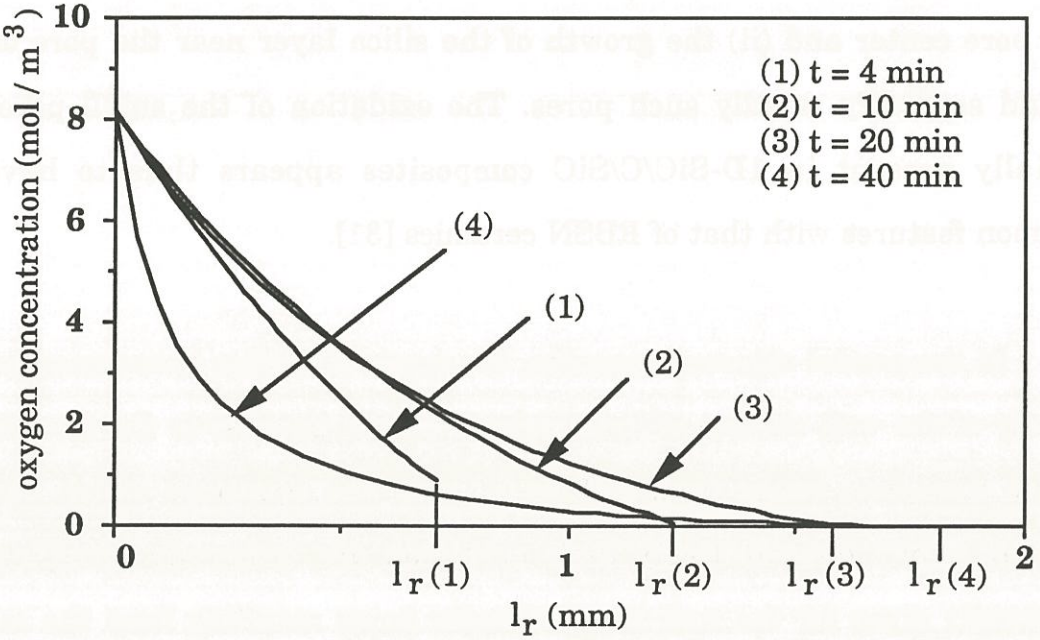

Fig. 4 : Changes of the calculated oxygen concentration profile along the annular pore as a function of time in a model 1D-SiC/C/SiC microcomposite (e = 0.1 μm) simulating an oxidation treatment in pure oxygen (P = 100 kPa) at 1200°C.

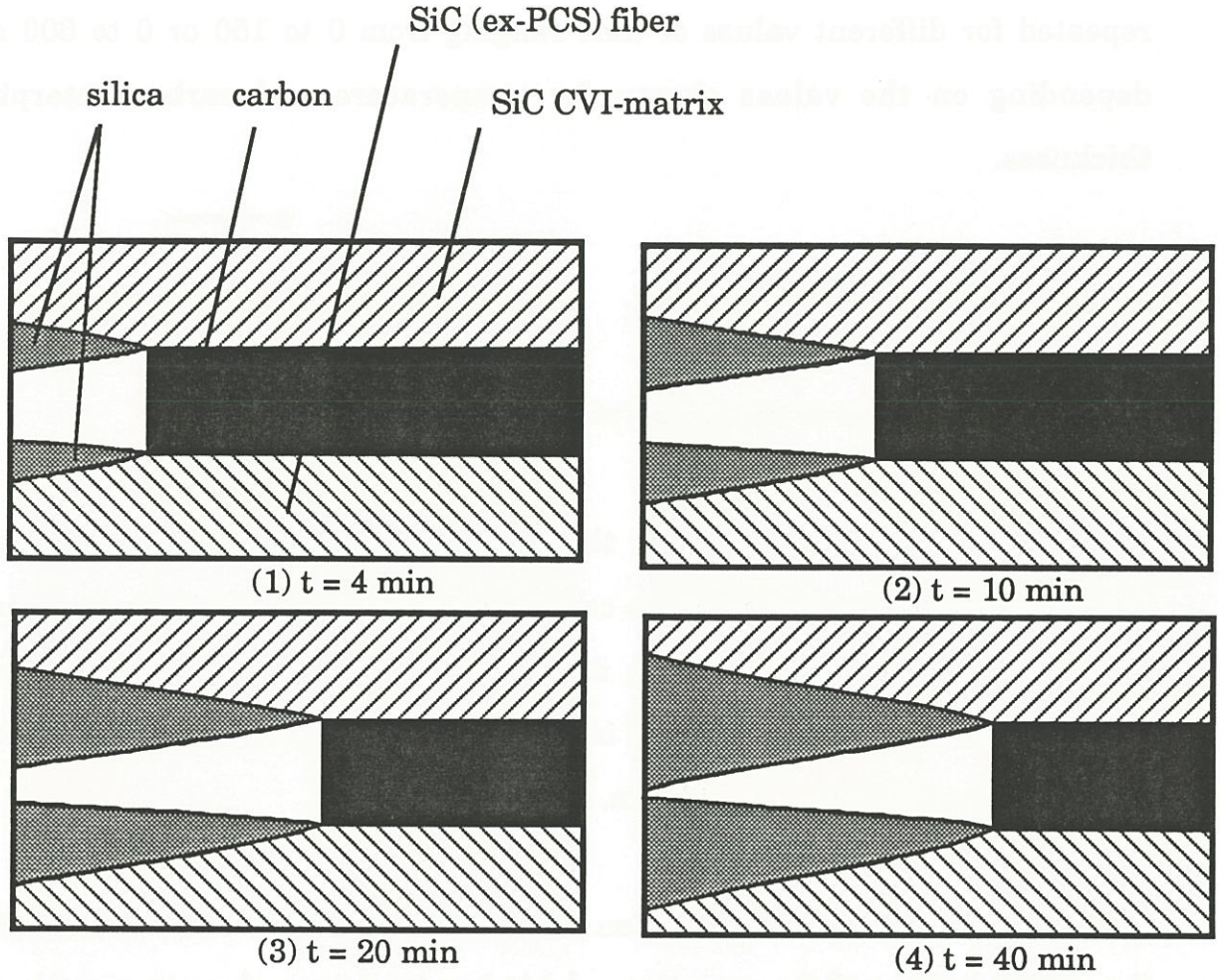

Fig. 5 : Changes of the annular pore geometry as a function of time in a model 1D-SiC/C/SiC microcomposite (e = 0.1 μm) simulating an oxidation treatment in pure oxygen (P = 100 kPa) at 1200°C

according to the equations given in appendix A4. The calculation is then repeated for different values of time ranging from 0 to 150 or 0 to 600 min, depending on the values chosen for temperature and carbon interphase thickness.

3 - RESULTS AND DISCUSSION

3.1 - Examples of numerical simulations

Oxygen concentration and silica thickness profiles along the annular pore resulting from the oxidation of the carbon interphase are shown in fig. 4 and 5. They have been calculated for an interphase thickness of 0.1 μm in order to simulate oxidation tests performed in pure oxygen (P = 100 kPa) at 1200°C with durations ranging from 4 to 40 min.

As shown in fig. 4, the oxygen concentration at the carbon reaction front (i.e. at the bottom of the pore or $x = l_r$) is low (and even close to zero in some cases). This feature means that the carbon reaction rate is fast with respect to the diffusion mass transfers along the pore. Furthermore and as shown in fig. 5, the length of the annular pore increases versus time whereas its width decreases owing to the formation of the silica scale on the pore walls, at the exposure of SiC and Si-C-O.

If one assumes that the oxygen consumption by the pore walls could be neglected, the equation (18) can be rewritten, for a straight pore of constant cross-section at the bottom of which carbon is consumed according to equation (1), as :

$$\frac{d}{dx}\left(\frac{dC_A}{dx}\right) = 0 \qquad (18')$$

Under such conditions, the integration of equation (18') yields concentration profiles along the annular pore which are linear. The **non-linearity** which is observed for the concentration profiles calculated according to the present model is due to : (i) the reaction of the pore wall with the oxidizing species and (ii) the pore geometry change versus time. It clearly appears from fig. 4 that the concentration profiles near the pore entrance become steeper when the oxidation duration increases.

The pore geometry change which is obtained when the oxidation proceeds, increases the diffusion resistance in the annular pore. It is thus logical that the concentration profiles along the pore are observed to become steeper versus time. Thus, for an oxidation duration close to that corresponding to pore sealing, i.e. t = 40 min, the chemical reaction between the oxidizing species and the pore wall is found to **deplete rapidly the gas phase** in oxidizing species when moving from the pore entrance towards the pore center.

Carbon length consumed l_r

The variation of the oxidizing species concentration profiles and its depletion in the gas phase at $x = l_r$, lower the oxygen flux available for the oxidation of the carbon interphase at the bottom of the annular pore. Therefore, the rate at which the carbon interphase is consumed is expected to decrease as the oxidation duration is increased.

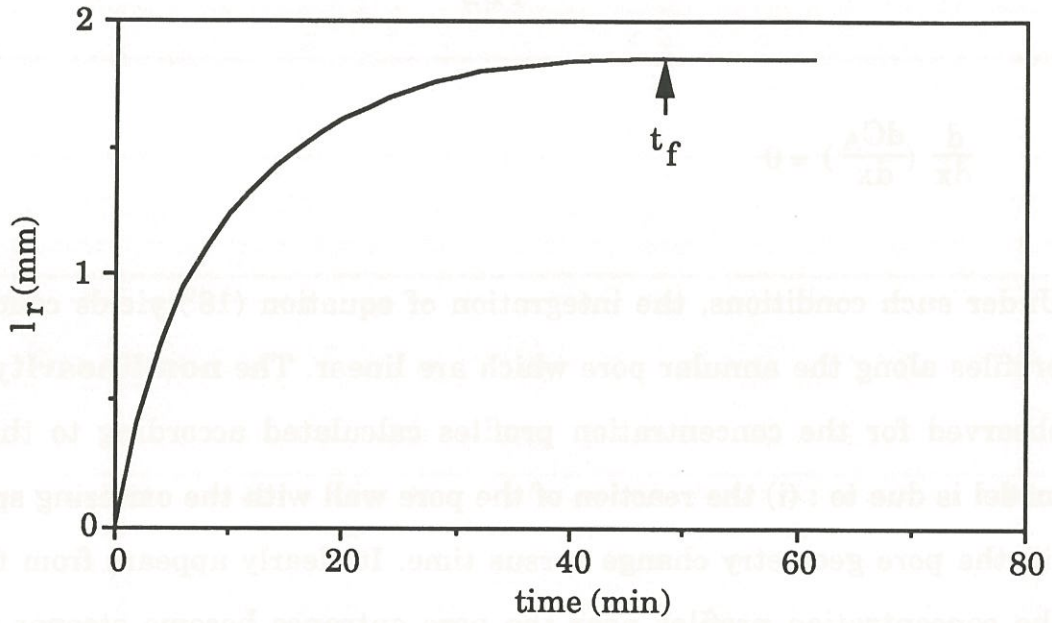

Fig. 6 : Variations of the calculated carbon interphase length consumed by oxidation in a model 1D-SiC/C/SiC microcomposite (e = 0.1 μm) during an oxidation treatment in pure oxygen (P = 100 kPa) at 1200°C (the arrow indicates pore sealing at t_f)

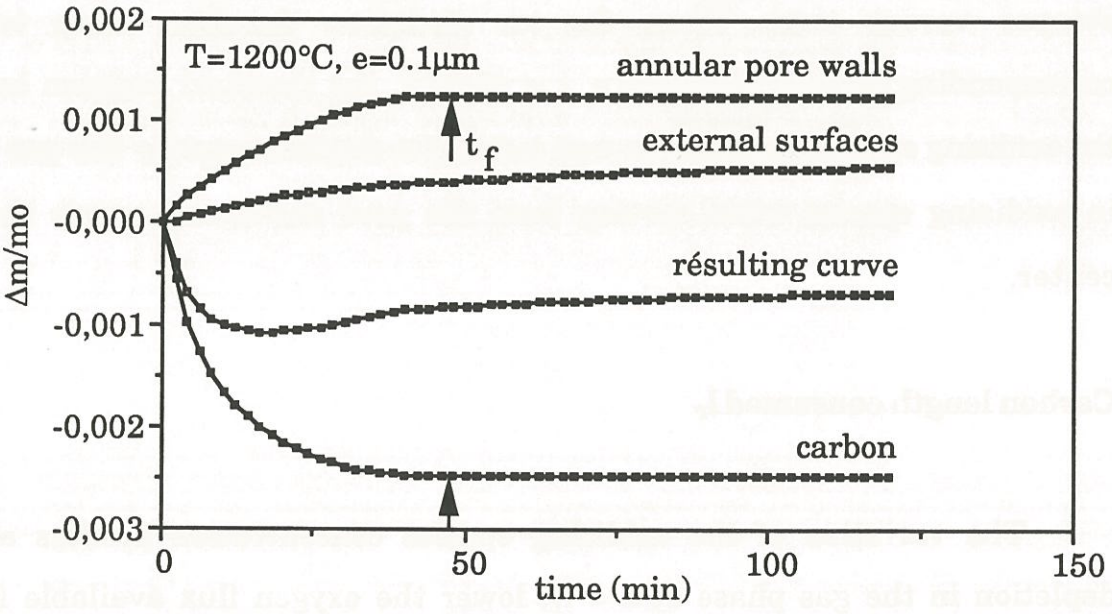

Fig. 7 : Variations of the relative weight change as a function of time calculated for a 1D-SiC/C/SiC microcomposite (e = 0.1 μm) simulating an oxidation treatment in pure oxygen (P = 100 kPa) at 1200°C (the arrows indicate pore sealing at t_f)

The variations of the length of carbon interphase consumed by oxidation as a function of time, calculated from the model, are shown in fig. 6. As expected, the kinetics of growth of l_r decrease rapidly with increasing oxidation duration to become nil (arrow) when the silica layers seal the pore.

Relative weight change $\Delta m/m_o$

The variations of $\Delta m/m_o$ as a function of time are shown in fig. 7 with the three components : (i) the oxidation of the carbon interphase (weight loss), (ii) the oxidation of the annular pore walls (weight increase) and (iii) the oxidation of the so-called external surface (weight increase). Note that the weight change related to (i) + (ii) is $(\Delta m/m_o)_i$; and that related to (iii) is $(\Delta m/m_o)_e$. Furthermore and as already mentioned, the oxidation of both the carbon interphase and the pore wall stops when the annular pore becomes sealed (arrows) whereas that of the external surface continues.

The **resulting curve** (obtained by adding the three components) shows first a weight loss followed by a weight increase whose rate decreases as the oxidation duration is raised beyond t_f (time necessary for pore sealing). Thus, the predominant mechanisms in the oxidation of the model microcomposite are successively : (i) the oxidation of carbon, (ii) the oxidation of the pore walls (SiC-matrix and Si-C-O fibers) and (iii) that of the external surface.

Quantitatively, such a sequence is in good agreement with the general features of the TGA curves which have been reported for actual 1D-SiC (ex-PCS)/C/SiC (CVI) composites, under the same oxidation conditions than those

considered here, in the companion article [10]. Thus, the results of the numerical simulations and more generally the model presented in section 2 are **qualitatively** in good agreement with the experimental data. However, before considering a more quantitative fit, some of the choices which have been done for the model parameters have to be discussed.

3.2 - Choice and influence of the model parameters

In the application of the model depicted in section 2 to the oxidation of 1D-SiC/C/SiC microcomposites, **most parameters have been given fixed values** (i.e. values from literature or which have been measured experimentally). Thus, the values of the diffusion coefficients, i.e. D_M and D_K, for the gas phase, have been calculated according to well-established laws, on the one hand, whereas the kinetic parabolic constants related to the oxidation of both the ex-PCS Si-C-O fibers(*) and SiC-CVI-matrix(**) have been measured previously, on the other hand [21,22]. However, some uncertainty remained concerning two important points : (i) the oxidation kinetic law of carbon and (ii) the related chemical reaction.

Carbon oxidation kinetic law

The oxidation kinetics of a pyrocarbon coating deposited on ex-PCS fibers, have not yet been, as far as we know, the subject of a specific experimental approach under conditions of reaction-rate control at high temperatures. As a matter of fact, the contribution of the diffusion mass transfers across the boundary layer to the carbon oxidation kinetics is known to be rate-controlling

(*) Nicalon (grade NLM 202) fibers from Nippon Carbon
(**) deposited from CH_3SiCl_3/H_2 at about 1000°C

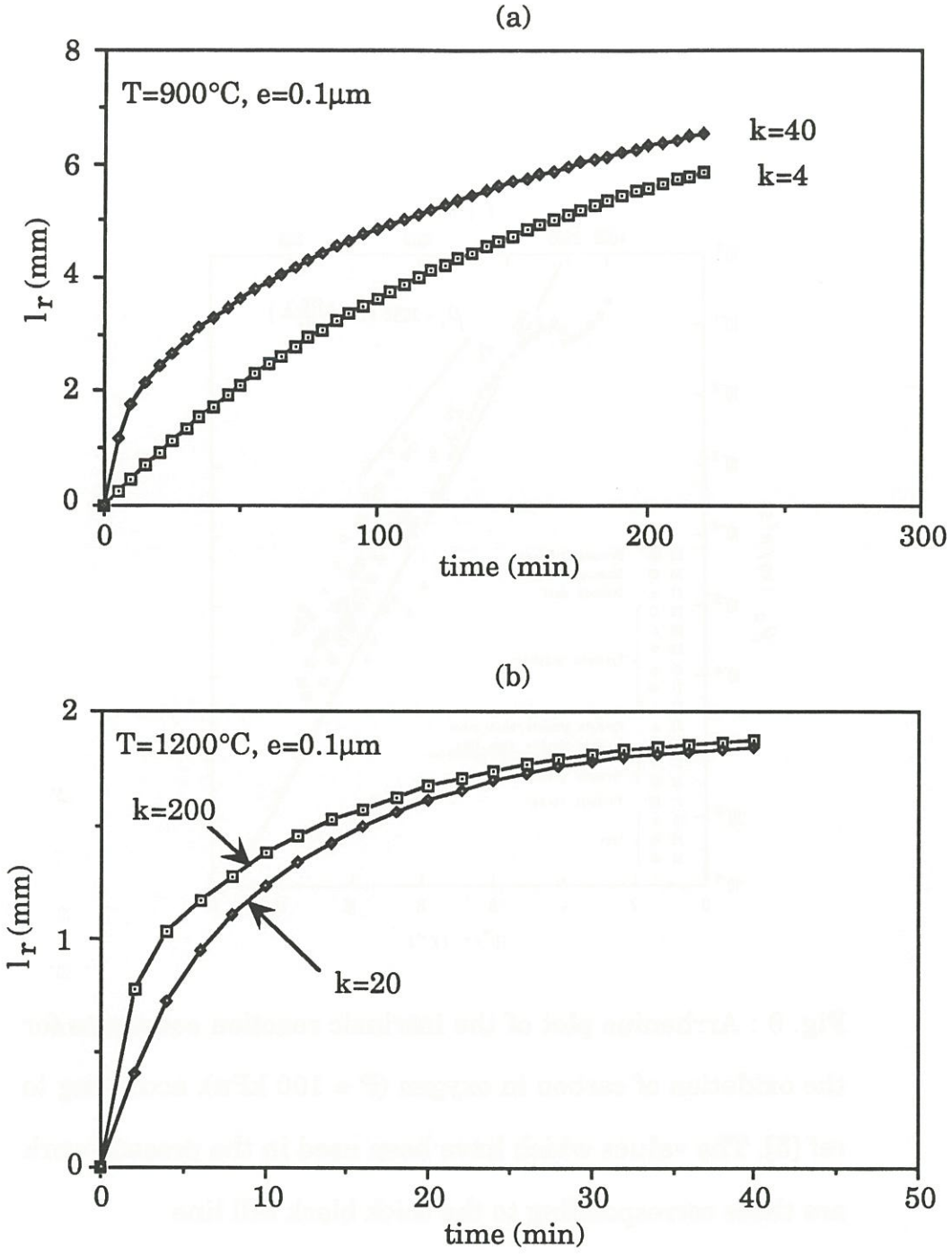

Fig. 8 : Influence of the reaction constant value k chosen for the oxidation of carbon on the calculated length of carbon interphase consumed in the model microcomposite (e = 0.1 µm) during an oxidation test in pure oxygen (P = 100 kPa) at : (a) 900°C and (b) 1200°C

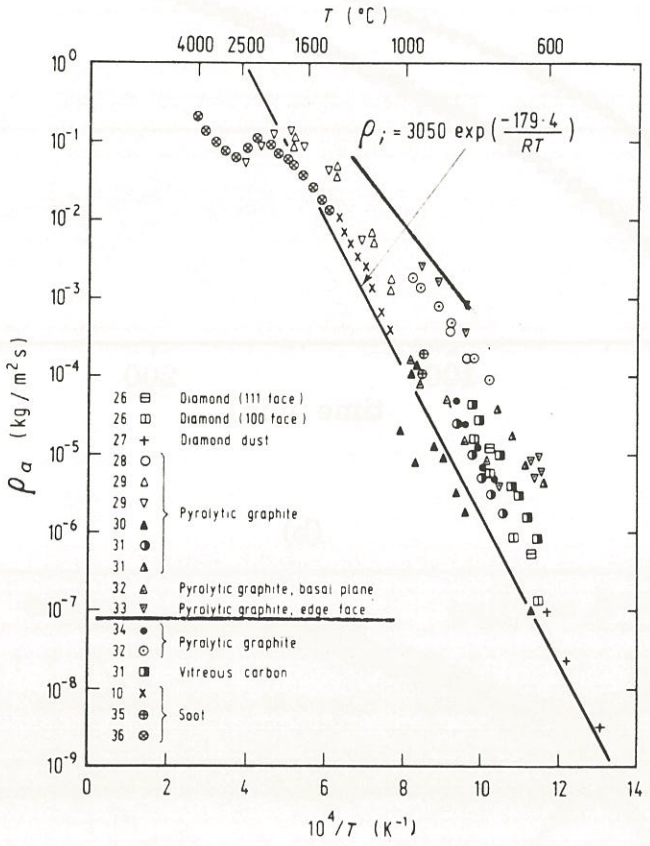

Fig. 9 : Arrhenius plot of the intrinsic reaction constants for the oxidation of carbon in oxygen (P = 100 kPa), according to ref [5]. The values which have been used in the present work are those corresponding to the thick black full line

at high temperatures and thus the measurement of the reaction constant characterizing the actual chemical phenomenon is difficult [17]. Consequently, the values of the reaction constants related to the oxidation of the carbon interphase which have been used in the present work have been chosen in order to lead to a satisfactory fit between the calculated and experimental $\Delta m/m_0$ curves presented in section 3.3.

The influence of the value given to the carbon oxidation reaction constant on the length of carbon consumed by oxidation, as it has been calculated from the model, is shown in fig. 8. As expected, at high temperatures, i.e. when the diffusion mass transfers in the gas phase become preponderant (fig. 8b), the effect of the value chosen for the reaction constant is weak and noticeable only for the pore of small lengths (i.e. at low l_r). As an example, for a model microcomposite with a thin carbon interphase (e = 0.1 μm), the length of carbon interphase that would be consumed in pure oxygen at 1200°C at t = tf increases only from 1.84 to 1.86 mm when the reaction rate constant is multiplied by ten. Conversely, at low oxidation temperatures (e.g. 900°C), the effect of the value given to the reaction constant, on l_r is more significant (fig. 8a). This result is surprising in first analysis since it is usually admitted that diffusion mass transfers are rate-controlling the oxidation of carbon beyond 700 - 800°C [2,5]. However, in the present model and as stated in section 2.1, it has been assumed that all the mass transfers outside the pore are very fast (i.e. the boundary layer thickness is nil), thus explaining that the reaction kinetics are observed to still have an influence on the length of carbon consumed at 900°C.

The values of the reaction constants which have been used in the present work for the oxidation of the carbon interphase are shown in fig. 9 [5]. The

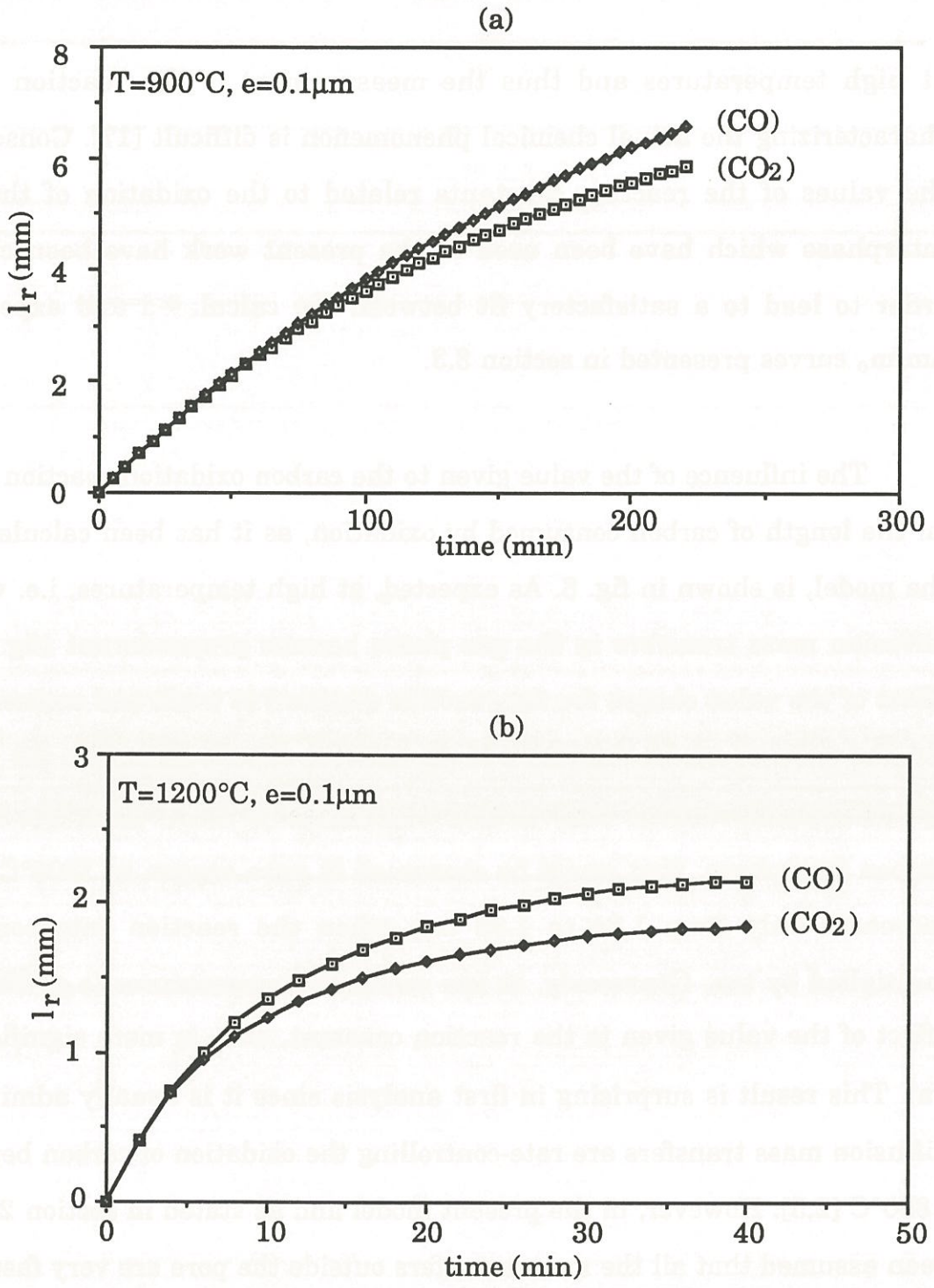

Fig. 10 : Influence of the choice of the gaseous reaction product on the length of carbon consumed by oxidation in a model 1D-SiC/C/SiC microcomposite (e = 0.1 µm) simulating an oxidation treatment in pure oxygen (P = 100 kPa) at : (a) 900°C ; (b) 1200°C

reaction order has been equal to 0.3 [18]. They are close to those reported for the oxidation of a pyrocarbon occurring parallel to the substrate surface, this configuration being also that of the TGA experiments reported in the companion article [10].

The kinetic law which has been used in the present work can be expressed according to the following equation :

$$V_i = kC_A^{p_c} \frac{M_c}{b} \qquad (21)$$

where V_i in kg m^{-2} s^{-1} is the intrinsic reaction rate, k the reaction rate constant, C_A the oxygen concentration, p_c the reaction order, M_c the molar mass of carbon and b is the mole number of carbon oxidized per mole of A.

Nature of the carbon oxidation chemical reaction

As already mentioned in section 2, the calculations concerning the oxidation of the model microcomposite have been performed assuming that CO_2 **or** CO is the reaction product. It is thought that these assumptions correspond to limit cases, the reaction product might be actually a mixture of both CO **and** CO_2.

The influence of the choice of the reaction set (i.e. reactions (1), (3) (3') or reactions (2) (4) (4')) on the calculated length of carbon interphase consumed by oxidation is shown in fig. 10 for the model microcomposite with a thin carbon interphase (e = 0.1 μm) and two different temperatures.

It clearly appears that the corresponding curves $l_r = f(t)$ are almost the same for short oxidation times, whatever temperature, but that they become divergent as the oxidation duration is further increased. As an example, at 1200°C, the value of l_r at $t = t_f$ increases from 1.84 to 2.16 mm when CO is replaced by CO_2 as the reaction product of the oxidation of the material components.

The effect of the reaction set on l_r can be explained by considering the values of the **stoichiometric coefficients** which are involved in the various reaction equations. Considering first equations (1) and (2), one mole of oxygen reacts with only one mole of carbon according to (1) whereas it reacts with two according to (2). However, the resulting effect (in term of carbon consumption) when CO_2 is replaced by CO is balanced by that related to the concomitant increase in the overall mole number of the gaseous species which is responsible for a higher product counterflux lowering thus the direct flux of oxygen in the pore. In the same manner comparing now equations (3) and (4) or (3') and (4'), it appears that the oxygen mole number consumed by reaction with the pore walls is less when CO is involved. Thus, the residual oxygen flux at $x = l_r$ available for the oxidation of the carbon interphase would be higher when the reaction product of SiC and SiC_xO_y is CO. Conversely, the change in the mole number of the gaseous species has an opposite effect on the flux of oxygen entering the pore. Finally and as shown in appendix 2, the binary diffusion coefficients calculated according to equations (A4) and (A5) are higher for the CO - O_2 mixtures than for the CO_2 - O_2 mixtures.

Obviously, all the differences which have been mentioned above when the reaction product CO is assumed to be replaced by the other possible reaction

product CO_2, would have a significant influence only when the oxidation process is rate-controlled by diffusion mass transfers in the gas phase. At the beginning of the oxidation process of the model composite, the annular pore is short with a rather large cross-section. As a result the depletion of the gas phase in the pore (due to reaction of oxygen with the pore walls) is low and thus the consumption rates of carbon assuming that CO or CO_2 are respectively formed, are almost the same (explaining that the values of l_r calculated for CO and CO_2 are very similar for short oxidation times) (fig. 10). Conversely, as the oxidation of the microcomposite proceeds, the pore length increases and the cross-section decreases with the result that mass transfers by diffusion along the pore are predominant explaining thus that the nature of the reaction product which is introduced in the model has now an influence.

Generally speaking and as shown in fig. 10, the main features of the $l_r = f(t)$ curves calculated for the CO/O_2 and CO_2/O_2 couples are similar, the difference between the two related values of l_r at a given t remaining small. It is thought that the actual value of l_r falls in between (as an example, for e = 0.1 μm ; T = 1200°C, t = tf, the mean value of l_r would be 2.00 mm which has to be compared with the extreme values, i.e. 1.84 and 2.16 mm). Therefore, all the numerical simulations presented in the following have been done considering that **CO_2 is the reaction product.**

3.3 - Comparison of the results of the numerical simulations with the experimental data

As described in the companion article, TGA experiments have been performed on parallelipiped samples (3 x 3 x 13 mm^3) of 1D-SiC (ex-PCS)/C/SiC

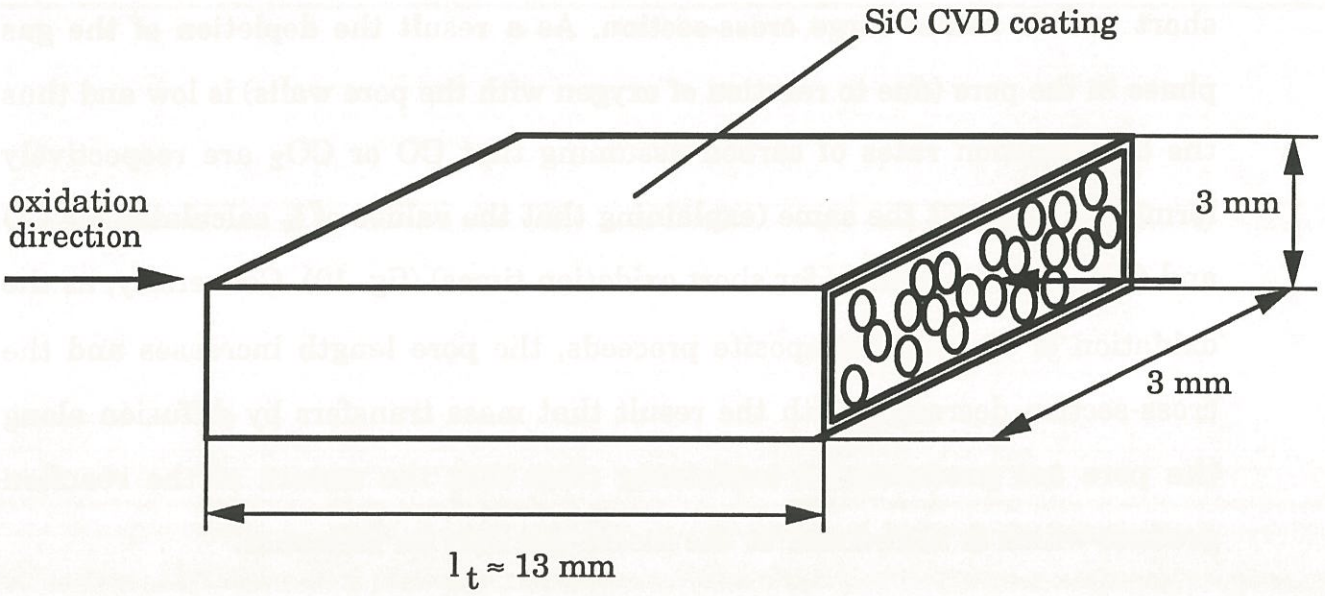

Fig. 11 : 1D-SiC (ex-PCS)/C/SiC (CVI) composite samples used for the TGA-experiments

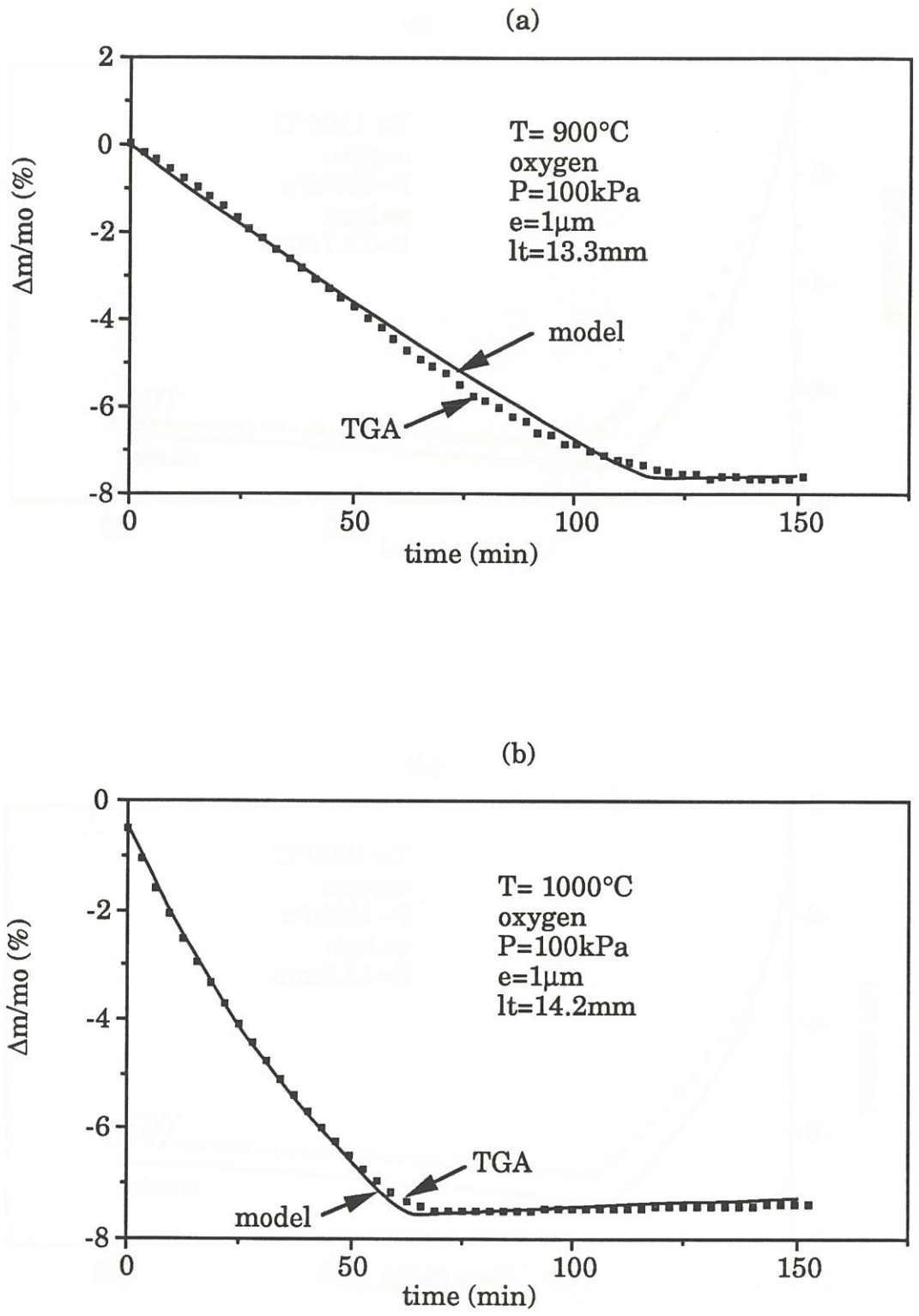

Fig. 12 : Variations versus time of the relative weight change, as established by TGA on actual 1D-SiC (ex-PCS)/C/SiC (CVI) composites (material B with a thick carbon interphase) and as calculated for the model microcomposite, for an isothermal treatment in pure oxygen (P = 100 kPa) at : (a) 900°C ; (b) 1000°C ; (c) 1100°C and (d) 1200°C

(c)

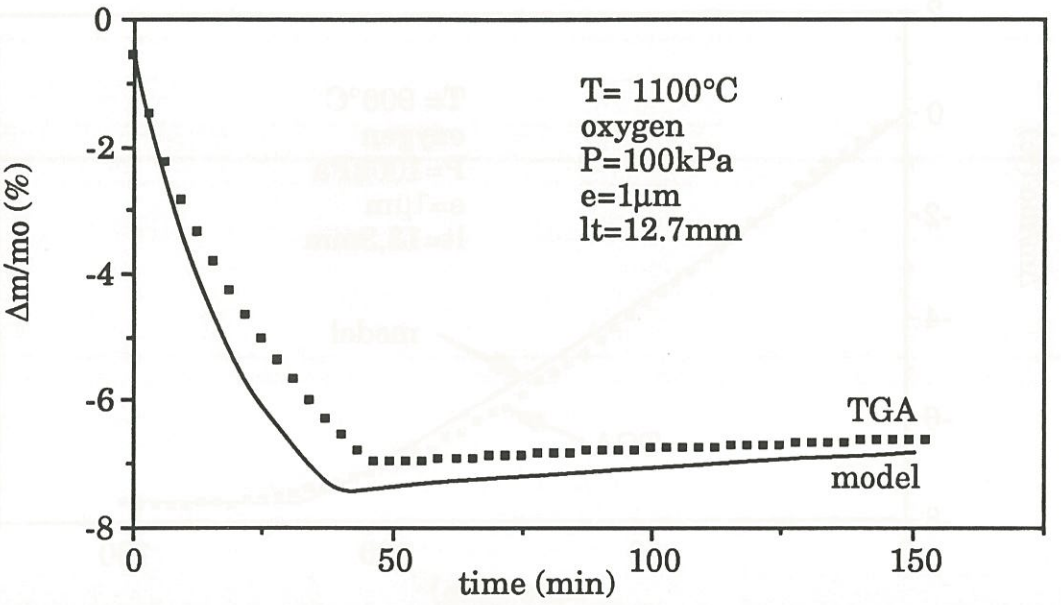
T= 1100°C
oxygen
P=100kPa
e=1µm
lt=12.7mm
TGA
model
Δm/mo (%)
time (min)
0
-2
-4
-6
-8
0
50
100
150

(d)

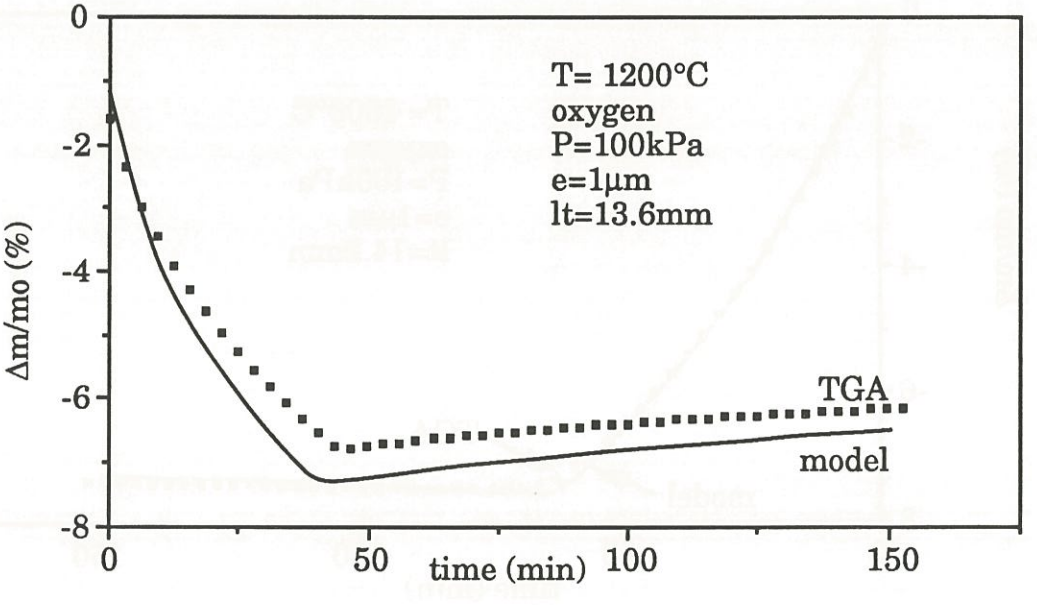
T= 1200°C
oxygen
P=100kPa
e=1µm
lt=13.6mm
TGA
model
Δm/mo (%)
time (min)
0
-2
-4
-6
-8
0
50
100
150

(CVI) composites which have received a SiC CVD-coating on all the faces parallel to the fiber direction (fig. 11). Under such conditions, oxidation proceeds unidirectionally along the fiber axis. Two different materials were studied : in materials A the thickness of the carbon interphase was e = 0.1 μm whereas in materials B it was e = 1 μm [10].

Materials B (e = 1 μm)

The $\Delta m/m_0 = f(t)$ curves obtained experimentally by TGA on the actual 1D-SiC (ex-PCS)/C/SiC (CVI) composites and calculated according to the model depicted in section 2 for the corresponding microcomposite, are shown in fig. 12 for temperatures ranging from 900°C to 1200°C. During the TGA experiments, the sample was heated in oxygen from room temperature to the test temperature (T_0). Since the curves presented here are isothermal curves, they do not include the transient initial regime with the result that at t = 0 (defined as the origin of the isothermal treatment), $\Delta m/m_0 \neq 0$ (i.e. $\Delta m/m_0$ at t = 0 is usually negative since under such conditions, the oxidation of the carbon interphase is predominant as already mentioned, its value being noticeable for the high test temperatures). To simulate this effect, the related microcomposite was considered in the calculations with an initial length of carbon already consumed at t = 0.

It clearly appears from fig. 12, that there is a **fair agreement** between the experimental data and the calculated curves. At low temperatures, i.e. T_0 = 900°C and 1000°C, the agreement is even excellent considering the nature of the actual 1D-SiC (ex-PCS)/C/SiC (CVI) composites. At high temperatures, i.e. T_0 = 1100°C and 1200°C, the agreement is somewhat less satisfactory although still

(a)

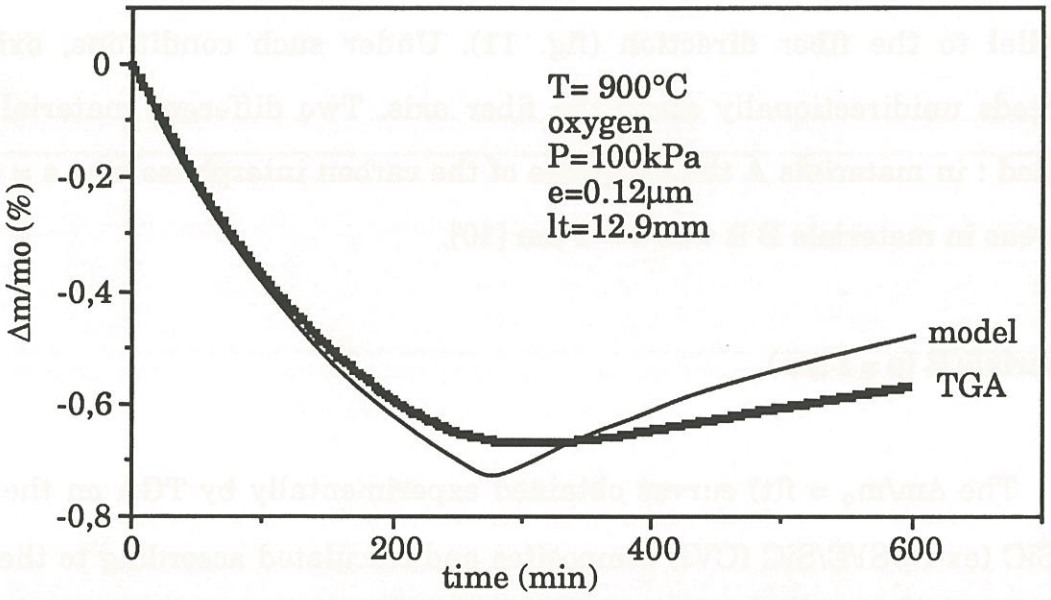

(b)

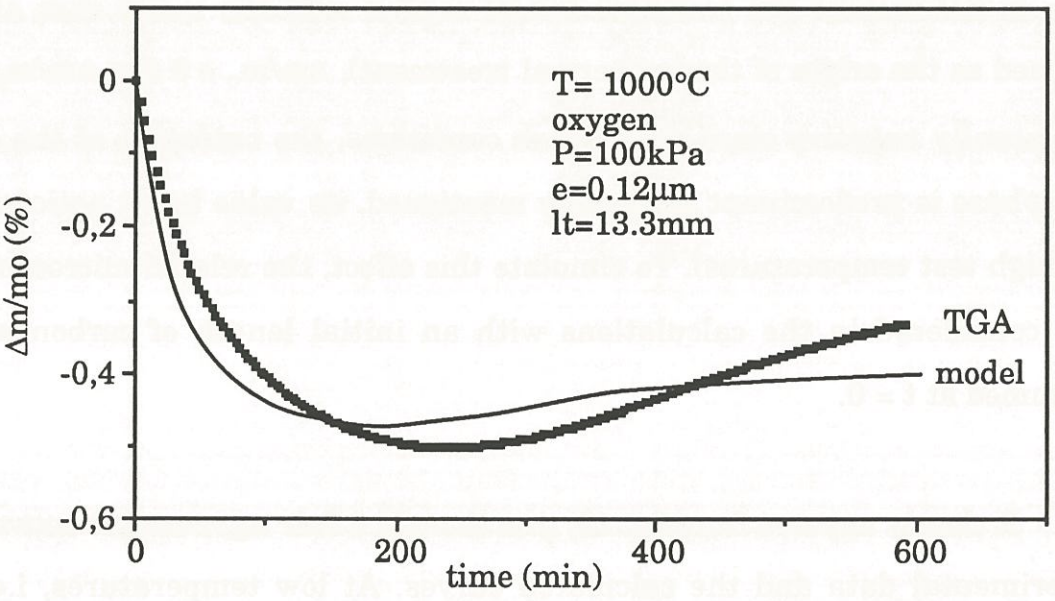

Fig. 13 : Variations versus time of the relative weight change, as established by TGA on actual 1D-SiC (ex-PCS)/C/SiC (CVI) composites (material A with a thin carbon interphase) and as calculated for the model microcomposite, for an isothermal treatment in pure oxygen (P = 100 kPa) at : (a) 900°C ; (b) 1000°C ; (c) 1100°C and (d) 1200°C

(c)

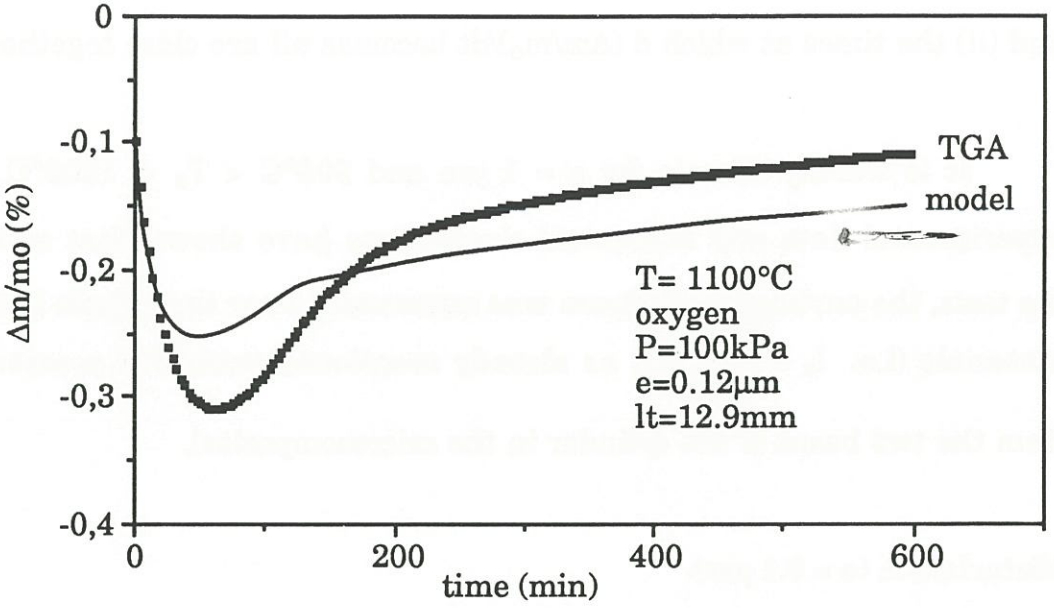
0
-0,1
-0,2
-0,3
-0,4
Δm/mo (%)
0
200
400
600
time (min)
TGA
model
T= 1100°C
oxygen
P=100kPa
e=0.12µm
lt=12.9mm

(d)

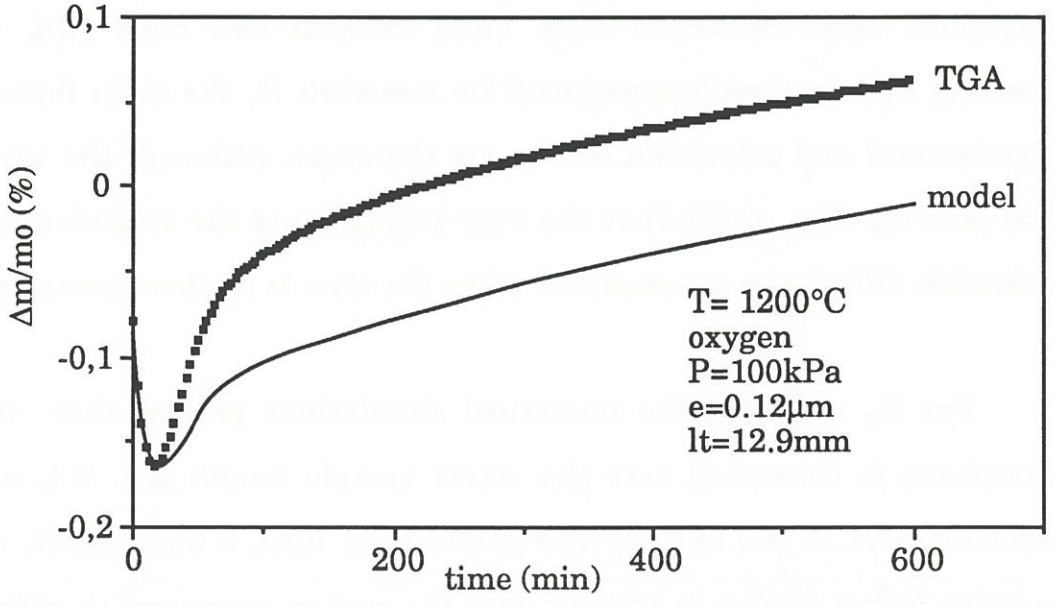
0,1
0
-0,1
-0,2
Δm/mo (%)
0
200
400
600
time (min)
TGA
model
T= 1200°C
oxygen
P=100kPa
e=0.12µm
lt=12.9mm

acceptable : (i) the TGA and calculated curves exhibit the same main features and (ii) the times at which d $(\Delta m/m_0)/dt$ becomes nil are close together.

It is worthy of note for e = 1 μm and 900°C < T_0 < 1200°C, both the experimental data and numerical simulations have shown that at the end of the tests, the **carbon interphase was consumed over the whole length** of the materials (i.e. $l_r = \frac{l_t}{2}$, since, as already mentioned oxidation proceeds equally from the two bases of the cylinder in the microcomposite).

Materials A (e = 0.1 μm)

The TGA and calculated $\Delta m/m_0 = f(t)$ curves are shown in fig. 13 for materials A with a nominal interphase thickness of 0.1 μm. However, in the numerical simulations, a thickness of e = 0.12 μm (corresponding to the maximum value measured from TEM images) was used [10]. Generally speaking and as already mentioned for materials B, the main features of the experimental and calculated curves are the same. Although the agreement is good (see fig. 13a, c and d) at the very beginning of the oxidation tests, some noticeable differences are observed when the time is further increased.

For T_0 = 900°C, the numerical simulations predict that the carbon interphase is consumed over the whole sample length (i.e. 2 l_r = lt) for an exposure close to 300 min. At this particularly time, d $(\Delta m/m_0)/dt$, which was negative before (owing to the fact that the carbon consumption with a weight loss is predominant at such a low temperature) becomes suddenly positive with a low absolute value (since the formation of silica takes place with a weight increase but with a low rate at 900°C). The corresponding transition in the

actual composites although it is indeed observed for a time close to that predicted by the model is much less sharp. For **T_o = 1000°C**, the annular pore in the model microcomposite should become sealed by silica before all the carbon interphase is consumed (arrow in fig. 13b). Beyond t_f, the value of d ($\Delta m/m_o$)/dt characterizing the weight increase related to the oxidation of the SiC CVI-matrix is much lower than that observed for T_o = 900°C since in this latter case the annular pore was not sealed and the surface seen by oxygen (i.e. the annular pore wall and external surface) much larger. This difference in the positive slopes of the curves is not observed on the TGA-curves recorded for the tests performed at 900°C and 1000°C.

For **T_o = 1100°C and 1200°C** still more significant differences are observed between the experimental and calculated $\Delta m/m_o$ = f(t) curves, the main difference being in the fact that : (i) the positive slope of the curve when the oxidation of SiC-based components becomes predominant is higher for the TGA-curves and (ii) the overall related weight increase is higher. Conversely, the main features of the experimental and calculated curves remain the same suggesting that the model depicts correctly the phenomena occurring during the oxidation of the actual materials.

The curves corresponding to T_o > 1200°C are not shown here since most of the interesting phenomena take place during the initial transient (i.e. non isothermal) regime (a different experimental procedure would have been necessary to study this temperature domain).

Finally, the **lengths of carbon interphase consumed** at the end of the tests (see fig. 13), as established experimentally (on the basis of electrical

length of carbon interphase consumed by oxidation	Temperature T_o (°C)				
	900	1000	1100	1200	1300
experimental (electrical measurement on composites) (mm)	> 6.5	> 6.6	3.4	2.2	1.5
calculated for model microcomposite with e = 0.12μm (mm)	11.2	6.2	3.7	2.4	1.8
calculated for model microcomposite with e = 0.11μm (mm)	10.0	5.5	3.3	2.2	1.6

Table III : Lengths of carbon interphase consumed by oxidation after an oxidation test performed in pure oxygen (P = 100 kPa ; t = 600 min) as established from electrical measurements on actual 1D-SiC (ex-PCS)/C/SiC(CVI) composites and from numerical simulation with the microcomposite model.

measurements described in the companion article) and calculated from the model, have been compared [10]. The data listed in table III show that the agreement is fair for e = 0.12 μm and becomes very good for e = 0.11 μm. One should again emphasize that the number of adjustable parameters in the model is limited to the carbon interphase thickness (chosen here close to that measured on TEM images) and nature of the reaction product (CO_2 in the present simulation). If CO_2 is replaced by CO, the length of carbon interphase consumed at 1200°C would be 2.16 mm, as shown in fig. 10b for e = 0.1 μm. Finally, it has been shown that the value chosen for the reaction constant related to the oxidation of carbon has but a low influence on the value of l_r (fig. 8).

Limitation of the model

The microcomposite model developed in section 2 depicts in a satisfactory manner the main features of the oxidation behavior of the actual 1D-SiC (exPCS)/C/SiC (CVI) composites. However, the differences which are observed between the TGA and calculated $\Delta m/m_0 = f(t)$ curves suggest that some of the assumptions of the model might be unapropriate to take into account the complexity of the materials and of the oxidation mechanisms.

First, the simple axisymmetrical geometry chosen for the microcomposite does not correspond exactly to the actual materials. In the microcomposite, the **thickness of the carbon interphase** is assumed to be constant whereas TEM images have shown that this is not the case [10]. Furthermore, the relative position of the fiber with respect to the matrix (which is assumed to remain axisymmetrical in the model) has been observed to

change versus time in the composites : when the annular pore is formed the fiber has a tendancy **to move off axis** towards the pore wall (the effect being more pronounced near the pore entrance than near the bottom where the carbon oxidation takes place). As a result, the **time necessary to seal the pore (t_f) can increase** considerably. When the annular pores, in the composites, become long and narrow, the oxidation of the pore wall are preponderant. Thus, the effect that the fiber moves off-axis enlarge the width of the annular pore and favors the oxygen diffusion and the formation of silica. The change in the pore geometry might thus partly explain the higher weight increase observed in the second part of the TGA curves with respect to the calculated curves (fig. 13 b-d).

The second limitation of the model deals with the assumptions made in the model about the **chemistry of the oxidation process** in the pore. The coexistence at high temperatures of oxygen with carbon monoxide remains hypothetical. Moreover, when CO_2 is assumed to be the reaction product, both the fiber and matrix pore walls see a O_2/CO_2 mixture. It has been reported by Fitzer and Ebi that SiC is oxidized by CO_2 with formation of silica [32], presumably according to the following overall equation :

$$SiC + 3\,CO_2 \rightarrow SiO_2 + 4CO \qquad (22)$$

Thus, near the carbon reaction front (i.e. at the pore bottom) where CO_2 is the main gaseous species, the silica formation and the related weight increase might be actually more significant than that calculated for the model microcomposite (since the reaction between SiC and CO_2 has not been taken into account). Finally, one should emphasize that the parabolic rate constants

corresponding to the oxidation of both the ex-PCS Si-C-O fibers and SiC-matrix in O_2-CO-CO_2 mixtures of various compositions (in the passive oxidation regime) have not been reported yet, as far as we know.

Another questionable point in the model deals with the ability of the **equations** which have been used to depict correctly the phenomena. Taking into account the way according to which the calculations are performed, it is assumed implicitly that the effective **diffusion coefficients** of O_2 and CO_2 are identical. Obviously, since the molar masses of these two species are different, the values of the Knudsen diffusion coefficients D_K (as calculated according to equation (A7') are themselves different. Thus, CO_2, the slower species, would have a tendency to stay within the pore, increasing locally the pressure and diminishing the direct flux of oxygen. This phenomenon, which has been also mentioned by Hewitt, is not taken into account in the equations used in the present model [27].

3.4 - Prospective use of the model

From a mechanical behavior standpoint, the main effect of oxidation, in 2D-SiC (ex-PCS)/C/SiC (CVI) composites, is not related to the weight change itself but rather to the change that occurs in the fiber/matrix bonding over a given fiber length. Although the model has some limitations, as discussed in section 3.3, it can be used nevertheless to foresee the influence of various material or/and test parameters on the rate at which the carbon interphase is consumed.

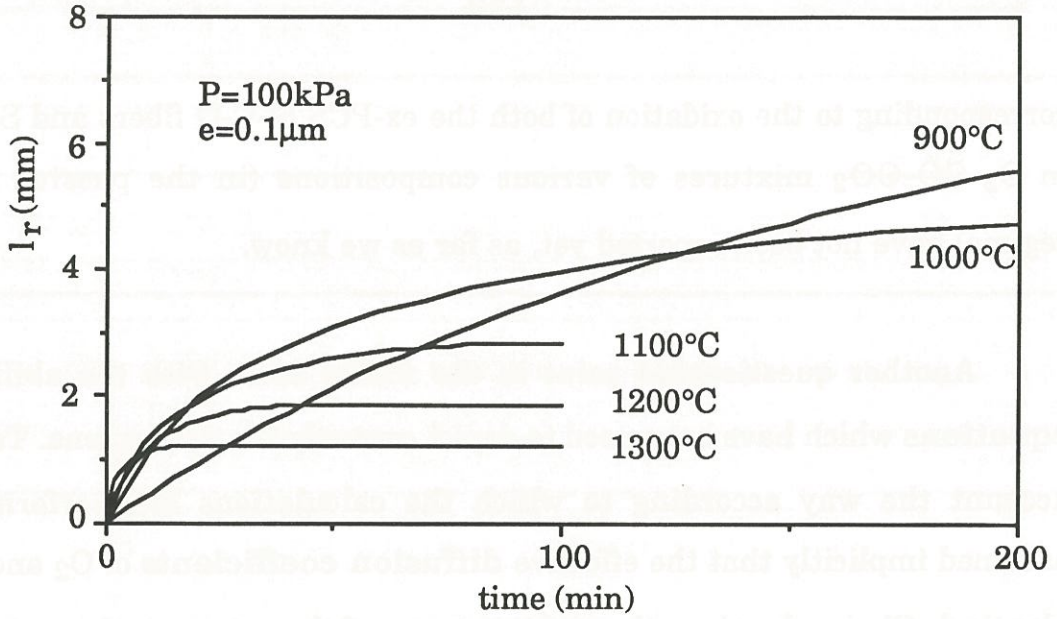

Fig. 14 : Influence of temperature on the calculated length of carbon interphase consumed by oxidation in pure oxygen versus time

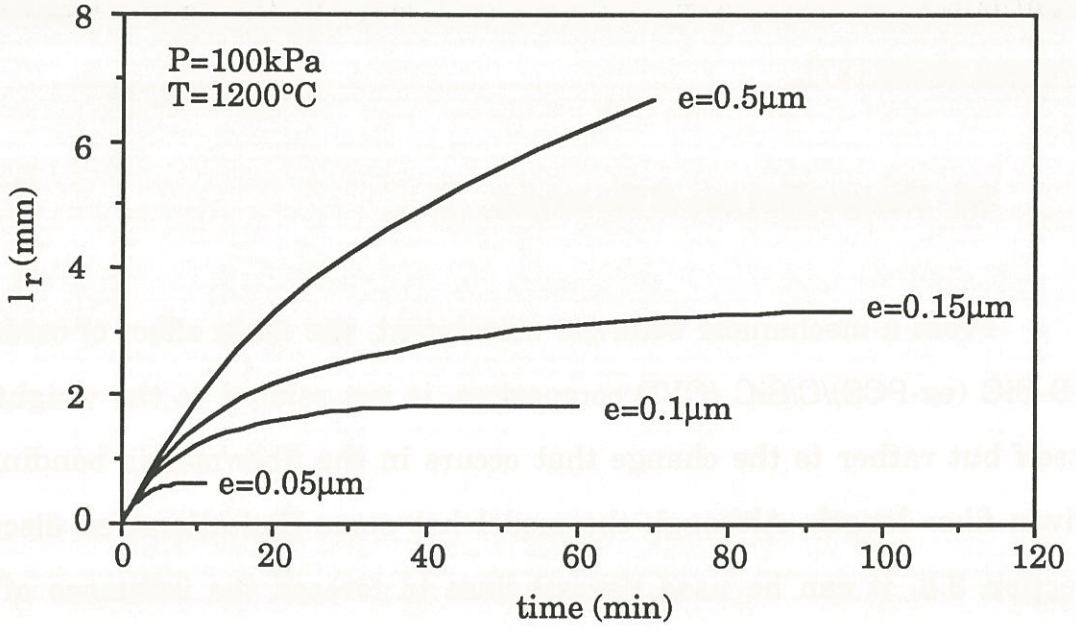

Fig. 15 : Influence of the interphase thickness on the calculated length of carbon consumed by oxidation in pure oxygen at 1200°C versus time

Effect of temperature

The variations of the calculated length of carbon interphase consumed l_r as a function of time are shown in fig. 14 for a model microcomposite (e = 0.1 μm) and various temperatures ranging from 900°C to 1300°C. As T_0 is raised, the initial oxidation rate (related mainly to the oxidation of carbon, as already mentioned) increases. Conversely, as the oxidation proceeds further, the reverse phenomenon is observed. As a matter of fact, when T_0 is raised, the value of t_f and that of the length of carbon interphase finally consumed both decrease. At **low temperatures**, the carbon interphase is consumed **slowly but over an important length** (in-depth oxidation) whereas at **high temperatures** the oxidation of the interphase is **rapid but limited to a short distance near the surface** (owing to the depletion of the oxidant concentration related to the oxidation of the pore walls). This important feature can be explained on the basis of the thermal dependence of the parabolic rate constants, on the one hand, and of the diffusion coefficients in the gas phase, on the other hand. It has been shown previously (see section 3.2) that the oxidation kinetics of the carbon interphase are very rapidly controlled by the diffusion mass transfers along the pore. As shown by equations (A4) and (A7'), the thermal dependence of the diffusion coefficients is less (i.e. D_M varies as $T^{1.75}$ and D_K as $T^{0.5}$). Conversely, the parabolic rate constants obey Arrhenius laws [21,22] and thus their thermal dependence is very high. Under such conditions, when T_0 is raised from 1000°C to 1200°C, the parabolic rate constant of the SiC-matrix is multiplied by 8 whereas the value of the effective diffusion coefficient (for oxygen in O_2-CO_2 mixtures and for e = 0.1 μm) increases only from $4.72\ 10^{-5}$ to $5.28\ 10^{-5}\ m^2s^{-1}$. Consequently : (i) the relative weight of the oxygen consumption by the pore wall increases when T_0 is raised and (ii) the pore width decreases

more rapidly than its length increases. The numerical simulations suggest that the use of unprotected SiC/C/SiC composites might be **more problematic at low temperatures** than at high temperatures since in this latter case the materials exhibit a **self-healing behavior** (at least under passive oxidation regime conditions).

Effect of the interphase thickness

The influence of e on l_r is shown in fig. 15 for an oxidation treatment in pure oxygen at 1200°C. Owing to the parabolic character of the growth laws of the silica scales on both the SiC-matrix and ex-PCS Si-C-O fibers, the value of t_f (time necessary to seal the pore entrance) is proportional to e^2. As an example, for e = 0.5 μm, t_f = 1200 min whereas for e = 0.05 μm, tf = 12 min only. Moreover, the value of the effective diffusion coefficient (O_2 in O_2-CO_2 mixtures) decreases when e is lowered. Thus, the thickness of the carbon interphase is a very important parameter in the oxidation of SiC/C/SiC composites : as shown in fig. 15, **when e is lowered**, the oxidation rate of SiC and Si-C-O decreases and the **pore sealing occurs more rapidly**.

Cao et al. have mentioned that the carbon interphase thickness in SiC/C/LAS composites can be **as low as 0.01 μm** while maintaining the tough mechanical behavior of the materials (in such composites, the carbon interphase is formed in-situ during processing and not deposited on the fibers prior to composite processing) [33]. If a similar carbon interphase thickness could be used in 1D-SiC/C/SiC composites, our numerical simulations show that it will be consumed only over 60 μm at 1200°C in pure oxygen.

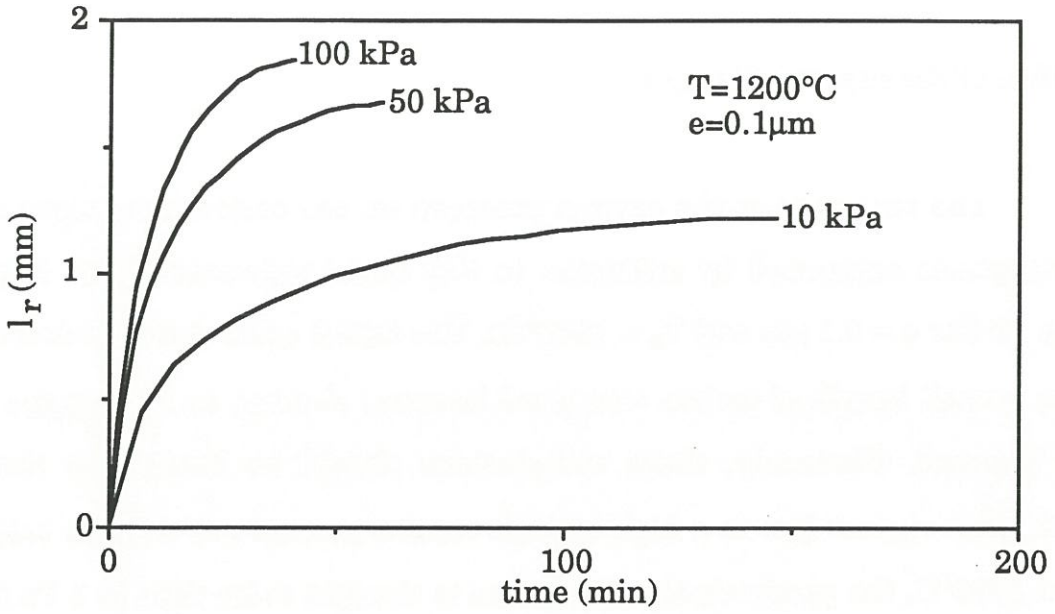

Fig. 16 : Influence of the oxygen pressure on the calculated length of carbon consumed by oxidation in pure oxygen at 1200°C vs time

Effect of the oxygen pressure

The influence of the oxygen pressure on the calculated length of carbon interphase consumed by oxidation in the model microcomposite is shown in fig. 16 (for e = 0.1 μm and T_0 = 1200°C). The initial oxidation rate decreases and the overall length of carbon consumed becomes shorter, as the oxygen pressure is lowered. Obviously, these calculations should be limited to the passive oxidation regime (i.e. to a high enough oxygen pressure at a given temperature : at 1200°C, the passive/active transition is thought to be close to 1 Pa in oxygen for pure SiC) [34]. When the oxygen pressure is lowered enough, the Knudsen diffusion becomes preponderant in the pore and thus the effective diffusion coefficients do not vary significantly with the pressure. However, since the concentration gradients decrease, the oxidation kinetics of the carbon interphase should decrease, according to equation (20). Taking into account the variations of the parabolic rate constants depicting the growth of the silica layers on both SiC and Si-C-O (equation (5)), it comes out that the overall carbon interphase length consumed by oxidation decreases when the oxygen pressure is lowered.

4 - CONCLUSION

A model, based on a simple axisymmetrical fiber/interphase/matrix assembly, has been developed to depict the oxidation behavior of 1D-SiC (ex-PCS)/C/SiC (CVI) composites. It takes into account the changes versus time of the geometry of the annular pore resulting from the oxidation of the carbon interphase, the diffusion of the gaseous species along the pore and their reaction with the pore walls (fiber and matrix) and bottom (carbon interphase).

Both the fibers and matrix react with oxygen to form gaseous carbon oxides and a condensed phase silica which tends to seal the pore. The oxidation of carbon yields gaseous oxides and simultaneously increases the length of the annular pore. The model gives : (i) the gaseous species concentration and silica thickness profiles along the pore, (ii) the length of carbon consumed and (iii) the relative weight change.

The model depicts in a satisfactory manner the main features of the TGA-curves recorded on actual 1D-SiC (ex-PCS)/C/SiC (CVI) composites. As the oxidation duration increases, the following phenomena are preponderant : (i) the oxidation of carbon, (ii) the oxidation of the fiber and matrix within the annular pore and (iii) the oxidation of the external surface. Quantitatively, an excellent agreement is observed between the observed and calculated overall lengths of carbon interphase consumed by oxidation.

The model, despite its limitations, is a good tool to study the influence of the material and test parameters on the oxidation behavior of 1D-SiC/C/SiC composites. Low temperatures favor in-depth oxidation whereas the oxidation of the composites is limited to the vicinity of the external surface at high temperatures, 1D-SiC/C/SiC unprotected composites exhibiting a **self-healing behavior** in this latter case. The most crucial material characteristics is the thickness of the carbon interphase, the best oxidation resistance being observed with thin carbon interphase.

ACKNOWLEDGEMENTS

This work has been supported by CNRS and SEP through a grant given to L. Filipuzzi. The carbon consolidation of the samples as well as the SiC-infiltration have been performed by SEP. The authors like to thank J. Thébault from SEP, G. Camus, J. Deuzet, F. Lamouroux and F. Langlais, (from LCTS) for fruitfull discussions on the mathematics of the model, the numerical treatment and the kinetic aspects.

NOTATION

a : number of mol of A' producted per mol of A.

b : number of mol of carbon consumed per mol of A.

B : parabolic rate constant ($m^2\ s^{-1}$).

C : concentration (mol m^{-3}).

C_o : total concentration (mol m^{-3}).

D : effective diffusion coefficient ($m^2\ s^{-1}$).

D_K : Knudsen diffusion coefficient ($m^2\ s^{-1}$).

D_M : molecular diffusion coefficient ($m^2\ s^{-1}$).

g : number of mol of A consumed per mol of silica.

G : molar weight variation during oxidation (kg mol^{-1}).

K : rate constant for carbon oxidation (m s^{-1} if reaction order = 1).

l_r : length of carbon consumed (m).

l_t : total length of the microcomposite (m).

m : mass (kg).

M : molar mass (kg mol^{-1}).

p : exponent of oxygen partial pressure dependence.

N : absolute molar flux.

n : number of mol A consumed per unit time and per unit length (mol s^{-1}).

P : pressure (Pa).

Pe : perimeter (m).

Q : flow x pressure drop (Pa m^3 s^{-1}).

R : term representing the consumption or production of gas mole by the walls.

Rg : universal gas constant (J mol^{-1} K^{-1}).

r : radius (m).

S : surface (m^2).

T : temperature (K).

t : time (s).

v_a : mean velocity of molecules (m s^{-1})..

v_i : intrinsic reaction rate of carbon oxidation (kg m^{-2} s^{-1}).

x : spatial coordinate (m).

y : thickness of silica (m).

Greek letters

α : molar flux ratio of A' over A.

∇ : gradient operator.

ΔP : pressure drop (Pa).

Δ_m : coefficient of volumique expansion for matrix oxidation

Σv : diffusion volume (m^3).

ρ : density (kg m^{-3}).

Subscripts and superscripts

A : reactant gas.

A' : product gas.

c : carbon.

e : external interface.

f : fiber.

i : internal interface.

m : matrix.

s : silica.

o : inlet conditions.

* : reference value.

APPENDIX - 1

A11 - The microcomposite is designed to have the same basic characteristics, i.e. density and fiber volume fraction, than the actual 1D-SiC/C/SiC composites. Referring to fig. 1c and assuming that the carbon interphase can be represented as a ring of uniform thickness, these conditions lead to the following two equations :

$$r_{fo}^2 / r_{comp}^2 = V_f \qquad \text{(A1)}$$

$$r_{comp}^2 \cdot \rho_{comp} = (r_t^2 - r_{mo}^2)\,\rho_m + (r_{mo}^2 - r_{fo}^2)\,\rho_c + r_{fo}^2 \cdot \rho_f \qquad \text{(A2)}$$

solving this system of two equations, with $r_{fo} = 7\ \mu m$; $r_{mo} = r_{fo} + e$ (with $e = 0.1$ or $1\ \mu m$) ; $\rho_{comp} = 2.56$ (material A) or 2.51 (material B) $g\ .cm^{-3}$; $\rho_m = 3.2\ g\ cm^{-3}$; $\rho_c = 2.0\ g\ cm^{-3}$; $\rho_f = 2.55\ g\ cm^{-3}$ and $V_f = 0.42$, yields the values of r_t and r_{comp} necessary to fully define the microcomposite.

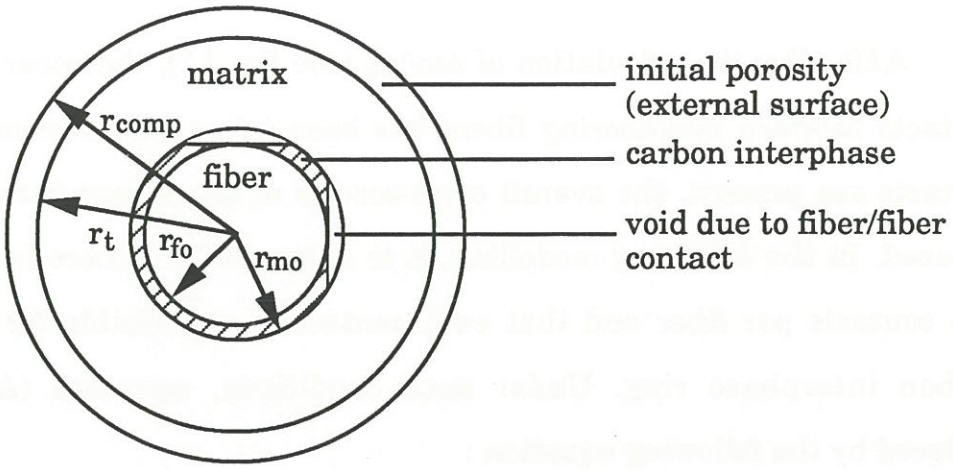

Fig. A1 : Cross-section of the model composite showing the voids in the carbon interphase related to the occurrence of fiber/fiber contacts in actual composites

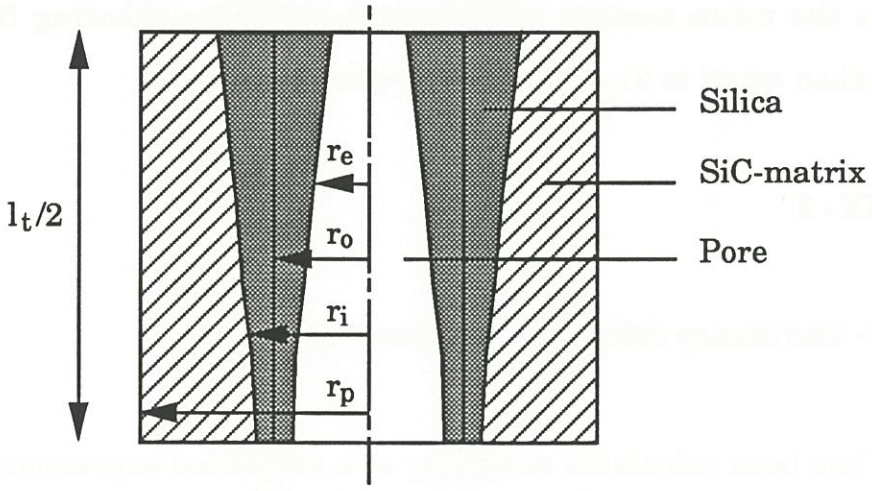

Fig. A2 : Longitudinal section of a cylindrical pore assumed to be present in the model microcomposite

A12 - For the calculation of $\Delta m/m_o$ (see fig. A1), the occurrence of direct contacts between neighboring fibers has been taken into account. When such contacts are present, the overall cross-section of the carbon interphase ring is reduced. In the following modelling, it is assumed that there is an average of two contacts per fiber and that each contact is responsible for a void in the carbon interphase ring. Under such conditions, equation (A2) has to be replaced by the following equation :

$$r_{comp}^2 \cdot \rho_{comp} = (r_t^2 - r_{mo}^2)\,\rho_m + \frac{S_c}{\pi}\,\rho_c + r_{fo}^2\,\rho_f \qquad (A'2)$$

with

$$S_c = \pi((r_{fo} + e)^2 - r_{fo}^{\ 2}) - n\,[(r_{fo} + e)^2\,(\frac{\pi}{2} - \mathrm{Arcsin}(\frac{r_{fo}}{r_{fo} + e})) - r_{fo}\,\sqrt{(r_{fo} + e)^2 - r_{fo}^{\ 2}}\,] \qquad (A3)$$

where n is the mean number of contacts between neighboring fibers (here n has been taken equal to 2), equation (A1) remaining valid.

APPENDIX - 2

A21 - The binary diffusion coefficient D_M

D_M has been calculated according to a simplified expression proposed by Fuller et al. [28] :

$$D_M = \frac{0.00143\ T^{1.75}}{P\ M_{AA'}^{1/2}\,[(\Sigma v)_A^{1/3} + (\Sigma v)_{A'}^{1/3}]^2} \qquad (A4)$$

with

$$M_{AA'} = \frac{2}{M_A^{-1} + M_{A'}^{-1}} \qquad (A5)$$

where M_A, $M_{A'}$ are the molar mass of the gaseous species A and A',$(\Sigma v)_A$, $(\Sigma v)_{A'}$ are the diffusion volumes of the molecules A and

A22 - The Knudsen diffusion coefficient in an annular pore

The Knudsen diffusion coefficient is usually given for a straight pore with a **circular** cross-section in which the collisions of the molecules with the pore walls occur equally in all radial directions. The situation is somewhat different in an **annular** pore (or in crack) since here the collisions of the molecules with the walls occur mainly in one single direction (i.e. that corresponding to the width of the ring of the crack). Therefore, the Knudsen diffusion in an annular pore is easier than that taking place in a cylindrical pore with a diameter equal to the width of the annular pore. Thus, the Knudsen diffusion coefficient has to be calculated for the specific geometry of the pore resulting from the consumption of the carbon interphase (i.e. a straight pore with an annular cross-section).

In his original work, Knudsen has established that the quantity Q (expressed in Pa $m^3 s^{-1}$), in a pore of length l and whose cross-section is characterized by an area S and a perimeter Pe, is related to the pressure drop ΔP along the pore, according to the following equation [29] :

$$Q = \frac{4}{3} v_a \frac{1}{\int_0^l \frac{Pe}{S^2} dl} \Delta P \qquad (A6)$$

with $$v_a = \left(\frac{8R_gT}{\pi M}\right)^{1/2} \qquad (A7)$$

where v_a is the mean velocity of the molecules. Assuming that the cross-section is constant, equation (A3) can be rewritten as :

$$Q = \frac{4}{3} v_a \frac{S^2}{Pe\, l} \Delta P \qquad (A6')$$

In the same manner, the **flux** of gaseous species flowing along a pore of same geometry is related to the concentration gradient in this direction, the proportionality coefficient in the Knudsen regime being D_K with :

$$D_K = \frac{4}{3} v_a \frac{S}{Pe} \qquad (A7')$$

It thus appears that D_K is itself proportional to the S/Pe ratio characterizing the cross-section of the pore. For a straight pore whose cross-section is annular (fig. 1), equation (A7) can be rewritten as :

$$D_K = \frac{2}{3} (r_m - r_f) \left(\frac{8R_gT}{\pi M}\right)^{1/2} \qquad (A7'')$$

The value of D_K for a crack whose width is $r_m - r_f$ is identical to that for the annular pore whereas that for a cylindrical pore of diameter $r_m - r_f$ is only one half that given by equation (A7'). D_K is thus a function of the pore cross-section geometry.

APPENDIX - 3

Referring to fig. A2, let us consider a single pore, with a circular cross-section, in the matrix. Let u be a geometrical parameter defined by :

$$u = \frac{r_i^2 - r_e^2}{r_o^2} \tag{A8}$$

then, the application of the first Fick's law to the growth of the silica layer on the pore wall leads to the following equation :

$$\frac{du}{dt} = \frac{2B_m^* \left(\frac{C_A}{C^*}\right)^{p_m}}{r_o^2 \, Ln \frac{\Delta_m + u}{\Delta_m + u\,(1 - \Delta_m)}} \tag{A9}$$

when Δ_m is the volumic expansion coefficient related to the SiC/SiO_2 conversion. Neglecting the Stefan flow and taking into account the cylindrical geometry, equation (18) can be rewritten as :

$$\frac{d}{dx}\left[r_e^2 D_A \frac{dC_A}{dx}\right] = \frac{2g_m B_m^* \left(\frac{C_A}{C^*}\right)^{p_m} \rho_S}{Ln\left[\frac{\Delta_m + u}{\Delta_m + u\,(1 - \Delta_m)}\right] M_s} \tag{A10}$$

with the following boundary conditions :

$$x = 0 \qquad C_A = C_o \tag{A11}$$

$$x = \frac{l_t}{2} \qquad \frac{dC_A}{dx} = 0 \tag{A11'}$$

APPENDIX - 4

The overall specific surface area measured by mercury porosimetry on 1D-SiC/C/SiC composites is about 0.06 $m^2\ g^{-1}$. As shown in fig. 3, it consists of **large pores** which account for a **constant** value of about 0.004 $m^2.g^{-1}$ (i.e. 7 % of the overall specific surface area) and a family of **small pores** whose equivalent pore diameters range from 0.02 to 0.5 μm. This family is divided into **12 classes of pores** (each of them being associated with a given specific surface area value).

As shown in fig. 2, the calculation of the overall relative weight change $\Delta m/m_o$ related to the oxidation of the model microcomposite involves four intermediate steps corresponding to the relative weight changes related to the oxidation of : (i) the annular pore $(\Delta m/m_o)i$; (ii) the specific surface Sp_1 corresponding to the external faces of the actual composite, $(\Delta m/m_o)_1^e$, (iii) the specific surface area Sp_2, related to the pores of large diameters, $(\Delta m/m_o)_2^e$ and (iv) the specific surface area Sp_3 of the 12 classes of small pores, $(\Delta m/m_o)_3^e$. The equations which have been used to calculate the various $\Delta m/m_o$ contributions are the following :

$$\left(\frac{\Delta m}{m_o}\right)i = \frac{\frac{G_m\rho_m}{M_m}\int_0^{l_r}(r_{mi}^2 - r_{m_o}^2)dx + \frac{G_f\rho_f}{M_f}\int_0^{l_r}(r_{fo}^2 - r_{rfi}^2)dx - l_r\frac{S_c}{M_c}\rho_c}{\frac{l_t}{2}\left[(r_{fo}^2\rho_f) + \left(\frac{S_c}{\pi}\rho_c\right) + (r_t^2 - r_{m_o}^2)\rho_m\right]} \quad \text{(A12)}$$

$$\left(\frac{\Delta m}{m_o}\right)_1^e + \left(\frac{\Delta m}{m_o}\right)_2^e = \frac{(Sp_1 + Sp_2)\left[B^*\left(\frac{C_A}{C^*}\right)\rho_m\, t\right]^{1/2}\rho_m\, G_m}{\Delta m\,.\,M_m} \quad \text{(A13)}$$

$$\left(\frac{\Delta m}{m_o}\right)_3^e = \sum_{j=1}^{j=12} \frac{S_{pj} F_j \rho_m G_m (r_p^2 - r_{oj}^2)}{2 M_m r_{oj}} \qquad \text{(A14)}$$

$$\text{with} \quad F_j = \frac{\int_0^{l_t/2} (r_i^2 - r_o^2)\, dl}{(r_p^2 - r_o^2)\, l_t/2} \qquad \text{(A15)}$$

where Fj is the average conversion rate for the pore of initial equivalent radius $r_{o.j}$. S_{pj} is the specific surface area related to the class j.

REFERENCES

[1] R.F. ADAMSKY, J. Phys. Chem., 63 305-07 (1959).

[2] K.L. LUTHRA, Carbon, 26 [2] 217-224 (1988).

[3] A.J. CAPUTO, D.P. STINTON, R.A. LOWDEN and T.M. BESMANN, Am. Ceram. Soc. Bull., 66 [2] 368-72 (1987).

[4] R. CHAIM and A.H. HEUER,J. Mater. Sci., 2 154-58 (1987).

[5] H. MARSH and K. KUO in Introduction to Carbon Science Edited by H. Marsh pp 107-51 (1989).

[6] N. FRETY and M. BOUSSUGE Comp. Sci. Tech., 37 177-189 (1990).

[5] L. FILIPUZZI, G. CAMUS, J. THEBAULT and R. NASLAIN, 11th RISO International Symposium on Metallurgy and Materials Science, Eds. J.J. Bentzen, J.B. Bilde-Sorensen, N. Christiansen, A. Horsewell, B. Ralph, Roskilde Denmark, 1990 pp 283-289.

[8] O. SBAIZERO and C. SCHMIDT, Materials Engineering, 1 [1] 273-80 (1989).

[9] D.H. GRANDE, J.F. MANDELL and H.C.C. HONG "Fibre-Matrix Bond Strengh Studies of Glass, Ceramic and Metal Matrix Composites", J. Mater. Sci., 23 311-328 (1988).

[10] L. FILIPUZZI, G. CAMUS, and R. NASLAIN, (submitted to J. Am. Ceram. Soc.).

[11] R. NASLAIN, J.Y. ROSSIGNOL, P. HAGENMULLER, F. CHRISTIN, L. HERAUD and J.J. CHOURY, Synthesis Properties of New Composite Materials for High Temperature Applications Based on Carbon Fibers and C-SiC or C-TiC Hybrid Matrices Rev. Chimie Minérale, 18 544-564 (1981).

[12] J. BERNSTEIN and T.B. KOGER, J. Electrochem. Soc. Solid State Science and Technol., 135 [8] 2086-90 (1988).

[13] E.W. THIELE, Industrial and Engineering Chemistry, 31 [7] 916-20 (1939).

[14] E.E. PETERSEN, AIChe J., 3 [4] 443-48 (1957).

[15] P.A. RAMACHANDRAN and J.M. SMITH, AIChe J., 23 [3] 353-61 (1977).

[16] J.W. CHROSTOWSKI and C. GEORGAKIS, in "ACS Symposium Series", V. W. WEEKMAN and D. LUN, Editors, p 225 Houston, TX (1978).

[17] F. LOUYS, Thesis, Univ. Mulhouse, (1987).

[18] J.M. THOMAS, Chemistry and Physics of Carbon (Edited by P.L. Walker, Jr) Vol 1, Marcel Dekker, Inc New York, 135-68 (1965).

[19] S. YAJIMA, K. OKAMURA, T. MATSUZAWA, Y. HASEGAWA, T. SHISHIDO, Nature (London), 279 [5715] 706-707 (1979).

[20] R. HAGEGE et Al, J. Mater. Sci., 24 1503-12 (1989)

[21] L. FILIPUZZI and R. NASLAIN, 7th Cimtec, Montecatini Terme, June 24-30 1990.

[22] L. FILIPUZZI, R. NASLAIN and C. JAUSSAUD, (Submitted to J. Mater. Sci.).

[23] R.E. TRESSLER, J.A. COSTELLO and Z. ZHENG, ASM Pittsburgh, Pennsylvania 6-8 November 307-13 (1985).

[24] Z. ZHENG, R.E. TRESSLER and K.E. SPEAR, J. Electrochem. Soc., 137 [9] 2812-16 (1990).

[25] L. FILIPUZZI, Unpublished work.

[26] R.B. BIRD, W.E. STEWART and E. N. LIGHTFOOT, "Transport phenomena", John Wiley and Sons, New York (1960).

[27] G.F. HEWITT, Chemistry and Physics of Carbon (Edited by P.C. Walker, Jr) Vol 1 Marcel Dekker Inc., New York, 73-120 (1965) .

[28] E.N. FULLER and J.C. GIDDINGS, Ind. Eng. Chem. 58 [5] 18 (1966).

[29] M. KNUDSEN, Ann. Physik, 28 75-130 (1909).

[30] M. CROUZEIX and A.L. MIGNOT, Edited by Masson 95-119 (1989).

[31] F. PORZ and F. THUMMLER, J. Mater. Sci., 19 1283-1295 (1984).

[32] E. FITZER and R. EBI in Silicon Carbide 1973, (R.C. Marshall, J.W. Faust and C.E. RYAN, eds.) University of South Carolina Press, Columbia SC, 320-28 (1973).

[33] M.C. CAO, E. BISCHOFF, O. SBAIZERO, Manfred RÜHLE, A.G. EVANS, D.B. MARSHALL and J.J. BRENNAN, J. Am. Ceram. Soc., 73 [6] 1691-99 (1990).

[34] E.A. GULBRANSEN and S.A. JANSSON Oxid.Met. 4 [3] 181-201 (1972).

CHAPITRE V

EFFECT OF HIGH TEMPERATURE AGEING TREATMENTS ON THE MECHANICAL BEHAVIOUR OF UNIDIRECTIONAL SiC/SiC FIBROUS COMPOSITES

INTRODUCTION AU CHAPITRE V

Le but de toutes les études précédentes était de comprendre comment et à quelle vitesse les composites SiC/C/SiC s'oxydaient. Cependant, la finalité de ce travail était de bien comprendre l'évolution des propriétés mécaniques des matériaux avec les traitements oxydants. L'étude de l'influence de vieillissements à haute température sur les caractéristiques mécaniques était la conclusion logique de ce travail. Les éprouvettes choisies (de traction) présentaient une texture unidirectionnelle. Malheureusement, et en raison de cette texture, les traitements oxydants ont permis de caractériser uniquement une oxydation se propageant orthogonalement à l'axe des fibres et non parallèlement comme cela avait été préférentiellement le cas dans les études précédentes. Il résulte que si ce dernier chapitre est finalement une illustration intéressante des résultats précédents, elle reste essentiellement qualitative. Il faut enfin préciser que tous les matériaux étudiés ont été oxydés alors qu'ils n'étaient pas contraints mécaniquement.

Proceedings of the 11th. Risø International Symposium
on Metallurgy and Materials Science:
Structural Ceramics-Processing, Microstructure and properties
Editors : J.J. Bentzen, J.B. Bilde Sørensen, N. Christiansen, A. Horsewell, B. Ralph,
Risø National Laboratory, Roskilde, Denmark, 1990

EFFECT OF HIGH TEMPERATURE AGEING TREATMENTS ON THE MECHANICAL BEHAVIOUR OF UNIDIRECTIONAL SiC/SiC FIBROUS COMPOSITES

L.Filipuzzi*, G. Camus*, J. Thébault** and R. Naslain*

* Laboratoire des Composites Thermostructuraux,
UMR 47, CNRS-SEP-UB1, 1 - 3 Avenue Léonard de Vinci, F-33600 Pessac
** Société Européenne de Propulsion
BP 37, F-33165 Saint Médard en Jalles

ABSTRACT

Room temperature tensile tests were performed on two types of unidirectional SiC/SiC composites with different carbon interphase thicknesses after ageing at 1173 K and 1673 K for durations up to 100 h in air and in helium. The observed changes in the tensile behaviour appear to be strongly related to both the ageing treatments and the initial carbon interphase thickness. Experimental data are presented and possible correlations between the microstructural changes and the resulting modifications in tensile strength as well as in the observed fracture surfaces are discussed.

KEY WORDS : SiC/SiC Composites, Environmental Effects, Oxidation, Mechanical Properties

1 - INTRODUCTION

SiC/SiC composites are potential candidates for high temperature structural applications. Although each of their constituents is brittle, they

behave in a non-brittle manner when mechanically tested, displaying exceptional strain tolerance, high strength and fracture toughness (Lamicq, Bernhart, Dauchier and Macé, 1986). Besides, they offer good oxidation resistance -when protected- as they have been shown to retain a large part of their strength when tested after exposures to oxidizing environments at temperatures as high as 1673 K (1400°C) for 20 hours durations (Cavalier, Lacombe and Rouges 1989).

Enhancement and reproducibility of the mechanical properties are usually achieved through the interposition of a thin carbon layer between the fibers and the matrix. This C-layer indeed provides a lower shear strength interface which allows the fibers to remain intact and to bridge the cracks behind the crack tips. Yet, the reactivity of this carbon interphase towards oxygen constitutes undoubtedly a weak point for the material when exposed to oxidative atmospheres at elevated temperatures. Frety and Boussuge (1990) have thus recently shown, by studying the effect of high temperature ageings on the flexural strength of both carbon coated and uncoated 2D woven SiC/SiC composites, that modifications in the strength of the fiber-matrix bond gives rise to significant changes in the composites ultimate strength and failure mode. However, the use of bending tests/bidimensional woven composites and the fact that, even with initially uncoated fibers, an uncontrolled carbon layer may be generated in situ during the processing/heat treatment cycles (Caputo, Stinton, Lowden and Besmann 1987) made uneasy the interpretation of some of the results.

The effect of oxidation on the microstructural and chemical evolutions of SiC/C/SiC composites has recently been examined (Filipuzzi, Naslain and

Thébault 1990), using unsealed unidirectional model materials with two different carbon interphase thicknesses (0.1 μm and 1 μm, respectively), in order to magnify and better understand the involved phenomena. It has thus been decided to use the same model materials to study the effect of high temperature oxidizing treatments on their room temperature tensile behaviour, with a view to correlate the observed microstructural changes due to oxidation with possible resulting modifications in the composites strength as well as in the fracture mode. In order to properly separate the temperature effect from the oxidizing environment effect, additional ageing treatments under an inert atmosphere were performed.

2 - EXPERIMENTAL PROCEDURE

The composite(*) materials consisted of a CVI-processed SiC matrix reinforced with 0° plies of ex-PCS(**) fibers unidirectional layers. Before infiltration by the matrix, the fibers were precoated with carbon layers of either 0.1 μm or 1 μm in thickness. These materials will be further referred to as material A(0.1) and material B(1), respectively. The fiber content was calculated to be approximatly 45 vol% in both cases, and measured apparent densities gave values of about 2.6 and 2.5 for material A(0.1) and B(1), respectively. Prior to the various ageing treatments, the tensile specimens (10x3x94 mm^3) were ground on their wide faces, on a 40 mm length extended along the center, so that fibers and interphases remain unsealed.

(*) Produced by the Société Européenne de Propulsion
(**) Nicalon fibers (NLM 202 grade)

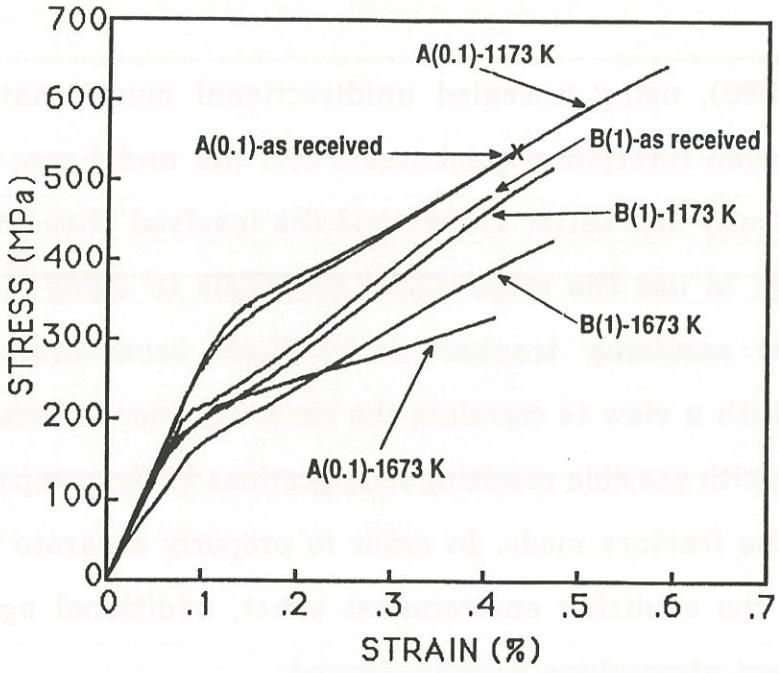

Fig.1 : 0° R.T. tensile stress-strain curves for unidirectional SiC/C/SiC composites untreated and/or aged 100 h in helium.

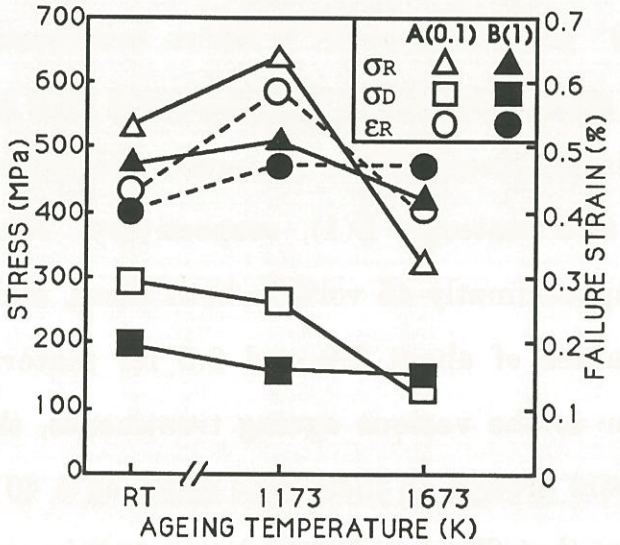

Fig.2 : Changes in strength stress at first damage and strain to failure versus temperature for 100 h ageing treatments in helium

The ageing treatments were conducted in flowing air and/or flowing helium, at a flow rate of approximatly 1 l/h, in a resistively heated furnace. Both materials were aged at 1173 K (900°C) and 1673 K (1400°C), for durations of 10 and 100 hours in air, and 100 hours in helium. Room temperature tensile tests were then performed on the as-received and variously aged composites at a constant strain rate of 0.02 % mn^{-1} with a servohydraulic machine. Specimen strain was measured using strain gauges on both wide specimen faces. In addition, acoustic emission monitoring was used during the loading to follow the occurrence and the propagation of damage into the materials. Fracture surfaces of broken specimens were examined in a scanning electron microscope.

3 - EXPERIMENTAL RESULTS

The room temperature tensile properties of the as received and variously aged SiC/C/SiC composite materials are summarized in Table 1 along with an indication of the appearance of the resultant fracture surfaces, quoted as fibrous (limited or extensive), brittle and/or mixed. In the latter case, the embrittled regions always start from the specimen outer surface.

3.1 - Effects of ageing treaments performed in helium

Room temperature axial tensile stress-strain curves of both untreated and helium aged materials A(0.1) and B(1) are shown in Fig.1. The tensile strengths (σ_R), stresses at first damage (σ_D, determined by acoustic emission monitoring) and strains to failure (ε_R) are plotted as a function of ageing

Ageing condition	material A(0.1)					material B(1)				
	E GPa *	σ_D MPa *	σ_R MPa *	ε_R % *	Fracture Mode **	E GPa	σ_D MPa	σ_R MPa	ε_R %	Fracture Mode
As received	270	295	535	0.43	LF	245	200	479	0.40	LF
1173 K - 100 h helium	280	265	642	0.59	LF	250	160	513	0.47	LF
1673 K - 100 h helium	260	130	326	0.41	EF	190	150	422	0.47	EF
1173 K - 10 h air	260	185	520	0.50	b + LF	220	30	342	0.39	EF
1173 K - 100 h air	280	110	238	0.26	B + LF	210	30	145(+)	0.11(+)	/(+)
1673 K - 10 h air	250	180	341	0.58	b + LF	230	35	119	0.49	B +EF
1673 K - 100 h air	240	175	398	0.65	b+ EF	235	30	45	0.02	B

* E, σ_R, σ_D, ε_R are the Young's modulus, the tensile strength, the stress at first damage and the strain to failure, respectively

** LF = limited fiber pull-out ; EF = extensive fiber pull-out ; B , b = brittle fractures

(+) specimens broke in the grips

Table 1 : 0° tensile test data for unidirectional SiC/C/SiC composites

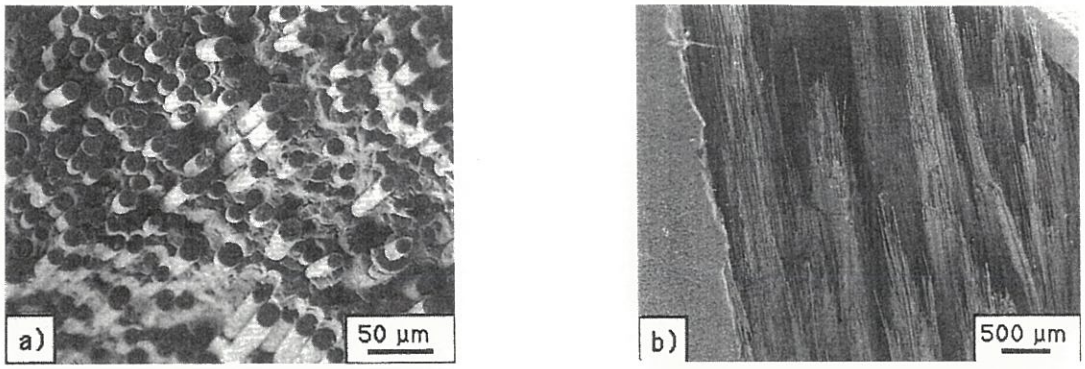

Fig.3. Fracture surfaces of broken tensile specimens; a)material A(0.1) as received, b) material A(0.1) aged 100 h at 1673 K in helium.

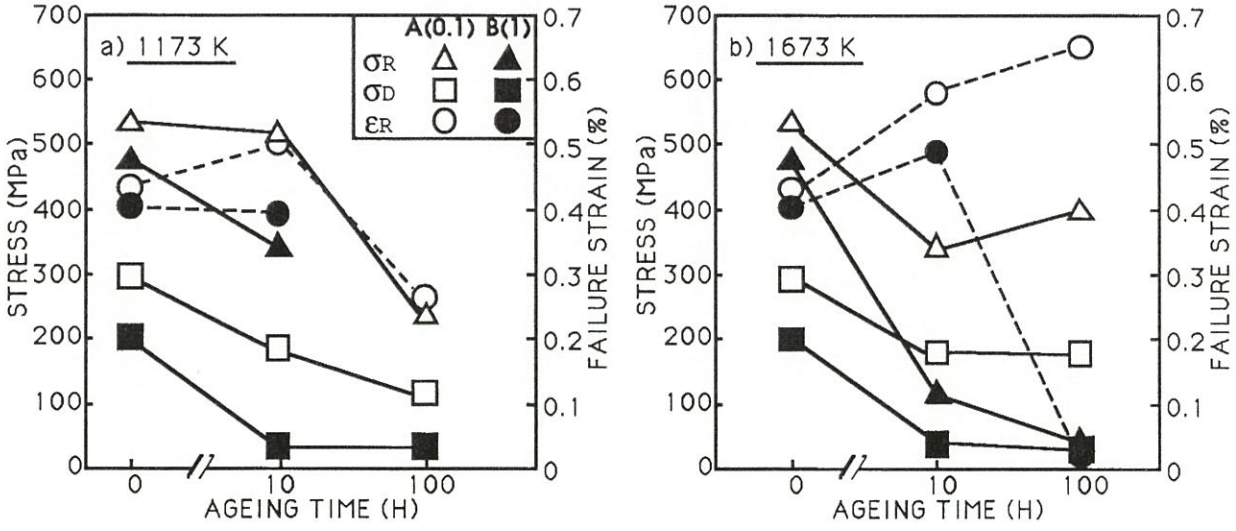

Fig. 4. Changes in tensile strength, stress at first damage and strain to failure versus ageing time for heat treatments performed in air at : a) 1173 K ; b) 1673 K.

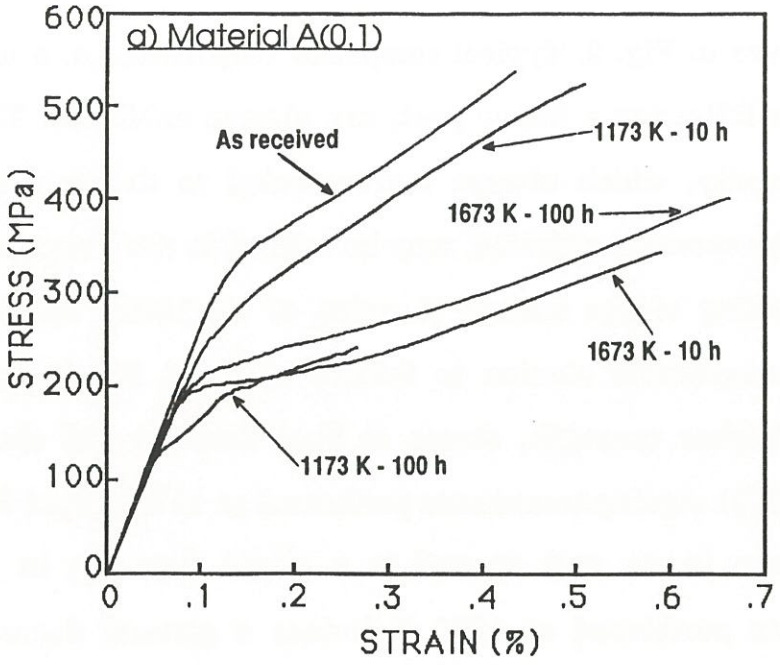

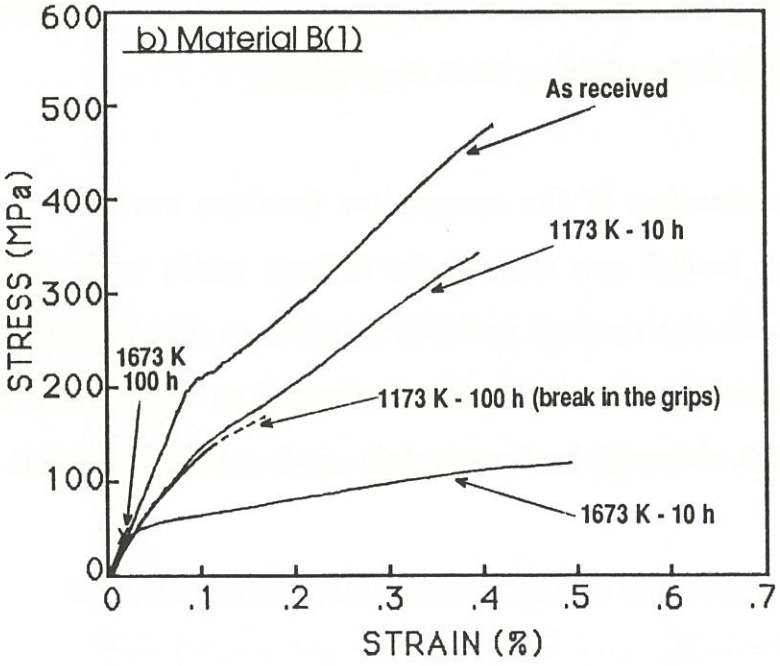

Fig. 5 : 0° R.T. tensile stress-strain curves for unidirectional SiC/C/SiC composites aged in air: a) material A(0.1), b) material B(1).

temperature in Fig. 2. Typical composite responses, i.e. a markedly non-linear behaviour following a linear part, are always exhibited. The initial deviation from linearity, which always corresponded to the first significant damage detected by acoustic emission, may be related to the occurrence of a progressive microcracking of the matrix (Lamicq et al. 1986). As received composites display comparable strains to failure of about 0.4 %, but material A(0.1) exhibits higher strength, stress at first damage and elastic modulus than material B(1). Ageing treatments performed at 1173 K lead for both materials to an increase in σ_R and ε_R and to a slight decrease in σ_D, while ageing treatments performed at 1673 K induce a general decrease of these three parameters. These trends are, besides, significantly emphasized when material A(0.1) is compared to material B(1). From Table 1, it can be seen that the composites elastic moduli are mostly unaffected by the various heat treatments performed under helium, with yet the exception of material B(1) aged at 1673 K for which a 22 % drop occurs.

Examination of the composites fracture surfaces revealed that all the specimens tested are fibrous in failure mode with still some noticeable differences in the average pull-out lengths, as illustrated by Fig. 3. As received conditions and ageing treatments performed at 1173 K lead to limited fiber pull-out (Fig. 3a), although both materials aged at 1673 K exhibit extensive pull-out.

3.2 - Effects of ageing treatments performed in air

Plots of the tensile strengths, stresses at first damage and strains to failure, and room temperature axial tensile stress-strain curves of composites aged in air are shown in Fig. 4 and Fig. 5, respectively. For material B(1), an

increase in the duration and/or in the temperature of the ageing treatment induces a consistent decrease in strength and stress at first damage while the strain to failure remains nearly constant, except for a 1673 K/100 h ageing where ε_R drops by almost 95 %. In this latter case, the composite displays severe embrittlement with a very low strength of 45 MPa and a linear stress-strain behaviour up to the point of fracture. Material A(0.1), on the other hand, behaves in a quite different manner. Ageing at 1173 K induces a strong decrease in σ_R and σ_D when the duration of the heat treatment is increased while, in contrast, if the material is noticeably weakened by a 10 hours treatment at 1673 K, no consistent difference in σ_R, σ_D and ε_R may be further noted with longer exposures. Comparisons between both composites show that the strongest damage associated with ageing treatments performed in air occurs at 1173 K for material A(0.1) and at 1673 K for material B(1). However, it can be seen from the values of elastic moduli reported in Table 1 that the composites stiffness is affected in the exact opposite manner : the largest observed decrease in modulus occurs with heat treatments performed at 1173 K for material B(1) and at 1673 K for material A(0.1).

Examination of fracture surfaces reveals marked differences in failure mode, which ranges from extensively fibrous to entirely brittle, depending on the heat treatment performed and the material considered. For any of the ageing conditions explored, material A(0.1) always fails in a mixed mode, i.e. with a fracture surface exhibiting both brittle and fibrous parts, the brittle parts being always connected to the specimen surfaces. Moreover, the width of the embrittled portions appears to increase with the duration of the ageing treatments, the more extended being for the specimen aged 100 h at 1173 K. For material B(1), failure surfaces exhibit either an extensive fiber pull-out (1173 K

- 10 h), or an entirely brittle fracture (1673 K-100 h, Fig. 6a) or a mixed mode (1673 K- 10 h, Fig. 6b). In this latter case, both the average pull-out length and the embrittled parts are widely extended.

4 - DISCUSSION

The axial tensile stress-strain behaviour of unidirectional SiC/C/SiC composites is shown to be strongly influenced by high temperature ageing treatments performed in air and/or in an helium inert atmosphere. The magnitude of the induced changes depends in both cases on the time and temperature of exposure as well as on the initial composite carbon interphase thickness. Although the mechanisms involved during the ageing treatments performed in air and in an helium (i.e. the oxidizing environment effect and the temperature effect respectively) are very likely strongly interrelated, it is convenient to discuss them separately.

Howewer, it should be noted first, that variations of the initial carbon interphase thickness already causes significant differences in the as received composite stress-strain behaviour. Thus, if both materials exhibit a typical highly non linear response with comparable strains to failure, an increase in the interphase thickness results in lower stiffness, strength and stress at first damage. The drop in the elastic modulus is, according to the rule of mixture, likely related to a lower matrix content, since the fiber content remains constant (45 vol%) while the interphase thickness (i.e. the carbon content) is increased. The observed lower strain at first damage, which accounts for an

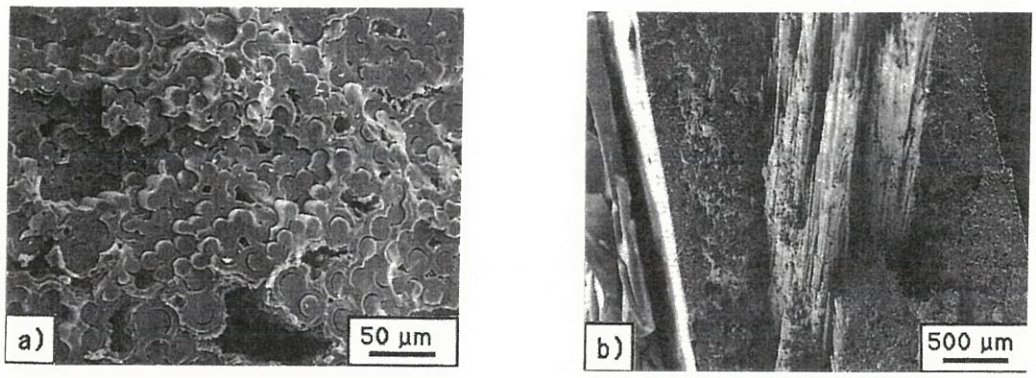

Fig. 6 : Fracture surfaces of tensile specimens aged in air

a) material B (1) : 1673 K / 100h

b) material B (1) : 1673 K / 10h

earlier occurrence of matrix microcracking, may be related to a less efficient fiber matrix load transfer induced by the thicker initial carbon interphase.

4.1 - Effects of ageing treatments performed in helium

The overall tensile stress-strain behaviour and the resulting fracture mode of the composites aged in helium prove to be highly temperature dependent.

Ageing at 1673 K causes the greatest change in both materials response. Elastic modulus values are lower, tensile strengths as well as stresses at first damage are significantly reduced and the fracture surfaces exhibit extensive fiber pull-out. These alterations can be most readily associated with the degradation of the Nicalon fiber which is known to be unstable over 1273 K. Such thermal instabilities have been shown to decrease the fiber mechanical properties. Inside the composite, these effects are probably delayed and degradations at the interfaces are expected. Thus, extensive pull-out as well as earlier matrix cracking and reduced modulus are observed.

At 1173 K less interface modifications are expected. The overall shape of the stress-strain curves are retained, but matrix cracking starts at lower stresses and strains to failure are higher. Howewer, these effects remain low in magnitude and may as well not be very significant.

4.2 - Effects of ageing treatments performed in air

The effects of oxidation on the microstructural and chemical evolutions of the unidirectional SiC/C/SiC composites used in the present work has been previously examined (Filipuzzi et al. 1990). Results have shown that several phenomena occur: (i) oxidation of the carbon interphase which leaves interstitial cavities between the fibers and the matrix, (ii) subsequent gaseous diffusion of oxygen in interstitial cavities and (iii) growth of silica layers through oxidation of both the matrix and the fibers which tends to progressively fill up these cavities. Eventually, connections between the silica films occur and the oxidation along the fibers is strongly reduced.

Comparisons between both composites have shown that the use of a thick interphase leads to a lower oxidation resistance. The major reasons were found to be related to: (i) the strong transverse interconnection of the carbon interphases which provides therefore an easy path to the oxygen diffusion perpendicularly to the fibers, (ii) the long time to close the interstitial cavities and (iii) a higher diffusion inside the cavities. For material A(0.1), cavities closure were shown to occur faster as temperature was increased, and more severe oxidation in the bulk at lower temperatures was observed.

Observed modifications in the room temperature tensile behaviour of the composites aged in air are indeed very consistent with these induced microstructural and chemical changes. For material B(1), the thick interconnected carbon interphase is rapidly consumed and lost nearly all over the material at any of the ageing temperature and/or duration explored and load transfers are therefore less efficient, as shown by the very low and mostly

identical stresses at first damage as well as by the extended fiber pull-out exhibited by the material aged 10 h at 1173 K. Then, as the duration and/or the temperature of the ageing treatments are increased, a progressive junction of the silica layers growing from both the fibers and the matrix takes place. Thus, the material aged 10 h at 1673 K exhibits brittle fracture in the outer regions as strong brittle bonds have been formed by the silica layers between the fibers and the matrix. The extensive pull-out observed in the center of the fractured surface suggests that unbonded fibers remain and explains the unaffected strain to rupture. The severe embrittlement observed for the composite aged at 1673 K for 100 h, i.e. an entirely brittle low strength fracture and a tensile stress-strain curve remaining linear up to the point of fracture, suggests that the fibers are, in this case, bonded at some extend to the matrix through silica layers all over the material. Evolutions of the elastic moduli are consistent with these interpretations since the oxidation of the carbon interphase should favour a decrease in the overall stiffness, while it should increase again with the progressive formation of silica layers (Gault and Huger 1990).

For material A(0.1), the cavities left by the oxidation of the carbon interphases located near the surface are filled up before the carbon is consumed all over the material. The more pronounced weakening of the material aged at 1173 K is related to a deeper oxygen penetration, as illustrated by the fact that the larger brittle zone is exhibited by the sample aged at 1173 K for 100 h. As oxidation at 1673 K remains at the near surface, material is not so severely affected by long time exposures. All the specimens tested fail in a mixed mode and the limited pull-out observed in the center of the fracture surfaces further corroborates the hypothesis that the carbon interphase has not been oxidized. The exception of the ageing treatment performed at 1673 K for

100 h which induces extensive pull-out has to be related to effects similar to those induced by ageing under helium (i.e. modifications in the fiber-matrix bonding) since oxygen does not have access to the interior of the specimen.

In any case, these results show that, as long as some fiber-matrix bonding remain weak enough, the main damage consists in drops of both the strength and the stress at first damage, while non linear stress-strain behaviours are still exhibited. Moreover, comparisons between both composites show that a thin initial carbon interphase procures a better resistance towards oxidation and therefore a better preservation of the mechanical integrity.

5 - CONCLUSION

The effect of high temperature oxidizing and inert ageing treatments on the room temperature tensile behaviour of unsealed unidirectional model SiC/C/SiC composites has been studied. Results show that ageing temperature, duration and environment, as well as the initial interphase thickness have a strong influence on the resulting mechanical behaviour. Exposure in an inert helium atmosphere at 1673K weakens the composites, most probably through the degradation of the fibers which in turn might induce modifications in the fiber-matrix bonding. Ageing in air causes a progressive weakening and embrittlement of the materials through the disappearing of the initial carbon interphase and the subsequent growth of silica layers which can form a strong brittle bond between the fibers and the matrix. Howewer, as long as some fiber-matrix bondings remain weak enough, main damage consists in drops of both strengths and stresses at first damage, while markedly non linear composite

behaviours are still observed. If the composite with the smaller initial interphase thickness exhibits a higher susceptibility towards ageing treatments performed in helium, its mechanical integrity is, in any case, better preserved after high temperature exposures in an oxidative atmosphere.

ACKNOWLEDGEMENTS

The authors are thankfull to SEP for providing the materials, B. Humez for performing the tensile tests, N. David for preparing the samples and P. Pluvinage for usefull discussions.

REFERENCES

Caputo, A.J., Stinton, D.P., Lowden, R.A. and Besmann, T.M. (1987). Fiber-Reinforced SiC Composites with Improved Mechanical Properties. Am. Ceram. Soc. Bull. 66 [2], 368-372.

Cavalier, J.C., Lacombe, A., and Rouges, J.M., (1989). Composites à Matrice Céramique, Nouveaux Matériaux à très hautes Performances. In : Developments in the science and technology of composite Materials, ECCM3 Proc. Edited by A.R. Bunsell, P. Lamicq and A. Massiah (Elsevier Applied Science, London and New-York) , 99 - 110.

Filipuzzi, L., Naslain R. and Thébault, J. (1990). Etude de l'oxydation de composites unidirectionnels SiC(Nicalon)/SiC(CVI) à interphase pyrocarbone. In: Matériaux Composites pour applications à hautes températures, Proc. Edited by R. Naslain, J. Lamalle and J.L. Zulian (AMAC/CODEMAC publications, Paris and Bordeaux), 289-301.

Frety, N. and Boussuge, M. (1990). Relationship between high-temperature Development of fibre-matrix Interfaces and the Mechanical Behaviour of SiC-SiC composites. Composites Sci. and Tech. 37, 177-189.

Gault, C. and Huger, M., (1990), Caractérisation ultrasonore à haute température des évolutions microstructurales de composites fibreux céramique-céramique. Influence de l'atmosphère. In : Matériaux Composites pour applications à hautes températures, Proc., Edited by R. Naslain, J. Lamalle and J.L. Zulian (AMAC/CODEMAC publications, Paris and Bordeaux), 303-314.

Lamicq, P.J., Bernhart, G.A., Dauchier, M.M. and Macé, J.G. (1986). SiC/SiC Composite Ceramics. Am. Ceram. Soc. Bull. 65 [2], 336-338.

CONCLUSIONS GENERALES

CONCLUSIONS GENERALES

Ce travail s'inscrit dans le cadre plus général des études poursuivies au Laboratoire des Composites Thermostructuraux (LCTS) sur les composites fibreux à matrice céramique. Les composites SiC/SiC à interphase de pyrocarbone(*), sont des matériaux destinés à de nombreuses applications à haute température en environnement oxydant. La connaissance de leur comportement à l'oxydation apparaît donc essentielle dans le cadre de leur utilisation.

L'objectif de ce travail était la compréhension des mécanismes d'oxydation des composites SiC/SiC à interphase de carbone (SiC/C/SiC) et des effets résultants de l'oxydation sur le comportement mécanique.

La démarche adoptée a consisté à étudier, dans un premier temps, le comportement à l'oxydation des constituants pris isolément. Dans une seconde étape, l'étude de l'oxydation de composites SiC/C/SiC à texture **unidirectionnelle** a été abordée. Le choix de cette texture a été motivé par le souci de simplification du problème, la compréhension des processus fondamentaux impliqués étant le but principal de ce travail. Le dépouillement des résultats expérimentaux a mis en évidence les divers phénomènes mis en jeu lors de l'oxydation de ces matériaux. Il est alors apparu nécessaire d'avoir une approche théorique globale servant de support à l'interprétation des résultats expérimentaux. Un **modèle théorique** permettant de prédire le comportement à l'oxydation des composites SiC/C/SiC a été développé. Enfin, l'influence de traitements

---

(*) industrialisés en France par SEP et aux USA par du Pont de Nemours.

oxydants à haute température sur le comportement mécanique des composites a été étudiée.

Les cinétiques d'oxydation des **fibres Si-C-O** ex-PCS ont été étudiées par analyse thermogravimétrique (ATG) entre 800°C et 1500°C sous oxygène ou sous air sec (P=100 kPa). Dans tous les cas, un **régime passif** d'oxydation a été mis en évidence avec formation d'une couche de silice amorphe ou cristallisée (sous forme de cristobalite). Entre 800°C et 1200°C, les variations de masse relative au carré sont proportionnelles au temps, suggérant ainsi que des mécanismes **diffusionnels** à travers la couche d'oxyde contrôlent la cinétique. Au-delà de 1200°C, le régime parabolique n'est plus respecté. La cristallisation du film d'oxyde, la formation de fissures et la stabilité intrinsèque des fibres à haute température expliquent les modifications des cinétiques d'oxydation. Entre 800°C et 1200°C, les valeurs des énergies apparentes d'activation (69-77 kJ mol^{-1}) sont relativement basses par rapport aux valeurs reportées pour l'oxydation du SiC pur ou du silicium. La présence d'hydrogène résiduel qui réagit probablement avec la silice et/ou celle de micropores pourraient expliquer ces faibles valeurs. Notons que le coefficient d'expansion volumique de Si-C-O ex-PCS (≈ 1,35) est inférieur à celui de SiC pur (≈ 2). Les contraintes dans la couche d'oxyde doivent donc être moins importantes. Enfin, les valeurs des constantes paraboliques de vitesse du SiC ex-PCS sont plus élevées que celles reportées pour du SiC pur, particulièrement à basse température. Cette étude a révélé que les fibres SiC ex-PCS présentent un comportement à l'oxydation particulier. L'influence de la pression partielle d'oxygène sur les cinétiques d'oxydation pourrait apporter un éclairage nouveau à ce problème.

Les cinétiques d'oxydation de la **matrice SiC,** déposée chimiquement en phase vapeur à partir d'un mélange CH_3SiCl_3/H_2 dans des conditions de CVI, ont été étudiées entre 900°C et 1500°C sous oxygène sec par mesure de l'épaisseur des couches d'oxyde . Les échantillons contenaient des traces de silicium libre. Les cinétiques de croissance des couches d'oxyde suivent des lois paraboliques. Entre 1100°C et 1400°C, les processus d'oxydation sont thermiquement activés avec une énergie apparente d'activation de 128 kJ mol^{-1}. Cette valeur est comparable à celles trouvées dans la bibliographie pour des conditions similaires. Au-dessus de 1400°C, une augmentation de l'énergie apparente d'activation est observée et attribuée à un changement progressif du mode de transport de l'oxygène dans la couche de silice. A haute température, la diffusion de l'oxygène ionique dans le réseau devient prépondérante devant la perméation de l'oxygène moléculaire. En dessous de 1100°C, la valeur de l'énergie apparente d'activation augmente par rapport à celle obtenue entre 1100°C et 1400°C. Les effets de contraintes, générées par l'accroissement de volume associé à la transformation du SiC en SiO_2, pourraient intervenir et expliquer l'augmentation de l'énergie apparente d'activation à basse température.

Les mécanismes d'oxydation des **composites 1D SiC/C/SiC** ont été abordés, dans un premier temps, avec une **approche expérimentale**. Des études cinétiques et morphologiques ont permis de préciser l'influence de plusieurs paramètres et d'identifier les principaux mécanismes mis en jeu lors de l'oxydation de ces matériaux.

Des analyses ATG, en atmosphère inerte, ont permis de montrer que la stabilité thermique des composites SiC/C/SiC était sensiblement supérieure à celles des fibres seules. En atmosphère oxydante (sous forte

pression partielle d'oxygène), les principaux processus d'oxydation sont: (i) la réaction de l'oxygène avec le carbone qui crée des pores autour des fibres, (ii) la diffusion de l'oxygène, ainsi que des espèces produites, dans ces pores pour accéder au front de carbone et (iii) la réaction de l'oxygène avec les parois du pore qui conduit à la formation de couches de silice sur les fibres et la matrice qui réduisent progressivement la section du pore. Suivant les conditions, l'oxydation peut intervenir parallèlement ou perpendiculairement à l'axe des fibres. Il a été montré que l'oxydation du carbone est plus rapide lorsque les épaisseurs d'interphase sont grandes. D'autre part, lorsque les matériaux présentent des interphases de carbone de faible épaisseur (0,1 μm), l'**augmentation** des températures d'oxydation conduit à une **réduction** des longueurs où le carbone est gazéifié. Les couches d'oxyde qui croissent sur les fibres et la matrice peuvent au bout d'un temps donné, le temps de fermeture, boucher l'entrée des pores et réduire considérablement l'oxydation du carbone. Les dépendances thermiques en exp(-Ea/RT) pour la croissance des couches de silice (forte dépendance) et en $T^{0,5}$ ou $T^{1,75}$ pour les transferts de masse en phase gazeuse au sein des pores (faible dépendance) expliquent ce paradoxe.

La réduction de la pression partielle d'oxygène se traduit toujours par une diminution de la cinétique d'oxydation du carbone.

Notons enfin, qu'un mécanisme d'endommagement par microfissuration de la matrice a été observé pour des traitements prolongés à **basses températures**. Il a été attribué à des contraintes mécaniques internes générées par l'augmentation de volume associée à l'oxydation de SiC qui se poursuit après le temps de fermeture. Ces contraintes ne peuvent pas être relaxées en raison de la forte viscosité de la silice à basse température.

Pour aller au-delà de l'interprétation qualitative et pour vérifier les hypothèses émises, un **modèle théorique** décrivant le comportement à l'oxydation des composites 1D SiC/C/SiC a été développé. Il prend en compte l'évolution de la géométrie du pore créé par l'oxydation du carbone, la diffusion et la réaction simultanées de l'espèce oxydante au sein de ce pore avec les différents constituants que sont la fibre, la matrice et le carbone. La fibre et la matrice réagissent avec l'oxygène en formant à la fois des oxydes gazeux et de la silice qui tend à fermer progressivement le pore. Le carbone, en se gazéifiant sous forme d'oxydes volatils, augmente la longueur du pore. Ce modèle permet d'accéder à la **cinétique d'oxydation du carbone interfacial** dans les composites unidirectionnels SiC/C/SiC.

Les simulations numériques effectuées ont été comparées aux variations de masse relative obtenues par ATG et aux longueurs correspondant à la consommation du carbone. Le modèle rend compte qualitativement des variations de masse relative observées expérimentalement avec notamment la prépondérance successive de l'oxydation : (i) du carbone, (ii) des carbures (fibre et matrice) au sein du pore et (iii) des surfaces externes. Un bon accord est obtenu entre les longueurs, expérimentales et calculées, où le carbone a été consommé.

Ce modèle théorique, malgré ses limitations, fournit un support pour interpréter le comportement à l'oxydation des composites SiC/C/SiC. Il permet en outre de prédire l'influence de plusieurs paramètres. Ainsi, il a été montré que les basses températures favorisent une oxydation à coeur des matériaux alors que les hautes températures mènent à une disparition du carbone limitée à la surface. Enfin, le paramètre crucial est probablement la valeur de l'épaisseur de l'interphase de carbone. En effet, avec de faibles

épaisseurs, le carbone s'oxyde moins vite et moins longtemps, il est donc mieux protégé.

Enfin, après avoir étudié le comportement à l'oxydation des composites SiC/C/SiC d'un point de vue cinétique et microstructural, l'influence de traitements à haute température sur les **propriétés mécaniques** de ces matériaux était la conclusion logique de ce travail. Les **vieillissements sous atmosphère inerte** à 900°C n'ont pas d'influence notable sur le comportement mécanique. En revanche, à 1400°C les propriétés mécaniques des composites sont affectées probablement en raison de la dégradation des fibres SiC ex-PCS et/ou des liaisons fibre-matrice. Ces résultats sont en accord avec les analyses physico-chimiques qui ont mis en évidence la décomposition des fibres au sein du composite à partir de 1400°C.

Les **vieillissements sous air,** effectués à basse et haute températures, sur des composites avec des interphases de carbone de faible et forte épaisseurs sont une illustration intéressante des conclusions précédentes. Les matériaux avec de fortes épaisseurs d'interphase de carbone présentent une décroissance de leurs caractéristiques mécaniques avec l'augmentation des temps et des températures de traitements. Dans les conditions les plus sévères, un comportement de type fragile, avec rupture sans déchaussement des fibres est observé. Dans ce cas, le carbone est consommé assez rapidement et la croissance des couches d'oxyde n'est pas suffisante pour obstruer les pores. Les composites avec une interphase de carbone de faible épaisseur subissent aussi une diminution de leurs propriétés mécaniques qui, à basse température (900°C), augmente avec le temps. Par contre, à haute température (1400°C), après une chute initiale

des caractéristiques, il n'y a plus d'évolution sensible. Le **matériau s'auto-protège** et seule sa surface est affectée par le milieu oxydant.

En résumé, cette thèse se voulait être une contribution à la compréhension des mécanismes d'oxydation des composites SiC/SiC à interphase de carbone. S'appuyant sur des études expérimentales et théoriques, elle aura permis, notamment, d'expliquer le rôle paradoxal de la température et celui, primordial, de l'épaisseur d'interphase.

Un approfondissement de ce travail, notamment en ce qui concerne l' approche théorique, devrait sans doute passer par une meilleure connaissance de la chimie des réactions (approche thermodynamique et cinétique). Cette étude garde un certain caractère général. Elle pourrait, par exemple, être étendue sans trop de difficultés aux composites unidirectionnel à matrice verre (ou vitrocéramique) et fibres SiC ex-PCS dans lesquels une interphase à base de carbone est également présente. Par ailleurs, les résultats acquis au cours de ce travail ont été développés et servent de support à l'interprétation de l'oxydation des composites C/SiC en cours d'étude au LCTS.

ANNEXE 1

DETECTION DE SiO_2 PAR CATHODOLUMINESCENCE DANS LES COMPOSITES SiC/SiC OXYDES

ANNEXE 1

DETECTION DE SiO_2 PAR CATHODOLUMINESCENCE DANS LES COMPOSITES SiC/SiC OXYDES

1 - INTRODUCTION

Cette étude* se proposait de mettre en place une méthode capable de détecter la silice, formée lors de oxydation des composites SiC/SiC, sur une coupe polie. La cathodoluminescence présentait, a priori, l'avantage d'obtenir un signal propre à la silice qu'il était ensuite possible d'exploiter afin de définir une cartographie de répartition.

2 - LA CATHODOLUMINESCENCE (CL)

La cathodoluminescence est l'émission de lumière provoquée par le bombardement électronique d'un matériau isolant ou semi-conducteur. Elle se traduit par des processus de désexcitation radiative des électrons des couches périphériques des atomes. Les énergies mises en jeu au moment des désexcitations sont de quelques eV, ce qui se traduit par une émission dans le domaine allant des ultraviolets aux infrarouges [1-3].

---

* conduite avec la collaboration du CRIAA de l'université de Bordeaux III pour les analyses par cathodoluminescence

3 - APPAREILLAGES UTILISES

3.1 - Appareillage de cathodoluminescence couplé avec un système optique

Il permet l'observation directe, avec une loupe ou un microscope, du phénomène de cathodoluminescence ainsi que son enregistrement photographique. Il est composé d'une alimentation à haute tension, d'un canon à électrons à cathode froide qui fournit le faisceau électronique, d'une chambre d'analyse de cathodoluminescence où est placé l'échantillon à analyser (vide primaire) et d'un système de grandissement (loupe ou microscope). Le grandissement maximum avec cette technique est limité à 200 fois.

3.2 - Appareillage de cathodoluminescence couplé avec un microscope électronique à balayage

A l'intérieur de la chambre d'analyse du MEB, un miroir ellipsoïdal percé est placé à la verticale de l'échantillon étudié. Le percement permet le passage du faisceau d'électrons. Le miroir peut être déplacé au dessus de l'échantillon. Il collecte le signal de cathodoluminescence et le focalise hors de la chambre d'analyse vers un périscope. Le signal peut être dirigé vers un tube avec ou sans sélection chromatique (filtre interférentiel ou monochromateur à réseau). Il est amplifié et renvoyé vers l'écran vidéo du microscope électronique à balayage. Cette technique permet d'accéder à des grandissements beaucoup

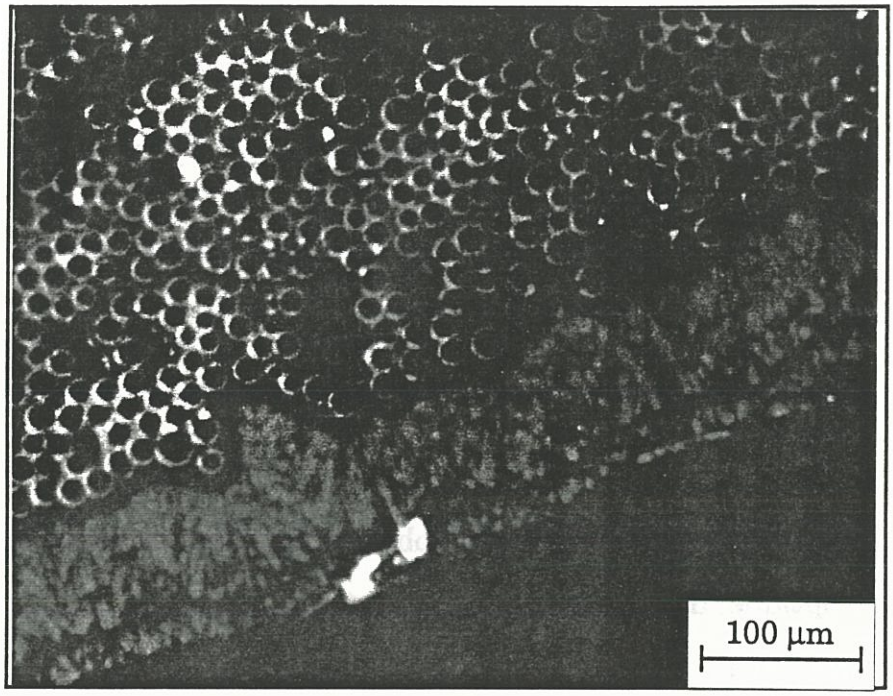

Figure 1 : Cliché de cathodoluminescence avec microscope optique sur coupe polie d'un SiC/SiC avec une interphase de faible épaisseur oxydé 140 h à 900°C sous air.

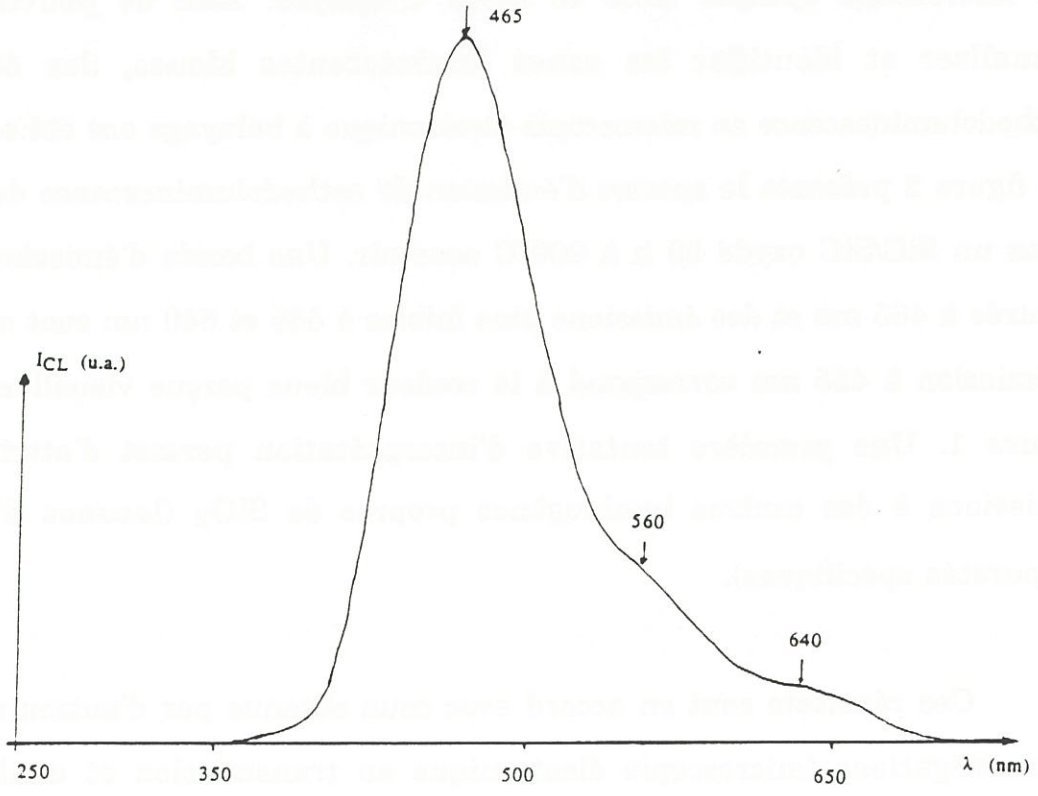

Figure 2 : Spectre d'émission de cathodoluminescence de la silice dans un SiC/SiC oxydé 20 à 900°C sous air. la surface de l'échantillon n'a pas été polie après oxydation.

plus importants que ceux des ensembles optiques. Un analyseur d'image permet de numériser et traiter les informations.

4 - RESULTATS

La figure 1 présente un cliché, obtenu en cathodoluminescence avec un microscope optique, d'un échantillon SiC/SiC oxydé 140 h à 900°C sous air. Une luminescence bleue est clairement localisée autour des fibres. Par ailleurs, une zone correspondant à de la matrice au bord de l'échantillon luminesce en rouge. Cette luminescence rouge, associée à des défauts cristallins de SiC, n'a pas été étudiée car elle se situait en dehors des objectifs de ce travail. Ce cliché à la figure 1 correspond au grandissement maximum qui peut être obtenu avec un microscope optique dans ce mode d'analyse. Afin de pouvoir mieux visualiser et identifier les zones luminescentes bleues, des études de cathodoluminescence en microscopie électronique à balayage ont été effectuées. La figure 2 présente le spectre d'émission de cathodoluminescence de la silice dans un SiC/SiC oxydé 20 h à 900°C sous air. Une bande d'émission intense centrée à 465 nm et des émissions plus faibles à 565 et 640 nm sont observées. L'émission à 465 nm correspond à la couleur bleue perçue visuellement à la figure 1. Une première tentative d'interprétation permet d'attribuer ces émissions à des centres luminogènes propres de SiO_2 (lacunes d'oxygène, impuretés spécifiques).

Ces résultats sont en accord avec ceux obtenus par d'autres méthodes d'investigations (microscopie électronique en transmission et analyses par pertes d'énergie notamment).

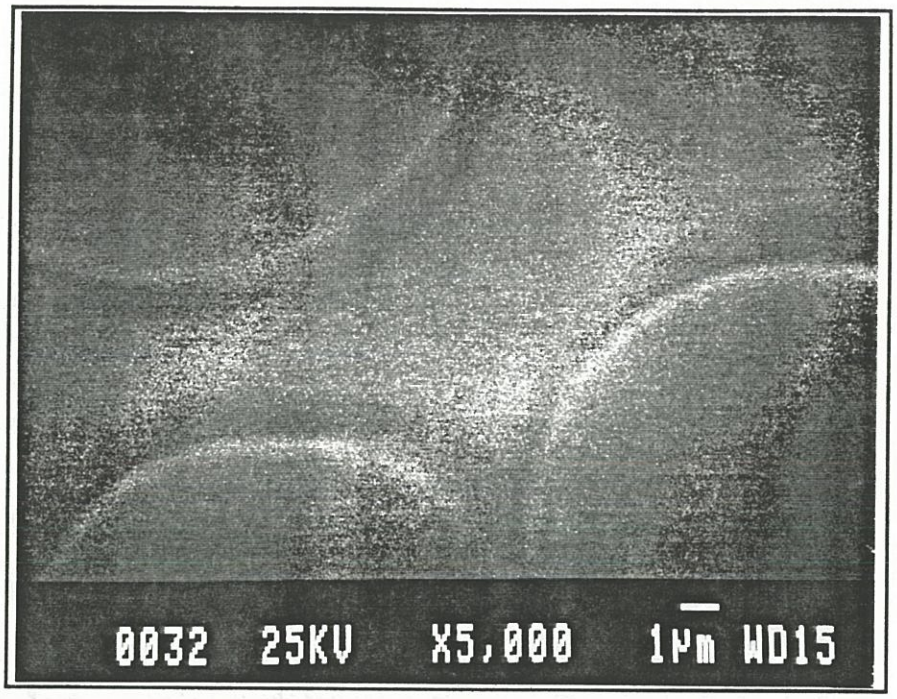

Figure 3 : Cliché de cathodoluminescence en microscopie électronique à balayage sur coupe polie d'un SiC/SiC avec interphase de forte épaisseur oxydé 65 h à 900°C sous air.

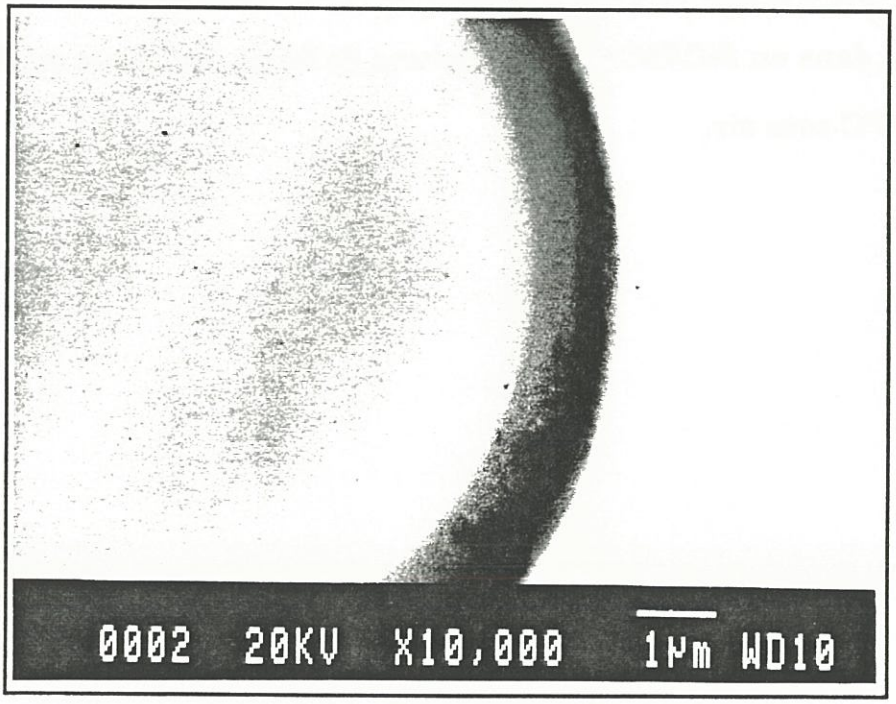

Figure 4 : Micrographie en microscopie électronique à balayage, obtenue en mode d'électrons rétrodiffusés, sur coupe polie d'un SiC/SiC avec interphase de forte épaisseur oxydé 140 h à 900°C sous air.

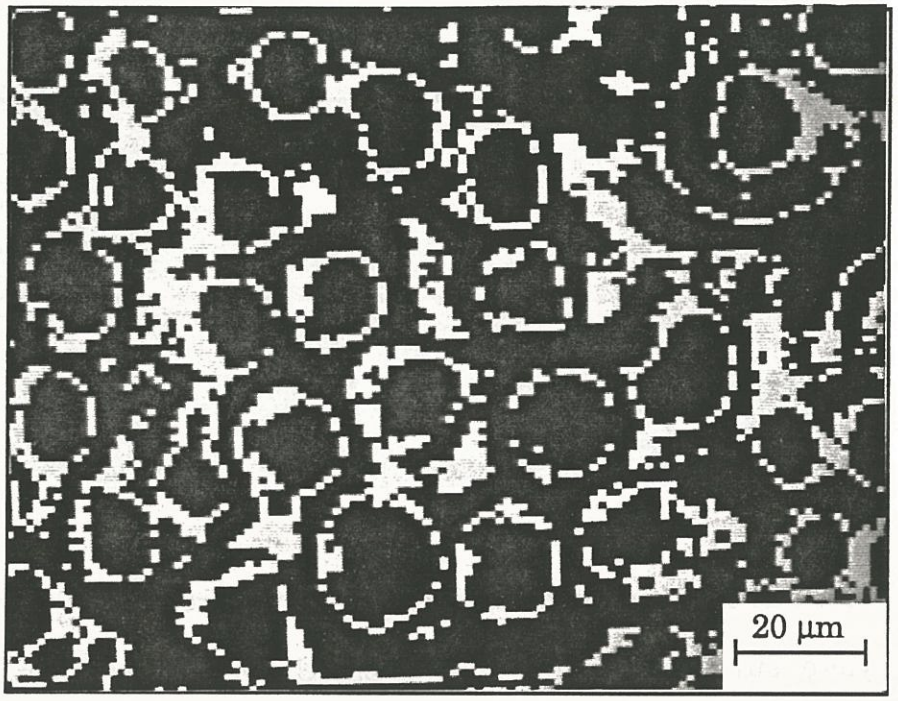

Figure 5 : Image en fausses couleurs de la cathodoluminescence de la silice dans un SiC/SiC avec interphase de faible épaisseur oxydé 300 h à 900°C sous air.

La figure 3 présente un cliché de cathodoluminescence obtenu en microscopie électronique à balayage sur coupe polie d'un échantillon oxydé 20h à 900°C sous air. Le contraste est donné par la luminescence. Les zones luminescentes apparaissent claires. Ce cliché permet de distinguer une zone luminescente intense autour des fibres, qui elles ne luminescent pratiquement pas alors que la matrice présente une certaine intensité de luminescence. Aucun signal intense de luminescence n'est observé en bordure de la matrice.

Pour comparaison, la figure 4 présente une micrographie obtenue en mode d'électrons rétrodiffusés sur coupe polie d'un échantillon oxydé dans des conditions voisines. Une couche de SiO_2 sur la fibre et une couche sur la matrice sont observées dans ce cas (zones grises).

La figure 5 présente une image en fausses couleurs de la cathodoluminescence de SiO_2 dans un composite SiC/SiC oxydé 300 h à 900°C. La silice est visualisée en bleue, elle apparait autour des fibres et des porosités. Ce type d'image est encore difficilement exploitable quantitativement.

5 - CONCLUSION

Une technique originale pour détecter et cartographier la présence de silice dans un composite SiC/SiC a été développée. Elle est basée sur l'émission de luminescence de la silice lorsqu'elle est irradiée par un faisceau électronique (cathodoluminescence). Cette méthode permet d'obtenir d'excellentes informations qualitatives lorsqu'elle est couplée à un ensemble optique (loupe ou microscope) et a été utilisée au cours de ce travail. Par contre,

les analyses fines en microscopie électronique à balayage ont été perturbées par la luminescence intrinsèque de la matrice SiC. Des modifications concernant la détection du signal, le filtrage et le traitement informatique des données devraient permettre d'améliorer la qualité des resultats.

REMERCIEMENTS

Cette étude a été réalisée au CRIAA avec la collaboration de Messieurs M. Schvoerer et R. Chapoulie. J.L. Bobet et F. Régnier ont contribué à ce travail.

REFERENCES

[1] R. Chapoulie
Thèse de l'Université de Bordeaux III, 1988

[2] H.W. Leverentz
" An Introduction to Luminescence of solids", New York, John Wiley inc. 1950

[3] F. Régnier
Mémoire de la série "Formation à et par la Recherche" n°178 CRIAA-ENSERB mars 90

ANNEXE 2

VERIFICATION DE L'HYPOTHESE DU REGIME QUASI-STATIONNAIRE

ANNEXE 2

VERIFICATION DE L'HYPOTHESE DU REGIME QUASI-STATIONNAIRE

Cette vérification a été éffectuée dans le cas d'un pore de révolution dont le diamètre est proche de l'épaisseur d'interphase d'un composite.

E.E. Petersen [1] a étudié la réaction d'un solide poreux avec un gaz. Cet auteur pour justifier l'hypothèse du régime établi a fait les hypothèses suivantes :

- le pore est cylindrique, sa longueur est grande par rapport au rayon r_o,
- il n'y a pas de convection dans le pore,
- la réaction est irréversible, et hétérogène du 1er ordre,
- la diffusion de Knudsen n'est pas prise en compte,
- la concentration C à l'entrée du pore est constante et égale à Co.

L'équation générale à résoudre est :

$$\frac{\partial C}{\partial t} = \frac{D}{r^2} \frac{\partial}{\partial x} \left(r^2 \frac{\partial C}{\partial x}\right) - \frac{2k}{r} C \qquad (1)$$

Soit en coordonnées réduites avec $\psi = \frac{C}{Co}$; $\eta = \frac{x}{L}$; $\tau = \frac{Dt}{L^2}$; $\alpha = (\frac{2k}{ro})^{1/2} L$; $\xi = \frac{r}{ro}$

où ψ est la concentration réduite ; η la distance réduite ; τ le temps adimensionnel ; α le nombre de Thiele (adimensionnel) et ξ le rayon réduit :

$$\frac{\partial \psi}{\partial \tau} = \frac{1}{\xi^2} \frac{\partial}{\partial \eta} (\xi^2 \frac{\partial \psi}{\partial \eta}) - \alpha^2 \frac{\psi}{\xi} \qquad (2)$$

Pour des temps courts, la morphologie du pore est supposée ne pas beaucoup évoluer, l'équation (2) devient :

$$\frac{\partial \psi}{\partial \tau} = \frac{\partial^2 \psi}{\partial \eta^2} - \alpha^2 \psi \qquad (3)$$

L'intégration de cette équation au dérivées partielles peut s'effectuer en utilisant la méthode des transformées de Laplace. Les conditions intiales et aux limites sont les suivantes :

$$\psi(\tau;o) = 1 \qquad (4)$$

$$(\frac{\partial \psi(\tau;\eta)}{\partial \eta})_{\eta = 1} = 0 \qquad (5)$$

$$\psi(o;\eta) = 0 \qquad \forall \eta \qquad (6)$$

Petersen propose la solution suivante :

$$\psi(\tau;\eta) = \frac{ch\alpha(1-\eta)}{ch\alpha} - \frac{4}{\pi}\sum_{n=0}^{\infty} \frac{(-1)^n \exp\left[-\left(\frac{\alpha^2-(2n+1)^2\pi^2}{4}\right)\tau\right]\cos\left[\frac{(2n+1)(1-\eta)\pi}{2}\right]}{(2n+1)\left[1+\frac{4}{(2n+1)^2\pi^2}\right]} \quad (7)$$

Dans l'équation (7), le terme général de la série ne tend pas vers 0 lorsque n croît. Par conséquent, cette série est divergente.

De plus, lorsque $\tau = 0$ et, par exemple, $\eta = 1$ l'équation (7) devient :

$$\psi(0;1) = \frac{1}{ch\alpha} - \frac{4}{\pi}\sum_{n=0}^{\infty} \frac{(-1)^n}{(2n+1)\left(1+\frac{4}{(2n+1)^2\pi^2}\right)} \quad (8)$$

La condition initiale $\psi(0;\eta) = 0$ ne peut pas être respectée quel que soit α.

Ces anomalies ont conduit à réeffectuer l'intégration en utilisant la méthode des transformées de Laplace, l'équation suivante est proposée :

$$\psi(\tau;\eta) = \frac{ch\alpha(1-\eta)}{ch\alpha} - \pi\sum_{n=0}^{\infty} \frac{(-1)^n(2n+1)\exp\left[-\left(\alpha^2+\frac{(2n+1)^2\pi^2}{4}\right)\tau\right]\cos\left[\frac{(2n+1)(1-\eta)\pi}{2}\right]}{\alpha^2+\frac{(2n+1)^2\pi^2}{4}} \quad (9)$$

Il a été vérifié, numériquement, que la condition initiale $\psi(0,1) = 0$ était satisfaite quel que soit α.

L'utilisation de l'équation (9) permet de connaître le temps nécessaire pour s'approcher du régime quasi-stationnaire, c'est à dire t tel que $\psi(\tau,\eta) = \frac{ch\alpha(1-\eta)}{ch\alpha} + \varepsilon$

Dans l'équation (9), lorsque α croît, la convergence de la somme de la série avec τ est accélérée. Le cas $\alpha \neq 0$ est donc le moins favorable à l'hypothèse du régime établi.

L'utilisation de l'équation (9) donne les résultats suivants :

$\alpha = 10^{-2}$	$\psi(3;1)$	$= 1 - 8\,10^{-4} + 1{,}2\,10^{-29} - \ldots$
$\alpha = 1$	$\psi(2;1)$	$= 0{,}65 - 9\,10^{-4} + \ldots$
$\alpha = 10$	$\psi(0{,}2;1)$	$= 9\,10^{-5} - 3{,}9\,10^{-11} + \ldots$

Dans le cas le plus défavorable, pour $\tau = 3$, le profil de concentration est égal à mieux que 10^{-3} près au profil stationnaire. Cela correspond, tenant compte des conditions utilisées, à des temps inférieures à 5 s, temps pendant lequel le profil de SiO_2 dans le pore n'a pas sensiblement évolué. Par conséquent, le **découplage des variables de temps et d'espace est acceptable.** L'équation (1) peut **être simplifiée** en utilisant $\frac{\partial C}{\partial t} = 0$.

REFERENCE

1 - E.E. Petersen
AICHE Journal, 3 [4] (1957) 443-448

ANNEXE 3

METHODE DE RESOLUTION NUMERIQUE

ANNEXE 3

METHODE DE RESOLUTION NUMERIQUE

Les équations à intégrer se présentent sous forme d'équations différentielles ordinaires, non linéaires du second ordre. Les conditions aux limites à respecter sont placées, dans tous les cas, aux deux bornes de l'intervalle d'espace.

La méthode de Runge et Kutta classique (d'ordre 4) a été utilisée pour intégrer ces équations [1]. Les équations permettant de calculer l'approximation y_{n+1} de la fonction $y(x_{n+1})$ à partir de l'approximation y_n est :

$$y_{n,1} = y_n$$

$$y_{n,2} = y_n + \frac{h_n}{2} f(x_n; y_{n,1})$$

$$y_{n,3} = y_n + \frac{h_n}{2} f\left(x_n + \frac{h_n}{2}; y_{n,2}\right)$$

$$y_{n,4} = y_n + h_n f\left(x_n + \frac{h_n}{2}; y_{n,3}\right)$$

$$y_{n+1} = y_n + h_n \left[\frac{1}{6} f(x_n; y_n) + \frac{1}{3} f\left(x_n + \frac{h_n}{2}; y_{n,2}\right) + \frac{1}{3} f\left(x_n + \frac{h_n}{2}; y_{n,3}\right) + \frac{1}{6} f(x_{n+1}; y_{n,4})\right]$$

Une méthode itérative a dû être utilisée pour déterminer les conditions initiales (valeurs des approximations à la première borne d'intégration x_0) permettant le respect des conditions aux limites (en $x=x_1$).

Soit le système à résoudre :

$$\begin{cases} z' = f(x, y, y') \\ y' = z \end{cases}$$

Soit u la condition initiale à déterminer

$$u = z(x_0)$$

On définit :

$$\begin{cases} v = \dfrac{\partial y}{\partial u} \\ \\ w = \dfrac{\partial z}{\partial u} \end{cases}$$

En intégrant le système :

$$\begin{cases} \dfrac{\partial w}{\partial x} = \dfrac{\partial}{\partial u}(z') \\ \\ \dfrac{\partial v}{\partial x} = w \end{cases}$$

il est possible d'obtenir la variation de l'approximation, y ou z, à la seconde borne d'intégration en fonction de la condition initiale u. En utilisant un algorithme de Newton, il est possible de choisir la nouvelle valeur de u permettant de respecter ou d'obtenir une valeur de l'approximation proche de la valeur à respecter. Ainsi la correction, Δu, à apporter à la valeur de u si la condition à respecter en $x = x_1$ est $y_{n+1} = y_1$, est définie par :

$$\Delta u = \frac{y_{n+1} - y_1}{v_{n+1}}$$

La figure 1 présente un organigramme du progamme de résolution.

REFERENCE

[1] M. Crouzeix et A.L. Mignot
"Analyse numérique des équations différentielles", Masson, 2nde édition, 1989

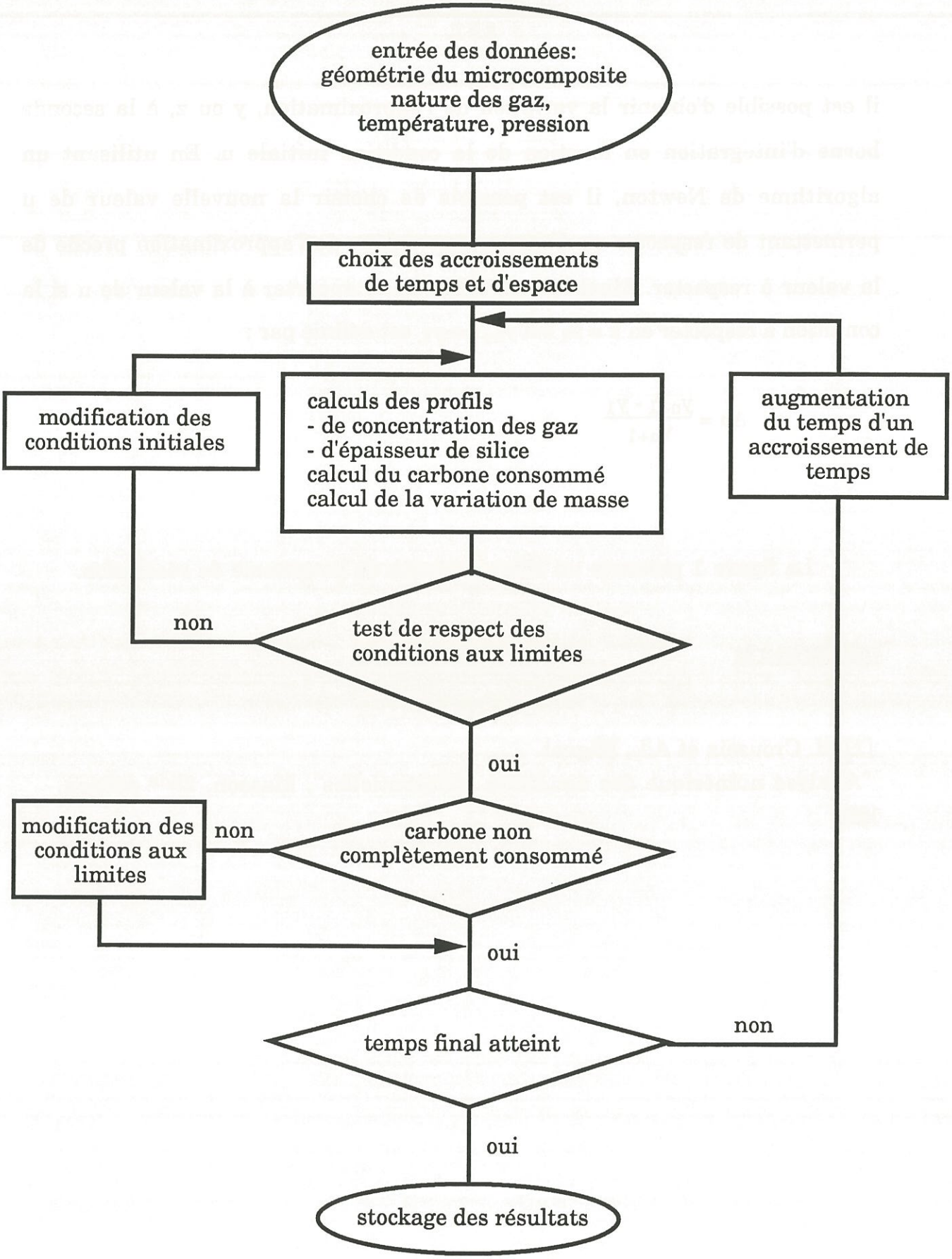

Figure 1 : Organigramme du programme de résolution

RESUME

La connaissance des mécanismes d'oxydation des composites SiC/C/SiC est essentielle pour l'utilisation de ces matériaux à hautes températures en environnement oxydant. Dans cette étude, sont présentées dans un premier temps les cinétiques d'oxydation des fibres SiC ex-polycarbosilane et de la matrice SiC déposée chimiquement à partir d'un mélange CH_3SiCl_3/H_2. Le comportement à l'oxydation des composites SiC/C/SiC unidirectionnel a été étudié expérimentalement. Les principaux mécanismes mis en jeu ont été identifiés et l'influence de plusieurs paramètres a été mise en évidence. Un modèle théorique prenant en compte les phénomènes de diffusion et de réaction simultanée de l'espèce oxydante avec les différents constituants (fibre, matrice, interphase) a été développé. Ce modèle, qui permet d'accéder à la cinétique d'oxydation du carbone interfacial, montre le rôle déterminant de l'épaisseur d'interphase. Il permet d'expliquer qu'à hautes températures les matériaux s'auto-protègent. Ce type de comportement a été confirmé par l'étude de l'influence de vieillissements à hautes températures sur les caractéristiques mécaniques résiduelles de ces composites.

MOTS CLES

Fibres ex-PCS, Carbure de silicium (SiC), Carbone, Composites SiC/C/SiC, Cinétique, Oxydation, Effets d'environnement, Diffusion

ABSTRACT

The knowledge of the oxidation mechanisms of SiC/C/SiC composites is essential regarding the use of these materials at high temperatures in oxidizing environment. The oxidation kinetics of SiC ex-polycarbosilane fibers and SiC matrix chemically deposited from a CH_3SiCl_3/H_2 mixture are presented. The oxidation behaviour of unidirectional SiC/C/SiC composites has been studied experimentally. The main mechanisms have been identified and the influence of several parameters on the oxidation kinetics has been investigated. A theoretical model, accounting for simultaneous diffusion and reaction of the oxidizing species with the different constituents (fiber, interphase, matrix) has been developed. This model allows the calculation of the carbon interphase oxidation kinetics. It shows the strong influence of the carbon interphase thickness and explains the self-healing behaviour observed at high temperatures with thin interphase thickness. This particular behaviour is in good agreement with the effects of high temperature ageing treatments on the mechanical properties of unidirectional SiC/C/SiC composites.

KEY WORDS

Ex-PCS fibers, Silicon Carbide (SiC), Carbon, SiC/C/SiC Composites Kinetics, Oxidation, Environmental effects, Diffusion

RESUME

La connaissance des mécanismes d'oxydation des composites SiC/C/SiC est essentielle pour l'utilisation de ces matériaux à hautes températures en environnement oxydant. Dans cette étude, sont présentées dans un premier temps les cinétiques d'oxydation des fibres SiC ex-polycarbosilane et de la matrice SiC déposée chimiquement à partir d'un mélange CH_3SiCl_3/H_2. Le comportement à l'oxydation des composites SiC/C/SiC unidirectionnel a été étudié expérimentalement. Les principaux mécanismes mis en jeu ont été identifiés et l'influence de plusieurs paramètres a été mise en évidence. Un modèle théorique prenant en compte les phénomènes de diffusion et de réaction simultanée de l'espèce oxydante avec les différents constituants (fibre, matrice, interphase) a été développé. Ce modèle, qui permet d'accéder à la cinétique d'oxydation du carbone interfacial, montre le rôle déterminant de l'épaisseur d'interphase. Il permet d'expliquer qu'à hautes températures les matériaux s'auto-protègent. Ce type de comportement a été confirmé par l'étude de l'influence de vieillissements à hautes températures sur les caractéristiques mécaniques résiduelles de ces composites.

MOTS CLES

Fibres ex-PCS, Carbure de silicium (SiC), Carbone, Composites SiC/C/SiC, Cinétique, Oxydation, Effets d'environnement, Diffusion

ABSTRACT

The knowledge of the oxidation mechanisms of SiC/C/SiC composites is essential regarding the use of these materials at high temperatures in oxidizing environment. The oxidation kinetics of SiC ex-polycarbosilane fibers and SiC matrix chemically deposited from a CH_3SiCl_3/H_2 mixture are presented. The oxidation behaviour of unidirectional SiC/C/SiC composites has been studied experimentally. The main mechanisms have been identified and the influence of several parameters on the oxidation kinetics has been investigated. A theoretical model, accounting for simultaneous diffusion and reaction of the oxidizing species with the different constituents (fiber, interphase, matrix) has been developed. This model allows the calculation of the carbon interphase oxidation kinetics. It shows the strong influence of the carbon interphase thickness and explains the self-healing behaviour observed at high temperatures with thin interphase thickness. This particular behaviour is in good agreement with the effects of high temperature ageing treatments on the mechanical properties of unidirectional SiC/C/SiC composites.

KEY WORDS

Ex-PCS fibers, Silicon Carbide (SiC), Carbon, SiC/C/SiC Composites Kinetics, Oxidation, Environmental effects, Diffusion